Aus dem Institut für Virologie

der Medizinischen Fakultät Charité – Universitätsmedizin Berlin

DISSERTATION

Innate Immune Sensing and Viral Evasion Mechanisms of HIV-1 and SARS-CoV-2

-

Angeborene Immunität gegen und Virale Evasionsmechanismen von HIV-1 und SARS-CoV-2

zur Erlangung des akademischen Grades

Doctor of Philosophy (PhD)

vorgelegt der Medizinischen Fakultät

Charité – Universitätsmedizin Berlin

von

Julia Kazmierski, M.Sc.

Datum der Promotion: 30.11.2023

I. Content

II. Table of figures

III. Table of abbreviations

Abbreviation	Definition
AIDS	Aquired immunodeficiency syndrome
ART	Antiretroviral therapy
CA	Capsid
c-di-UMP	Cyclic di-UMP
cGAMP	Cyclic GMP-AMP
cGAS	Cyclic GMP-AMP synthase
COVID-19	Coronavirus disease 2019
DC	Dendritic cell
dNTPs	Desoxy nucleosid triphsphates
EFV	Efavirenz
Env	Envelope
ER	Endoplasmic reticulum
ERGIC	ER-Golgi intermediate compartment
Gp	Glycoprotein
H	Histidine
HIV-1	Human immunodeficiency virus
IFN	Interferon
IFNAR	Interferon-α/β-receptor
IN	Integrase
ISD	Immunostimmulatory DNA
ISG	Interferon-stimulated gene
KO	Knock out
LPS	Lipopolysaccharide
M	Membrane
MDDCs	Monocyte-derived dendritic cells
MDMs	Monocyte-derived macrophages
N	Nucleocapsid

Abbreviation	Definition
Nsps	Non-structural proteins
ORF	Open reading frame
P	Proline
PAMP	Pathogen-associated molecular pattern
PBMCs	Peripheral blood mononuclear cells
pDC	Plasmacytoid dendritic cell
PRR	Pattern recognition receptor
RT	Reverse transcriptase
S	Spike
SARS-CoV	Severe acure respiratory syndrome coronavirus
sg	Subgenomic
SNP	Single nucleotide polymorphism
ss	Single strand
TLR	Toll-like receptor
UTR	Untranslated Regions
WT	Wildtype

IV. Zusammenfassung

Das angeborene Immunsystem ist die erste Abwehrlinie gegen eindringende Pathogene. Zelluläre Mustererkennungsrezeptoren (*engl. PRRs*) detektieren konservierte Pathogen-assoziierte molekulare Muster (*engl. PAMPs*) und initiieren eine Signaltransduktionskaskade, die in der Sekretion von Typ I Interferonen (IFN) und pro-inflammatorischen Zytokinen mündet, welche durch parakrine und autokrineMechanismen die Immunantwort amplifizieren. Typ I IFN sind universelle, antivirale Zytokine, die nach Bindung an den IFN-α/β-Rezeptor die JAK/STAT-abhängige Expression hunderter antiviraler Moleküle, der so genannten IFN-stimulierten Gene, auslöst. Irrtümlich im zellulären Zytosol lokalisierte DNA ist ein besonders potenter Auslöser von Typ I IFN-vermittelter Immunität. Das Enzym zyklische GMP-AMP Synthase (*engl. cGAS*) katalysiert nach Bindung an zytosolischer DNA die Synthese des sekundären Botenstoffes zyklisches GMP-AMP (cGAMP), welches eine STING/TBK1/IRF3-abhängige Signalkaskade zur Produktion von Typ I IFN auslöst. Die frühe Initiierung einer solchen angeborenen Immunantwort ist entscheidend für die Restriktion viraler Replikation, die Eliminierung infizierter Zellen und die Einleitung der adaptiven Immunantwort zur effizienten Kontrolle der Infektion und der Abmilderung des Krankheitsverlaufs *in vivo*. Folglich haben Viren Evasionsmechanismen entwickelt, um der Typ I IFN-vermittelten Restriktion zu entgehen und die virale Replikation zu fördern, zum Beispiel durch die Expression antagonistischer viraler Proteine, die PRR-ausgelöste Signalketten zum Erliegen bringen oder durch die Entwicklung anspruchsvoller Replikationsstrategien, die die Exposition viraler PAMPs gegenüber den zellulären PRRs auf ein Minimum reduziert.

Diese Dissertation basiert auf den drei kürzlich unter meiner maßgeblichen Mitarbeit veröffentlichten Publikationen, die jeweils Schlüsselfragen der angeborenen Immunität und viraler Evasion im Kontext der HIV-1- und SARS-CoV-2-Infektion adressieren. Die erste Studie untersucht die strukturellen und funktionellen Konsequenzen der am häufigsten natürlich vorkommenden cGAS-Variante, rs610913, in Bezug auf deren Fähigkeit DNA-vermittelte Immunantworten im Kontext viraler Infektionen auszulösen (1). Die zweite Studie evaluiert den Beitrag der cGAS-vermittelten Detektion proviraler DNA zur intrinsischen Immunantwort in HIV-1-infizierten $CD4^+$ T-Zellen, den Hauptzielzellen von HIV-1 *in vivo* (2). In der dritten Studie wird die Infektionsempfänglichkeit und initiierte

angeborene Immunantwort in peripheren mononukleären Zellen des Blutes nach *ex vivo* Inokulation mit SARS-CoV-2 unter Anderem mittels Einzelzellsequenzierung analysiert (3).

V. Abstract

The innate immune system is the first line of defence against invading pathogens. Pattern recognition receptors (PRRs) sense conserved pathogen-associated molecular patterns (PAMPs) and initiate a signal transduction cascade that culminates in the secretion of type I interferons (IFNs), pro-inflammatory cytokines and amplification of innate immunity through autocrine and paracrine signalling. Type I IFNs are universal, antiviral cytokines that bind to the IFN-α/β-receptor (IFNAR) and induce the JAK/STAT-dependent expression of hundreds of antiviral molecules, known as IFN-stimulated genes (ISGs). Aberrantly located, cytosolic DNA is a potent activator of type I IFN responses upon detection by the cytosolic DNA sensor cyclic GMP-AMP synthase (cGAS). Upon DNA sensing, cGAS catalyses the formation of the second messenger cyclic GMP-AMP (cGAMP) that subsequently induces a STING/TBK1/IRF3-driven signalling cascade and the production of type I IFNs. Early initiation of intrinsic immunity is crucial for viral restriction, elimination of infected cells and orchestration of adaptive immunity to sufficiently control the viral infection and dampen disease progression *in vivo*. Consequently, multiple viruses have evolved mechanisms to counteract restrictive type I IFN immunity to facilitate continuous viral replication, e.g. through expression of antagonistic viral proteins that modulate PRR-induced signalling or the development of sophisticated replication strategies to minimize viral PAMP exposure to cellular PRRs.

This dissertation is based on my three recent publications addressing key questions in the field of innate sensing and viral evasion of HIV-1 and SARS-CoV-2 infections. The first study investigated the structural and functional consequences of the most frequent naturally occurring variant rs610913 in the cGAS-encoding gene in the context of DNA sensing upon viral infections (1). The second study carefully re-evaluates the contribution of cGAS-mediated sensing of reverse transcription products to the induction of intrinsic immunity in HIV-1-infected $CD4^+$ T-cells, the major HIV-1 target cell *in vivo* (2). In the third study, the susceptibility to infection and ability to mount cell-intrinsic immunity in peripheral blood mononuclear cells upon *ex vivo* SARS-CoV-2 exposure were investigated and delineated to individual cell types using, among other methods, single cell RNA-sequencing (3).

1. Introduction

The innate immune system serves as the first line of defence against invading pathogens. Sensing of the virus components elicits an innate antiviral immune response that restricts virus replication and spread, aids at identifying and eliminating infected cells and alarms local and systemic immune effector mechanisms to eventually achieve viral clearance. Virus sensing is accomplished by pattern recognition receptors (PRRs) that, upon recognition of conserved pathogen-associated molecular patterns (PAMPs), initiate a signalling cascade culminating in the production of soluble mediators, such as type I interferons (IFNs) and pro-inflammatory cytokines that - through both autocrine and paracrine signalling - restrict virus replication. Type I IFNs are universal, antiviral cytokines that bind to the Interferon-α/β- receptor (IFNAR) and induce a downstream JAK/STAT-dependent signalling cascade resulting in the expression of hundreds of antiviral molecules, known as IFN-stimulated genes (ISGs). Aberrantly located, cytosolic DNA is a potent activator of such type I IFN responses (4). Upon infection or cellular stress responses, viral or host DNAs can leak into the cytosol and be detected by the cytosolic DNA sensor cyclic GMP-AMP synthase (cGAS) in a sequence-independent manner (5, 6). Following binding to double-stranded DNA, cGAS catalyses the synthesis of the second messenger cyclic GMP-AMP (cGAMP) which subsequently binds to and activates the Stimulator of IFN Genes (STING) (7–11). Activation of STING results in its translocation to the Golgi, activation and phosphorylation of the TANK-binding kinase 1 (TBK1) and eventually the phosphorylation, dimerization and nuclear translocation of the transcription factor IFN regulatory factor (IRF) 3, resulting in the enhanced expression of type I IFNs and other antiviral IRF3-target genes. Conclusively, the DNA sensor cGAS is an essential component of innate immunity for immediate recognition of invading pathogens and establishment of a type I IFN response (12).

Innate sensing of pathogens´ components is decisive for disease outcome and their insufficient recognition enables unrestricted viral spread. Consequently, viruses have evolved sophisticated replication strategies to counteract innate sensing and down-stream signalling by various mechanisms (13, 14). In the following chapters, I will introduce the characteristics of HIV-1 and SARS-CoV-2 replication that trigger intrinsic immunity and the corresponding viral strategies that have evolved to minimize these occasions.

1.1. Molecular biology of HIV-1 infection

Originating from distinct zoonotic transmission events in the early 20th century, HIV-1 has slowly spread and gave rise to the acquired immunodeficiency syndrome (AIDS) pandemic starting in the early 1980s (15, 16). To date, HIV infection remains a global health threat, with the Joint United Nations Program on AIDS (UNAIDS) estimating a total of 79.3 million people have become infected and 36.3 million have died from AIDS-related illness since the start of the pandemic (17).

HIV-1 is transmitted by sexual contact across mucosal surfaces, percutaneous inoculation and perinatal from mother to child. The infection manifests itself in an initial phase of acute infection, but slowly progresses through an asymptomatic phase characterized by high viral loads and massive $CD4^+$ T-cell depletion to the irreversible, final stage of the infection defined as AIDS, in which patients suffer from life-threatening immune deficiency and susceptibility to opportunistic infections (18, 19). The development of a potent antiretroviral therapy (ART) has substantially improved the life expectancy and quality of individuals with HIV by suppressing virus replication, transmission and disease progression. HIV-1, however, establishes a persistent infection upon integration of the viral genome into the host cells' DNA thereby forming a viral reservoir with minimal viral RNA and protein expression. Latent infection allows the virus to persist in an ART-insensitive stage and to maintain its reservoir through low-level viral replication and homeostatic proliferation in $CD4^+$ T-cells as the main HIV-1 target cells displaying a particularly long life span (20). The existence of this long-lasting, viral reservoir remains the main obstacle to HIV-1 eradication and cure.

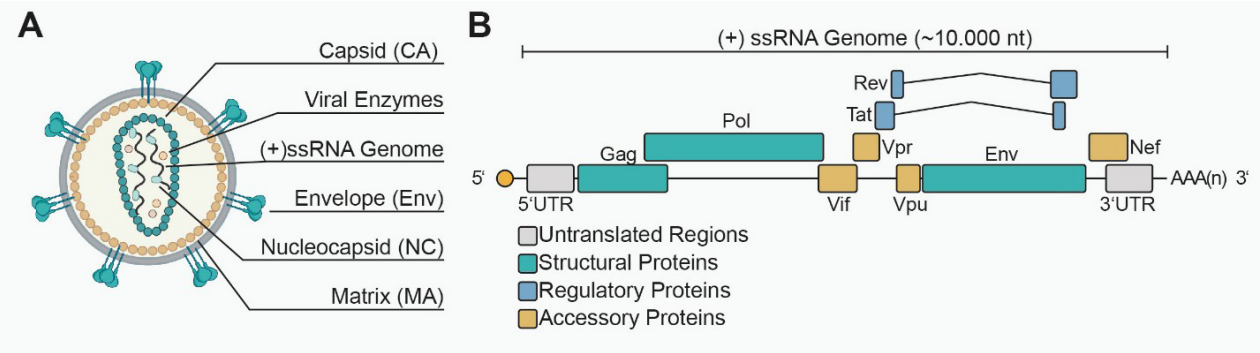

Figure 1. HIV-1 virion and genome organisation. (A) *The trimeric envelope glycoprotein (Env) is composed of gp41/gp120 embedded in the HIV-1 lipid envelope. The structural proteins matrix (MA), capsid (CA) and nucleocapsid (NC) and the viral enzymes, such as the reverse transcriptase and integrase are derived from the Gag and Gag/Pol polyproteins.* ***(B)*** *The 10.000 nucleotide-long HIV-1 genome is composed of the 5' and 3' untranslated regions (UTRs), the structural polyprotein-encoding genes Gag, Pol and Env, the regulatory genes Tat and Rev as well as the accessory genes Vif, Vpr, Vpu and Nef.(Source: own figure).*

The HIV-1 virion is composed of a lipid envelope embedding the viral envelope glycoproteins (Env) (**Fig. 1A**). The capsid (CA) encloses the ~10.000 nucleotide long, positive-sense, single-stranded (ss) RNA genome, containing untranslated regions (UTRs), structural, regulatory and accessory genes (**Fig. 1B**). Additionally, HIV-1 virions contain viral enzymes that are essential for mediating early post-entry steps of the replication cycle, including reverse transcriptase (RT) and integrase (IN). HIV-1 host cell entry is mediated by Env, a trimeric complex of the non-covalently associated glycoproteins (gp) 120 and 41. Sequential binding of gp120 to the CD4 receptor and co-receptor, either CCR5 and/or CXCR4, triggers conformational changes and insertion of a viral fusion peptide into the cellular membrane, resulting in a fusion pore to bridge viral and host cell membranes and allow the release of the capsid into the target cell (**Fig. 2**)

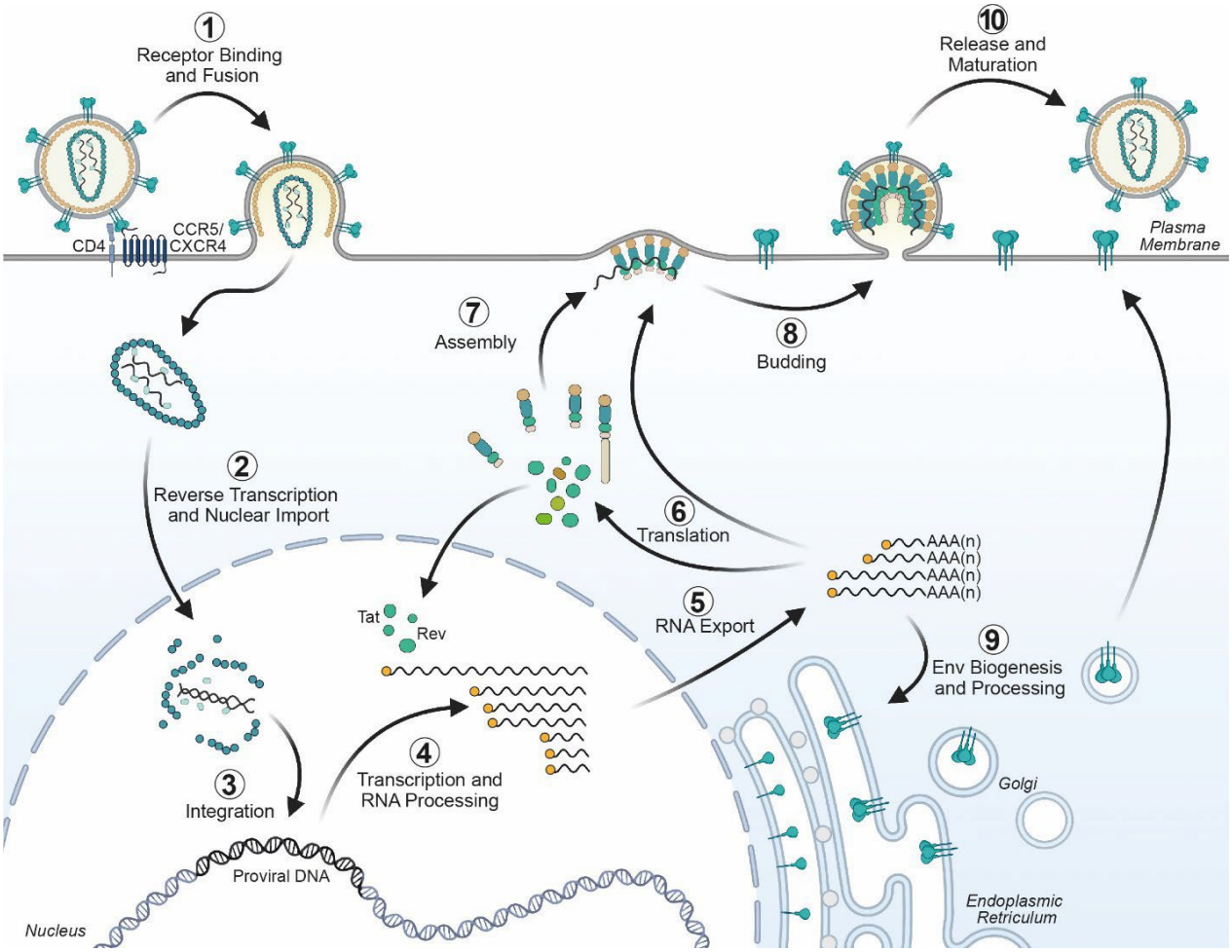

Figure 2. HIV-1 replication cycle. *HIV-1 enters via engagement of the CD4 receptor and one of the co-receptors CCR5 or CXCR4 ①. Following reverse transcription, nuclear import ② and integration ③, the proviral DNA is transcribed ④ and the viral RNAs are processed and exported from the nucleus ⑤ where they are translated ⑥. The regulatory proteins Tat and Rev translocate to the nucleus to facilitate viral transcription and RNA export, respectively. The structural polyproteins Gag and Gag/Pol assemble at the plasma membrane ⑦ upon recruitment of the genomic RNA to the budding virions ⑧.The glycoprotein Env is translated at the rough ER, processed and glycosylated in the Golgi apparatus and presented on the cell surface via the secretory pathway ⑨. Finally, progeny virions are released from the plasma membrane and undergo protease-mediated maturation within the virion ⑩. (Source: own figure).*

(21–23). Following entry, the HIV-1 genomic RNA is reverse transcribed into complementary double-stranded DNA which is integrated into the host cell genome, mediated by the viral RT and IN enzymes, respectively. It is established that reverse transcription and integration are closely linked to capsid disassembly, however, recent studies propose that nuclear import precedes uncoating and the completion of reverse transcription (24–27). The host cell RNA polymerase II transcribes the integrated proviral DNA (the provirus) and generated viral RNAs are either fully spliced and exported by hijacking the cellular mRNA export machinery, or incompletely spliced or non-spliced and dependent on the Rev-mediated RNA export mechanism (28, 29). After RNA export, the structural polyproteins Gag and Gag/Pol, the regulatory proteins Tat and Rev as well as the accessory proteins Vpr, Vif and Nef are translated in the cytosol. Env and Vpu are translated separately from a bicistronic, singly spliced RNA at the rough ER, following Env translocation to the Golgi for processing and glycosylation and finally transport to the plasma membrane. In parallel, Gag and Gag/Pol polyproteins assemble at the plasma membrane and recruit two copies of the full-length genomic RNA (30, 31). Eventually, the budding particles are released from the plasma membrane using the cellular ESCRT-machinery followed by protease-mediated cleavage of Gag and Gag/Pol to generate mature, infectious HIV-1 particles.

1.2. HIV-1 innate immune sensing and viral evasion strategies

The main HIV-1 target cells, $CD4^+$ T-cells, macrophages and dendritic cells (DCs), harbour a set of potent, constitutively expressed or IFN-induced anti-HIV-1 restriction factors, of which APOBEC3G, Tetherin, TRIM5α, SAMHD1 and SERINC5 have been identified as the most potent ones (32). However, HIV-1 aquired the accessory proteins Vif, Vpr, Vpu and Nef that target specific restriction factors for degradation by hijacking diverse cellular mechanisms, thus nullifying their antiviral activity (13, 32). Notably, SAMHD1, a triphosphohydrolase that degrades cytosolic dNTPs required for HIV-1 replication, is targeted by the HIV-2/SIV-encoded protein Vpx, but none of the HIV-1 accessory proteins. Therefore, resting $CD4^+$ T-cells, macrophages and DCs expressing active SAMHD1 are more refractory to HIV-1 infection as compared to activated $CD4^+$ T-cells that lack SAMHD1 activity (33, 34). *Ex vivo* studies report an overall stronger innate immune response in monocyte-derived macrophages (MDMs) or DCs (MDDCs)

compared to CD4$^+$ T-cells potentially accounting for their lower susceptibility to HIV-1 infection (13, 35). The innate sensing of HIV-1 infection, however, is exclusively monitored under certain experimental conditions, including the co-packaging of HIV-2/SIV Vpx for eliminating SAMHD1 and replenishing cellular dNTP concentrations (36–38), and genetic or pharmacological destabilization of the HIV-1 CA (39–41). In these studies, HIV-1 sensing was dependent on cGAS/STING signalling, suggesting recognition of leaking RT products into the cytosol (37, 42, 43). In contrast, the role of cytosolic DNA sensing upon HIV-1 infection in CD4$^+$ T-cells, the main target cell for HIV-1 *in vivo*, is less well understood. One study reported a cGAS-mediated, post-integration, type I IFN response, potentially through sensing of mtDNA released from ruptured mitochondria (44), while another study questioned the overall intactness of the cGAS/STING signalling pathway in primary CD4$^+$ T-cells (45). In contrast, another cytosolic DNA sensor, IFI16, was reported to sense abortive HIV-1 infection in CD4$^+$ T-cells, however exclusively in lymphoid tissue-derived T-cells. Specifically, IFI16 recognized the accumulation of RT products upon abortive CD4$^+$ T-cell infection and triggered a caspase-1-driven inflammasome activation, resulting in pyroptotic cell death (46–48). Pyroptosis is therefore proposed to be the main driver of the massive CD4$^+$ T-cell depletion upon untreated HIV-1 infection *in vivo* (49).

In addition to evolution of accessory proteins, HIV-1 displays a sophisticated replication strategy to evade intrinsic immunity by hijacking cellular host factors to mask or protect viral PAMPs from sensing. For example, HIV-1 CA recruits CPSF6 and the cyclophilins Nup358 and CypA through highly conserved amino acids to maintain the CA lattice integrity and prevent untimely nucleic acid leakage into the cytosol (39). Further, the cytosolic exonuclease TREX1 impedes the accumulation of excessive cytosolic DNAs, including HIV-1 RT products, thereby protecting HIV-1 from cGAS-mediated immunity (50, 51). Finally, HIV-1 RNAs are shielded from the cytosolic RNA sensor MDA-5, through the cellular FTSJ3, an RNA 2'-*O*-methyltransferase that installs a 2'O-methylation at the 5' end of the viral RNAs, a modification whose absence triggers MDA-5 activation (52).

Despite potent evasion mechanisms of HIV-1 *ex vivo,* acute HIV-1 and SIV infections trigger transient and subtle type I IFN responses *in vivo* (53), the quality of which negatively correlates with viral load (54). The early type I IFN response is thought to originate primarily from plasmacytoid DCs (pDCs) due to their ability to detect HIV-1

ssRNA, potentially released from cytopathic HIV-1-infected cells, in a Toll-like receptor (TLR) 7/8-dependent manner (55, 56) and their timely arrival at the primary site of infection (53, 57). Remarkably, transmitted founder viruses, in contrast to variants circulating during the chronic phase of infection, harbour a distinct resistance profile to type I IFNs, suggesting that the early type I IFN response partially prevents transmission events of most IFN-sensitive viruses, which potentially accounts for the relatively poor HIV-1 transmission rates *in vivo* (58–60). The type I IFN levels in serum, together with $CD4^+$ T-cell counts and viral loads, normalize after ART initiation (54, 61). Conversely, individuals receiving ART still suffer from chronic immune activation and exhaustion characterized by elevated expression of activation markers and cytokine levels, which may result from reoccurring, transient viral antigen exposure to cytotoxic T-cells from the persisting viral reservoirs, rather than cell-intrinsic sensing of HIV-1 PAMPs (62, 63).

1.3. SARS-CoV-2 infection biology

The Severe Acute Respiratory Syndrome Coronavirus 2 (SARS-CoV-2) is a highly transmissive, human-pathogenic coronavirus and the causative agent of the coronavirus disease 2019 (COVID-19). Since its emergence in 2019, SARS-CoV-2 rapidly spread across the globe, with an estimate of more than 592 million infections and 6.4 million deaths owing to infection (as of 08/2022) (64). SARS-CoV-2 establishes upper and lower respiratory tract infections, mostly accompanied by mild symptoms; however, some cases experience clinical deterioration with systemic inflammation, acute respiratory distress syndrome, multiple organ failure and fatal disease outcome (65, 66). Despite the licencing of multiple effective vaccines, control of the COVID-19 pandemic is jeopardized by the emergence of variants, such as Alpha, Beta, Delta and Omicron, conferring enhanced transmissibility and immune evasion, hence SARS-CoV-2 remains a global health threat (67, 68).

The SARS-CoV-2 virion contains the positive-sense, ssRNA genome coated by the viral nucleocapsid (N) and enclosed by a lipid bilayer embedding the viral envelope (E), membrane (M) and spike (S) proteins (**Fig. 3A**). The viral genome of nearly 30.000 nucleotides length contains 5’ and 3’ regulatory UTRs, and encodes for non-structural proteins (nsps), structural and accessory proteins (**Fig. 3B**).

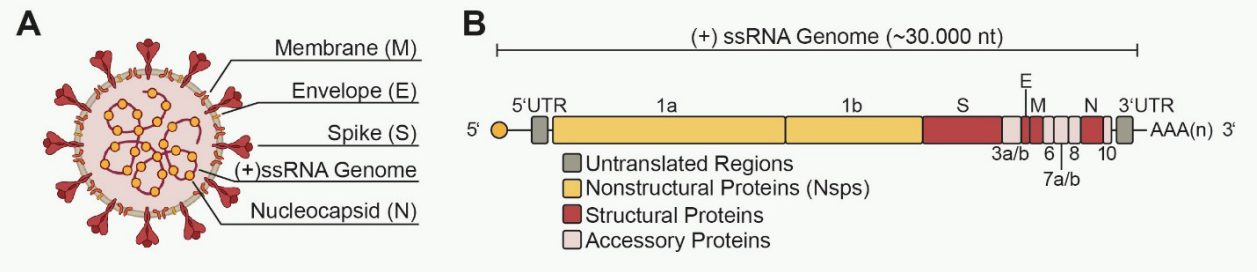

Figure 3. SARS-CoV-2 particle and genome organisation. (A) *The SARS-CoV-2 virion consists of the structural proteins membrane (M), envelope (E), spike (S) embedded in the lipid envelope and nucleocapsid (N) coating the viral ssRNA genome incorporated in the viral particle.* ***(B)*** *The nearly 30.000 nucleotides (nt) long viral genome is equipped with a 5' capping structure and 3' poly-A-tail and encodes regulatory, untranslated regions (UTRs) on the 5' and 3' ends, ORF1a and ORF1b encoding for the non-structural proteins (nsps) 1-16, the four structural proteins S, E, M and N as well as the accessory proteins ORF3a, ORF3b, ORF6, ORF7a, ORF7b, ORF8 and ORF10. (Source: own figure).*

SARS-CoV-2 infection is initiated through specific binding of the S protein to the cellular entry receptor ACE2 (69, 70). Membrane fusion following ACE2 engagement requires the proteolytic cleavage of the S2' site which is executed by the cellular proteases TMPRSS2 or the less favoured Cathepsin L, present on the plasma membrane and the endosomal compartment, respectively **(Fig. 4**) (69, 71). Following entry, the RNA genome is released in the cytosol and initiates the immediate translation of the open reading frame (ORF) 1a- and 1b-encoded polyproteins, followed by their proteolytic cleavage and the subsequent release of 16 nsps (72–74). The early nsp1 mediates a selective host shutoff (75), while nsp2-16 assemble to the viral replication and transcription complex including the RNA-dependent RNA polymerase (nsp12) and all factors required for genome replication and subgenomic (sg) RNA transcription (72, 73). Notably, the interaction of nsp3-5 with cellular factors generates a designated, ER-derived, viral replication organelle which consists of interconnected, convoluted membranes and double-membrane vesicles that concentrates all components of the replication machinery (76, 77). Within this virus-specific replication organelle, the viral genome replication is executed via generation of a full-length, negative-sense ssRNA intermediate used as a template for generation of new positive-sense ssRNA genomes that are subsequently packaged into progeny virions. Additionally, a set of sgRNAs is transcribed to serve as templates for translation to structural and accessory proteins through a CoV-attributed, discontinuous transcription mechanism (78). The sgRNAs are then 5'-capped and 3'-polyadenylated and translated into the structural and accessory CoV proteins. The envelope proteins E, M and S are translated at the ER and subsequently retained at the ER-Golgi intermediate compartment (ERGIC) where S is additionally primed by furin-like proteases. Finally, the

N condensates the genomic RNA, virus particles bud into the ERGIC membranes and virions exit the cell via exocytosis.

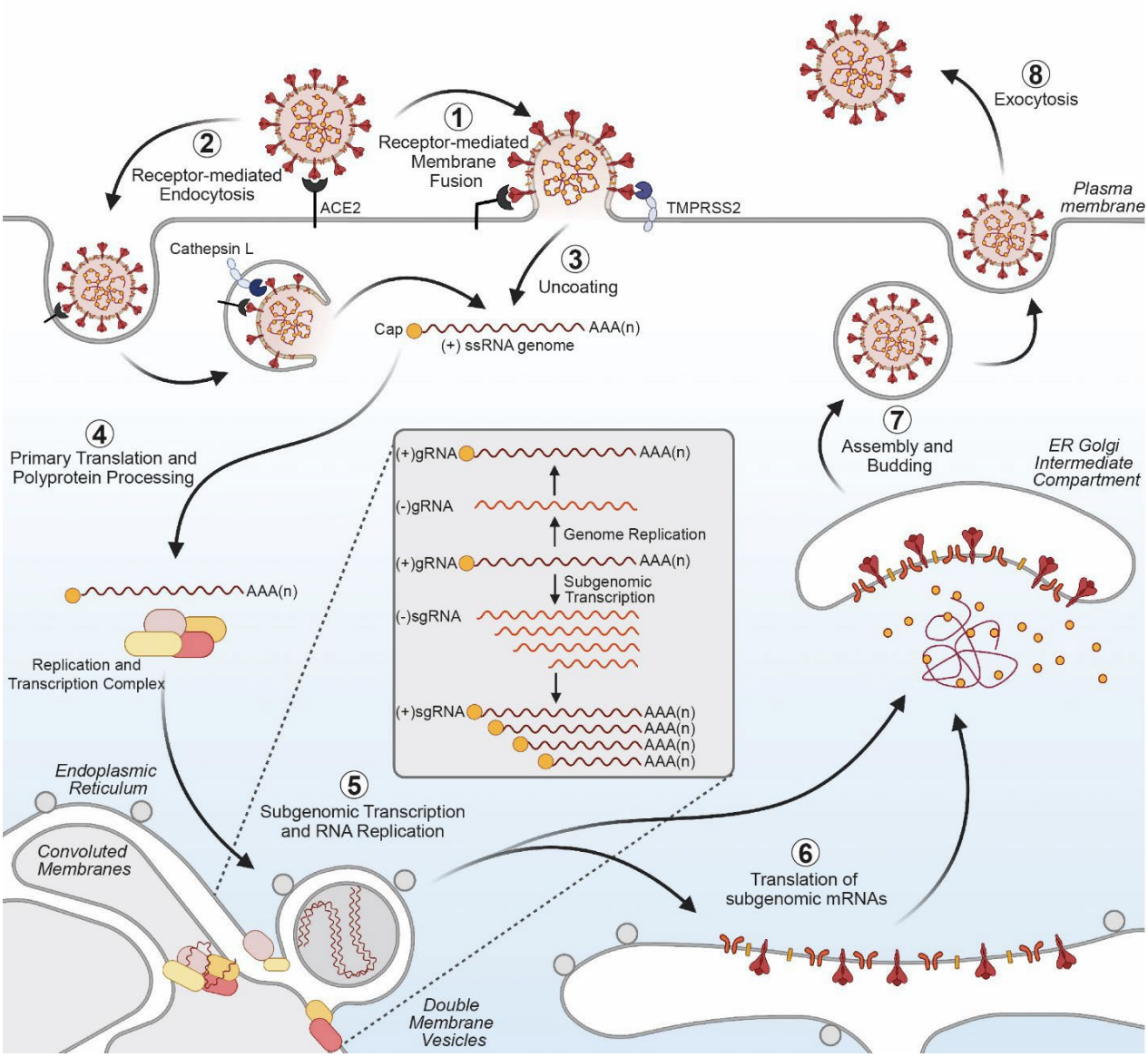

Figure 4. SARS-CoV-2 replication cycle. *SARS-CoV-2 enters the cell via receptor-mediated membrane fusion ① or endocytosis ②, following the activation of the S protein by the proteases TMPRSS2 or Cathepsin L, respectively. Uncoating releases the genomic viral RNA ③, from which the non-structural proteins (nsps) are translated and released by proteolytic cleavage ④. The replication complex of nsps and genomic RNA creates a virus-specific replication organelle where subgenomic transcription and RNA replication takes place ⑤. The subgenomic RNAs are translated and structural proteins assemble together with the genomic RNA at the ER Golgi intermediate compartment ⑥ where progeny virions bud ⑦ and exit the cell via the secretory pathway ⑧. (Source: own figure).*

1.4. The role of innate immunity and type I IFN signalling in SARS-CoV-2 infection and COVID-19 disease progression

The expression of ACE2 and TMPRSS2 principally defines the cellular susceptibility to SARS-CoV-2 entry. Both factors are found on epithelial cells of the respiratory tract (79), suggesting that these cell types are the first to encounter and induce an innate immune response upon SARS-CoV-2 exposure. Despite the protected replication in the ER-derived replication organelle, genomic and sgRNAs are exposed to the cytosolic RNA sensors MDA-5 and RIG-I. MDA-5, that favours the binding of long, partially double-stranded RNAs, was reported to mount IRF3- and NF-κB-driven type I IFN and pro-inflammatory cytokine responses in Calu-3 lung epithelial cells (80, 81), while the contribution of RIG-I to SARS-CoV-2 sensing is still under debate (81–83). In addition, membrane-bound TLRs located at the plasma membrane or the endosomal compartment, whose expression is reserved to specialized immune cell subsets have been attributed to sensing of SARS-CoV-2 infection (84–87). For example, SARS-CoV-2 RNA, isolated or packaged into virions, is a potent inducer of a TLR7/MyD88-dependent type I IFN responses in pDCs *ex vivo* (86, 88, 89).

Despite the observation of type I IFN and pro-inflammatory cytokine responses upon infection, SARS-CoV-2 encodes numerous viral proteins with reported immune antagonistic properties (90). Specifically nsp6, nsp13, ORF6 or ORF7 erase the downstream signalling cascades of PRRs by inhibiting IRF3 activity (nsp6, ORF6) or blocking STAT phosphorylation (nsp13, ORF7), thereby blunting innate immune signalling irrespective of the emitting sensor (91–93). It should be noted that the ability of SARS-CoV-2 to evade cell-intrinsic immunity or conversely the cellular ability to mount a restrictive immune response is closely linked to the quantities of the initial viral inoculum (92, 94, 95).

In vivo, SARS-CoV-2 infection triggers the secretion of IRF3/IRF7-driven type I and III IFNs, such as IFN-α2, IFN-β and IFN-λ, and NF-κB-driven pro-inflammatory cytokines, such as IL-1β, IL-6, TNF, IL-12 or IL-17, mainly at the site of acute infection, the respiratory tract (96, 97). Profiling of infection-induced cytokines in patient sera and different cell culture models revealed a dampened production of type I IFNs, but not pro-inflammatory cytokines, upon infection with SARS-CoV-2 as opposed to other respiratory viruses, such as Influenza A (98, 99) or Respiratory Syncytial Virus (100, 101), suggesting

that IRF3/IRF7-driven transcription is the prime target of SARS-CoV-2 immune antagonists (94, 96, 102). *Ex vivo*, SARS-CoV-2 displays an exceptionally high sensitivity to type I IFN-pre-treatment (92, 95) and pre-existing PRR-induced antiviral states (103, 104) in contrast to the closely related SARS-CoV, emphasizing the necessity of SARS-CoV-2 to efficiently evade type I IFN induction *in vivo* (95). In agreement with this observation, longitudinal monitoring of SARS-CoV-2-infected individuals revealed that the quality of the early type I IFN production inversely correlates with disease progression in general (94, 96, 105, 106). More precisely, patients presenting reduced type I IFN levels in the first week after symptom onset were more prone to clinical deterioration after 10 days post symptom onset, accompanied by exceeding cytokine levels, chronic inflammation and tissue damage in contrast to mild-diseased patients, for whom cytokine expression gradually decreases from 10 days post symptom onset on (94, 96, 105, 106). Consequently, inborn loss-of-function mutations or genetic variants of the *IRF7*, *OAS1*, *TLR3* or *TLR7* genes, all of which are connected to type I IFN signalling, as well as pre-existing, type I IFN-neutralizing autoantibodies have been identified as high risk factors for life-threatening COVID-19, underlining the importance of intact type I IFN signalling for SARS-CoV-2 control *in vivo* (107–112).

1.5. Research Questions

A profound understanding of virus-specific intrinsic immunity and evasion strategies is essential for the future development of novel therapeutics and treatment strategies. In the present dissertation, I will summarize and discuss the main findings of three publications that I significantly contributed to (1–3). Each of them addresses specific aspects of innate sensing and viral evasion mechanisms upon HIV-1 and SARS-CoV-2 infection.

1.5.1. A baseline cellular antiviral state is maintained by cGAS and its most frequent naturally occurring variant rs610913

The cGAS/STING signalling pathway is an essential part of the cell-intrinsic defence against invading pathogens, through sensing aberrantly-located cytosolic DNA and subsequently mounting a type I IFN response (12). Single nucleotide polymorphisms (SNPs) in genes encoding PRRs or other downstream adaptors have the potential to significantly alter an individual’s susceptibility to infection and potentially predicts disease

outcome (113, 114). Data from the “International Collaboration for the Genomics of HIV” (115) suggested that rs610913, the most frequently occurring natural variant of cGAS, nominally associates with HIV-1 acquisition *in vivo*. To date, functional studies on the rs610913-encoded proline (P) to histidine (H) substitution at position 261 in the cGAS protein are missing. Therefore, this study is the first to combine genetic, structural and functional analysis for systematic comparison of the rs610913-encoded cGAS(P261H) variant with cGAS(WT) in the context of viral infections (1).

1.5.2. Absence of cGAS-mediated type I IFN responses in HIV-1-infected CD4⁺ T-cells

The contribution of cGAS-mediated sensing for HIV-1-induced intrinsic immunity has been primarily studied in macrophages and DCs (37–39, 42). In contrast, conflicting results were obtained for cGAS/STING signalling functionality (45) and the extend of cGAS-induced innate responses in HIV-1-infected CD4⁺ T-cells (44), the primary target cells of HIV-1 infection *in vivo*. This study re-evaluates the overall intactness of the cGAS/STING cytosolic DNA-sensing pathway in human and mouse CD4⁺ T-cells and carefully characterizes cGAS’ contribution in mediating type I IFN responses upon HIV-1 infection (2).

1.5.3. Non-productive exposure of PBMCs to SARS-CoV-2 induces cell-intrinsic innate immune responses

The quality of type I IFN-induced immunity is crucial for controlling SARS-CoV-2 infection *in vivo*. Peripheral immune cells are major contributors to the cellular immune response in COVID-19 upon recruitment to the site of infection and in response to cytokines originating from the respiratory tract (105). Further, viral RNA has been reported in the peripheral blood of up to 10% of severe COVID-19 patients (116), allowing the assumption that peripheral immune cells are exposed to SARS-CoV-2 virions and RNA. The susceptibility of peripheral immune cells to SARS-CoV-2 infection and their ability to respond to SARS-CoV-2 exposure, however, remains understudied. Here, we provide a comprehensive analysis on the susceptibility and cellular immune response of peripheral blood mononuclear cells (PBMCs) upon *ex vivo* SARS-CoV and SARS-CoV-2 inoculation (3).

2. Methods

This section describes the key methodology and experimental models used to obtain the main findings of the three presented studies. A detailed description of the methods including equipment, materials and reagents used to generate and analyse the data, can be found in the designated publications (1–3).

2.1. Cell culture-based assays and experiments

2.1.1. Cell culture and primary cell models

Different immortalized cell lines, such as Calu-3, HEK293T, Jurkat, PM1, THP-1 and Vero E6 cells were used to generate virus stocks and analyse cellular immunity upon virus exposure and infection (*2.1.2*) or *ex vivo* stimulation (*2.1.3*). HEK293T cells were used to generate VSV-G-pseudotyped lentiviral particles upon transient transfection which were concentrated by ultracentrifugation from virus-containing supernatants through a sucrose cushion and subjected to two rounds of DNase I treatments in order to degrade excessive plasmid DNAs. PM1 cells were used to propagate HIV-1_{BaL} (117) by several rounds of passaging and collection of the virus-containing supernatant. SARS-CoV and SARS-CoV-2 stocks were grown on Vero E6 cells and subsequently concentrated using size-exclusion columns. Among other cell lines, HEK293T, PM1 and THP-1 cells were genetically modified by CRISPR/Cas9-mediated editing or lentiviral transduction to achieve genetic ablation or overexpression of specific genes, respectively.

Additionally, primary cells isolated from blood donations of healthy individuals with approval of the local ethics committee were used (Ethical review committee of Charité Berlin, votes EA4/166/19 and EA4/167/19 and University of Tübingen, votes 156-2012BO1 and 354-2012BO2). Human peripheral mononuclear cells (PBMCs) or $CD4^+$ T-cells from buffy coats were isolated by Ficoll-Hypaque centrifugation or direct negative selection, respectively. For specific experiments, PBMCs were stimulated with IL-2 (10 ng/ml) and phytohaemagglutinin (1 µg/ml) for 3-4 days to obtain $CD3^+$ T-cell cultures with typically >90% purity, the same treatment regimen was used for $CD4^+$ T-cell activation after isolation.

2.1.2. Virus exposure and infection assays

The following viruses were used: Chikungunya virus 181/25 (118), VSV-G pseudotyped HIV-1 NL4.3 Δ*Env*, Δ*Vpr* (119), VSV-G pseudotyped lentiviral vectors (120), HSV-1 Δ*UL41*N (121), HIV-1_{BaL} (117), SARS-CoV HKU-39849 (122), SARS-CoV-2 B.1 EPI_ISL_406862 (123). The indicated cells were inoculated with virus-containing supernatants for a defined amount of time before harvesting cells and supernatants for quantitative real time (RT)-PCR, immunoblotting, flow cytometry, bulk or single cell RNA sequencing and IFN release assays, respectively.

2.1.3. Ex vivo *stimulation assays*

Primary $CD4^+$ T-cells, PBMCs, PM1 and THP-1 cells were stimulated *ex vivo* using endotoxin-free plasmid DNA, cGAMP, c-di-UMP, short immuno-stimulatory DNA (ISD), Lipopolysaccharide (LPS) or poly(I:C). Stimulations were conducted by electroporation of cells with DNA, cGAMP or c-di-UMP, to deliver the reagents across plasma membranes or, in case of LPS and poly(I:C), directly added to the culture medium. Cells and supernatants were harvested at different time points post treatment start and subjected to quantitative RT-PCR, immunoblotting and IFN release assays.

2.2. Characterization of cellular and viral gene and protein expression

2.2.1. Quantitative real time PCR

Cellular and viral RNA expression were quantified using Taqman-based quantitative RT-PCR. Viral RNA from cell culture supernatants was extracted using the NucleoSpin RNA virus isolation kit (Macherey-Nagel) and total RNA from cells was extracted using the Direct-zol RNA extraction kit (Zymo Research) or RNeasy Mini Kit (Qiagen). To analyse cellular gene expression, extracted RNA was subjected to cDNA synthesis (NEB, Invitrogen) before quantification of relative mRNA levels using the Taq-Man-based PCR technology in LightCycler 480 II (Roche) or OneStep Plus (Applied Biosystems) machines. Relative mRNA levels were determined in multiplexed reactions using the $\Delta\Delta C_T$ method and *RNASEP* mRNA levels as internal control (124). To quantify SARS-

CoV and SARS-CoV-2 viral genome equivalents or sgRNAs, total RNA was directly subjected to quantitative one-step Taqman-based PCR reactions using primer pairs and probes detecting a conserved region within the E sequence of both viruses or the N sequence of SARS-CoV-2 specifically (125).

2.2.2. Flow cytometry

Flow cytometry was used to quantify the expression of cell surface markers or the percentage of infected cells in the culture. Cell surface immunostaining of cellular markers was performed using fluorochrome-labelled, specific antibodies, followed by PFA fixation and signal acquisition. Intracellular immunostaining of viral proteins was performed in PBS-washed, PFA-fixed cells using specific antibodies against viral proteins, such as p24-Capsid (HIV-1), VP5-Capsid (HSV-1) or Nucleocapsid (SARS-CoV-2), diluted in 0.1% Triton X-100/PBS. The primary antibodies were either directly fluorochrome-conjugated or stained with a fluorochrome-conjugated, species-specific secondary antibody before acquisition of the samples on the FACS Lyric or FACS Celesta (both BD) devices. Data analysis was performed using the BD Suite or FlowJo software.

2.2.3. Immunoblotting

To detect total and phosphorylated proteins, cell lysates were generated using the M-PER Mammalian Protein Extraction Reagent (Thermo Fisher Scientific), run on an SDS-PAGE, transferred onto nitrocellulose membranes using a semi-dry transfer system (Bio-Rad Laboratories) followed by blocking of the membranes in 5% BSA/PBS solutions and olver-night incubation with specific primary antibodies. For detection and quantification of the individual proteins, secondary antibodies conjugated to AlexaFluor680 or AlexaFluor800 and the Odyssey Infrared Imaging System (Both LI-COR) were used.

2.2.4. IFN reporter assay

HL116 cells that express a luciferase reporter gene under the control of an IFN-inducible 6-16 promoter (126) were incubated with culture supernatants from individual experiments or defined IFN-α2a (Roferon) dilutions and incubated for 6 hours. Following incubation, cells were PBS-washed and luciferase expression was quantified using the

Cell Culture Lysis Buffer and Luciferase Assay System (both Promega). Concentration of bioactive IFN was quantified using an IFN-α2a standard curve.

2.2.5. Bulk RNA-sequencing

Total RNA was extracted from cells using the RNeasy Mini and RNase-free DNase kit (both Qiagen) and quality was verified on an Agilent 2100 Bioanalyzer (Agilent Technologies) before proceeding with the sequencing library preparation using the TruSeq Stranded mRNA Library Prep Kit (Illumina). The generated libraries were sequenced on Illumina HiSeq4000 (2x75 base pairs, paired-end run) or Illumina NovaSeq 6000 (2x50 base pairs, paired-end run) machines with an average of 9 x 10^7 reads per RNA sample. The generated data were either analysed using Geneious Prime (Version 2020.0.4, Biomatters) or CLC Genomic Workbench (Version 12.0.3, Qiagen) by mapping the individual reads against the hg38 human reference genome and the HIV-1_{BaL} sequence (GenBank: AY713409) for (2)). Gene expression was calculated as reads per kilobase per million bases mapped (RPKM) and differentially expressed genes (DEGs) were identified by calculating the gene expression fold change and p-values by comparing two individual samples. P-values were corrected by taking false discovery rates for multiple testing into account.

2.2.6. Single cell RNA-sequencing

Single cell RNA-Sequencing experiments of *ex vivo* SARS-CoV-, SARS-CoV-2- or mock-exposed PBMCs, as described in (3), were performed using the 10x Genomics platform and the Chromium Next GEM Single Cell 3' Reagent Kits (Version 3.1) following the manufacturer's instruction. Briefly, single cell suspensions were subjected to a microfluidic device that creates single vesicles within an oil emulsion, also called Gel Beads in Emulsion (GEMs), each containing a single cell, reagents for the reverse transcription reaction and a gel bead decorated with barcoded, poly-T-tailed oligonucleotides. Following GEM generation, the cells within the individual GEM reaction vesicle were lysed and the barcoded oligonucleotides caught polyadenylated cellular and viral transcripts via the poly-T tail to initiate reverse transcription and generation of the complementary DNA (cDNA) molecules. Importantly, besides the genetic information, the newly synthesized cDNA contained a 16 nucleotide, bead-specific barcode and a 20

nucleotide, molecule-specific unique molecular identifier (UMI), to eventually assign transcripts originating from the same cell and eliminate PCR duplicates in the bioinformatic analysis, respectively. After completion of the RT reaction, GEMs were dissolved and the released cDNAs were pooled and subjected to bulk amplification and library construction followed by sequencing using HiSeq4000 to achieve ~ 20.000 reads per cell. The generated data were processed and analysed using the Cell Ranger pipeline (Version 3.1.0 10x Genomics) and the Seurat package (Version 3.1.4, (127)) in R (Version 3.6), which includes the mapping of reads to the human and viral genomes, barcode-based assignment of sequencing reads to a specific cell, the counting of total and mitochondria-derived transcripts for dead cell exclusion as well as secondary analyses' such as dimensional reduction and cell clustering, identification of cell types based on the discriminatory marker genes and differential gene expression analysis.

3. Results

This chapter will describe the results obtained in the three studies this dissertation is based on, with an emphasis on the experiments and analysis conducted by myself as stated in the declaration (**chapter VI**). References for figures and tables in the text refer to the original publications (1–3) (**chapter VIII**).

3.1. A baseline cellular antiviral state is maintained by cGAS and its most frequent naturally occurring variant rs610913

3.1.1. cGAS WT and P261H maintain a baseline antiviral state in vitro

In this publication, we investigate the functional consequences of the most frequent naturally occurring variant in the cGAS-encoding gene *MB21D1*, rs610913, harbouring an allele frequency >0.5 (1). First, the structural consequences of the rs610913-encoded proline-to-histidine substitution at position 261 were assessed using structural modelling. The H261 residue is located at the head-to-head interface between two cGAS monomers bound to a DNA molecule in a ladder-like assembly (**Fig. 2** in (1)). Another H261 residue from the neighbouring cGAS molecule is located in close proximity and together the two histidines create a positively charged surface, predestined for the creation of an additional co-factor binding site.

Next, the functional consequences of cGAS(P261H) were assessed in THP-1 cGAS KO cells reconstituted with individual cGAS variants each fused to a GFP reporter (**Fig. 3** in (1)). As a negative control, the catalytically inactive cGAS(G212A/S213A) variant was introduced (128). Expression of the essential cGAS-signalling pathway components STING, IRF3 and TREX1 was not affected upon introduction of different cGAS variants. In contrast, steady-state mRNA levels of the ISG *IFIT1*, and to a minor extend also *MX2* and *IFNB1*, significantly increased upon re-introduction of cGAS(WT) and cGAS(P261H), but not cGAS(G212A/S213A). To reveal the extent of cGAS-induced gene expression under steady-state conditions, bulk sequencing of RNAs isolated from THP-1 cells expressing the individual cGAS variants was performed (**Fig. 4**, **Sup. Fig. 1** in (1)). Comparison of the global transcriptomes of cGAS(WT)- and cGAS(P261H)-expressing

cells showed only little heterogeneity, but revealed 38 and 29 genes to be moderately increased and decreased in cGAS(WT) compared to cGAS(P261H) samples, respectively. Re-probing of the ten most differentially expressed genes by RT-Q-PCR, however, confirmed only TCP-1 to be expressed to higher levels in cGAS(P261H)- compared to cGAS(WT)-expressing cells.

The transcriptomic differences between cells harbouring active cGAS variants compared to the catalytically inactive cGAS(G212A/S213A) were more pronounced (**Fig. 4** in (1)). To elaborate further, cGAS(WT)- and cGAS(P261H)-expressing cells compared to cells expressing the inactive cGAS variant exhibited elevated expression of *IFI44L*, *IFI27*, *MX1*, *IFI6* and multiple other ISGs culminating in the enrichment of “type I IFN signalling” and “immune response to virus” gene sets. The induction of this baseline antiviral state was identified as the major attribute following the functional cGAS expression in THP-1 cells that might result from constant, low-level cGAS-mediated sensing of endogenous ligands (129). Importantly, the cGAS-maintained, baseline antiviral state was equally pronounced in cGAS(WT) and cGAS(P261H) samples.

3.1.2. Steady-state cGAS activity renders cells refractory to virus infection

As previously reported, rs610913 may be enriched in HIV-1-positive individuals as compared to healthy control groups (115), suggesting that cGAS(P261H) might facilitate HIV-1-acquisition *in vivo*. To test this hypothesis, THP-1 cells were inoculated with VSV-G-pseudotyped lentiviral vectors or HIV-1 NL4-3 for 72 hours before quantification of infection levels by luciferase reporter assays (**Fig. 5** in (1)). Both catalytically active cGAS variants, cGAS(WT) and cGAS(P261H), significantly decreased the cellular susceptibility to lentiviral transduction and HIV-1 infection as opposed to cells devoid of functional cGAS expression. Of note, no differential susceptibility was observed comparing cells expressing cGAS(WT) and cGAS(P261H). To verify if the increased resistance of cGAS-expressing cells originates from cGAS-mediated DNA sensing of the reverse transcribed viral DNAs, *IFIT1*, *MX2* and *IFNB1* mRNA levels and the secretion of bioactive IFNs in the culture supernatants were quantified upon transduction. Despite transient fluctuations of *IFIT1* mRNA expression, no cGAS-dependent type I IFN response was detectable upon lentiviral transduction. In parallel, the experiments were conducted in cultures supplemented with the RT inhibitor efavirenz (EFV) that prevents the generation of viral

RT DNAs, but yielded the same ISG mRNA expression dynamic. These data demonstrate that, cGAS expression might protect cells from lentiviral transduction through the maintenance of the pre-existing antiviral state, rather than the induction of type I IFN responses upon sensing of viral DNAs upon infection. To test the antiviral breadth of cGAS, cGAS/STING-expressing HEK293T cells were infected with HSV-1 and Chikungunya virus, a prototypic DNA and RNA virus, respectively (**Fig. 6**, **Sup. Fig. 2** in (1)). The expression of cGAS(WT) or cGAS(P261H), but not cGAS(G212A/S213A) provided a partial protection against both HSV-1 and Chikungunya virus infections, further supporting the hypothesis that both cGAS(WT) and cGAS(P261H) are equally capable of restricting diverse viruses through the maintenance of an antiviral state even prior to infection.

3.1.3. cGAS WT and cGAS P261H share intact DNA-sensing ability

Despite equal restrictive potential, cGAS(WT) and cGAS(P261H) might exert different DNA-sensing and STING/TBK1/IRF3-signalling abilities. Therefore, cGAS-expressing THP-1 cells were challenged with endotoxin-free plasmid DNAs or cGAMP, the product of catalytically active cGAS. Mock-electroporation or electroporation of c-di-UMP, a non-stimulating cyclic di-nucleotide, were used as negative controls (**Fig. 7** in (1)). The culture supernatants from cGAS(WT)- and cGAS(P261H)-expressing cells contained equal levels of bioactive IFNs after plasmid DNA challenge, as opposed to samples derived from cells lacking cGAS activity whose IFN levels did not exceed those in mock-treated cultures. As expected, cGAMP challenge triggered cGAS-independent IFN production in all cell lines. Furthermore, cGAS-induced signal transduction was monitored by quantification of phosphorylated STING, TBK1 and IRF3 as an indicator of their activation. Phosphorylation of STING, TBK1 and IRF3 occurred 0.5 and 1 hours post DNA electroporation, respectively, but did not reveal quantitative differences between cGAS(WT)- and cGAS(P261H)-expressing cells. Next, the effect of different DNA lengths and quantities on cGAS-dependent immunity was investigated by titration of plasmid DNAs and shorter 18-, 45- and 70-bp long dsDNA fragments. Notably, *IFIT1* mRNA levels, but not IFN production, was slightly impaired in cGAS(P261H)- compared to cGAS(WT)-expressing cells upon electroporation with suboptimal plasmid DNA quantities. In contrast, no difference in the magnitude of *IFIT1* mRNA induction upon challenge with short dsDNA fragments was observed (**Sup. Fig. 3** in (1)). To conclude

the functional studies on cGAS(WT) and cGAS(P261H), we aimed at validating cGAS' ability to sense DNA in the context of endogenous expression. To this end, blood samples obtained from healthy donors were genotyped for homozygous expression of rs610913 or the WT allele, followed by PBMC isolation and analysis of baseline and LPS-, poly(I:C)- or plasmid DNA-induced *IFIT1* mRNA expression (**Fig. 8** in (1)). Base line *IFIT1* mRNA expression was equally distributed among the two groups, in line with the previously obtained data. LPS and poly(I:C) stimulations thus tended towards higher *IFIT1* expression in the rs610913-carrying PBMCs compared to the WT-allele-carrying PBMCs, a trend that was reverted upon plasmid DNA stimulation, however, none of the results reached statistical significance.

3.2. Absence of cGAS-mediated type I IFN responses in HIV-1-infected T-cells

3.2.1. Probing the functionality of cGAS/STING signalling in CD4⁺ T-cells

In this publication, the functionality and efficiency of the cGAS/STING DNA-sensing pathway in the context of HIV-1-infections was investigated in different $CD4^+$ T-cell models of human and mouse origin (2). Activated $CD4^+$ T-cells from healthy human donors and wild-type mice expressed detectable level of cGAS, STING and TREX1 (**Fig. 1** in (2)). A first notable observation was that T-cells derived from cGAS or TREX1 KO mice exhibited a decreased or increased baseline expression of the ISGs *Ifit1* and *Mx2*, respectively. To probe the integrity of the cGAS/STING signalling pathway, IL-2/PHA-activated $CD4^+$ T-cells were electroporated with endotoxin-free plasmid DNAs, short DNA fragments or cGAMP, the product of catalytically active cGAS that binds to and activates downstream STING signalling. Human $CD4^+$ T-cells responded to both plasmid DNA and cGAMP stimulation with an increased *IFIT1* mRNA expression and the production of bioactive IFNs. Parallel experiments in murine $CD4^+$ T-cells isolated from WT and cGAS KO animals revealed a completely ablated *Ifit1* mRNA induction in cGAS-deficient cells in contrast to cells derived from WT animals, following DNA challenge. As expected, cells derived from WT- and cGAS KO-animals equally responded to cGAMP stimulation with *Ifit1* mRNA induction and type I IFN secretion.

Additionally, analysis of the cGAS/STING pathway was extended to T-cell lines of human and mouse origin. Surprisingly, we observed a high degree of variability in endogenous cGAS expression levels that largely overlapped with the individual cell lines' ability to respond to plasmid DNA challenge (**Fig. 4, 6, Sup. Fig. S5, S7** in (2)). More precisely, the human Jurkat, SupT1 and CEM T-cell lines presented low to undetectable endogenous cGAS quantities and only moderately induced *IFIT1* mRNA levels following plasmid DNA stimulation, in contrast to PM1 cells that exhibited reasonable cGAS expression and a strong *IFIT1* mRNA upregulation upon DNA stimulation. A similar observation was made for the murine YAC-1 T-cell line which together with the human PM1 cells were selected for further experimental investigations. Importantly, CRISPR/Cas9-mediated KO of cGAS in both cell lines eliminated the *IFIT1* mRNA induction following plasmid DNA, but not cGAMP challenge, highlighting a strong cGAS-dependency for DNA-mediated innate immune responses in both PM1 and YAC-1 cells.

3.2.2. Absence of a type I IFN response in HIV-1-infected CD4⁺ T-cells

To interrogate the relevance of DNA-sensing in CD4⁺ T-cells upon HIV-1 *de novo* infection, primary human CD4⁺ T-cells were infected with the R5-tropic HIV-1_{BaL} strain, that caused only moderate cytopathic effects and therefore allowed the long-term observation of infected cultures (**Fig. 2** in (2)). Parallel experiments were carried out in cell cultures supplemented with the RT inhibitor EFV to assign potentially observed innate immune responses to the presence of viral RT products. As a positive control for a virus that causes strong cGAS-induced innate immunity in other cell types, the HSV-1 Δ*UL41*N strain, deficient for the viral cGAS-antagonist UL41 (121), was used. Although around 20% of the CD4⁺ T-cells were HIV-1 p24-CA-positive six days post infection and viral RT products were detectable from eight hours post infection on, no EFV-sensitive *IFIT1*, *MX2* or *IFNB1* mRNA induction was observed over the course of 13 days. Of note, the destabilization of HIV-1 CA structures by PF74, a small molecule binding the HIV-1 CA and thereby perturbing uncoating (130), was previously reported to cause cGAS-mediated sensing of HIV-1-infection in monocytic cells (40, 41). Upon infection of primary CD4⁺ T-cells, PF74 treatment only yielded a moderate and not statistically significant increase in ISG mRNA levels upon HIV-1-infection (**Sup. Fig. 4** in (2)). In stark contrast, inoculation with HSV-1, induced a strong type I IFN response in the CD4⁺ T-cell cultures starting eight hours post infection and was characterized by the strong induction of *IFIT1*,

MX2 and *IFNB1* mRNA levels. The HSV-1-induced response was insensitive to treatment with the nucleoside analogue acyclovir, indicating the sensing of incoming viral genomes independent of viral replication.

In addition, RNAs isolated from HIV-1-infected $CD4^+$T-cells were subjected to transcriptomic profiling at 3, 8 and 144 hours post infection in the presence or absence of EFV (**Fig. 3** in (2)). In agreement with previous results, ISGs and IFN gene expression were not upregulated after HIV-1-infection. Strikingly, HIV-1 infection only induced 34, 10 and 78 differentially expressed genes in an EFV-sensitive manner at 3, 8 and 144 hours post infection, respectively, the majority of which was related to cell cycle progression.

3.2.3. Characterization of cGAS-dependent innate immune responses upon HIV-1-infection

To characterize the extent of cGAS-sensing in HIV-1 infection, PM1 T-cells were inoculated with replication-deficient, VSV-G-pseudotyped lentiviral vectors that lack HIV-1 accessory gene expression (**Fig. 5** in (2)). Despite the 30% transduction efficiency in parental and cGAS KO cells after 72 hours post transduction, *IFIT1* and *MX2* mRNA levels remained equally low in both cell lines over time. The absence cGAS-dependent type I IFN responses was corroborated in the murine YAC-1 parental, cGAS and TREX1 KO cells upon transduction with either lentiviral vectors of VSV-G-pseudotyped murine leukemia virus (MLV) (**Fig. 7**, **Sup. Fig. S8** in (2)). Notably, also HIV-1 harbouring the CA mutants P90A and N74A failed to induce an innate immune response in PM1 cells (**Sup. Fig. S6** in (2)). In stark contrast, HSV-1 Δ*UL41*N infection triggered a cGAS-dependent *IFIT1* and *MX2* mRNA upregulation starting from six hours post infection on in PM1 and YAC-1 cells (**Fig. 5, 7** in (2)). To test the hypothesis whether lentiviral transduction, despite absence of accessory gene expression, specifically counteracts cGAS/STING-mediated immunity, PM1 cells were transduced for 24 hours, followed by co-infection with HSV-1 Δ*UL41*N and *IFIT1* mRNA quantification at a total of 72 hours post transduction. Importantly, HSV-1 Δ*UL41*N-infected cultures, irrespective of the preceding lentiviral transduction, displayed a strong, cGAS-dependent *IFIT1* mRNA upregulation, indicative for the absence of a HIV-1-imposed block of cGAS-signalling.

3.3. Non-productive exposure of PBMCs to SARS-CoV-2 induces cell-intrinsic innate immune responses

3.3.1. PBMCs are refractory to ex vivo SARS-CoV and SARS-CoV-2 infection

In this study, the susceptibility of peripheral immune cells to SARS-CoV and SARS-CoV-2 infection and their ability to respond to viral exposure was probed using PBMCs isolated from healthy donors (3). First, the ability of SARS-related CoVs to establish a productive infection in peripheral immune cells was probed by isolating PBMCs from healthy individuals following exposure to SARS-CoV or SARS-CoV-2. Abundance of infectious particles and viral RNA in the supernatant as well as cell-associated genomic RNA and sgRNAs were monitored for up to eight days post exposure (**Fig. 1**, **Fig. EV1** in (3)). Infectious viral particles in the cell culture drastically decreased over time and became undetectable after 72 hours post exposure for both viruses, irrespective of the pre-incubation with the JAK/STAT-inhibitor ruxolitinb. In contrast, viral RNA in the culture supernatant remained stable for up to eight days post exposure. Notably, the same observation was made in cell cultures treated with the replication inhibitor remdesivir or inoculated with heat-inactivated, replication-defective SARS-CoV-2 particles, implying an unexpectedly high stability of extracellular RNA molecules derived from the virus inoculum rather than replenishing viral RNAs derived from *de novo* production. To assess whether, PBMCs nevertheless support SARS-CoV or SARS-CoV-2 initial replication, despite the absence of productive infection, cell-associated genomic RNAs and sgRNAs were quantified in pooled and, after two days of culture, separated adherent and suspension cell fractions. The relative levels of cell-associated viral RNA decreased over time in all cell fractions independent of ruxolitinib co-treatment. Additionally, sgRNA quantities were very low, but remained at a constant level for up to eight days post exposure, suggesting that these were sgRNA molecules derived from the inoculum rather than *de novo* intracellular sgRNA transcription.

Taken together, *ex vivo*-inoculated PBMCs are refractory to SARS-CoV or SARS-CoV-2 infection. The susceptibility to infection did not changed upon blockage of the JAK/STAT signalling pathway by ruxolitinib, suggesting the absence of an IFN-imposed block of infection and rather a lack of essential host factors to support SARS-CoV and SARS-CoV-2 infection. In agreement, mRNA and protein expression of the main entry receptor

ACE2 and the alternative entry factor NRP1 were absent in PBMC as quantified by RT-Q-PCR, immunoblotting and flow cytometry (**Fig. EV2** in (3)).

3.3.2. SARS-CoV-2, but not SARS-CoV, triggers a robust type I IFN response

To unravel the extent of cell-intrinsic innate immunity despite the absence of productive infection, *IFIT1* and *IL6* mRNA expression was monitored as an indicator of IRF3 and NF-κB transcription factor activity, respectively (131) (**Fig. 2**, **Fig. EV3** in (3)). SARS-CoV-2 exposure induced a strong, ruxolitinib-sensitive *IFIT1*, but not *IL6*, mRNA induction in both adherent and suspension PBMC fractions at 16, 24 and 48 hours post exposure. Surprisingly, SARS-CoV exposure failed to trigger significant *IFIT1* or *IL6* mRNA upregulation at any of the analysed time points. Preceding *IFNA1* and *IFNB1* mRNA expression levels displayed high donor-variability and failed to display any discrepancy between SARS-CoV- and SARS-CoV-2-exposed cultures, but cytokine quantification from culture supernatants confirmed a higher abundance of IFN-α2 and to a lower extent also the ISG products IP-10, MCP-1 and MCP-3 in SARS-CoV-2-, as opposed to SARS-CoV-inoculated cultures. Accordingly, the reporter cell-based quantification of bioactive IFNs in the supernatant over time, showed detectable amounts of IFNs starting from 24 hours post exposure on, again to a higher extent in SARS-CoV-2 compared to SARS-CoV-treated cultures. Notably, both CoVs induced detectable IFN secretion upon PBMC exposure. However, the inferior amounts of SARS-CoV-induced IFNs might not reach the necessary threshold to switch on the downstream JAK/STAT-signalling and robust ISG expression.

PBMCs are a diverse cell population. To disentangle the individual cells' contribution to the type I IFN response, scRNA-sequencing of mock-, SARS-CoV- and SARS-CoV-2 inoculated PBMCs 24 hours post exposure was performed (**Fig. 3** in (3)). The major PBMC-containing cell types, monocytes, B-cells, NK cells, $CD4^+$ and $CD8^+$ T-cells were identified based on cell-specific marker genes, the relative distribution of which was not affected by virus exposure, as monitored by flow cytometry in parallel. Differential gene expression analysis identified the majority of upregulated genes as known ISGs (defined by the interferome database), including *IFI6*, *IFI44L*, *ISG15*, *MX1*, and *OAS1*, which were found to be upregulated in all cell types upon SARS-CoV-2, but not SARS-CoV exposure (**Fig. 4** in (3)). Assignment of an IFN module score that accounts for the expression levels

of numerous ISGs, identified monocytes as the strongest contributor to SARS-CoV-2-specific type I IFN responses. Importantly, combining IFN module scores with a pseudotime analysis, which is used to order cells based on their progression towards a dynamic cellular response, revealed that SARS-CoV-2-triggered ISG signatures are the major driver for cellular heterogeneity in the overall culture, but most pronounced in monocytes. In line with the existing data, pro-inflammatory cytokines, such as *IL6*, *IL1B*, *CCL8* and *TNF*, were not upregulated after SARS-CoV- or SARS-CoV-2 inoculation. Together, SARS-CoV-2, but not SARS-CoV, provokes a type I IFN-derived, antiviral ISG expression profile in PBMCs that is most pronounced in monocytes.

3.3.3. SARS-CoV and SARS-CoV-2-specific RNAs associated with monocytes

In addition to cellular transcripts, we were able to retrieve virus-specific reads potentially originating from the poly-adenylated genomic and sgRNAs of cell-attached or internalized viral particles (**Fig. 5** in (3)). As a result from poly-A-based catching, the majority of viral reads located to the 3'part of the viral genome, harbouring the 3'UTR and N sequences. In SARS-CoV- and SARS-CoV-2-inoculated cultures, 2.13% and 2.88% of all cells were identified positive for viral RNAs, respectively, the majority of which were monocytes. Although differential gene expression analysis yielded no significantly dysregulated genes, SARS-CoV-2-RNA-positive monocytes tended towards a higher expression of genes with profibrotic functions, such as *CD163*, *LGMN*, *THBS1* or *FN*, and marginally lower quantities of ISGs, such as *ISG15*, *IFITM3*, *LY6E* or *IFI27* as compared to viral-RNA-negative monocytes from the same culture. Intriguingly, this notion was confirmed by a statistically significant decreased IFN module score in SARS-CoV-2-RNA-positive monocytes as opposed to viral RNA-negative monocytes, a phenotype which was not observed in SARS-CoV-RNA-exposed cultures.

4. Discussion

4.1. A baseline cellular antiviral state is maintained by cGAS and its most frequent occurring variant rs610913

This study investigated the structural and functional consequences of the proline-to-histidine substitution at position 261 in the cGAS protein that is encoded in the most-frequently occurring natural cGAS variant rs610913 (1).

Committed to identify crucial differences between cGAS(WT) and cGAS(P261H) in response to cytosolic DNA challenge, this study highlights the important contribution of cGAS to maintain a cellular antiviral state beyond direct sensing of pathogen-derived DNA molecules. The concept of the broad antiviral activity of cGAS has been initially suggested after the discovery of cGAS-dependent RNA virus control (132) and was verified with the identification of cGAS/STING-specific evasion mechanisms in different RNA virus families (133), e.g., the targeting of cGAS and STING for degradation by Dengue virus NS2B and Hepatitis C virus NS4B proteins, respectively (134, 135). cGAS has a preference for long, double-stranded DNA (136, 137), thus the underlying mechanism for restricting RNA virus infection appears to be independent of direct viral nucleic acid sensing. Accordingly, this study reports the decreased susceptibility of cGAS-expressing cells to lentiviral transduction in the absence of HIV-1 RT product sensing (**Fig. 5** in (1)). Further, this study proposes a cGAS-dependent cellular antiviral state contributing to the restriction of virus infection in the absence of viral nucleic acid sensing. Baseline cGAS expression results in enhanced levels of ISGs, of which some harbour direct antiviral properties, such as *ISG15*, *IFIMT1* or *GBP4*, and essential components of PRR-signalling pathways, such as *IRF7*, *IRF9* or *STAT1*, in the absence of exogenous stimuli (**Fig. 3, 4** in (1)). These results are reminiscent of observations we made in murine cGAS and TREX1 KO $CD4^+$ T-cells, where baseline expression of *Ifit1* was decreased and increased in cGAS KO and TREX1 KO cells, respectively, indicating that TREX1 is responsible for preventing the over-amplification of cGAS-induced baseline immunity (2). The observation is in agreement with accumulation of cytosolic DNAs in TREX1-deficient patients, that suffer from elevated type I IFN signalling and a sterile, cGAS-dependent auto-immune disorder, defined as the *Aicardi-Goutières syndrome* (138, 139). Different sources for cytosolic DNAs underlying baseline cGAS-sensing have been identified, including tumor-derived

DNAs (140), mtDNAs leaking to the cytosol upon mitochondrial rupture and cellular stress responses or endogenous retroviral elements (129, 133). Interestingly, mtDNA leakage is also triggered upon viral infection, providing another mechanism by which cGAS initiates infection-induced antiviral immune responses without detecting viral PAMPs (12, 133).

To elucidate differential responses to DNA stimulation by cGAS(WT) and cGAS(P261H), cells were challenged with suboptimal DNA quantities or DNAs of different lengths (**Fig. 7**, **Sup. Fig. 3** in (1)). Despite the only minor differences in cGAS(WT)- compared to cGAS(P261H)-mediated responses in time course experiments and stimulations with short DNA fragments, suboptimal quantities of long plasmid DNAs triggered a slightly reduced *IFIT1* mRNA induction, but not type I IFN production. This observation, although not statistically significant, was paralleled upon plasmid DNA challenge of PBMCs derived from homozygous WT- or rs610913-carrying donors (**Fig. 8** in (1)), suggesting only a modest, if any, difference of cGAS(WT) and cGAS(P261H) DNA sensing capability. However, the cGAS signalling pathway is involved in multiple biological processes beyond antiviral responses, including autoimmunity, senescence, DNA repair and cancer immunology (12). The simplified view of cGAS as a dominant cytosolic DNA sensor has recently been challenged by reports of nuclear cGAS (141). In parallel, both canonical and non-canonical, STING-independent functions devoted to cGAS' nuclear localisation, such as sensing of nuclear HIV-1 or herpesviruses (43, 141), inhibition of DNA repair through homologous recombination (142, 143) or genome integrity maintenance and DNA replication (144) were identified. This study, however, did not investigate aspects of cGAS beyond innate immune sensing, thus the consequences of cGAS(P261H) in non-canonical cGAS pathways remains to be discovered.

Together, we propose the establishment of a pre-existing cellular state exhibiting elevated levels of antiviral ISGs and PRR-signalling components by cGAS that primes cells for a rapid control and restriction of evading pathogens. Importantly, the ability to induce a baseline antiviral state and an intact DNA-sensing capacity was shared between cGAS(WT) and its most frequent naturally occurring variant cGAS(P261H).

4.2. Absence of cGAS-mediated type I IFN responses in HIV-1-infected T-cells

This study investigated the functionality of the cGAS-mediated DNA sensing pathway in $CD4^+$ T-cells, the primary target cell for HIV-1 infection *in vivo* (2). We report that despite an intact cGAS/STING signalling axis, HIV-1 fails to trigger any type I IFN response mediated by cGAS sensing of viral RT products.

A first interesting observation was that primary $CD4^+$ T-cells derived from cGAS KO mice displayed a lower baseline expression of *Ifit1* and *Mx2* mRNA as compared to cells derived from WT animals (**Fig. 1** in (2)), in agreement with our data obtained from cGAS-overexpressing THP-1 cells (1). Further, the absence of the cellular exonuclease TREX1 enhanced baseline *Ifit1* and *Mx2* levels and allowed cells to detect short DNA fragments that are otherwise degraded by TREX1, adding weight to the notion that cGAS activity is tightly controlled by cellular factors such as TREX1 also in T-cells.

Previous studies on cGAS-sensing of HIV-1 infections were mainly conducted in HIV-1-infected macrophages or DCs that exhibit cGAS-mediated sensing of RT products under certain experimental conditions, including the absence of TREX1 (50, 51), genetic or pharmacological destabilization of the HIV-1 CAs (39–41) or co-supplementation of the HIV-2/SIV Vpx protein (37, 38, 42). Here, HIV-1-infected $CD4^+$ T-cells showed no EFV-sensitive ISG mRNA induction at either early or late time points, accounting for the possible early sensing of RT products before integration or the recognition of infection-induced cytopathic effects through cytosolic mtDNA exposure (**Fig. 2** in (2)). Further, neither the absence of TREX1 in murine $CD4^+$ T-cells nor pharmacological or genetic CA destabilization by PF74 or CA N74D and P90A mutations in human $CD4^+$ T-cells or PM1 cells, respectively, triggered an intrinsic immune response above the levels of EFV-treated cultures upon HIV-1 exposure (**Fig. 7**, **Sup. Fig. S4,S6** in (2)). One interesting future scientific question is whether cGAS sensing occurs upon CA destabilization in TREX1-deficient cells, which would suggest a more advanced role for TREX1 in degrading CA-escaping RT products in T-cells as opposed to monocytic cells. Nevertheless, these results further support the hypothesis of cell type-specific differences in the cGAS/STING signalling pathway with an emphasis on HIV-1 infection, in agreement with the identification of myeloid cell-specific cGAS interaction partners, like PQBP1 (37) and NONO (43).

Despite the vast majority of studies that were conducted in myeloid cells, the study of Vermeire and colleagues suggests cGAS-dependent sensing of HIV-1 infection in $CD4^+$ T-cells (44). There are two possible reasons for the discrepancies observed between our and their studies. First, Vermeire *et al.*, hypothesize cGAS sensing of cytosolic mtDNA whose release might be triggered by a post-integration step of HIV-1-infection (44). Indeed, cytopathic effects following the loss of mitochondria integrity and mtDNA leakage and are a well-known characteristic of HIV-1-infection (145), especially for X4-tropic viruses such as HIV-1 NL4-3 (146), which was primarily used for the conducted experiments (44). In contrast, we used the R5-tropic $HIV\text{-}1_{BaL}$ strain to circumvent massive cell death, which allowed us to monitor infected T-cell cultures for up to 13 days without detectable loss in cell viability (**Fig. 2** in (2)), thereby potentially attributing the observed cGAS activity to HIV-1 strain-specific induction of cell death. Second, $HIV\text{-}1_{BaL}$ is generated upon passaging on susceptible PM1 cells as opposed to transient transfection of proviral DNAs in producer cells. The latter protocol, e.g. used for HIV-1 NL4-3, requires extensive DNase treatment to remove excessive immuno-stimulatory plasmid DNAs attached to the virus particles and circumvent false-positive signals (40). Notably, preliminary data from our group indicate that insufficient DNase treatment results in strong cGAS-dependent *IFIT1* mRNA induction upon lentiviral transduction in PM1 cells. Additionally, virus stocks generated by transient transfection with LPS-contaminated plasmids sensitize for cGAS-mediated HIV-1 sensing (147) which is another remarkable example for the necessity to thoroughly validate reagents and virus stocks used for delicate sensing experiments.

In conclusion, this study provides a thorough understanding on the lack of HIV-1-induced intrinsic immunity in $CD4^+$ T-cells. More precisely, despite the intactness of cytosolic DNA sensing pathways, human and murine $CD4^+$ T-cells fail to detect HIV-1 RT products in a cGAS-dependent manner and do not contribute to type I IFN immunity upon HIV-1 infection, probably not through an active counteraction mechanism, but rather through a sophisticated replication strategy with minimal viral PAMP generation and exposure to respective PRRs.

4.3. Non-productive exposure of PBMCs to SARS-CoV-2 induces cell-intrinsic innate immune responses

Antiviral immunity orchestrated by different cell types and signalling pathways is essential for controlling SARS-CoV-2 infection *in vivo*. This study is the first to carefully characterize replication and resulting immune responses of the closely related, but functionally distinct SARS-CoV and SARS-CoV-2 in *ex vivo*-inoculated PBMC cultures at the single cell level (3). Although both viruses failed to establish a productive infection upon *ex vivo* challenge, SARS-CoV-2, but not SARS-CoV, exposure triggered a potent, JAK/STAT-dependent antiviral response mostly driven by monocytes.

The experimental data imply the lack of essential host factors in PBMCs that are required for SARS-CoV and SARS-CoV-2 infection. Conclusively, mRNA and protein expression of ACE2 was virtually absent in PBMCs and gene expression of NRP1 was detectable in monocytes, but cell surface protein expression was barely detectable (**Fig. EV 1** in (3)), in line with current literature (79, 148). To date a comprehensive assessment of the susceptibility of peripheral immune cells to SARS-related CoV infection is missing. In the context of SARS-CoV infection one study reported the absence of infection even upon usage of high MOIs (149) while another study documented contradictory results of productive infection of PBMCs with high inter-donor variability (150). In our study, monocytes were identified as the primary interactors with and responders to SARS-CoV-2 (**Fig. 5** in (3)). In line with our data, a recent study reports the absence of productive monocyte infection explained by the lack of ACE2 expression (151), while another report links abortive SARS-CoV-2 infection in monocytes to FcγR-mediated particle uptake of antibody-opsonized virions (152). Further, the virion-associated protein ORF7 facilitates interactions between monocytes and SARS-CoV-2 virions (153), potentially contributing to the observed interaction of specifically monocytes and SARS-CoV-2 in this study. Interestingly, pre-stimulation of PBMCs with cytokine-containing sera or virus-free supernatants from SARS-CoV-2-infected Calu-3 cells sensitized cells for viral uptake potentially as a result of monocytic activation and increased phagocytosis (**Fig. EV 5** (3)). However, the enhanced particle uptake did not result in detectable virus replication, hinting towards the existence of an additional post-entry block of SARS-CoV-2-specific replication in monocytes that manifests upon bypassing the initial viral entry (152) or the internalization of particles via a dead-end entry route. Notably, virus replication in

monocytic cells was observed before for other human CoVs, such as MERS (154) and 229E (155), however, these CoVs utilize DPP4 and CD13/APN as host entry receptors, respectively, thereby harbouring a different cell tropism and potential entry routes compared to SARS-related CoVs upon infection of monocytes.

The second major finding of our study is the ability of SARS-CoV-2, but not SARS-CoV, to initiate a potent JAK/STAT-dependent, antiviral response despite the lack of productive infection. SARS-CoV-2-induced *IFIT1* mRNA induction resisted virus heat-inactivation, suggesting the sensing of virion-associated viral PAMPs (**Appendix Fig. S2** in (3)). Recent evidence suggests that extracellular SARS-CoV-2 envelope proteins can trigger NF-κB-dependent, pro-inflammatory responses following TLR2 engagement in monocytes and macrophages, whereas conflicting results were obtained for isolated E and S proteins to be responsible for this effect (85, 87). Another study delineated the relative contribution of TLR2 and TLR7 in responding to SARS-CoV-2 exposure in DCs, showing that TLR2 initiated pro-inflammatory cytokine release in contrast to TLR7 that primarily induced type I IFN responses (86). TLR7-mediated sensing of SARS-CoV-2 genomic RNAs in the endosomal compartment triggers a MyD88-driven type I IFN response in cells of the myeloid compartment (86, 88, 89), that is reminiscent of the observed JAK/STAT-dependent type I IFN response in SARS-CoV-2-inoculated PBMCs in this study (**Fig. 2** in (3)). However, despite being closely related, SARS-CoV induced inferior levels of bioactive IFNs that failed to establish an ISG signature, potentially due to minor, yet essential, differences between SARS-CoV and SARS-CoV-2 virion immunogenicity. Intriguingly, SARS-CoV-2 RNA encodes a significantly higher amount of TLR7-stimulating GU-rich RNA sequences compared to SARS-CoV (89), providing one reasonable explanation for insufficient type I IFN responses upon SARS-CoV inoculation.

Finally, SARS-CoV-2 exposed cultures showed a striking cell-intrinsic immune response that likely arise from incomplete viral countermeasures, that typically requires both translation of early nsps and late accessory proteins in productively infected cells, to unfold its full IFN-antagonistic potential (72, 90). However, scRNA-sequencing of virus-exposed PBMC cultures disentangled cellular transcription profiles specifically in SARS-CoV-2 RNA-positive and -negative monocytes. SARS-CoV-2-RNA-positivity showed a mildly inverse correlation with cellular ISG expression when analysed at the individual ISG level, but reaching statistical significance upon averaging ISG expression within the

IFN module score (**Fig. 5** in (3)). One plausible explanation is that despite the absence of productive infection, virus-associated proteins execute their IFN-antagonistic potential upon exposure to PBMCs. Notably, the SARS-CoV-2 envelope proteins E, M and N themselves were reported to exhibit IFN-antagonistic activities (90, 156, 157) the extent of which in the absence of sufficient viral replication, however, remains elusive.

In summary, our study contributes to the understanding of SARS-CoV-2-induced immunity by defining cell-specific responses in an *ex vivo* PBMC model that is refractory to infection. The data suggest that especially monocytes contribute to the type I IFN-specific antiviral immune response upon physical interaction with SARS-CoV-2 virions despite lacking evidence for productive virus infection.

VI. References

1. Kazmierski, J., C. Elsner, K. Döhner, S. Xu, A. Ducroux, F. Pott, J. Jansen, C. W. Thorball, O. Zeymer, X. Zhou, R. Fedorov, J. Fellay, M. W. Löffler, A. N. R. Weber, B. Sodeik, and C. Goffinet. 2022. A Baseline Cellular Antiviral State Is Maintained by cGAS and Its Most Frequent Naturally Occurring Variant rs610913. *J Immunol* ji2100685.

2. Elsner, C., A. Ponnurangam, J. Kazmierski, T. Zillinger, J. Jansen, D. Todt, K. Döhner, S. Xu, A. Ducroux, N. Kriedemann, A. Malassa, P.-K. Larsen, G. Hartmann, W. Barchet, E. Steinmann, U. Kalinke, B. Sodeik, and C. Goffinet. 2020. Absence of cGAS-mediated type I IFN responses in HIV-1–infected T cells. *Proc. Natl. Acad. Sci. U.S.A.* 117: 19475–19486.

3. Kazmierski, J., K. Friedmann, D. Postmus, J. Emanuel, C. Fischer, J. Jansen, A. Richter, L. Bosquillon de Jarcy, C. Schüler, M. Sohn, S. Sauer, C. Drosten, A.-E. Saliba, L. E. Sander, M. A. Müller, D. Niemeyer, and C. Goffinet. 2022. Nonproductive exposure of PBMCs to SARS-CoV-2 induces cell-intrinsic innate immune responses. *Mol Syst Biol* 18: e10961.

4. Stetson, D. B., and R. Medzhitov. 2006. Recognition of cytosolic DNA activates an IRF3-dependent innate immune response. *Immunity* 24: 93–103.

5. Sun, L., J. Wu, F. Du, X. Chen, and Z. J. Chen. 2013. Cyclic GMP-AMP synthase is a cytosolic DNA sensor that activates the type I interferon pathway. *Science* 339: 786–791.

6. Wu, J., L. Sun, X. Chen, F. Du, H. Shi, C. Chen, and Z. J. Chen. 2013. Cyclic GMP-AMP is an endogenous second messenger in innate immune signaling by cytosolic DNA. *Science* 339: 826–830.

7. Zhang, X., H. Shi, J. Wu, X. Zhang, L. Sun, C. Chen, and Z. J. Chen. 2013. Cyclic GMP-AMP containing mixed phosphodiester linkages is an endogenous high-affinity ligand for STING. *Mol Cell* 51: 226–235.

8. Ablasser, A., M. Goldeck, T. Cavlar, T. Deimling, G. Witte, I. Röhl, K.-P. Hopfner, J. Ludwig, and V. Hornung. 2013. cGAS produces a 2’-5’-linked cyclic dinucleotide second messenger that activates STING. *Nature* 498: 380–384.

9. Diner, E. J., D. L. Burdette, S. C. Wilson, K. M. Monroe, C. A. Kellenberger, M. Hyodo, Y. Hayakawa, M. C. Hammond, and R. E. Vance. 2013. The innate immune DNA sensor cGAS produces a noncanonical cyclic dinucleotide that activates human STING. *Cell Rep* 3: 1355–1361.

10. Gao, P., M. Ascano, Y. Wu, W. Barchet, B. L. Gaffney, T. Zillinger, A. A. Serganov, Y. Liu, R. A. Jones, G. Hartmann, T. Tuschl, and D. J. Patel. 2013. Cyclic [G(2’,5’)pA(3’,5’)p] is the metazoan second messenger produced by DNA-activated cyclic GMP-AMP synthase. *Cell* 153: 1094–1107.

11. Ishikawa, H., and G. N. Barber. 2008. STING is an endoplasmic reticulum adaptor that facilitates innate immune signalling. *Nature* 455: 674–678.

12. Hopfner, K.-P., and V. Hornung. 2020. Molecular mechanisms and cellular functions of cGAS–STING signalling. *Nat Rev Mol Cell Biol* 21: 501–521.

13. Yin, X., S. Langer, Z. Zhang, K. M. Herbert, S. Yoh, R. König, and S. K. Chanda. 2020. Sensor Sensibility—HIV-1 and the Innate Immune Response. *Cells* 9: 254.

14. Kasuga, Y., B. Zhu, K.-J. Jang, and J.-S. Yoo. 2021. Innate immune sensing of coronavirus and viral evasion strategies. *Exp Mol Med* 53: 723–736.

15. Barré-Sinoussi, F., J. C. Chermann, F. Rey, M. T. Nugeyre, S. Chamaret, J. Gruest, C. Dauguet, C. Axler-Blin, F. Vézinet-Brun, C. Rouzioux, W. Rozenbaum, and L. Montagnier. 1983. Isolation of a T-lymphotropic retrovirus from a patient at risk for acquired immune deficiency syndrome (AIDS). *Science* 220: 868–871.

16. Sharp, P. M., and B. H. Hahn. 2011. Origins of HIV and the AIDS pandemic. *Cold Spring Harb Perspect Med* 1: a006841.

17. 2021 UNAIDS Global AIDS Update — Confronting inequalities — Lessons for pandemic responses from 40 years of AIDS. .

18. Deeks, S. G., J. Overbaugh, A. Phillips, and S. Buchbinder. 2015. HIV infection. *Nat Rev Dis Primers* 1: 1–22.

19. Nyamweya, S., A. Hegedus, A. Jaye, S. Rowland-Jones, K. L. Flanagan, and D. C. Macallan. 2013. Comparing HIV-1 and HIV-2 infection: Lessons for viral immunopathogenesis. *Rev Med Virol* 23: 221–240.

20. Cohn, L. B., N. Chomont, and S. G. Deeks. 2020. The Biology of the HIV-1 Latent Reservoir and Implications for Cure Strategies. *Cell Host Microbe* 27: 519–530.

21. Ma, X., M. Lu, J. Gorman, D. S. Terry, X. Hong, Z. Zhou, H. Zhao, R. B. Altman, J. Arthos, S. C. Blanchard, P. D. Kwong, J. B. Munro, and W. Mothes. 2018. HIV-1 Env trimer opens through an asymmetric intermediate in which individual protomers adopt distinct conformations. *Elife* 7: e34271.

22. Ivan, B., Z. Sun, H. Subbaraman, N. Friedrich, and A. Trkola. 2019. CD4 occupancy triggers sequential pre-fusion conformational states of the HIV-1 envelope trimer with relevance for broadly neutralizing antibody activity. *PLoS Biol* 17: e3000114.

23. Chen, B. 2019. Molecular Mechanism of HIV-1 Entry. *Trends Microbiol* 27: 878–891.

24. Burdick, R. C., C. Li, M. Munshi, J. M. O. Rawson, K. Nagashima, W.-S. Hu, and V. K. Pathak. 2020. HIV-1 uncoats in the nucleus near sites of integration. *Proceedings of the National Academy of Sciences* 117: 5486–5493.

25. Dharan, A., N. Bachmann, S. Talley, V. Zwikelmaier, and E. M. Campbell. 2020. Nuclear pore blockade reveals that HIV-1 completes reverse transcription and uncoating in the nucleus. *Nat Microbiol* 5: 1088–1095.

26. Li, C., R. C. Burdick, K. Nagashima, W.-S. Hu, and V. K. Pathak. 2021. HIV-1 cores retain their integrity until minutes before uncoating in the nucleus. *Proceedings of the National Academy of Sciences* 118: e2019467118.

27. Selyutina, A., M. Persaud, K. Lee, V. KewalRamani, and F. Diaz-Griffero. 2020. Nuclear Import of the HIV-1 Core Precedes Reverse Transcription and Uncoating. *Cell Rep* 32: 108201.

28. Ocwieja, K. E., S. Sherrill-Mix, R. Mukherjee, R. Custers-Allen, P. David, M. Brown, S. Wang, D. R. Link, J. Olson, K. Travers, E. Schadt, and F. D. Bushman. 2012. Dynamic regulation of HIV-1 mRNA populations analyzed by single-molecule enrichment and long-read sequencing. *Nucleic Acids Res* 40: 10345–10355.

29. Fang, X., J. Wang, I. P. O'Carroll, M. Mitchell, X. Zuo, Y. Wang, P. Yu, Y. Liu, J. W. Rausch, M. A. Dyba, J. Kjems, C. D. Schwieters, S. Seifert, R. E. Winans, N. R. Watts,

S. J. Stahl, P. T. Wingfield, R. A. Byrd, S. F. J. Le Grice, A. Rein, and Y.-X. Wang. 2013. An unusual topological structure of the HIV-1 Rev response element. *Cell* 155: 594–605.

30. Rein, A. 2019. RNA Packaging in HIV. *Trends Microbiol* 27: 715–723.

31. Keane, S. C., X. Heng, K. Lu, S. Kharytonchyk, V. Ramakrishnan, G. Carter, S. Barton, A. Hosic, A. Florwick, J. Santos, N. C. Bolden, S. McCowin, D. A. Case, B. Johnson, M. Salemi, A. Telesnitsky, and M. F. Summers. 2015. Structure of the HIV-1 RNA Packaging Signal. *Science* 348: 917–921.

32. Colomer-Lluch, M., A. Ruiz, A. Moris, and J. G. Prado. 2018. Restriction Factors: From Intrinsic Viral Restriction to Shaping Cellular Immunity Against HIV-1. *Front Immunol* 9: 2876.

33. Laguette, N., B. Sobhian, N. Casartelli, M. Ringeard, C. Chable-Bessia, E. Ségéral, A. Yatim, S. Emiliani, O. Schwartz, and M. Benkirane. 2011. SAMHD1 is the dendritic– and myeloid–cell–specific HIV–1 restriction factor counteracted by Vpx. *Nature* 474: 654–657.

34. Baldauf, H.-M., X. Pan, E. Erikson, S. Schmidt, W. Daddacha, M. Burggraf, K. Schenkova, I. Ambiel, G. Wabnitz, T. Gramberg, S. Panitz, E. Flory, N. R. Landau, S. Sertel, F. Rutsch, F. Lasitschka, B. Kim, R. König, O. T. Fackler, and O. T. Keppler. 2012. SAMHD1 restricts HIV-1 infection in resting CD4(+) T cells. *Nat Med* 18: 1682–1687.

35. Altfeld, M., and M. Gale. 2015. Innate immunity against HIV-1 infection. *Nat Immunol* 16: 554–562.

36. Lahaye, X., T. Satoh, M. Gentili, S. Cerboni, C. Conrad, I. Hurbain, A. El Marjou, C. Lacabaratz, J.-D. Lelièvre, and N. Manel. 2013. The Capsids of HIV-1 and HIV-2 Determine Immune Detection of the Viral cDNA by the Innate Sensor cGAS in Dendritic Cells. *Immunity* 39: 1132–1142.

37. Yoh, S. M., M. Schneider, J. Seifried, S. Soonthornvacharin, R. E. Akleh, K. C. Olivieri, P. D. De Jesus, C. Ruan, E. de Castro, P. A. Ruiz, D. Germanaud, V. des Portes, A. García-Sastre, R. König, and S. K. Chanda. 2015. PQBP1 is a Proximal Sensor of the cGAS-dependent Innate Response to HIV-1. *Cell* 161: 1293–1305.

38. Manel, N., B. Hogstad, Y. Wang, D. E. Levy, D. Unutmaz, and D. R. Littman. 2010. A cryptic sensor for HIV-1 activates antiviral innate immunity in dendritic cells. *Nature* 467: 214–217.

39. Rasaiyaah, J., C. P. Tan, A. J. Fletcher, A. J. Price, C. Blondeau, L. Hilditch, D. A. Jacques, D. L. Selwood, L. C. James, M. Noursadeghi, and G. J. Towers. 2013. HIV-1 evades innate immune recognition through specific co-factor recruitment. *Nature* 503: 402–405.

40. Sumner, R. P., L. Harrison, E. Touizer, T. P. Peacock, M. Spencer, L. Zuliani-Alvarez, and G. J. Towers. 2020. Disrupting HIV-1 capsid formation causes cGAS sensing of viral DNA. *EMBO J* 39: e103958.

41. Siddiqui, M. A., A. Saito, U. D. Halambage, D. Ferhadian, D. K. Fischer, A. C. Francis, G. B. Melikyan, Z. Ambrose, C. Aiken, and M. Yamashita. 2019. A Novel Phenotype Links HIV-1 Capsid Stability to cGAS-Mediated DNA Sensing. *J Virol* 93: e00706-19.

42. Gao, D., J. Wu, Y.-T. Wu, F. Du, C. Aroh, N. Yan, L. Sun, and Z. J. Chen. 2013. Cyclic GMP-AMP synthase is an innate immune sensor of HIV and other retroviruses. *Science* 341: 903–906.

43. Lahaye, X., M. Gentili, A. Silvin, C. Conrad, L. Picard, M. Jouve, E. Zueva, M. Maurin, F. Nadalin, G. J. Knott, B. Zhao, F. Du, M. Rio, J. Amiel, A. H. Fox, P. Li, L. Etienne, C. S. Bond, L. Colleaux, and N. Manel. 2018. NONO Detects the Nuclear HIV Capsid to Promote cGAS-Mediated Innate Immune Activation. *Cell* 175: 488-501.e22.

44. Vermeire, J., F. Roesch, D. Sauter, R. Rua, D. Hotter, A. Van Nuffel, H. Vanderstraeten, E. Naessens, V. Iannucci, A. Landi, W. Witkowski, A. Baeyens, F. Kirchhoff, and B. Verhasselt. 2016. HIV Triggers a cGAS-Dependent, Vpu- and Vpr-Regulated Type I Interferon Response in CD4+ T Cells. *Cell Rep* 17: 413–424.

45. Berg, R. K., S. H. Rahbek, E. Kofod-Olsen, C. K. Holm, J. Melchjorsen, D. G. Jensen, A. L. Hansen, L. B. Jørgensen, L. Ostergaard, M. Tolstrup, C. S. Larsen, S. R. Paludan, M. R. Jakobsen, and T. H. Mogensen. 2014. T cells detect intracellular DNA but fail to induce type I IFN responses: implications for restriction of HIV replication. *PLoS One* 9: e84513.

46. Doitsh, G., M. Cavrois, K. G. Lassen, O. Zepeda, Z. Yang, M. L. Santiago, A. M. Hebbeler, and W. C. Greene. 2010. Abortive HIV Infection Mediates CD4 T-Cell Depletion and Inflammation in Human Lymphoid Tissue. *Cell* 143: 789–801.

47. Monroe, K. M., Z. Yang, J. R. Johnson, X. Geng, G. Doitsh, N. J. Krogan, and W. C. Greene. 2014. IFI16 DNA Sensor Is Required for Death of Lymphoid CD4 T-cells Abortively Infected with HIV. *Science* 343: 428–432.

48. Muñoz-Arias, I., G. Doitsh, Z. Yang, S. Sowinski, D. Ruelas, and W. C. Greene. 2015. Blood-Derived CD4 T Cells Naturally Resist Pyroptosis During Abortive HIV-1 Infection. *Cell Host Microbe* 18: 463–470.

49. Doitsh, G., and W. C. Greene. 2016. Dissecting How CD4 T Cells Are Lost During HIV Infection. *Cell Host & Microbe* 19: 280–291.

50. Kumar, S., J. H. Morrison, D. Dingli, and E. Poeschla. 2018. HIV-1 Activation of Innate Immunity Depends Strongly on the Intracellular Level of TREX1 and Sensing of Incomplete Reverse Transcription Products. *J Virol* 92: e00001-18.

51. Yan, N., A. D. Regalado-Magdos, B. Stiggelbout, M. A. Lee-Kirsch, and J. Lieberman. 2010. The cytosolic exonuclease TREX1 inhibits the innate immune response to human immunodeficiency virus type 1. *Nat Immunol* 11: 1005–1013.

52. Ringeard, M., V. Marchand, E. Decroly, Y. Motorin, and Y. Bennasser. 2019. FTSJ3 is an RNA 2′-O-methyltransferase recruited by HIV to avoid innate immune sensing. *Nature* 565: 500–504.

53. Bruel, T., S. Dupuy, T. Démoulins, C. Rogez-Kreuz, J. Dutrieux, A. Corneau, A. Cosma, R. Cheynier, N. Dereuddre-Bosquet, R. Le Grand, and B. Vaslin. 2014. Plasmacytoid Dendritic Cell Dynamics Tune Interferon-Alfa Production in SIV-Infected Cynomolgus Macaques. *PLoS Pathog* 10: e1003915.

54. Stylianou, E., P. Aukrust, K. Bendtzen, F. Müller, and S. S. Frøland. 2000. Interferons and interferon (IFN)-inducible protein 10 during highly active anti-retroviral therapy (HAART)—possible immunosuppressive role of IFN-α in HIV infection. *Clin Exp Immunol* 119: 479–485.

55. Meier, A., G. Alter, N. Frahm, H. Sidhu, B. Li, A. Bagchi, N. Teigen, H. Streeck, H.-J. Stellbrink, J. Hellman, J. van Lunzen, and M. Altfeld. 2007. MyD88-Dependent Immune Activation Mediated by Human Immunodeficiency Virus Type 1-Encoded Toll-Like Receptor Ligands. *J Virol* 81: 8180–8191.

56. Heil, F., H. Hemmi, H. Hochrein, F. Ampenberger, C. Kirschning, S. Akira, G. Lipford, H. Wagner, and S. Bauer. 2004. Species-specific recognition of single-stranded RNA via toll-like receptor 7 and 8. *Science* 303: 1526–1529.

57. Kwa, S., S. Kannanganat, P. Nigam, M. Siddiqui, R. D. Shetty, W. Armstrong, A. Ansari, S. E. Bosinger, G. Silvestri, and R. R. Amara. 2011. Plasmacytoid dendritic cells are recruited to the colorectum and contribute to immune activation during pathogenic SIV infection in rhesus macaques. *Blood* 118: 2763–2773.

58. Parrish, N. F., F. Gao, H. Li, E. E. Giorgi, H. J. Barbian, E. H. Parrish, L. Zajic, S. S. Iyer, J. M. Decker, A. Kumar, B. Hora, A. Berg, F. Cai, J. Hopper, T. N. Denny, H. Ding, C. Ochsenbauer, J. C. Kappes, R. P. Galimidi, A. P. West, P. J. Bjorkman, C. B. Wilen, R. W. Doms, M. O'Brien, N. Bhardwaj, P. Borrow, B. F. Haynes, M. Muldoon, J. P. Theiler, B. Korber, G. M. Shaw, and B. H. Hahn. 2013. Phenotypic properties of transmitted founder HIV-1. *Proc Natl Acad Sci U S A* 110: 6626–6633.

59. Iyer, S. S., F. Bibollet-Ruche, S. Sherrill-Mix, G. H. Learn, L. Plenderleith, A. G. Smith, H. J. Barbian, R. M. Russell, M. V. P. Gondim, C. Y. Bahari, C. M. Shaw, Y. Li, T. Decker, B. F. Haynes, G. M. Shaw, P. M. Sharp, P. Borrow, and B. H. Hahn. 2017. Resistance to type 1 interferons is a major determinant of HIV-1 transmission fitness. *Proc Natl Acad Sci U S A* 114: E590–E599.

60. Kirchhoff, F. 2010. Immune Evasion and Counteraction of Restriction Factors by HIV-1 and Other Primate Lentiviruses. *Cell Host & Microbe* 8: 55–67.

61. Mitchell, J. L., H. Takata, R. Muir, D. J. Colby, E. Kroon, T. A. Crowell, C. Sacdalan, S. Pinyakorn, S. Puttamaswin, K. Benjapornpong, R. Trichavaroj, R. L. Tressler, L. Fox, V. R. Polonis, D. L. Bolton, F. Maldarelli, S. R. Lewin, E. K. Haddad, P. Phanuphak, M. L. Robb, N. L. Michael, M. de Souza, N. Phanuphak, J. Ananworanich, and L. Trautmann. 2020. Plasmacytoid dendritic cells sense HIV replication before detectable viremia following treatment interruption. *J Clin Invest* 130: 2845–2858.

62. Wang, S., Q. Zhang, H. Hui, K. Agrawal, M. A. Y. Karris, and T. M. Rana. 2020. An atlas of immune cell exhaustion in HIV-infected individuals revealed by single-cell transcriptomics. *Emerging Microbes & Infections* 9: 2333–2347.

63. Khaitan, A., and D. Unutmaz. 2011. Revisiting Immune Exhaustion During HIV Infection. *Curr HIV/AIDS Rep* 8: 4–11.

64. Dong, E., H. Du, and L. Gardner. 2020. An interactive web-based dashboard to track COVID-19 in real time. *The Lancet Infectious Diseases* 20: 533–534.

65. Osuchowski, M. F., M. S. Winkler, T. Skirecki, S. Cajander, M. Shankar-Hari, G. Lachmann, G. Monneret, F. Venet, M. Bauer, F. M. Brunkhorst, S. Weis, A. Garcia-Salido, M. Kox, J.-M. Cavaillon, F. Uhle, M. A. Weigand, S. B. Flohé, W. J. Wiersinga, R. Almansa, A. de la Fuente, I. Martin-Loeches, C. Meisel, T. Spinetti, J. C. Schefold, C. Cilloniz, A. Torres, E. J. Giamarellos-Bourboulis, R. Ferrer, M. Girardis, A. Cossarizza, M. G. Netea, T. van der Poll, J. F. Bermejo-Martín, and I. Rubio. 2021. The COVID-19 puzzle: deciphering pathophysiology and phenotypes of a new disease entity. *Lancet Respir Med* 9: 622–642.

66. Mazzoni, A., L. Salvati, L. Maggi, F. Annunziato, and L. Cosmi. 2021. Hallmarks of immune response in COVID-19: Exploring dysregulation and exhaustion. *Semin Immunol* 55: 101508.

67. Harvey, W. T., A. M. Carabelli, B. Jackson, R. K. Gupta, E. C. Thomson, E. M. Harrison, C. Ludden, R. Reeve, A. Rambaut, COVID-19 Genomics UK (COG-UK) Consortium, S. J. Peacock, and D. L. Robertson. 2021. SARS-CoV-2 variants, spike mutations and immune escape. *Nat Rev Microbiol* 19: 409–424.

68. Jung, C., D. Kmiec, L. Koepke, F. Zech, T. Jacob, K. M. J. Sparrer, and F. Kirchhoff. 2022. Omicron: What Makes the Latest SARS-CoV-2 Variant of Concern So Concerning? *J Virol* 96: e0207721.

69. Hoffmann, M., H. Kleine-Weber, S. Schroeder, N. Krüger, T. Herrler, S. Erichsen, T. S. Schiergens, G. Herrler, N.-H. Wu, A. Nitsche, M. A. Müller, C. Drosten, and S. Pöhlmann. 2020. SARS-CoV-2 Cell Entry Depends on ACE2 and TMPRSS2 and Is Blocked by a Clinically Proven Protease Inhibitor. *Cell* 181: 271-280.e8.

70. Letko, M., A. Marzi, and V. Munster. 2020. Functional assessment of cell entry and receptor usage for SARS-CoV-2 and other lineage B betacoronaviruses. *Nat Microbiol* 5: 562–569.

71. Bayati, A., R. Kumar, V. Francis, and P. S. McPherson. 2021. SARS-CoV-2 infects cells after viral entry via clathrin-mediated endocytosis. *Journal of Biological Chemistry* 296: 100306.

72. V'kovski, P., A. Kratzel, S. Steiner, H. Stalder, and V. Thiel. 2021. Coronavirus biology and replication: implications for SARS-CoV-2. *Nat Rev Microbiol* 19: 155–170.

73. Kung, Y.-A., K.-M. Lee, H.-J. Chiang, S.-Y. Huang, C.-J. Wu, and S.-R. Shih. 2022. Molecular Virology of SARS-CoV-2 and Related Coronaviruses. *Microbiol Mol Biol Rev* 86: e00026-21.

74. Hartenian, E., D. Nandakumar, A. Lari, M. Ly, J. M. Tucker, and B. A. Glaunsinger. 2020. The molecular virology of coronaviruses. *Journal of Biological Chemistry* 295: 12910–12934.

75. Schubert, K., E. D. Karousis, A. Jomaa, A. Scaiola, B. Echeverria, L.-A. Gurzeler, M. Leibundgut, V. Thiel, O. Mühlemann, and N. Ban. 2020. SARS-CoV-2 Nsp1 binds the ribosomal mRNA channel to inhibit translation. *Nat Struct Mol Biol* 27: 959–966.

76. Knoops, K., M. Kikkert, S. H. E. van den Worm, J. C. Zevenhoven-Dobbe, Y. van der Meer, A. J. Koster, A. M. Mommaas, and E. J. Snijder. 2008. SARS-Coronavirus Replication Is Supported by a Reticulovesicular Network of Modified Endoplasmic Reticulum. *PLoS Biol* 6: e226.

77. Snijder, E. J., R. W. A. L. Limpens, A. H. de Wilde, A. W. M. de Jong, J. C. Zevenhoven-Dobbe, H. J. Maier, F. F. G. A. Faas, A. J. Koster, and M. Bárcena. 2020. A unifying structural and functional model of the coronavirus replication organelle: Tracking down RNA synthesis. *PLoS Biol* 18: e3000715.

78. Sawicki, S. G., and D. L. Sawicki. 1995. Coronaviruses use discontinuous extension for synthesis of subgenome-length negative strands. *Adv Exp Med Biol* 380: 499–506.

79. Sungnak, W., N. Huang, C. Bécavin, M. Berg, R. Queen, M. Litvinukova, C. Talavera-López, H. Maatz, D. Reichart, F. Sampaziotis, K. B. Worlock, M. Yoshida, J. L. Barnes, and HCA Lung Biological Network. 2020. SARS-CoV-2 entry factors are highly expressed in nasal epithelial cells together with innate immune genes. *Nat Med* 26: 681–687.

80. Rebendenne, A., A. L. Chaves Valadão, M. Tauziet, G. Maarifi, B. Bonaventure, J. McKellar, R. Planès, S. Nisole, M. Arnaud-Arnould, O. Moncorgé, and C. Goujon. 2021.

SARS-CoV-2 Triggers an MDA-5-Dependent Interferon Response Which Is Unable To Control Replication in Lung Epithelial Cells. *J Virol* 95: e02415-20.

81. Yin, X., L. Riva, Y. Pu, L. Martin-Sancho, J. Kanamune, Y. Yamamoto, K. Sakai, S. Gotoh, L. Miorin, P. D. De Jesus, C.-C. Yang, K. M. Herbert, S. Yoh, J. F. Hultquist, A. García-Sastre, and S. K. Chanda. 2021. MDA5 Governs the Innate Immune Response to SARS-CoV-2 in Lung Epithelial Cells. *Cell Reports* 34: 108628.

82. Thorne, L. G., A. Reuschl, L. Zuliani-Alvarez, M. V. X. Whelan, J. Turner, M. Noursadeghi, C. Jolly, and G. J. Towers. 2021. SARS-CoV-2 sensing by RIG-I and MDA5 links epithelial infection to macrophage inflammation. *The EMBO Journal* 40.

83. Yamada, T., S. Sato, Y. Sotoyama, Y. Orba, H. Sawa, H. Yamauchi, M. Sasaki, and A. Takaoka. 2021. RIG-I triggers a signaling-abortive anti-SARS-CoV-2 defense in human lung cells. *Nat Immunol* 22: 820–828.

84. Fitzgerald, K. A., and J. C. Kagan. 2020. Toll-like Receptors and the Control of Immunity. *Cell* 180: 1044–1066.

85. Zheng, M., R. Karki, E. P. Williams, D. Yang, E. Fitzpatrick, P. Vogel, C. B. Jonsson, and T.-D. Kanneganti. 2021. TLR2 senses the SARS-CoV-2 envelope protein to produce inflammatory cytokines. *Nat Immunol* 22: 829–838.

86. van der Sluis, R. M., L. B. Cham, A. Gris-Oliver, K. R. Gammelgaard, J. G. Pedersen, M. Idorn, U. Ahmadov, S. S. Hernandez, E. Cémalovic, S. H. Godsk, J. Thyrsted, J. D. Gunst, S. D. Nielsen, J. J. Jørgensen, T. W. Bjerg, A. Laustsen, L. S. Reinert, D. Olagnier, R. O. Bak, M. Kjolby, C. K. Holm, M. Tolstrup, S. R. Paludan, L. S. Kristensen, O. S. Søgaard, and M. R. Jakobsen. 2022. TLR2 and TLR7 mediate distinct immunopathological and antiviral plasmacytoid dendritic cell responses to SARS-CoV-2 infection. *EMBO J* 41: e109622.

87. Khan, S., M. S. Shafiei, C. Longoria, J. W. Schoggins, R. C. Savani, and H. Zaki. 2021. SARS-CoV-2 spike protein induces inflammation via TLR2-dependent activation of the NF-κB pathway. *eLife* 10: e68563.

88. Salvi, V., H. O. Nguyen, F. Sozio, T. Schioppa, C. Gaudenzi, M. Laffranchi, P. Scapini, M. Passari, I. Barbazza, L. Tiberio, N. Tamassia, C. Garlanda, A. Del Prete, M. A. Cassatella, A. Mantovani, S. Sozzani, and D. Bosisio. 2021. SARS-CoV-2-associated ssRNAs activate inflammation and immunity via TLR7/8. *JCI Insight* 6: e150542.

89. Moreno-Eutimio, M. A., C. López-Macías, and R. Pastelin-Palacios. 2020. Bioinformatic analysis and identification of single-stranded RNA sequences recognized by TLR7/8 in the SARS-CoV-2, SARS-CoV, and MERS-CoV genomes. *Microbes Infect* 22: 226–229.

90. Lee, J.-H., L. Koepke, F. Kirchhoff, and K. M. J. Sparrer. 2022. Interferon antagonists encoded by SARS-CoV-2 at a glance. *Med Microbiol Immunol* .

91. Yuen, C.-K., J.-Y. Lam, W.-M. Wong, L.-F. Mak, X. Wang, H. Chu, J.-P. Cai, D.-Y. Jin, K. K.-W. To, J. F.-W. Chan, K.-Y. Yuen, and K.-H. Kok. 2020. SARS-CoV-2 nsp13, nsp14, nsp15 and orf6 function as potent interferon antagonists. *Emerg Microbes Infect* 9: 1418–1428.

92. Schroeder, S., F. Pott, D. Niemeyer, T. Veith, A. Richter, D. Muth, C. Goffinet, M. A. Müller, and C. Drosten. 2021. Interferon antagonism by SARS-CoV-2: a functional study using reverse genetics. *Lancet Microbe* 2: e210–e218.

93. Xia, H., Z. Cao, X. Xie, X. Zhang, J. Y.-C. Chen, H. Wang, V. D. Menachery, R. Rajsbaum, and P.-Y. Shi. 2020. Evasion of Type I Interferon by SARS-CoV-2. *Cell Rep* 33: 108234.

94. Blanco-Melo, D., B. E. Nilsson-Payant, W.-C. Liu, S. Uhl, D. Hoagland, R. Møller, T. X. Jordan, K. Oishi, M. Panis, D. Sachs, T. T. Wang, R. E. Schwartz, J. K. Lim, R. A. Albrecht, and B. R. tenOever. 2020. Imbalanced Host Response to SARS-CoV-2 Drives Development of COVID-19. *Cell* 181: 1036-1045.e9.

95. Lokugamage, K. G., A. Hage, M. de Vries, A. M. Valero-Jimenez, C. Schindewolf, M. Dittmann, R. Rajsbaum, and V. D. Menachery. 2020. Type I Interferon Susceptibility Distinguishes SARS-CoV-2 from SARS-CoV. *J Virol* 94: e01410-20.

96. Lucas, C., P. Wong, J. Klein, T. B. R. Castro, J. Silva, M. Sundaram, M. K. Ellingson, T. Mao, J. E. Oh, B. Israelow, T. Takahashi, M. Tokuyama, P. Lu, A. Venkataraman, A. Park, S. Mohanty, H. Wang, A. L. Wyllie, C. B. F. Vogels, R. Earnest, S. Lapidus, I. M. Ott, A. J. Moore, M. C. Muenker, J. B. Fournier, M. Campbell, C. D. Odio, A. Casanovas-Massana, Yale IMPACT Team, R. Herbst, A. C. Shaw, R. Medzhitov, W. L. Schulz, N. D. Grubaugh, C. Dela Cruz, S. Farhadian, A. I. Ko, S. B. Omer, and A. Iwasaki. 2020. Longitudinal analyses reveal immunological misfiring in severe COVID-19. *Nature* 584: 463–469.

97. Hadjadj, J., N. Yatim, L. Barnabei, A. Corneau, J. Boussier, N. Smith, H. Péré, B. Charbit, V. Bondet, C. Chenevier-Gobeaux, P. Breillat, N. Carlier, R. Gauzit, C. Morbieu, F. Pène, N. Marin, N. Roche, T.-A. Szwebel, S. H. Merkling, J.-M. Treluyer, D. Veyer, L. Mouthon, C. Blanc, P.-L. Tharaux, F. Rozenberg, A. Fischer, D. Duffy, F. Rieux-Laucat, S. Kernéis, and B. Terrier. 2020. Impaired type I interferon activity and inflammatory responses in severe COVID-19 patients. *Science* 369: 718–724.

98. Nguyen, T. H., J. L. McAuley, Y. Kim, M. Z. Zheng, N. A. Gherardin, D. I. Godfrey, D. F. Purcell, L. C. Sullivan, G. P. Westall, P. C. Reading, K. Kedzierska, and L. M. Wakim. 2021. Influenza, but not SARS-CoV-2, infection induces a rapid interferon response that wanes with age and diminished tissue-resident memory CD8+ T cells. *Clinical & Translational Immunology* 10: e1242.

99. Mudd, P. A., J. C. Crawford, J. S. Turner, A. Souquette, D. Reynolds, D. Bender, J. P. Bosanquet, N. J. Anand, D. A. Striker, R. S. Martin, A. C. M. Boon, S. L. House, K. E. Remy, R. S. Hotchkiss, R. M. Presti, J. A. O'Halloran, W. G. Powderly, P. G. Thomas, and A. H. Ellebedy. 2020. Distinct inflammatory profiles distinguish COVID-19 from influenza with limited contributions from cytokine storm. *Science Advances* 6: eabe3024.

100. Hasan, M. Z., S. Islam, K. Matsumoto, and T. Kawai. 2021. SARS-CoV-2 infection initiates interleukin-17-enriched transcriptional response in different cells from multiple organs. *Sci Rep* 11: 16814.

101. Rajan, A., A. M. Weaver, G. M. Aloisio, J. Jelinski, H. L. Johnson, S. F. Venable, T. McBride, L. Aideyan, F.-A. Piedra, X. Ye, E. Melicoff-Portillo, M. R. K. Yerramilli, X.-L. Zeng, M. A. Mancini, F. Stossi, A. W. Maresso, S. A. Kotkar, M. K. Estes, S. Blutt, V. Avadhanula, and P. A. Piedra. 2022. The Human Nose Organoid Respiratory Virus Model: an Ex Vivo Human Challenge Model To Study Respiratory Syncytial Virus (RSV) and Severe Acute Respiratory Syndrome Coronavirus 2 (SARS-CoV-2) Pathogenesis and Evaluate Therapeutics. *mBio* 13: e03511-21.

102. Trouillet-Assant, S., S. Viel, A. Gaymard, S. Pons, J.-C. Richard, M. Perret, M. Villard, K. Brengel-Pesce, B. Lina, M. Mezidi, L. Bitker, A. Belot, and COVID HCL Study

group. 2020. Type I IFN immunoprofiling in COVID-19 patients. *J Allergy Clin Immunol* 146: 206-208.e2.

103. Cheemarla, N. R., T. A. Watkins, V. T. Mihaylova, B. Wang, D. Zhao, G. Wang, M. L. Landry, and E. F. Foxman. 2021. Dynamic innate immune response determines susceptibility to SARS-CoV-2 infection and early replication kinetics. *Journal of Experimental Medicine* 218: e20210583.

104. Li, M., M. Ferretti, B. Ying, H. Descamps, E. Lee, M. Dittmar, J. S. Lee, K. Whig, B. Kamalia, L. Dohnalová, G. Uhr, H. Zarkoob, Y.-C. Chen, H. Ramage, M. Ferrer, K. Lynch, D. C. Schultz, C. A. Thaiss, M. S. Diamond, and S. Cherry. 2021. Pharmacological activation of STING blocks SARS-CoV-2 infection. *Sci Immunol* 6: eabi9007.

105. Schulte-Schrepping, J., N. Reusch, D. Paclik, K. Baßler, S. Schlickeiser, B. Zhang, B. Krämer, T. Krammer, S. Brumhard, L. Bonaguro, E. De Domenico, D. Wendisch, M. Grasshoff, T. S. Kapellos, M. Beckstette, T. Pecht, A. Saglam, O. Dietrich, H. E. Mei, A. R. Schulz, C. Conrad, D. Kunkel, E. Vafadarnejad, C.-J. Xu, A. Horne, M. Herbert, A. Drews, C. Thibeault, M. Pfeiffer, S. Hippenstiel, A. Hocke, H. Müller-Redetzky, K.-M. Heim, F. Machleidt, A. Uhrig, L. Bosquillon de Jarcy, L. Jürgens, M. Stegemann, C. R. Glösenkamp, H.-D. Volk, C. Goffinet, M. Landthaler, E. Wyler, P. Georg, M. Schneider, C. Dang-Heine, N. Neuwinger, K. Kappert, R. Tauber, V. Corman, J. Raabe, K. M. Kaiser, M. T. Vinh, G. Rieke, C. Meisel, T. Ulas, M. Becker, R. Geffers, M. Witzenrath, C. Drosten, N. Suttorp, C. von Kalle, F. Kurth, K. Händler, J. L. Schultze, A. C. Aschenbrenner, Y. Li, J. Nattermann, B. Sawitzki, A.-E. Saliba, and L. E. Sander. 2020. Severe COVID-19 Is Marked by a Dysregulated Myeloid Cell Compartment. *Cell* 182: 1419-1440.e23.

106. Ou, X., Y. Liu, X. Lei, P. Li, D. Mi, L. Ren, L. Guo, R. Guo, T. Chen, J. Hu, Z. Xiang, Z. Mu, X. Chen, J. Chen, K. Hu, Q. Jin, J. Wang, and Z. Qian. 2020. Characterization of spike glycoprotein of SARS-CoV-2 on virus entry and its immune cross-reactivity with SARS-CoV. *Nat Commun* 11: 1620.

107. Asano, T., B. Boisson, F. Onodi, D. Matuozzo, M. Moncada-Velez, M. R. L. Maglorius Renkilaraj, P. Zhang, L. Meertens, A. Bolze, M. Materna, et al., 2021. X-linked recessive TLR7 deficiency in ~1% of men under 60 years old with life-threatening COVID-19. *Sci. Immunol.* 6: eabl4348.

108. van der Made, C. I., A. Simons, J. Schuurs-Hoeijmakers, G. van den Heuvel, T. Mantere, S. Kersten, R. C. van Deuren, M. Steehouwer, S. V. van Reijmersdal, M. Jaeger, T. Hofste, G. Astuti, J. Corominas Galbany, V. van der Schoot, H. van der Hoeven, W. Hagmolen Of Ten Have, E. Klijn, C. van den Meer, J. Fiddelaers, Q. de Mast, C. P. Bleeker-Rovers, L. A. B. Joosten, H. G. Yntema, C. Gilissen, M. Nelen, J. W. M. van der Meer, H. G. Brunner, M. G. Netea, F. L. van de Veerdonk, and A. Hoischen. 2020. Presence of Genetic Variants Among Young Men With Severe COVID-19. *JAMA* 324: 663–673.

109. Bastard, P., A. Gervais, T. Le Voyer, J. Rosain, Q. Philippot, J. Manry, E. Michailidis, H.-H. Hoffmann, S. Eto, M. Garcia-Prat, L. Bizien, A. Parra-Martínez, R. Yang, L. Haljasmägi, M. Migaud, K. Särekannu, J. Maslovskaja, N. de Prost, Y. Tandjaoui-Lambiotte, C.-E. Luyt, B. Amador-Borrero, A. Gaudet, J. Poissy, P. Morel, P. Richard, F. Cognasse, J. Troya, S. Trouillet-Assant, A. Belot, K. Saker, P. Garçon, J. G. Rivière, J.-C. Lagier, S. Gentile, L. B. Rosen, E. Shaw, T. Morio, J. Tanaka, D. Dalmau, P.-L. Tharaux, D. Sene, A. Stepanian, B. Megarbane, V. Triantafyllia, A. Fekkar, J. R. Heath, J. L. Franco, J.-M. Anaya, J. Solé-Violán, L. Imberti, A. Biondi, P. Bonfanti, R. Castagnoli, O. M. Delmonte, Y. Zhang, A. L. Snow, S. M. Holland, C. M. Biggs, M. Moncada-Vélez,

A. A. Arias, L. Lorenzo, S. Boucherit, B. Coulibaly, D. Anglicheau, A. M. Planas, F. Haerynck, S. Duvlis, R. L. Nussbaum, T. Ozcelik, S. Keles, A. A. Bousfiha, J. El Bakkouri, C. Ramirez-Santana, S. Paul, Q. Pan-Hammarström, L. Hammarström, A. Dupont, A. Kurolap, C. N. Metz, A. Aiuti, G. Casari, V. Lampasona, F. Ciceri, L. A. Barreiros, E. Dominguez-Garrido, M. Vidigal, M. Zatz, D. van de Beek, S. Sahanic, I. Tancevski, Y. Stepanovskyy, O. Boyarchuk, Y. Nukui, M. Tsumura, L. Vidaur, S. G. Tangye, S. Burrel, D. Duffy, L. Quintana-Murci, A. Klocperk, N. Y. Kann, A. Shcherbina, Y.-L. Lau, D. Leung, M. Coulongeat, J. Marlet, R. Koning, L. F. Reyes, A. Chauvineau-Grenier, F. Venet, G. Monneret, M. C. Nussenzweig, R. Arrestier, I. Boudhabhay, H. Baris-Feldman, D. Hagin, J. Wauters, I. Meyts, A. H. Dyer, S. P. Kennelly, N. M. Bourke, R. Halwani, N. S. Sharif-Askari, K. Dorgham, J. Sallette, S. Mehlal Sedkaoui, S. AlKhater, R. Rigo-Bonnin, F. Morandeira, L. Roussel, D. C. Vinh, S. R. Ostrowski, A. Condino-Neto, C. Prando, A. Bondarenko, A. N. Spaan, L. Gilardin, J. Fellay, S. Lyonnet, K. Bilguvar, R. P. Lifton, S. Mane, HGID Lab, COVID Clinicians, COVID-STORM Clinicians, NIAID Immune Response to COVID Group, NH-COVAIR Study Group, Danish CHGE, Danish Blood Donor Study, St. James's Hospital SARS CoV2 Interest group, French COVID Cohort Study Group, Imagine COVID-Group, The Milieu Intérieur Consortium, CoV-Contact Cohort, Amsterdam UMC Covid-19 Biobank Investigators, COVID Human Genetic Effort, CONSTANCES cohort, 3C-Dijon Study, Cerba HealthCare, Etablissement du Sang study group, M. S. Anderson, B. Boisson, V. Béziat, S.-Y. Zhang, E. Andreakos, O. Hermine, A. Pujol, P. Peterson, T. H. Mogensen, L. Rowen, J. Mond, S. Debette, X. de Lamballerie, X. Duval, F. Mentré, M. Zins, P. Soler-Palacin, R. Colobran, G. Gorochov, X. Solanich, S. Susen, J. Martinez-Picado, D. Raoult, M. Vasse, P. K. Gregersen, L. Piemonti, C. Rodríguez-Gallego, L. D. Notarangelo, H. C. Su, K. Kisand, S. Okada, A. Puel, E. Jouanguy, C. M. Rice, P. Tiberghien, Q. Zhang, A. Cobat, L. Abel, and J.-L. Casanova. 2021. Autoantibodies neutralizing type I IFNs are present in ~4% of uninfected individuals over 70 years old and account for ~20% of COVID-19 deaths. *Science Immunology* 6: eabl4340.

110. Zhang, Q., P. Bastard, Z. Liu, J. Le Pen, M. Moncada-Velez, J. Chen, M. Ogishi, I. K. D. Sabli, S. Hodeib, C. Korol, J. Rosain, K. Bilguvar, J. Ye, A. Bolze, B. Bigio, R. Yang, A. A. Arias, Q. Zhou, Y. Zhang, F. Onodi, S. Korniotis, L. Karpf, Q. Philippot, M. Chbihi, L. Bonnet-Madin, K. Dorgham, N. Smith, W. M. Schneider, B. S. Razooky, H.-H. Hoffmann, E. Michailidis, L. Moens, J. E. Han, L. Lorenzo, L. Bizien, P. Meade, A.-L. Neehus, A. C. Ugurbil, A. Corneau, G. Kerner, P. Zhang, F. Rapaport, Y. Seeleuthner, J. Manry, C. Masson, Y. Schmitt, A. Schlüter, T. Le Voyer, T. Khan, J. Li, J. Fellay, L. Roussel, M. Shahrooei, M. F. Alosaimi, D. Mansouri, H. Al-Saud, F. Al-Mulla, F. Almourfi, S. Z. Al-Muhsen, F. Alsohime, S. Al Turki, R. Hasanato, D. van de Beek, A. Biondi, L. R. Bettini, M. D'Angio', P. Bonfanti, L. Imberti, A. Sottini, S. Paghera, E. Quiros-Roldan, C. Rossi, A. J. Oler, M. F. Tompkins, C. Alba, I. Vandernoot, J.-C. Goffard, G. Smits, I. Migeotte, F. Haerynck, P. Soler-Palacin, A. Martin-Nalda, R. Colobran, P.-E. Morange, S. Keles, F. Çölkesen, T. Ozcelik, K. K. Yasar, S. Senoglu, Ş. N. Karabela, C. Rodríguez-Gallego, G. Novelli, S. Hraiech, Y. Tandjaoui-Lambiotte, X. Duval, C. Laouénan, COVID-STORM Clinicians, COVID Clinicians, Imagine COVID Group, French COVID Cohort Study Group, CoV-Contact Cohort, Amsterdam UMC Covid-19 Biobank, COVID Human Genetic Effort, NIAID-USUHS/TAGC COVID Immunity Group, A. L. Snow, C. L. Dalgard, J. D. Milner, D. C. Vinh, T. H. Mogensen, N. Marr, A. N. Spaan, B. Boisson, S. Boisson-Dupuis, J. Bustamante, A. Puel, M. J. Ciancanelli, I. Meyts, T. Maniatis, V. Soumelis, A. Amara, M. Nussenzweig, A. García-Sastre, F. Krammer, A. Pujol, D. Duffy, R. P. Lifton, S.-Y. Zhang, G. Gorochov, V. Béziat, E. Jouanguy, V. Sancho-Shimizu, C. M. Rice, L.

Abel, L. D. Notarangelo, A. Cobat, H. C. Su, and J.-L. Casanova. 2020. Inborn errors of type I IFN immunity in patients with life-threatening COVID-19. *Science* 370: eabd4570.

111. Bastard, P., L. B. Rosen, Q. Zhang, E. Michailidis, H.-H. Hoffmann, Y. Zhang, K. Dorgham, Q. Philippot, J. Rosain, V. Béziat, J. Manry, E. Shaw, L. Haljasmägi, P. Peterson, L. Lorenzo, L. Bizien, S. Trouillet-Assant, K. Dobbs, A. A. de Jesus, A. Belot, A. Kallaste, E. Catherinot, Y. Tandjaoui-Lambiotte, J. Le Pen, G. Kerner, B. Bigio, Y. Seeleuthner, R. Yang, A. Bolze, A. N. Spaan, O. M. Delmonte, M. S. Abers, A. Aiuti, G. Casari, V. Lampasona, L. Piemonti, F. Ciceri, K. Bilguvar, R. P. Lifton, M. Vasse, D. M. Smadja, M. Migaud, J. Hadjadj, B. Terrier, D. Duffy, L. Quintana-Murci, D. van de Beek, L. Roussel, D. C. Vinh, S. G. Tangye, F. Haerynck, D. Dalmau, J. Martinez-Picado, P. Brodin, M. C. Nussenzweig, S. Boisson-Dupuis, C. Rodríguez-Gallego, G. Vogt, T. H. Mogensen, A. J. Oler, J. Gu, P. D. Burbelo, J. I. Cohen, A. Biondi, L. R. Bettini, M. D'Angio, P. Bonfanti, P. Rossignol, J. Mayaux, F. Rieux-Laucat, E. S. Husebye, F. Fusco, M. V. Ursini, L. Imberti, A. Sottini, S. Paghera, E. Quiros-Roldan, C. Rossi, R. Castagnoli, D. Montagna, A. Licari, G. L. Marseglia, X. Duval, J. Ghosn, HGID Lab, NIAID-USUHS Immune Response to COVID Group, COVID Clinicians, COVID-STORM Clinicians, Imagine COVID Group, French COVID Cohort Study Group, Milieu Intérieur Consortium, CoV-Contact Cohort, Amsterdam UMC Covid-19 Biobank, COVID Human Genetic Effort, J. S. Tsang, R. Goldbach-Mansky, K. Kisand, M. S. Lionakis, A. Puel, S.-Y. Zhang, S. M. Holland, G. Gorochov, E. Jouanguy, C. M. Rice, A. Cobat, L. D. Notarangelo, L. Abel, H. C. Su, and J.-L. Casanova. 2020. Autoantibodies against type I IFNs in patients with life-threatening COVID-19. *Science* 370: eabd4585.

112. Banday, A. R., M. L. Stanifer, O. Florez-Vargas, O. O. Onabajo, B. W. Papenberg, M. A. Zahoor, L. Mirabello, T. J. Ring, C.-H. Lee, P. S. Albert, E. Andreakos, E. Arons, G. Barsh, L. G. Biesecker, D. L. Boyle, M. S. Brahier, A. Burnett-Hartman, M. Carrington, E. Chang, P. G. Choe, R. L. Chisholm, L. M. Colli, C. L. Dalgard, C. M. Dude, J. Edberg, N. Erdmann, H. S. Feigelson, B. A. Fonseca, G. S. Firestein, A. J. Gehring, C. Guo, M. Ho, S. Holland, A. A. Hutchinson, H. Im, L. Irby, M. G. Ison, N. T. Joseph, H. B. Kim, R. J. Kreitman, B. R. Korf, S. M. Lipkin, S. M. Mahgoub, I. Mohammed, G. L. Paschoalini, J. A. Pacheco, M. J. Peluso, D. J. Rader, D. T. Redden, M. D. Ritchie, B. Rosenblum, M. E. Ross, H. P. S. Anna, S. A. Savage, S. Sharma, E. Siouti, A. K. Smith, V. Triantafyllia, J. M. Vargas, J. D. Vargas, A. Verma, V. Vij, D. R. Wesemann, M. Yeager, X. Yu, Y. Zhang, S. Boulant, S. J. Chanock, J. J. Feld, and L. Prokunina-Olsson. 2022. Genetic regulation of OAS1 nonsense-mediated decay underlies association with COVID-19 hospitalization in patients of European and African ancestries. *Nat Genet* 1–14.

113. Jin, L., L.-G. Xu, I. V. Yang, E. J. Davidson, D. A. Schwartz, M. M. Wurfel, and J. C. Cambier. 2011. Identification and characterization of a loss-of-function human MPYS variant. *Genes Immun* 12: 263–269.

114. Patel, S., S. M. Blaauboer, H. R. Tucker, S. Mansouri, J. S. Ruiz-Moreno, L. Hamann, R. R. Schumann, B. Opitz, and L. Jin. 2017. The Common R71H-G230A-R293Q Human TMEM173 Is a Null Allele. *J Immunol* 198: 776–787.

115. McLaren, P. J., C. Coulonges, S. Ripke, L. van den Berg, S. Buchbinder, M. Carrington, A. Cossarizza, J. Dalmau, S. G. Deeks, O. Delaneau, A. De Luca, J. J. Goedert, D. Haas, J. T. Herbeck, S. Kathiresan, G. D. Kirk, O. Lambotte, M. Luo, S. Mallal, D. van Manen, J. Martinez-Picado, L. Meyer, J. M. Miro, J. I. Mullins, N. Obel, S. J. O'Brien, F. Pereyra, F. A. Plummer, G. Poli, Y. Qi, P. Rucart, M. S. Sandhu, P. R. Shea, H. Schuitemaker, I. Theodorou, F. Vannberg, J. Veldink, B. D. Walker, A. Weintrob, C. A. Winkler, S. Wolinsky, A. Telenti, D. B. Goldstein, P. I. W. de Bakker, J.-F. Zagury, and J.

Fellay. 2013. Association study of common genetic variants and HIV-1 acquisition in 6,300 infected cases and 7,200 controls. *PLoS Pathog* 9: e1003515.

116. Prebensen, C., P. L. Myhre, C. Jonassen, A. Rangberg, A. Blomfeldt, M. Svensson, T. Omland, and J.-E. Berdal. 2021. Severe Acute Respiratory Syndrome Coronavirus 2 RNA in Plasma Is Associated With Intensive Care Unit Admission and Mortality in Patients Hospitalized With Coronavirus Disease 2019. *Clin Infect Dis* 73: e799–e802.

117. Popovic, M., S. Gartner, E. Read-Connole, B. Beaver, and M. Reitz. 1989. Retroviruses of human AIDS and related animal diseases. *France: Pasteur Vaccins: Marnes-La-Coquette* 219.

118. Levitt, N. H., H. H. Ramsburg, S. E. Hasty, P. M. Repik, F. E. Cole, and H. W. Lupton. 1986. Development of an attenuated strain of chikungunya virus for use in vaccine production. *Vaccine* 4: 157–162.

119. Connor, R. I., B. K. Chen, S. Choe, and N. R. Landau. 1995. Vpr is required for efficient replication of human immunodeficiency virus type-1 in mononuclear phagocytes. *Virology* 206: 935–944.

120. Zufferey, R., D. Nagy, R. J. Mandel, L. Naldini, and D. Trono. 1997. Multiply attenuated lentiviral vector achieves efficient gene delivery in vivo. *Nat Biotechnol* 15: 871–875.

121. Strelow, L. I., and D. A. Leib. 1995. Role of the virion host shutoff (vhs) of herpes simplex virus type 1 in latency and pathogenesis. *J Virol* 69: 6779–6786.

122. Zeng, F. Y., C. W. M. Chan, M. N. Chan, J. D. Chen, K. Y. C. Chow, C. C. Hon, K. H. Hui, J. Li, V. Y. Y. Li, C. Y. Wang, P. Y. Wang, Y. Guan, B. Zheng, L. L. M. Poon, K. H. Chan, K. Y. Yuen, J. S. M. Peiris, and F. C. Leung. 2003. The Complete Genome Sequence of Severe Acute Respiratory Syndrome Coronavirus Strain HKU-39849 (HK-39). *Exp Biol Med (Maywood)* 228: 866–873.

123. Wölfel, R., V. M. Corman, W. Guggemos, M. Seilmaier, S. Zange, M. A. Müller, D. Niemeyer, T. C. Jones, P. Vollmar, C. Rothe, M. Hoelscher, T. Bleicker, S. Brünink, J. Schneider, R. Ehmann, K. Zwirglmaier, C. Drosten, and C. Wendtner. 2020. Virological assessment of hospitalized patients with COVID-2019. *Nature* 581: 465–469.

124. Livak, K. J., and T. D. Schmittgen. 2001. Analysis of relative gene expression data using real-time quantitative PCR and the 2(-Delta Delta C(T)) Method. *Methods* 25: 402–408.

125. Corman, V. M., O. Landt, M. Kaiser, R. Molenkamp, A. Meijer, D. K. Chu, T. Bleicker, S. Brünink, J. Schneider, M. L. Schmidt, D. G. Mulders, B. L. Haagmans, B. van der Veer, S. van den Brink, L. Wijsman, G. Goderski, J.-L. Romette, J. Ellis, M. Zambon, M. Peiris, H. Goossens, C. Reusken, M. P. Koopmans, and C. Drosten. 2020. Detection of 2019 novel coronavirus (2019-nCoV) by real-time RT-PCR. *Eurosurveillance* 25.

126. Uzé, G., S. Di Marco, E. Mouchel-Vielh, D. Monneron, M. T. Bandu, M. A. Horisberger, A. Dorques, G. Lutfalla, and K. E. Mogensen. 1994. Domains of interaction between alpha interferon and its receptor components. *J Mol Biol* 243: 245–257.

127. Butler, A., P. Hoffman, P. Smibert, E. Papalexi, and R. Satija. 2018. Integrating single-cell transcriptomic data across different conditions, technologies, and species. *Nat Biotechnol* 36: 411–420.

128. Civril, F., T. Deimling, C. C. de Oliveira Mann, A. Ablasser, M. Moldt, G. Witte, V. Hornung, and K.-P. Hopfner. 2013. Structural mechanism of cytosolic DNA sensing by cGAS. *Nature* 498: 332–337.

129. West, A. P., W. Khoury-Hanold, M. Staron, M. C. Tal, C. M. Pineda, S. M. Lang, M. Bestwick, B. A. Duguay, N. Raimundo, D. A. MacDuff, S. M. Kaech, J. R. Smiley, R. E. Means, A. Iwasaki, and G. S. Shadel. 2015. Mitochondrial DNA stress primes the antiviral innate immune response. *Nature* 520: 553–557.

130. Shi, J., J. Zhou, V. B. Shah, C. Aiken, and K. Whitby. 2011. Small-molecule inhibition of human immunodeficiency virus type 1 infection by virus capsid destabilization. *J Virol* 85: 542–549.

131. Honda, K., and T. Taniguchi. 2006. IRFs: master regulators of signalling by Toll-like receptors and cytosolic pattern-recognition receptors. *Nat Rev Immunol* 6: 644–658.

132. Schoggins, J. W., D. A. MacDuff, N. Imanaka, M. D. Gainey, B. Shrestha, J. L. Eitson, K. B. Mar, R. B. Richardson, A. V. Ratushny, V. Litvak, R. Dabelic, B. Manicassamy, J. D. Aitchison, A. Aderem, R. M. Elliott, A. García-Sastre, V. Racaniello, E. J. Snijder, W. M. Yokoyama, M. S. Diamond, H. W. Virgin, and C. M. Rice. 2014. Pan-viral specificity of IFN-induced genes reveals new roles for cGAS in innate immunity. *Nature* 505: 691–695.

133. Webb, L. G., and A. Fernandez-Sesma. 2022. RNA viruses and the cGAS-STING pathway: reframing our understanding of innate immune sensing. *Curr Opin Virol* 53: 101206.

134. Aguirre, S., P. Luthra, M. T. Sanchez-Aparicio, A. M. Maestre, J. Patel, F. Lamothe, A. C. Fredericks, S. Tripathi, T. Zhu, J. Pintado-Silva, L. G. Webb, D. Bernal-Rubio, A. Solovyov, B. Greenbaum, V. Simon, C. F. Basler, L. C. F. Mulder, A. García-Sastre, and A. Fernandez-Sesma. 2017. Dengue virus NS2B protein targets cGAS for degradation and prevents mitochondrial DNA sensing during infection. *Nat Microbiol* 2: 17037.

135. Nitta, S., N. Sakamoto, M. Nakagawa, S. Kakinuma, K. Mishima, A. Kusano-Kitazume, K. Kiyohashi, M. Murakawa, Y. Nishimura-Sakurai, S. Azuma, M. Tasaka-Fujita, Y. Asahina, M. Yoneyama, T. Fujita, and M. Watanabe. 2013. Hepatitis C virus NS4B protein targets STING and abrogates RIG-I-mediated type I interferon-dependent innate immunity. *Hepatology* 57: 46–58.

136. Luecke, S., A. Holleufer, M. H. Christensen, K. L. Jønsson, G. A. Boni, L. K. Sørensen, M. Johannsen, M. R. Jakobsen, R. Hartmann, and S. R. Paludan. 2017. cGAS is activated by DNA in a length-dependent manner. *EMBO Rep* 18: 1707–1715.

137. Andreeva, L., B. Hiller, D. Kostrewa, C. Lässig, C. C. de Oliveira Mann, D. Jan Drexler, A. Maiser, M. Gaidt, H. Leonhardt, V. Hornung, and K.-P. Hopfner. 2017. cGAS senses long and HMGB/TFAM-bound U-turn DNA by forming protein-DNA ladders. *Nature* 549: 394–398.

138. Stetson, D. B., J. S. Ko, T. Heidmann, and R. Medzhitov. 2008. Trex1 prevents cell-intrinsic initiation of autoimmunity. *Cell* 134: 587–598.

139. Crow, Y. J., B. E. Hayward, R. Parmar, P. Robins, A. Leitch, M. Ali, D. N. Black, H. van Bokhoven, H. G. Brunner, B. C. Hamel, P. C. Corry, F. M. Cowan, S. G. Frints, J. Klepper, J. H. Livingston, S. A. Lynch, R. F. Massey, J. F. Meritet, J. L. Michaud, G. Ponsot, T. Voit, P. Lebon, D. T. Bonthron, A. P. Jackson, D. E. Barnes, and T. Lindahl.

2006. Mutations in the gene encoding the 3’-5’ DNA exonuclease TREX1 cause Aicardi-Goutières syndrome at the AGS1 locus. *Nat Genet* 38: 917–920.

140. Deng, L., H. Liang, M. Xu, X. Yang, B. Burnette, A. Arina, X.-D. Li, H. Mauceri, M. Beckett, T. Darga, X. Huang, T. F. Gajewski, Z. J. Chen, Y.-X. Fu, and R. R. Weichselbaum. 2014. STING-Dependent Cytosolic DNA Sensing Promotes Radiation-Induced Type I Interferon-Dependent Antitumor Immunity in Immunogenic Tumors. *Immunity* 41: 843–852.

141. Orzalli, M. H., N. M. Broekema, B. A. Diner, D. C. Hancks, N. C. Elde, I. M. Cristea, and D. M. Knipe. 2015. cGAS-mediated stabilization of IFI16 promotes innate signaling during herpes simplex virus infection. *Proc Natl Acad Sci U S A* 112: E1773-1781.

142. Liu, H., H. Zhang, X. Wu, D. Ma, J. Wu, L. Wang, Y. Jiang, Y. Fei, C. Zhu, R. Tan, P. Jungblut, G. Pei, A. Dorhoi, Q. Yan, F. Zhang, R. Zheng, S. Liu, H. Liang, Z. Liu, H. Yang, J. Chen, P. Wang, T. Tang, W. Peng, Z. Hu, Z. Xu, X. Huang, J. Wang, H. Li, Y. Zhou, F. Liu, D. Yan, S. H. E. Kaufmann, C. Chen, Z. Mao, and B. Ge. 2018. Nuclear cGAS suppresses DNA repair and promotes tumorigenesis. *Nature* 563: 131–136.

143. Jiang, H., X. Xue, S. Panda, A. Kawale, R. M. Hooy, F. Liang, J. Sohn, P. Sung, and N. O. Gekara. 2019. Chromatin-bound cGAS is an inhibitor of DNA repair and hence accelerates genome destabilization and cell death. *EMBO J* 38: e102718.

144. Chen, H., H. Chen, J. Zhang, Y. Wang, A. Simoneau, H. Yang, A. S. Levine, L. Zou, Z. Chen, and L. Lan. 2020. cGAS suppresses genomic instability as a decelerator of replication forks. *Sci Adv* 6: eabb8941.

145. Alimonti, J. B., T. B. Ball, and K. R. Fowke. 2003. Mechanisms of CD4+ T lymphocyte cell death in human immunodeficiency virus infection and AIDS. *J Gen Virol* 84: 1649–1661.

146. Penn, M. L., J.-C. Grivel, B. Schramm, M. A. Goldsmith, and L. Margolis. 1999. CXCR4 utilization is sufficient to trigger CD4+ T cell depletion in HIV-1-infected human lymphoid tissue. *Proc Natl Acad Sci U S A* 96: 663–668.

147. Siddiqui, M. A., and M. Yamashita. 2021. Toll-Like Receptor (TLR) Signaling Enables Cyclic GMP-AMP Synthase (cGAS) Sensing of HIV-1 Infection in Macrophages. *mBio* 12: e0281721.

148. Song, X., W. Hu, H. Yu, L. Zhao, Y. Zhao, X. Zhao, H.-H. Xue, and Y. Zhao. 2020. Little to no expression of angiotensin-converting enzyme-2 on most human peripheral blood immune cells but highly expressed on tissue macrophages. *Cytometry A* .

149. Castilletti, C., L. Bordi, E. Lalle, G. Rozera, F. Poccia, C. Agrati, I. Abbate, and M. R. Capobianchi. 2005. Coordinate induction of IFN-α and -γ by SARS-CoV also in the absence of virus replication. *Virology* 341: 163–169.

150. Ng, L. F. P., M. L. Hibberd, E.-E. Ooi, K.-F. Tang, S.-Y. Neo, J. Tan, K. R. K. Murthy, V. B. Vega, J.-M. Chia, E. T. Liu, and E.-C. Ren. 2004. A human in vitro model system for investigating genome-wide host responses to SARS coronavirus infection. *BMC Infect Dis* 4: 34.

151. Zankharia, U., A. Yadav, Y. Yi, B. H. Hahn, and R. G. Collman. 2022. Highly restricted SARS-CoV-2 receptor expression and resistance to infection by primary human monocytes and monocyte-derived macrophages. *J Leukoc Biol* .

152. Junqueira, C., Â. Crespo, S. Ranjbar, L. B. de Lacerda, M. Lewandrowski, J. Ingber, B. Parry, S. Ravid, S. Clark, M. R. Schrimpf, F. Ho, C. Beakes, J. Margolin, N. Russell,

K. Kays, J. Boucau, U. Das Adhikari, S. M. Vora, V. Leger, L. Gehrke, L. A. Henderson, E. Janssen, D. Kwon, C. Sander, J. Abraham, M. B. Goldberg, H. Wu, G. Mehta, S. Bell, A. E. Goldfeld, M. R. Filbin, and J. Lieberman. 2022. FcγR-mediated SARS-CoV-2 infection of monocytes activates inflammation. *Nature* 606: 576–584.

153. Wang, G., J. Guan, G. Li, F. Wu, Q. Yang, C. Huang, J. Shao, L. Xu, Z. Guo, Q. Zhou, H. Zhu, and Z. Chen. 2021. Effect of ORF7 of SARS-CoV-2 on the Chemotaxis of Monocytes and Neutrophils In Vitro. *Dis Markers* 2021: 6803510.

154. Chu, H., J. Zhou, B. H.-Y. Wong, C. Li, Z.-S. Cheng, X. Lin, V. K.-M. Poon, T. Sun, C. C.-Y. Lau, J. F.-W. Chan, K. K.-W. To, K.-H. Chan, L. Lu, B.-J. Zheng, and K.-Y. Yuen. 2014. Productive replication of Middle East respiratory syndrome coronavirus in monocyte-derived dendritic cells modulates innate immune response. *Virology* 454–455: 197–205.

155. Cheung, C. Y., L. L. M. Poon, I. H. Y. Ng, W. Luk, S.-F. Sia, M. H. S. Wu, K.-H. Chan, K.-Y. Yuen, S. Gordon, Y. Guan, and J. S. M. Peiris. 2005. Cytokine responses in severe acute respiratory syndrome coronavirus-infected macrophages in vitro: possible relevance to pathogenesis. *J Virol* 79: 7819–7826.

156. Qiao, J., Y.-S. Li, R. Zeng, F.-L. Liu, R.-H. Luo, C. Huang, Y.-F. Wang, J. Zhang, B. Quan, C. Shen, X. Mao, X. Liu, W. Sun, W. Yang, X. Ni, K. Wang, L. Xu, Z.-L. Duan, Q.-C. Zou, H.-L. Zhang, W. Qu, Y.-H.-P. Long, M.-H. Li, R.-C. Yang, X. Liu, J. You, Y. Zhou, R. Yao, W.-P. Li, J.-M. Liu, P. Chen, Y. Liu, G.-F. Lin, X. Yang, J. Zou, L. Li, Y. Hu, G.-W. Lu, W.-M. Li, Y.-Q. Wei, Y.-T. Zheng, J. Lei, and S. Yang. 2021. SARS-CoV-2 Mpro inhibitors with antiviral activity in a transgenic mouse model. *Science* 371: 1374–1378.

157. Hayn, M., M. Hirschenberger, L. Koepke, R. Nchioua, J. H. Straub, S. Klute, V. Hunszinger, F. Zech, C. Prelli Bozzo, W. Aftab, M. H. Christensen, C. Conzelmann, J. A. Müller, S. Srinivasachar Badarinarayan, C. M. Stürzel, I. Forne, S. Stenger, K.-K. Conzelmann, J. Münch, F. I. Schmidt, D. Sauter, A. Imhof, F. Kirchhoff, and K. M. J. Sparrer. 2021. Systematic functional analysis of SARS-CoV-2 proteins uncovers viral innate immune antagonists and remaining vulnerabilities. *Cell Rep* 35: 109126.

VII. Eidesstattliche Versicherung

„Ich, Julia Kazmierski, versichere an Eides statt durch meine eigenhändige Unterschrift, dass ich die vorgelegte Dissertation mit dem Thema „Innate Immune Sensing and Viral Evasion Mechanisms of HIV-1 and SARS-CoV-2“/ „Angeborene Immunität gegen und Virale Evasionsmechanismen von HIV-1 und SARS-CoV-2“ selbstständig und ohne nicht offengelegte Hilfe Dritter verfasst und keine anderen als die angegebenen Quellen und Hilfsmittel genutzt habe.

Alle Stellen, die wörtlich oder dem Sinne nach auf Publikationen oder Vorträgen anderer Autoren/innen beruhen, sind als solche in korrekter Zitierung kenntlich gemacht. Die Abschnitte zu Methodik (insbesondere praktische Arbeiten, Laborbestimmungen, statistische Aufarbeitung) und Resultaten (insbesondere Abbildungen, Graphiken und Tabellen) werden von mir verantwortet.

Ich versichere ferner, dass ich die in Zusammenarbeit mit anderen Personen generierten Daten, Datenauswertungen und Schlussfolgerungen korrekt gekennzeichnet und meinen eigenen Beitrag sowie die Beiträge anderer Personen korrekt kenntlich gemacht habe (siehe Anteilserklärung). Texte oder Textteile, die gemeinsam mit anderen erstellt oder verwendet wurden, habe ich korrekt kenntlich gemacht.

Meine Anteile an etwaigen Publikationen zu dieser Dissertation entsprechen denen, die in der untenstehenden gemeinsamen Erklärung mit dem/der Erstbetreuer/in, angegeben sind. Für sämtliche im Rahmen der Dissertation entstandenen Publikationen wurden die Richtlinien des ICMJE (International Committee of Medical Journal Editors; www.icmje.og) zur Autorenschaft eingehalten. Ich erkläre ferner, dass ich mich zur Einhaltung der Satzung der Charité – Universitätsmedizin Berlin zur Sicherung Guter Wissenschaftlicher Praxis verpflichte.

Weiterhin versichere ich, dass ich diese Dissertation weder in gleicher noch in ähnlicher Form bereits an einer anderen Fakultät eingereicht habe.

Die Bedeutung dieser eidesstattlichen Versicherung und die strafrechtlichen Folgen einer unwahren eidesstattlichen Versicherung (§§156, 161 des Strafgesetzbuches) sind mir bekannt und bewusst.“

_____ _____

Datum Unterschrift

VIII. Declaration of Own Contribution

Es folgt die Erklärung der eigenen Anteile von Julia Kazmierski an den drei Schlüsselpublikationen der vorliegenden Dissertation:

Publikation 1: A baseline cellular antiviral state is maintained by cGAS and its most frequent naturally occurring variant rs610913

Kazmierski J, Elsner C, Döhner K, Xu S, Ducroux A, Pott F, Jansen J, Thorball CW, Zeymer O, Zhou X, Fedorov R, Fellay J, Löffler MW, Weber ANR, Sodeik B, Goffinet C. A Baseline Cellular Antiviral State Is Maintained by cGAS and Its Most Frequent Naturally Occurring Variant rs610913. J Immunol. 2022 Jul 18:ji2100685. Epub ahead of print.

In *Journal of Immunology*, 2022

Als Erstautorin dieser Publikation habe ich, zusammen mit meiner PhD Thesis-Betreuerin Christine Goffinet, die Studie konzipiert und geplant. Der Großteil der durchgeführten Experimente inklusive Datenanalyse und Aufbereitung wurde von mir ausgeführt. Die von mir generierten Daten sind insbesondere in den Abbildungen 3 – 7 sowie S1-3 dargestellt. Ich habe die erste Fassung des Manuskripts erstellt, war an der anschließenden Überarbeitung des Manuskripts beteiligt und habe alle die für die Revision des Manuskripts geforderten Experimente durchgeführt.

Publikation 2: Non-productive exposure of PBMCs to SARS-CoV-2 induces cell-intrinsic innate immune responses

Kazmierski J*, Friedmann K*, Postmus D, Emanuel J, Fischer C, Jansen J, Richter A, Bosquillon de Jarcy L, Schüler C, Sohn M, Sauer S, Drosten C, Saliba AE, Sander LE, Müller MA, Niemeyer D#, Goffinet C#. Nonproductive exposure of PBMCs to SARS-CoV-2 induces cell-intrinsic innate immune responses. Mol Syst Biol. 2022 Aug;18(8):e10961. doi: 10.15252/msb.202210961.

* Geteilte Erstautorenschaft

Co-Korrespondierende Autoren

In *Molecular Systems Biology*, 2022

In dieser Publikation bin ich als geteilte Erstautorin an der Studienkonzeption, Planung und Durchführung der Experimente, Datenanalyse sowie dem Verfassen und Überarbeiten des Manuskripts maßgeblich beteiligt gewesen. Konkret habe ich in enger Zusammenarbeit mit Kirstin Friedmann gemeinsam alle im Manuskript enthaltenden

Experimente geplant, durchgeführt und größtenteils ausgewertet (Abb. 1-5, EV Abb. 1-5, Appendix Abb. 1-6). Darüber hinaus habe ich alle im Manuskript erhaltenen Abbildungen generiert und war an dem Entwurf und der Überarbeitung des Manuskripts beteiligt.

Publikation 3: Absence of cGAS-mediated type I IFN responses in HIV-1-infected T-cells

Elsner C*, Ponnurangam A*, Kazmierski J, Zillinger T, Jansen J, Todt D, Döhner K, Xu S, Ducroux A, Kriedemann N, Malassa A, Larsen PK, Hartmann G, Barchet W, Steinmann E, Kalinke U, Sodeik B, Goffinet C. Absence of cGAS-mediated type I IFN responses in HIV-1-infected T cells. Proc Natl Acad Sci U S A. 2020 Aug 11;117(32):19475-19486. doi: 10.1073/pnas.2002481117.

* Geteilte Erstautorenschaft

In *Proceedings of the National Academy of Sciences*, 2020

Zu dieser Veröffentlichung habe ich durch Konzeption, Durchführung und Analyse ausgewählter Experimente beigetragen. Die Resultate meiner Experimente sind in folgenden Abbildungen dargestellt: Abb. 1A, D, F; Abb. 2D-F; Abb. 4B-C; Abb. 5 sowie in den ergänzenden Abbildungen S2; S4; S6. Außerdem war ich an der finalen Überarbeitung des Manuskripts im Zuge der Revision beteiligt.

Prof. Dr. Christine Goffinet	Datum, Stempel

Dr. Kirstin Friedmann
(Shared first-author publication 2)

Julia Kazmierski

IX. Excerpt from the Journal Summary List

A. Publication 1: A baseline cellular antiviral state is maintained by cGAS and its most frequent naturally occurring variant rs610913

In *Journal of Immunology*, 2022

Journal Data Filtered By:

Selected JCR Year: 2020

Selected Editions: SCIE,SSCI

Selected Categories: **"Immunology"**

Selected Category Scheme: WoS

Gesamtanzahl: 162 Journale

Rank	Full Journal Title	Total Cites	Journal Impact Factor	Eigenfactor Score
1	NATURE REVIEWS IMMUNOLOGY	55,784	53.106	0.063920
2	IMMUNITY	70,517	31.745	0.122940
3	Annual Review of Immunology	20,292	28.527	0.017290
4	NATURE IMMUNOLOGY	54,588	25.606	0.080490
5	Science Immunology	5,232	17.727	0.022200
6	TRENDS IN IMMUNOLOGY	16,915	16.687	0.024570
7	JOURNAL OF EXPERIMENTAL MEDICINE	74,803	14.307	0.062280
8	Journal for ImmunoTherapy of Cancer	11,042	13.751	0.028830
9	ALLERGY	25,131	13.146	0.023300
10	IMMUNOLOGICAL REVIEWS	19,337	12.988	0.024380
11	Lancet HIV	5,368	12.767	0.022020
12	Cellular & Molecular Immunology	8,489	11.530	0.010550
13	Cancer Immunology Research	11,185	11.151	0.027290

14	SEMINARS IN IMMUNOLOGY	6,814	11.130	0.008220
15	JOURNAL OF ALLERGY AND CLINICAL IMMUNOLOGY	63,614	10.793	0.069980
16	AUTOIMMUNITY REVIEWS	13,493	9.754	0.014810
17	Seminars in Immunopathology	5,651	9.623	0.009960
18	CLINICAL INFECTIOUS DISEASES	89,276	9.079	0.113210
19	Journal of Allergy and Clinical Immunology-In Practice	9,255	8.861	0.019690
20	CLINICAL REVIEWS IN ALLERGY & IMMUNOLOGY	4,546	8.667	0.006270
21	Journal of Neuroinflammation	19,657	8.322	0.027070
22	JOURNAL OF CLINICAL IMMUNOLOGY	6,537	8.317	0.007110
23	OncoImmunology	14,987	8.110	0.030230
24	Frontiers in Immunology	84,852	7.561	0.182280
25	CURRENT OPINION IN IMMUNOLOGY	11,347	7.486	0.014270
26	IMMUNOLOGY	14,248	7.397	0.011160
27	Inflammation and Regeneration	743	7.354	0.001450
28	Journal of Innate Immunity	3,032	7.349	0.003370
29	npj Vaccines	1,342	7.344	0.003850
30	Mucosal Immunology	9,440	7.313	0.017940
31	BRAIN BEHAVIOR AND IMMUNITY	24,161	7.217	0.026930
32	Emerging Microbes & Infections	8,988	7.163	0.012560
33	JOURNAL OF AUTOIMMUNITY	10,437	7.094	0.012240

34	CANCER IMMUNOLOGY IMMUNOTHERAPY	11,382	6.968	0.012190
35	Journal of Inflammation Research	1,321	6.922	0.002130
36	EMERGING INFECTIOUS DISEASES	44,051	6.883	0.049780
37	Immunity & Ageing	1,468	6.400	0.001750
38	PEDIATRIC ALLERGY AND IMMUNOLOGY	5,778	6.377	0.005590
39	ANNALS OF ALLERGY ASTHMA & IMMUNOLOGY	10,809	6.347	0.011650
40	EXERCISE IMMUNOLOGY REVIEW	1,093	6.308	0.000710
41	Immune Network	1,629	6.303	0.002620
42	Clinical & Translational Immunology	1,574	6.161	0.003690
43	INFECTIOUS DISEASE CLINICS OF NORTH AMERICA	4,090	5.982	0.006870
44	Virulence	5,784	5.882	0.007420
45	ALLERGOLOGY INTERNATIONAL	3,122	5.836	0.004520
46	BIODRUGS	2,581	5.807	0.003770
47	Allergy Asthma & Immunology Research	2,345	5.764	0.003570
48	BIOLOGY OF BLOOD AND MARROW TRANSPLANTATION	17,149	5.742	0.026390
49	EUROPEAN JOURNAL OF IMMUNOLOGY	24,504	5.532	0.017040
50	BONE MARROW TRANSPLANTATION	16,801	5.483	0.015200
51	**JOURNAL OF IMMUNOLOGY**	**146,980**	**5.422**	**0.087490**

B. Publication 2: Non-productive exposure of PBMCs to SARS-CoV-2 induces cell-intrinsic innate immune responses

In *Molecular Systems Biology*, 2022

Journal Data Filtered By:

Selected JCR Year: 2021

Selected Editions: SCIE,SSCI

Selected Categories: **"BIOCHEMISTRY and MOLECULAR BIOLOGY"**

Selected Category Scheme: WoS

Gesamtanzahl: 296 Journale

Rank	Full Journal Title	Total Cites	Journal Impact Factor	Eigenfactor Score
1	NATURE MEDICINE	141,857	87.241	0.23255
2	CELL	362,236	66.850	0.53397
3	Molecular Cancer	32,250	41.444	0.03386
4	Signal Transduction and Targeted Therapy	11,026	38.104	0.01781
5	Annual Review of Biochemistry	25,139	27.258	0.01962
6	Molecular Plant	20,242	21.949	0.02339
7	MOLECULAR CELL	94,258	19.328	0.13937
8	NUCLEIC ACIDS RESEARCH	284,490	19.160	0.33755
9	NATURE STRUCTURAL & MOLECULAR BIOLOGY	33,999	18.361	0.04689
10	TRENDS IN MICROBIOLOGY	19,957	18.230	0.02015
11	CYTOKINE & GROWTH FACTOR REVIEWS	9,002	17.660	0.00625

12	MOLECULAR ASPECTS OF MEDICINE	8,986	16.337	0.00615
13	Nature Chemical Biology	31,125	16.174	0.04456
14	TRENDS IN MOLECULAR MEDICINE	14,585	15.272	0.01381
15	NATURAL PRODUCT REPORTS	14,564	15.111	0.01079
16	PROGRESS IN LIPID RESEARCH	7,982	14.673	0.00444
17	TRENDS IN BIOCHEMICAL SCIENCES	22,957	14.264	0.02170
18	EMBO JOURNAL	80,536	14.012	0.05438
19	MOLECULAR PSYCHIATRY	33,324	13.437	0.04914
20	**Molecular Systems Biology**	**11,036**	**13.068**	**0.01483**

C. Publication 3: Absence of cGAS-mediated type I IFN responses in HIV-1-infected T-cells

In *Proceedings of the National Academy of Sciences*, 2019

Journal Data Filtered By:

Selected JCR Year: 2019

Selected Editions: SCIE,SSCI

Selected Categories: **“MULTIDISCIPLINARY SCIENCES”**

Selected Category

Scheme: WoS

Gesamtanzahl: 71 Journale

Rank	Full Journal Title	Total Cites	Journal Impact Factor	Eigenfactor Score
1	NATURE	767,209	42.778	1.216730
2	SCIENCE	699,842	41.845	1.022660
3	National Science Review	2,775	16.693	0.009760

4	Science Advances	36,380	13.116	0.172060
5	Nature Human Behaviour	2,457	12.282	0.014190
6	Nature Communications	312,599	12.121	1.259510
7	Science Bulletin	5,172	9.511	0.014150
8	**PROCEEDINGS OF THE NATIONAL ACADEMY OF SCIENCES OF THE UNITED STATES OF AMERICA**	**676,425**	**9.412**	**0.931890**

X. Printed copies of publications

The Journal of Immunology

A Baseline Cellular Antiviral State Is Maintained by cGAS and Its Most Frequent Naturally Occurring Variant rs610913

Julia Kazmierski, Carina Elsner, Katinka Döhner, Shuting Xu, Aurélie Ducroux, Fabian Pott, Jenny Jansen, Christian W. Thorball, Ole Zeymer, Xiaoyi Zhou, Roman Fedorov, Jacques Fellay, Markus W. Löffler, Alexander N. R. Weber, Beate Sodeik and Christine Goffinet

J Immunol 2022; 209:535-547; Prepublished online 18 July 2022;
doi: 10.4049/jimmunol.2100685
http://www.jimmunol.org/content/209/3/535

The Journal of Immunology is published twice each month by
The American Association of Immunologists, Inc.,
1451 Rockville Pike, Suite 650, Rockville, MD 20852

Print ISSN: 0022-1767 Online ISSN: 1550-6606.

A Baseline Cellular Antiviral State Is Maintained by cGAS and Its Most Frequent Naturally Occurring Variant rs610913

Julia Kazmierski,[*,†,‡] Carina Elsner,[‡,§] Katinka Döhner,[¶] Shuting Xu,[‡] Aurélie Ducroux,[‡] Fabian Pott,[*,†,‡] Jenny Jansen,[*,†] Christian W. Thorball,[‖,#,] Ole Zeymer,[††,‡‡] Xiaoyi Zhou,[††,‡‡] Roman Fedorov,[††,‡‡] Jacques Fellay,[‖,#,**] Markus W. Löffler,[§§,¶¶,‖‖,##] Alexander N. R. Weber,[§§,##,***] Beate Sodeik,[¶,‡‡,†††] and Christine Goffinet[*,†,‡]**

Upon recognition of aberrantly located DNA, the innate immune sensor cyclic GMP-AMP synthase (cGAS) activates stimulator of IFN genes (STING)/IFN regulatory factor (IRF)3–driven antiviral responses. In this study, we characterized the ability of a specific variant of the human cGAS-encoding gene *MB21D1*, rs610913, to alter cGAS-mediated DNA sensing and viral infection. rs610913 is a frequent G>T polymorphism resulting in a P261H exchange in the cGAS protein. Data from the International Collaboration for the Genomics of HIV suggested that rs610913 nominally associates with HIV-1 acquisition in vivo. Molecular modeling of cGAS(P261H) hinted toward the possibility for an additional binding site for a potential cellular cofactor in cGAS dimers. However, cGAS(wild-type [WT]) or cGAS(P261H)-reconstituted THP-1 cGAS knockout cells shared steady-state expression of IFN-stimulated genes, as opposed to cells expressing the enzymatically inactive cGAS(G212A/S213A). Accordingly, cGAS(WT) and cGAS(P261H) cells were less susceptible to lentiviral transduction and infection with HIV-1, HSV-1, and Chikungunya virus as compared with cGAS knockout or cGAS(G212A/S^{213}A) cells. Upon DNA challenge, innate immune activation appeared to be mildly reduced upon expression of cGAS(P261H) compared with cGAS(WT). Finally, DNA challenge of PBMCs from donors homozygously expressing rs610913 provoked a trend toward a slightly reduced type I IFN response as compared with PBMCs from GG donors. Taken together, the steady-state activity of cGAS maintains a baseline antiviral state rendering cells more refractory to IFN-stimulated gene–sensitive viral infections. rs610913 failed to grossly differ phenotypically from the WT gene, suggesting that cGAS(P261H) and WT cGAS share a similar ability to sense viral infections in vivo. *The Journal of Immunology*, 2022, 209: 535–547.

Pattern recognition receptors of the innate immune system are crucial for the detection of invading pathogens and required to mount an effective immune response. Cyclic GMP-AMP synthase (cGAS) binds to dsDNA in the cytosol and nucleus, followed by its enzymatic activation and the production of the second messenger molecule 2′3′-cyclic GMP-AMP (cGAMP) (1, 2). This small molecule, in turn, binds to the stimulator of IFN genes (STING), leading to its activation, phosphorylation and eventually induction of a TANK-binding kinase 1 (TBK1)/IFN regulatory factor (IRF)3-dependent signaling cascade, resulting in the transcription

*Institute of Virology, Campus Charité Mitte, Charité–Universitätsmedizin Berlin, Berlin, Germany; †Berlin Institute of Health, Berlin, Germany; ‡Institute of Experimental Virology, Twincore Centre for Experimental and Clinical Infection Research, a Joint Venture between the Hannover Medical School and the Helmholtz Centre for Infection Research, Hannover, Germany; §Institute for Virology, University Hospital Essen, University of Duisburg–Essen, Essen, Germany; ¶Institute of Virology, Hannover Medical School, Hannover, Germany; ‖School of Life Sciences, École Polytechnique Fédérale de Lausanne, Lausanne, Switzerland; #Swiss Institute of Bioinformatics, Lausanne, Switzerland; **Precision Medicine Unit, Lausanne University Hospital and University of Lausanne, Lausanne, Switzerland; ††Institute for Biophysical Chemistry, Research Division for Structural Biochemistry, Hannover Medical School, Hannover, Germany; ‡‡RESIST–Cluster of Excellence, Hannover Medical School, Hannover, Germany; §§Department of Immunology, Interfaculty Institute for Cell Biology, University of Tübingen, Tübingen, Germany; ¶¶Department of General, Visceral and Transplant Surgery, University Hospital Tübingen, Tübingen Germany; ‖‖Department of Clinical Pharmacology, University Hospital Tübingen, Tübingen, Germany; ##iFIT–Cluster of Excellence (EXC 2180) "Image-Guided and Functionally Instructed Tumor Therapies," University of Tübingen, Tübingen, Germany; ***CMFI–Cluster of Excellence (EXC 2124) "Controlling Microbes to Fight Infection," University of Tübingen, Tübingen, Germany; and †††German Center for Infection Research, Hannover-Braunschweig Partner Site, Hannover, Germany

ORCIDs: 0000-0002-7962-2165 (J.K.), 0000-0001-6590-8413 (C.E.), 0000-0002-8222-3085 (K.D.), 0000-0003-3700-1691 (F.P.), 0000-0002-6869-6943 (C.W.T.), 0000-0002-5240-4205 (R.F.), 0000-0002-8240-939X (J.F.), 0000-0003-2513-1317 (M.W.L.), 0000-0003-4650-3036 (B.S.), 0000-0002-3959-004X (C.G.).

Received for publication July 12, 2021. Accepted for publication May 13, 2022.

This work was supported by a postdoctoral fellowship from the Foundation Ernst & Margarete Wagemann to A.D., by funding from German Research Foundation (Deutsche Forschungsgemeinschaft) to C.G. (Collaborative Research Centre SFB900 "Microbial Persistence and Its Control," project number 158989968, project C8, and priority program 1923 "Innate Sensing and Restriction of Retroviruses," Grant GO2153/4) and to B.S. (Grants SFB900 158989968; project C2, EXC2155 RESIST 390874280, and So 403/6-1), by funding from the Boehringer Ingelheim Foundation (Exploration Grant) to C.G., funding of the Helmholtz Center for Infection Research and of Berlin Institute of Health to C.G. R.F. was supported by Deutsche Forschungsgemeinschaft Grants FE 1510/2-1 and EXC 2155 "RESIST" – Project ID 39087428. A.N.R.W. was supported by the Else-Kröner-Fresenius Stiftung, the University Hospital Tübingen, the University of Tübingen, and by the Deutsche Forschungsgemeinschaft Clusters of Excellence "iFIT – Image-Guided and Functionally Instructed Tumor Therapies" (EXC 2180) (also to M.W.L.) and "CMFI – Controlling Microbes to Fight Infection" (EXC 2124). J.K. is supported by the Center of Infection Biology and Immunity.

J.K., C.E., S.X., and C.G. designed research; J.K., C.E., K.D., S.X., A.D., F.P., J.J., O.Z., X.Z., and R.F. performed research; M.W.L. and A.N.R.W. were involved in sample acquisition; J.K., C.E., S.X., A.D., F.P., C.W.T., O.Z., X.Z., R.F., J.F., A.N.R.W., B.S., and C.G. analyzed data; C.E., K.D., C.W.T., R.F., A.N.R.W., and B.S. contributed to writing the manuscript; and J.K. and C.G. wrote the paper.The RNA sequencing datasets presented in this article have been submitted to Gene Expression Omnibus under accession number GSE203334.

Address correspondence and reprint requests to Prof. Christine Goffinet, Institute of Virology, Campus Charité Mitte, Charité–Universitätsmedizin Berlin, Charitéplatz 1, 10117 Berlin, Germany. E-mail: christine.goffinet@charite.de

The online version of this article contains supplemental material.

Abbreviations used in this article: cGAMP, 2′3′-cyclic GMP-AMP; cGAS, cyclic GMP-AMP synthase; CHIKV, Chikungunya virus; DEG, differentially expressed gene; EFV, efavirenz; GO, Gene Ontology; hcGAS, human cGAS; IFIT1, IFN-induced protein with tetratricopeptide repeats 1; IRF, IFN regulatory factor; ISG, IFN-stimulated gene; KO, knockout; mcGAS, murine cGAS; MX2, MX dynamin-like GTPase 2; PDB, Protein Data Bank; poly(I:C), polyinosinic-polycytidylic acid; RPKM, reads per kilobase of transcript per million mapped reads; SNP, single nucleotide polymorphism; STING, stimulator of IFN genes; TBK1, TANK-binding kinase 1; TREX1, three prime repair exonuclease 1; VSV-G, vesicular stomatitis virus glycoprotein; WT, wild-type.

of IFNs and IFN-stimulated genes (ISGs), many of them exerting antiviral activity.

cGAS-mediated recognition of invading pathogens serves as a first-line defense mechanism against multiple viruses, which themselves evolved strategies to counteract cGAS-mediated sensing. The genome of invading DNA viruses, such as HSV-1 or Kaposi's sarcoma-associated herpesvirus, is recognized in a cGAS-dependent fashion (reviewed in Refs. 3–5). As a consequence, herpes viruses evolved specific antagonists that counteract cGAS/STING-mediated DNA sensing, including HSV-1 pUL41, which selectively targets cGAS mRNA for degradation (6), HSV-1 ICP27, which prevents cGAS phosphorylation (7), or HSV-1-pUL36, which targets STING to proteasomal degradation (8) and therefore interferes with the activation of the crucial transcription factor IRF3. Retroviruses, including HIV-1, evolved a sophisticated replication strategy. Specifically, reverse transcription of their RNA genome into a single DNA intermediate that is destined for integration into a host cell's chromosome allows retroviruses to largely escape general innate immune activation (9) and cGAS-dependent recognition (10). These observations are in line with studies reporting that innate sensing of HIV-1 infection only occurs upon pharmacological or genetic destabilization of the otherwise nucleic acid–shielding viral capsid (11, 12) and is enhanced in the absence of functional three prime repair exonuclease 1 (TREX1) expression, which otherwise degrades capsid-escaping and thus cytosolic HIV-1 DNA (13, 14). Interestingly, RNA viruses also have been considered to be inhibited by cGAS-exerted functions, although not mediated through sensing of viral nucleic acids. Rather, cGAS may maintain a basal antiviral state through recognition of self DNA, including endogenous retroelements (15) and/or sensing of DNA released from the nucleus or mitochondria through infection-associated stress induction (16, 17).

Single nucleotide polymorphisms (SNPs) in genes encoding pattern recognition receptors and downstream adapter molecules modulate infection susceptibility and disease outcome. A remarkable example is the variant of the STING-encoding *TMEM173* gene that contains three nonsynonymous SNPs referred to as "the HAQ haplotype." Homozygous expression of this haplotype is predominantly found in East Asian (16.07%) and South American (7.78%) populations (18). It is associated with lower susceptibility to stimulation by cyclic dinucleotides (19) and eventually a severely reduced ability to induce IFN-β expression (19, 20). Interestingly, among other homozygous SNPs in the *TMEM173* gene, the HAQ haplotype has a higher prevalence in HIV-1 long-term nonprogressors, as compared with HIV-1 noncontrollers (21). SNPs can be functionally important in the context of infectious disease in vivo, as illustrated by the impact of a minor IFITM3 allele (rs12252-C) of influenza-associated morbidity and mortality (22), and a polymorphism near the *IL28B* gene, encoding IFN-λ-3, associated with an ~2-fold change in response to treatment to HCV infection (23). However, accurate estimation of their impact requires a combination of structure–function analysis, functional and immunogenetic investigations, and genome-wide association studies in well-characterized cohorts.

To date, there is limited knowledge on the role of SNPs in the cGAS-encoding gene *MB21D1*, in particular on implications for DNA sensing and innate immune activation. The most frequent SNP in *MB21D1* is rs610913, a G>T polymorphism that displays a global allele frequency of 0.503 (24). The G to T nucleotide exchange results in a single amino acid exchange from proline (P) to histidine (H) at position 261 in the protein sequence. In this study, we report structural and functional consequences of the rs610913-encoded P261H single amino acid exchange in the cGAS protein in the context of DNA sensing and restriction of viral infections.

Materials and Methods

Genome-wide association analysis

Summary statistics for HIV-1 acquisition in the region of *MB21D1* were obtained from genome-wide association analyses previously performed by the International Collaboration for the Genomics of HIV (25). The summary statistics were available on a subgroup basis, with a total of six groups matched by geographic origin and genotyping platform, as previously described: group 1 (the Netherlands, Illumina), group 2 (France, Illumina), group 3 (North America, Illumina), group 4 (French European, Illumina), group 5 (North American, Affymetrix), and group 6 (non-Dutch/non-French European, Affymetrix). Association results across groups were combined using a fixed-effects inverse-variance weighted meta-analysis.

Molecular modeling

The structural model of human cGAS (hcGAS)(P261H)·dsDNA assembly in the active (ATP-bound) conformational state was created using the ladder-like crystal structure of mouse cGAS (mcGAS) in complex with dsDNA (Protein Data Bank [PDB] code 5N6I) (26) and the structure of the wild-type (WT) hcGAS·dsDNA·ATP complex (PDB code 6CTA) (27). The protein part of the hcGAS·dsDNA·ATP complex was used to generate a homology model of hcGAS(P261H) in the active conformational state. The homology model of hcGAS(P261H) was superimposed on the mcGAS molecules in the ladder-like assembly. The superposition was performed using the program package Coot (28). The secondary structure matching algorithm (29) was used to align the structurally conserved parts of the proteins. The resulting model was subjected to an energy minimization procedure using the program HyperChem (Hypercube) with an AMBER force field (30) and a distance-dependent dielectric constant. The structural analysis and rendering of Fig. 1B and 1C were performed with the final energy minimized model using the programs Coot and PyMOL (The PyMOL Molecular Graphics System, version 1.8, Schrödinger).

Healthy study subjects and blood sample acquisition

Healthy blood donors were recruited at the Interfaculty Institute of Cell Biology, Department of Immunology, University of Tübingen (Tübingen, Germany). All healthy blood donors included in this study provided their written informed consent before study participation. Approval for use of their biomaterials was obtained by the respective local ethics committees (approvals 156-2012BO1 and 354-2012BO2), in accordance with the principles laid down in the Declaration of Helsinki as well as applicable laws and regulations.

Cell lines and primary cells

cGAS knockout (KO) THP-1 cells (a gift from Veit Hornung, Ludwig Maximilians University, Munich, Germany) were cultured in RPMI 1640 medium supplemented with 10% FCS, 100 U/ml penicillin, 100 μg/ml streptomycin, 2 mM L-glutamine, 1× MEM nonessential amino acids solution, and 1 mM sodium pyruvate (Thermo Fisher Scientific, Waltham, MA). HEK293T, HEK293T STING-mCherry (1), and BHK-21 cells were maintained in DMEM cell culture medium supplemented with 10% FCS, 100 U/ml penicillin, 100 μg/ml streptomycin, and 2 mM L-glutamine. HL116 cells (31) were cultured under identical conditions, except for the addition of 1× hypoxanthine-aminopterin-thymidine (HAT) media supplement (Thermo Fisher Scientific, Waltham, MA). THP-1 cGAS KO cells and HEK293T STING-mCherry cells were reconstituted with individual cGAS-GFP variants by lentiviral transduction and were maintained under 1 μg/ml puromycin selection. After preparation of PBMCs from EDTA-anticoagulated blood by Ficoll-Hypaque centrifugation, cells were stimulated with IL-2 (10 ng/ml) and PHA (1 μg/ml) for 3–4 d, resulting in cultures containing >90% $CD3^+$ T cells. Cells were maintained in RPMI 1640 containing 10% heat-inactivated FCS, 100 U/ml penicillin, 100 μg/ml streptomycin, 2 mM L-glutamine, 1× MEM nonessential amino acids solution, and 1 mM sodium pyruvate (Thermo Fisher Scientific, Waltham, MA).

Generation of lentiviral vector particles and virus stocks

Vesicular stomatitis virus glycoprotein (VSV-G)–pseudotyped lentiviral vector particles encoding GFP or luciferase were generated by calcium phosphate–based transfection of HEK293T cells with the packaging plasmid pCMV ΔR8.91 (32), the lentiviral transfer plasmids pHR-GFP (33) or pie-EF-luciferase (34), and pCMV–VSV-G (35). For the generation of cGAS-transducing lentiviral particles, the transfer plasmids pWPI cGAS(WT)-GFP, pWPI cGAS(G212A/S213A)-GFP (36), and pWPI cGAS(P261H)-GFP were used. pWPI cGAS(P261H)-GFP was generated by site-directed mutagenesis (Stratagene California, La Jolla, CA), and the correct introduction of the mutation was confirmed by Sanger sequencing. Vector-containing supernatant was collected 40 and 64 h posttransfection and subjected to ultracentrifugation through a 20% sucrose cushion. To remove residual plasmid DNA,

concentrated virus stocks were DNase I digested twice and stored in aliquots at −80°C. VSV-G–pseudotyped HIV-1 NL4.3 luciferase reporter virus was produced by calcium phosphate–based transfection of HEK293T cells with a HIV-1 NL4.3 ΔEnv ΔVpr luciferase reporter plasmid (37) and a VSV-G–encoding plasmid. Virus-containing supernatants were harvested 60 h posttransfection and concentrated by ultracentrifugation.

HSV-1 Δ*UL41*N (HSV-1(KOS) UL41NHB) encoding a truncated version of pUL41 was provided by David A. Leib (38). To prepare concentrated stocks, extracellular virions were pelleted from the medium of cells infected at a multiplicity of infection of 0.01 PFU/cell for 3 d (39–41). Virus stocks were plaque titrated on Vero cells (40, 42). To determine the genome/PFU ratio of HSV-1 stocks, we quantified the number of HSV-1 genomes by quantitative PCR as described previously (39, 43).

Chikungunya virus (CHIKV) 181/25 infectious stock (44) expressing a nanoluciferase fused to the E2 glycoprotein (a gift from G. Simmons, Vitalant Research Institute) was produced by in vitro transcription of the full-length, linearized molecular DNA clone into RNA and subsequent RNA electroporation into BHK-21 cells. Virus-containing supernatant was collected 3 d after electroporation, filtered through membranes of 0.45-μm pores, and stored in aliquots at −80°C.

Flow cytometry

For quantification of cGAS-GFP expression in transduced THP-1 or HEK293T cells, cells were PFA fixed and GFP positivity was quantified by flow cytometry. HSV-1–challenged HEK293T cells were PBS washed, PFA fixed, and immunostained for intracellular HSV-1 VP5 using rabbit anti–HSV-1 VP5 (no. SY4563) and an appropriate fluorochrome-conjugated secondary Ab in 0.1% Triton X-100 in PBS (10, 45). Samples were analyzed on a FACSLyric device (Becton Dickinson, Franklin Lakes, NJ) with BD Suite software for analysis.

Immunoblotting

Cell lysates were generated with mammalian protein extraction reagent (M-PER; Thermo Fisher Scientific, Waltham, MA), run on a 10% SDS-PAGE, and transferred onto nitrocellulose using a semidry transfer system (Bio-Rad Laboratories, Hercules, CA). BSA-blocked membranes were incubated with the primary Abs mouse-anti human actin (no. 8226, Abcam, Cambridge, U.K.), rabbit-anti human cGAS (no. 15102, Cell Signaling Technology, Danvers, MA), rabbit-anti human IRF3 (no. 4302, Cell Signaling Technology), rabbit anti-human p-IRF3 (no. 29047, Cell Signaling Technology), rabbit anti-human p-STING (no.19781, Cell Signaling Technology), rabbit anti-human p-TBK1 (no. 5483, Cell Signaling Technology), rabbit anti-human STING (no. 13647S, Cell Signaling Technology), rabbit anti-human TBK1 (no. 3504, Cell Signaling Technology), or rabbit anti-human TREX1 (no. 185228, Abcam). Secondary Abs conjugated to Alexa Fluor 680/800 fluorescent dyes were used for detection and quantification by an Odyssey infrared imaging system (LI-COR Biosciences, Lincoln, NE).

Quantitative RT-PCR

Total RNA from cells was extracted using the RNeasy mini kit (Qiagen, Hilden, Germany), and residual DNA contaminations were removed with the RNase-free DNase set (Qiagen, Hilden, Germany). Following cDNA synthesis (New England Biolabs, Ipswich, MA), quantification of relative mRNA levels was performed using Taq-Man PCR technology (Thermo Fisher Scientific, Waltham, MA) with primer-probe kits (Applied Biosystems, Waltham, MA) for following genes: *ACTB* (Hs03023943_g1), *ARL16* (Hs01586770_g1), *BST2* (Hs00171632_m1), *cGAS* (Hs00403553_m1), *HAUS7* (Hs00213860_m1), *IFIT1* (IFN-induced protein with tetratricopeptide repeats 1; Hs01911452_s1), *IFN-β* (Hs01077958_s1), *IRF3* (Hs01547283_m1), *LYAR* (Hs00215132_m1), *MX2* (MX dynamin-like GTPase 2; Hs01550814_m1), *RPL30* (Hs00265497_m1), *RPS11* (Hs06642555_g1), *STING* (Hs00736958_m1), *TCP1* (Hs01053946_g1), *TREX1* (Hs03989617_s1), *TRMT10C* (Hs01933516_s1), *YBX1* (Hs00358903_g1).

Relative mRNA levels were determined in multiplex reactions using the ΔCt method with human *RNASEP* mRNA as an internal reference (Figs. 3B, 3C, 8, Supplemental Figs. 1C, 2C) or using the ΔΔCt method when normalizing mRNA levels to a nontreated or mock-infected control sample (Fig. 5C, Supplemental Fig. 3). Each sample was analyzed in technical triplicates and with parallel controls omitting reverse transcriptase. Assays were performed on an OneStepPlus machine (Applied Biosystems, Waltham, MA) or a LightCycler 480 II (Roche, Basel, Switzerland). Data analysis was performed using Applied Biosystems StepOne software (version 2.3) or LightCycler 480 software (version 1.5).

RNA sequencing

Total RNA extraction from cells and DNase treatment were performed with the RNeasy mini kit and RNase-free DNase set (Qiagen, Hilden, Germany). The quality and integrity of total RNA were verified on an Agilent Technologies 2100 Bioanalyzer (Agilent Technologies, Waldbronn, Germany). The RNA sequencing libraries were generated using TruSeq stranded mRNA library prep kits (Illumina, San Diego, CA) following the manufacturer's protocol. The libraries were sequenced on Illumina HiSeq 4000 (paired-end run 2 × 75 bp) with an average of 9×10^7 reads per RNA sample. Data generated from individual samples were mapped separately against the hg38 human reference genome. Gene expression was calculated for individual transcripts as reads per kilobase of transcript per million mapped reads (RPKM). All transcriptomic analyses were performed using Geneious Prime version 2020.0.4 (Biomatters, Auckland, New Zealand). Differentially expressed genes (DEGs) were identified by calculating fold changes in expression, and genes were considered to be expressed significantly differently when their expression was increased by at least a factor of two with a p value of <0.05. Gene Ontology (GO) enrichment analyses were performed using the Panther overrepresentation test (http://geneontology.org/), *Homo sapiens* reference list, and GO biological process complete annotation dataset. The p values were corrected using false discovery rates (46, 47).

Electroporation

Ten million THP-1 cells and PBMCs were electroporated (140 V, 1000 μF) in serum-free RPMI 1640 in the presence of endotoxin-free plasmid DNA (12 μg of DNA, or indicated quantities), 4 μg of cGAMP (InvivoGen, San Diego, CA), 4 μg of c-di-UMP (InvivoGen, San Diego, CA), or mock electroporated using a Gene Pulser Xcell electroporation instrument (Bio-Rad Laboratories, Hercules, CA) and 0.2-cm cuvettes.

HL116 cell–based detection of bioactive IFNs

Culture supernatants of individual cell lines were titrated on HL116 cells that express the luciferase gene under the control of the IFN-inducible 6-16 promoter (31). Six hours after inoculation, cells were PBS washed and luciferase expression was determined using cell culture lysis buffer (Promega, Madison, WI) and a luciferase assay system (Promega, Madison, WI). The concentration of IFN was quantified using an IFN-α2a (Roferon-A) standard curve.

Protein purification

The full-length human cGAS(WT) and cGAS(P261H) proteins were expressed in *Escherichia coli* BL21(DE3). The expression was induced by 0.5 M isopropyl β-D-thiogalactoside and incubated at 18°C for 18 h. After centrifugation at 5000 × *g* for 15 min, pellets were resuspended in 20 ml of PBS and centrifuged again at 5000 × *g* for 15 min. The cells were flash-frozen and stored at −80°C until purification. For purification, pellets were thawed and resuspended in a buffer containing 300 mM NaCl, 50 mM Na_3PO_4, and 10 mM imidazole (pH 7.5) with cOmplete protease inhibitor mixture (Roche, Basel, Switzerland) and lysed by sonification for 2 min, with 4-min breaks after each minute of sonification to prevent overheating of the lysate. DNase I was added to remove a possible impurity caused by the cellular DNA bound to cGAS. After 30 min of incubation at room temperature, the sample was centrifuged at 40,000 × *g* for 1 h. The supernatant was filtered using a 0.45-μm syringe filter and loaded onto a 5-ml Protino Ni-NTA column (Macherey-Nagel, Düren, Germany). The column was washed until UV280 had reached a steady value and eluted with 500 mM imidazole, 150 mM NaCl, and 50 mM Na_3PO_4 (pH 7.5). The pooled fractions were diluted with low-salt buffer (50 mM NaCl, 20 mM Tris [pH 7.5]) to prevent protein aggregation caused by a high salt concentration of the elution buffer. The diluted eluate was then loaded onto a 1-ml HiTrap heparin HP column (GE Healthcare, Chalfont St Giles, U.K.). After loading, the column was washed until UV280 reached a steady value before elution with an increasing salt gradient buffer: 50 mM–2 M NaCl, 20 mM Tris (pH 7.5). The elution was concentrated by centrifugation with 30,000 Da molecular mass cutoff Vivaspin-Hydrosart (Sartorius, Göttingen, Germany) and, if needed, diluted with low-salt buffer to the final protein concentration used for the in vitro activity assay. The purified protein was flash-frozen in liquid nitrogen and stored at −80°C.

In vitro cGAS activity assay

Recombinant human cGAS (2 μM) was incubated for 2 h at 37°C with the substrates 0.5 mM ATP and 0.5 mM GTP, in the presence of 1 ng/μl dsDNA fragments (NoLimits; Thermo Fisher Scientific, Waltham, MA) of 1, 4, or 6 kb length, in a buffer containing 120.25 mM $MnCl_2$, 20 mM NaCl, 2.5 mM $MgCl_2$, and 8 mM Tris-HCl (pH 7.5) in a total volume of 200 μl. Following incubation, samples were inactivated at 95°C for 20 min. Samples were centrifuged at 14,500 rpm for 15 min at 4°C, and the supernatant was diluted 1:100 with H_2O for HPLC measurement with the API 4000 liquid chromatography–tandem mass spectrometry system (Sciex, Framingham, MA) for cGAMP quantification. The gradient started with 100% buffer

A (3/97 [v/v] MeOH/H_2O, 50 mM NH_4Ac, 0.1% HAc) and reached 50% buffer A, 50% buffer B (97/3 [v/v] MeOH/H_2O, 50 mM NH_4Ac, 0.1% HAc) after 5 min. The sample was run over a ZORBAX Eclipse XDB-C18 1.8-μm, 50 × 4.6-mm (Agilent Technologies, Waldbronn, Germany) column. Measurements and data generation were controlled by Analyst software (version 1.5.2, Sciex). Calibration was conducted with 10 μl of synthetic-derived cGAMP mixed with 800 μl of extraction reagent (2/2/1 [v/v/v] methanol, acetonitrile, and water mixture) and 300 μl of extraction reagent (25 ng/ml tenofovir in extraction reagent) with tenofovir as the internal standard.

Infection and transduction assays

Thirty minutes prior to lentiviral transduction, cells were left untreated or treated with efavirenz (EFV; 100 nM). Inhibitor treatment was maintained during the subsequent virus inoculation. Transduction and virus infection assays were performed by spinoculation for 60 min at 32°C. Following spinoculation, cells were incubated at 37°C, 5% CO_2, and individual wells were harvested at the indicated time points.

Luciferase assay

Luciferase expression of cells challenged with VSV-G lentiviral vectors or VSV-G/HIV-1 NL4.3 was quantified at 72 h posttransduction. Cells were washed with PBS, lysed using cell culture lysis buffer (Promega, Madison, WI), and luciferase activity was quantified using a luciferase assay system (Promega, Madison, WI). To detect nanoluciferase expression in supernatants from CHIKV-infected cells, the Nano-Glo luciferase assay system (Promega, Madison, WI) was used according to the manufacturer's instructions.

LPS and polyinosinic-polycytidylic acid treatment

IL-2/PHA–activated PBMCs were treated with 40 ng/ml LPS or 20 μg/ml polyinosinic-polycytidylic acid (poly(I:C)) as previously described (48, 49).

Reagents and inhibitors

Fragmented dsDNA (NoLimits 100-bp DNA fragment) for in vitro experiments were obtained from Thermo Fisher Scientific. LPS and poly(I:C) were purchased from Sigma-Aldrich (St. Louis, MO). Human IFN-α2a (Roferon-A) was purchased from Roche. cGAMP and c-di-UMP were purchased from InvivoGen. EFV was purchased from Bristol Myers Squibb. The 18-bp dsDNA fragment (5′-CTACTAGTGATCTATGACTG-3′) (26) was purchased from Integrated DNA Technologies, and 45-bp DNA (ISD) and 70-bp DNA (VACV-70) were purchased from InvivoGen.

Genotyping of PBMCs for rs610913

Two hundred microliters of freshly drawn EDTA-anticoagulated venous whole blood (S-Monocette K3 EDTA, Sarstedt, Hümbrecht, Germany) was subjected to DNA isolation using the QIAamp DNA blood mini kit on a QIAcube (both from Qiagen) instrument following the manufacturer's instructions. For genotyping, an *MB21D1* rs610913-specific TaqMan primer set (Thermo Fisher Scientific, C_937459_20), diluted 20×, was used with 20 ng of genomic DNA, and the appropriate amounts of TaqMan Universal MasterMix II (Thermo Fisher Scientific) in a 10-μl reaction volume were run in triplicate wells of a 96-well MicroAmp plate run on a QuantStudio 7 quantitative PCR cycler (Thermo Fisher Scientific) and QuantStudio real-time PCR software v1.3.

DNA transfection assay

For transfection of short dsDNA fragments, THP-1 cells were PMA differentiated for 48 h using 25 nM PMA followed by a 24-h culture period in fresh RPMI 1640 medium. THP-1 cells were then transfected using Lipofectamine 2000 (Thermo Fisher Scientific) and the indicated dsDNA quantities. *IFIT1* mRNA was quantified 4 h after transfection.

Data availability

RNA sequencing datasets are deposited at the National Center for Biotechnology Information Gene Expression Omnibus database (accession number GSE203334; https://www.ncbi.nlm.nih.gov/geo/query/acc.cgi?acc=GSE203334).

Data presentation and statistical analysis

Unless otherwise stated, bars and symbols show the arithmetic mean and error bars the SEM of the indicated number of individual experiments. Statistical significance was calculated by performing a paired Student *t* test using GraphPad Prism 8 (*$p < 0.05$, **$p < 0.01$; not significant, $p \geq 0.05$).

Results

rs610913 may facilitate HIV-1 acquisition in vivo

In the human population, the coding region of the cGAS-encoding gene *MB21D1* harbors several nonsynonymous SNPs of different frequencies (Table I). The allele frequencies vary substantially across populations, with rs610913 being the most frequent nonsynonymous SNP (Table I). We searched for SNPs in *MB21D1* displaying an association with HIV-1 acquisition using summary statistics covering 6334 infected cases and 7247 controls of European ancestry (25) (Fig. 1A). Interestingly, we detected a nominal, but not genome-wide significant, overrepresentation of rs610913 ($p = 0.004$) in HIV-1–infected individuals as compared with the uninfected control cohort, suggesting that this SNP may associate with and/or facilitate HIV-1 acquisition. Analyzing rs610913 in more detail across the six included subgroups indicated that the signal was primarily arising from group 3, a group consisting of North American individuals and enriched for HIV controllers (25) (Fig. 1B). Given its high global frequency and its potential role in HIV-1 acquisition, we embarked on a functional study of rs610913.

Structural modeling of cGAS(P261H) reveals amino acid position at the "head-to-head" interface of the cGAS ladder-like assembly

To investigate the structural impact of the cGAS(P261H) mutation, we built a molecular model of the hcGAS(P261H)·dsDNA assembly in the active (ATP-bound) conformational state. The overall structure of this assembly is based on the experimental ladder-like cGAS·dsDNA crystallographic model obtained for the mouse enzyme (mcGAS) (26). The positions of mcGAS molecules in the ladder-like assembly were substituted by the homology model of the hcGAS(P261H) mutant based on the structure of the WT hcGAS·dsDNA·ATP complex (PDB code 6CTA) (27). The model of the hcGAS P261H·dsDNA·ATP ladder-like assembly was optimized, and the geometry of the resulting model (Fig. 2) appeared to be very close to the original mcGAS·dsDNA assembly due to the high structural and sequence similarity (root mean square deviation 1.0 Å, sequence identity 70%) between the human and mouse enzymes. In the hcGAS(P261H)·dsDNA·ATP ladder-like structure,

Table I. Allele frequency of most abundant nonsynonymous SNPs in the cGAS-encoding gene *MB21D1*

			Total		African		Europe	
SNP	Alleles	Amino Acids	Reference	Alternative	Reference	Alternative	Reference	Alternative
rs9352000	G>T	T35N	15.65	84.35	14.37	85.63	16.28	83.72
rs610913	G>T	P261H	49.72	50.28	63.09	36.91	35.59	64.41
rs35629782	G>T	A48E	94.98	5.02	98.44	5.51	94.49	5.51
rs141133909	C>T	G101R	97.95	2.05	99.38	0.62	97.79	2.21
rs145259959	A>G	L239P	99.80	0.20	99.98	0.02	99.78	0.22
rs138984002	T>A	Y483F	99.96	0.04	99.74	0.26	100.00	0.00
rs114473784	C>T	E422K	99.96	0.04	98.73	1.27	100.00	0.00
rs141390590	G>T	F433L	99.98	0.03	100.00	0.00	99.97	0.03
rs146116825	G>C	S393C	99.98	0.02	99.90	0.10	100.00	0.00

Shown are the respective single nucleotide exchange, resulting amino acid substitution, and relative allele frequencies of the reference and alternative alleles in the African, European, and global populations.

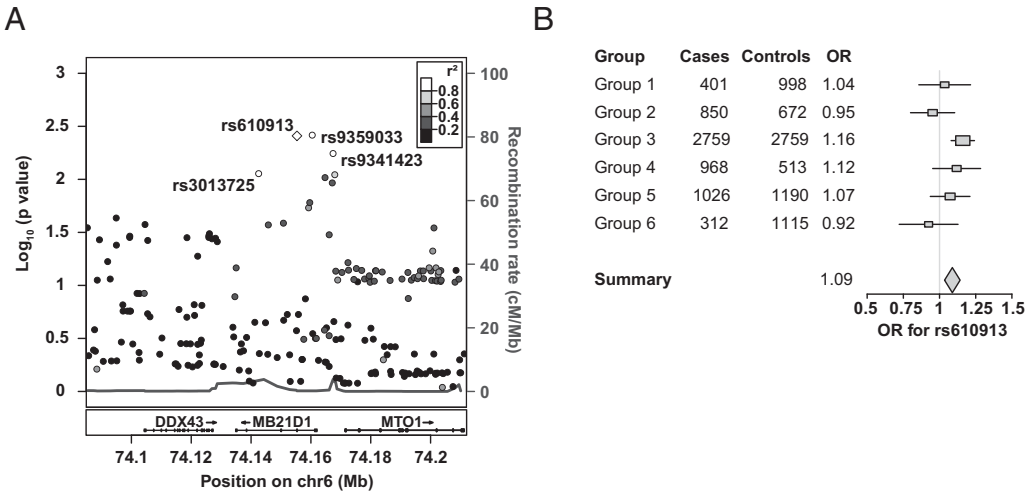

FIGURE 1. rs610913 may facilitate HIV-1 acquisition in vivo. (**A**) Regional association plot of the *MB21D1* region, containing all SNPs included in the meta-analysis and their respective *p* values. The plot is centered on rs610913 (white diamond), with white dots indicating SNPs in high linkage disequilibrium (LD) ($r^2 > 0.8$), and light gray dots representing SNPs in moderate or low LD. All SNPs in high LD with rs610913 are synonymous SNPs. (**B**) Forest plot of the odds ratios (OR) for rs610913 with 95% confidence intervals across all subgroups and after meta-analysis (diamond) within the International Collaboration for the Genomics of HIV genome-wide association studies of HIV-1 acquisition. The number of cases and controls are indicated for each group along with their respective odds ratios.

the H261 residue is located far away from the active site in the deep cleft created by the head-to-head interface between the two hcGAS monomers bound to the dsDNA (Fig. 2). Another H261 residue from the neighboring head-to-head hcGAS(P261H) molecule is located at the bottom of the same site. Together, two imidazole rings of the H261 residues create a positively charged surface at the bottom of the head-to-head hcGAS P261H cleft (Fig. 2D). The distance between the two H261 residues in the cleft is rather large (~11 Å), which makes direct interaction between them unlikely. The distances between H261 and the two dsDNA molecules (9.3 and 15.6 Å) also do not allow direct contact (Fig. 2C). At the same time, the side chain of H261 makes two new hydrogen bonds with the side chains of S201 and E259 of the same monomer, which is not possible for the proline side chain of P261 in the WT enzyme (Fig. 2C). These hydrogen bonds could provide additional stabilization of cGAS(P261H) monomers in the head-to-head cleft and may contribute to the overall stability of the cGAS·dsDNA assembly. Because S201, E259, and H261 residues are located in a solvent-accessible area, the free energy of their interaction may be expected to be diminished by the solvent effects. Thus, the modeling analysis indicates that cGAS P261H is not

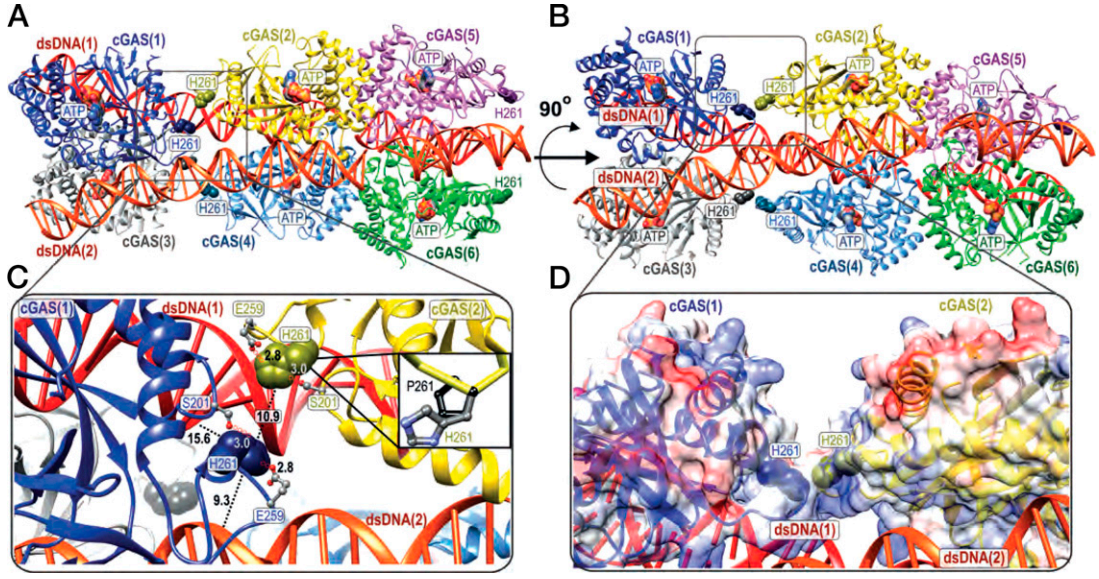

FIGURE 2. Structural model of cGAS(P261H) reveals amino acid position at head-to-head interface of the cGAS ladder-like assembly. (**A** and **B**) Structural models of human cGAS(P261H)·dsDNA oligomeric assembly created using the ladder-like crystal structure of mouse cGAS in complex with dsDNA (PDB ID 5N6I) and the structure of the hcGAS(WT)·dsDNA·ATP complex (PDB ID 6CTA) as starting coordinates. The cGAS(P261H) monomers are shown in blue, yellow, magenta, gray, cyan, and green. The two dsDNA molecules are shown in orange and red. The residues H261 in the cGAS(P261H) monomers are represented with a Corey–Pauling–Koltun model with the corresponding colors. The ATP binding sites are indicated using molecular surface representation. (**C**) Detailed view of H261 localization. The closest distances between H261 residues and the dsDNA molecules are shown with dotted black lines. The hydrogen bonds between H261, S201, and E259 are traced with red circles. The close-up panel in the black box shows the comparison of H261 and P261 side-chain structures. (**D**) Molecular surface representation of the head-to-head interface cleft between the two cGAS(P261H) monomers bound to the dsDNA molecules. The semitransparent surface is colored according to the molecular electrostatic potential with positive, negative, and neutral charges represented by the blue, red, and white colors, respectively. The residues H261 are shown using the Corey–Pauling–Koltun model representation.

expected to cause a significant discrepancy in enzymatic activity compared with the WT enzyme, although the overall stability of the multimeric complex with DNA could be affected slightly.

Catalytically active cGAS modulates baseline levels of IFIT1, MX2, *and* IFNB1 *mRNA expression*

To address functional consequences that may result from the proline-to-histidine exchange encoded by rs610913, we stably expressed individual cGAS-GFP variants in THP-1 cGAS KO cells by lentiviral transduction, including cGAS(WT)-GFP, catalytically inactive cGAS(G212A, S213A)-GFP (50), and cGAS(P261H)-GFP. Assessment of GFP expression by flow cytometry and of cGAS expression by immunoblotting confirmed similar expression levels of the transgenes in individual cell lines, as opposed to mock-transduced THP-1 cGAS KO cells (Fig. 3A). Other key components of the cGAS signaling cascade, such as STING, IRF3, and TREX1, were expressed at similar levels in the four cell lines (Fig. 3B), indicating that abrogation of cGAS expression or of its catalytic activity did not affect mRNA or protein quantities of gene products involved in this pathway. Interestingly, basal expression of *IFIT1* mRNA was clearly reduced in cells devoid of cGAS expression and in cells expressing catalytically inactive cGAS, as compared with cells expressing either cGAS(WT) or cGAS(P261H) (Fig. 3C). A similar trend was observed for *MX2* and *IFNB1* mRNA levels; however, only *MX2* mRNA levels in cGAS KO cells compared with cells expressing cGAS(WT) reached a statistically significant difference.

Expression of functional cGAS induces global transcriptomic alterations in THP-1 cells

To explore transcriptional profiles associated with expression of individual functional and nonfunctional cGAS variants, we subjected total RNA of indicated THP-1 cells to sequencing. Plotting of all RPKM values >0.5 revealed a high overall correlation in the gene expression profile between the individual samples (Fig. 4A). cGAS(WT) and cGAS(P261H) cells (Fig. 4A, top panel) shared a similar expression profile. Comparison of cGAS(WT) or cGAS(P261H) with the catalytically inactive cGAS(G212A/S213A) revealed a set of 77 and 115 genes significantly upregulated exclusively in the context of the functional cGAS variants, respectively, suggesting that expression of those genes requires cGAS base-level activity (Fig. 4B, middle and bottom panels). Interestingly, GO analysis revealed that the genes whose expression was overrepresented in cGAS(WT)- and cGAS(P261H)-expressing cells, as compared with cGAS (G212A/S213A) cells, joined common gene sets, including cellular defense mechanisms to invading pathogens (GO:0009615, response to virus; GO:0051607, defense response to virus) or type I IFN signaling (GO:0034340, response to type I IFN; GO:0060337, type I IFN signaling pathway) (Fig. 4C, middle and bottom panels). In accordance, the 50 most DEGs among all significant DEGs in cGAS(WT) compared with cGAS(G212A/S213A) samples represented mostly ISGs (43 ISGs out of 50 DEGs), such as *IFI44L*, *IFI27*, and *MX1* or important components of the type I IFN signaling axis, such as *STAT1* and *IRF7* (Fig. 4D). In line with previous experiments, known components or modulators of the cGAS/STING signaling axis were equally expressed throughout all cell lines, independent of functional cGAS expression (Supplemental Fig. 1A).

Although the overall transcriptome of cGAS(WT)- and cGAS(P261H)-expressing THP-1 cells appeared very homogeneous (Fig. 4A, top panel), 67 genes were DEGs that reached statistical significance (Fig. 4B, top panel). These genes, however, displayed low or moderate expression fold changes and *p* values. In addition, GO enrichment analysis revealed enrichment of gene sets with only moderate *p* values and divergent functions (Fig. 4C, top panel), indicating that expression of cGAS(P261H) does not severely modulate the cellular

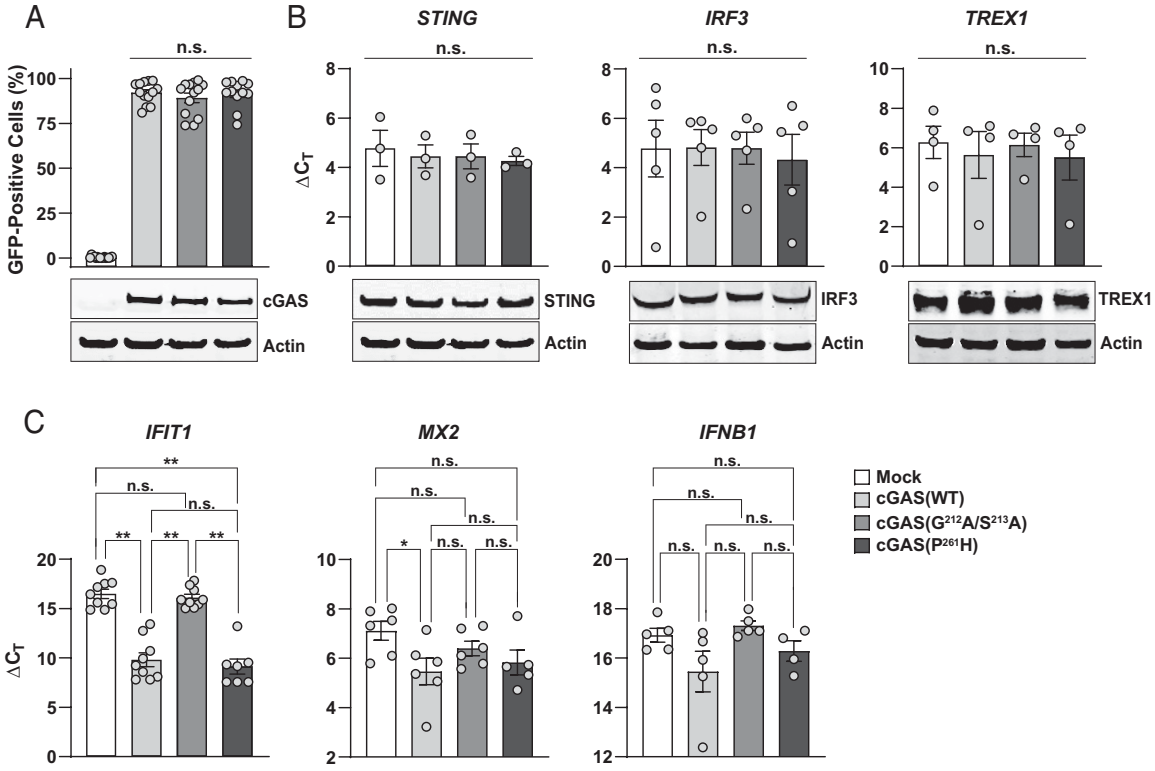

FIGURE 3. Catalytically active cGAS modulates baseline levels of *IFIT1*, *MX2*, and *IFNB1* mRNA expression. (**A**–**C**) THP-1 cGAS KO cells were stably transduced with indicated GFP-cGAS variants and analyzed for: (A) percentage of GFP-positive cells and steady-state cGAS protein expression by flow cytometry and immunoblotting, respectively; (B) relative expression of *STING*, *IRF3*, and *TREX1* mRNA by quantitative RT-PCR and immunoblotting of indicated proteins; and (C) relative *IFIT1*, *MX2*, and *IFNB1* mRNA expression levels by quantitative RT-PCR. Error bars indicate SEM from three or more independent experiments. Immunoblots shown are representative blots of two or more experiments. *$p < 0.05$, **$p < 0.01$; n.s., not significant.

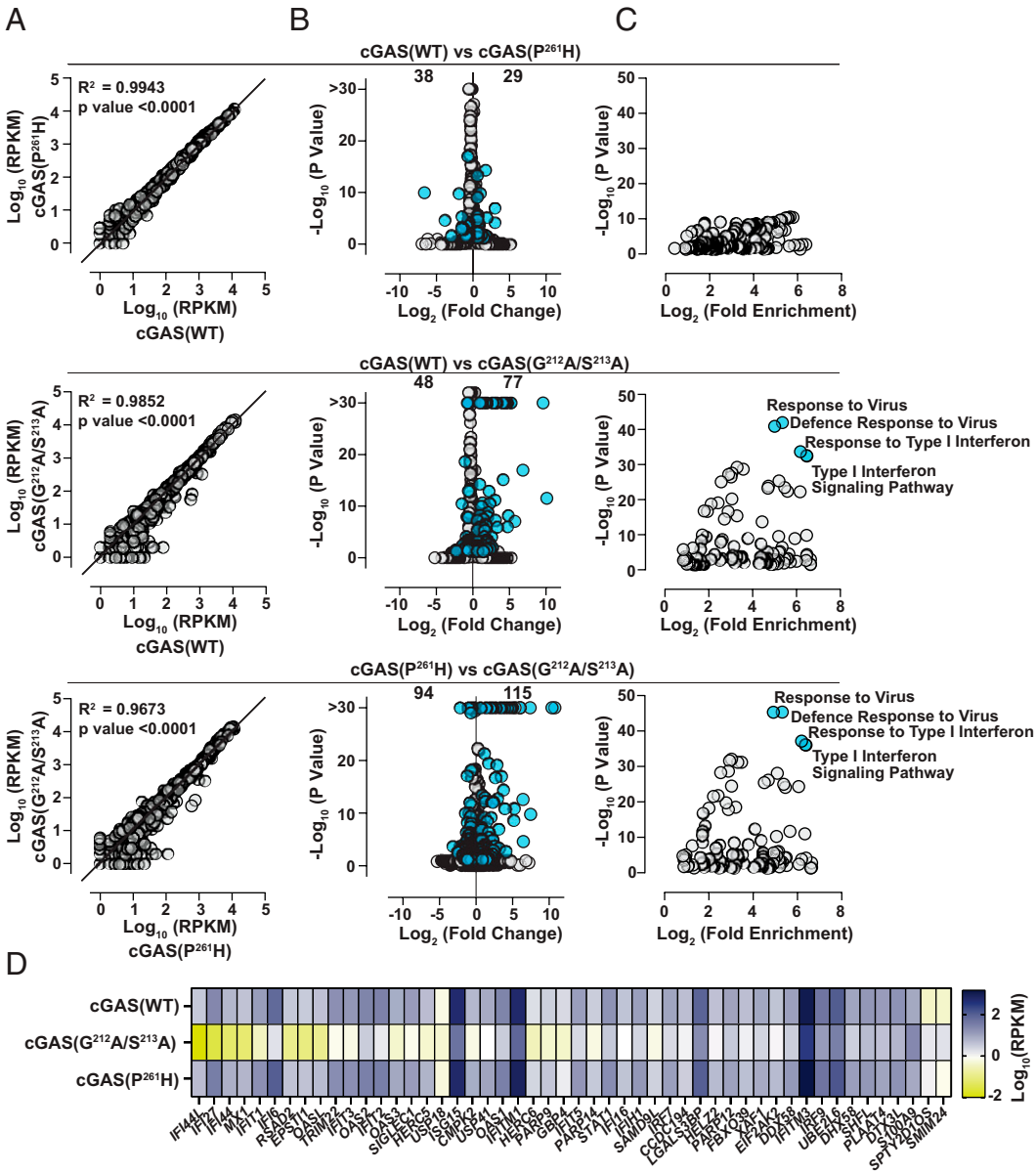

FIGURE 4. Expression of functional cGAS induces global transcriptomic alterations in THP-1 cells. (**A**–**D**) Bulk RNA sequencing analysis was conducted with total RNA extracted from THP-1 cGAS KO cells stably expressing indicated cGAS variants. (A) Plot of all raw RPKM values >0.5 of the indicated samples. (B) Identification of differentially expressed genes in cGAS(WT) versus cGAS(P261H), cGAS(WT) versus cGAS(G212A/S213A), or cGAS(P261H) versus cGAS(G212A/S213A) samples by plotting the gene expression fold change and *p* values of all differentially expressed genes. Genes with a *p* value <0.05 and a >2-fold change are highlighted in blue. (C) GO analysis of genes significantly upregulated in cGAS(P261H)- versus cGAS(WT)-, cGAS(WT)- versus cGAS(G212A/S213A)-, or cGAS(P261H)- versus cGAS(G212A/S213A)-expressing cells. (D) Heatmap showing the RPKM values of the 50 DEGs of highest absolute fold change of all statistically significant ($p < 0.05$) DEGs in cGAS(WT) versus cGAS(G212A/S213A) samples. Genes are ranked based on their absolute fold change.

transcriptome. We selected 10 candidate genes based on fold change and statistical significance (Supplemental Fig. 1B) and evaluated their expression by quantitative RT-PCR (Supplemental Fig. 1C), aiming at challenging the findings obtained with RNA sequencing. In line with the rather subtle differences in the transcriptomes of cGAS(WT)- and cGAS(P261H)-expressing cells, analysis of several independent samples by quantitative RT-PCR confirmed only *TCP-1* out of the 10 tested candidate genes as a true DEG whose expression is specifically increased in the context of cGAS(P261H) expression, thus displaying lower mRNA levels in cGAS(WT)-expressing cells.

In summary, the transcriptomic data provide further evidence for a baseline antiviral immunity in cells expressing functional cGAS(WT) or cGAS(P261H), and both cGAS variants control an overall highly similar cellular transcriptome. In contrast, the absence of cGAS expression or expression of a functionally inactive cGAS mutant decreased the antiviral state of the cell as reflected by lower expression of genes related to virus defense and the type I IFN response.

cGAS(WT) and cGAS(P261H) expression reduces susceptibility to lentiviral transduction in the absence of transduction-provoked innate immune responses

Because rs610913 may associate with increased probability of HIV-1 infection in vivo, we next investigated whether expression of cGAS(P261H) renders cells more susceptible to infection by HIV-1 and other viruses. Specifically, we challenged THP-1 cGAS KO cells reconstituted with cGAS(WT), cGAS(G212A/S213A), or cGAS(P261H)

with VSV-G–pseudotyped lentiviral particles or HIV-1 NL4.3 and monitored the transduction efficiency. Interestingly, cells devoid of cGAS expression or expressing the catalytically inactive mutant displayed higher susceptibility to lentiviral transduction as compared with cGAS(WT)- or cGAS(P261H)-expressing counterparts (Fig. 5A, 5B). However, cGAS(WT)- and cGAS(P261H)-expressing cells shared identical susceptibility to lentiviral transduction.

Importantly, transduction of cells with ablated cGAS expression or expressing individual cGAS variants did not induce expression of *IFIT1*, *MX2*, and *IFNB* mRNAs or secretion of bioactive IFN into the culture supernatant in an EFV-sensitive fashion (Fig. 5C). Lentiviral transduction triggered induction of *IFIT1* mRNA expression to a maximum of 2.9- to 7.1-fold in all four cell lines, irrespective of their cGAS expression status or EFV treatment. These results are consistent with absence of cGAS-mediated responses to lentiviral infection reported by others (9, 11) and us (10), suggesting that detectable differences in the susceptibility of our cell lines to transduction are linked to different antiviral states.

Baseline antiviral state mediated by cGAS(WT) and cGAS(P261H) expression renders cells less susceptible to HSV-1 and CHIKV infection

To explore the role of cGAS in the context of infection with other viruses displaying individual replication strategies and genomic architectures, we reconstituted HEK293T cells, which lack detectable cGAS and STING expression, and HEK293T mCherry-STING cells (1) with individual cGAS variants (Supplemental Fig. 2A, 2B). In line with results obtained in THP-1 cells, expression of STING,

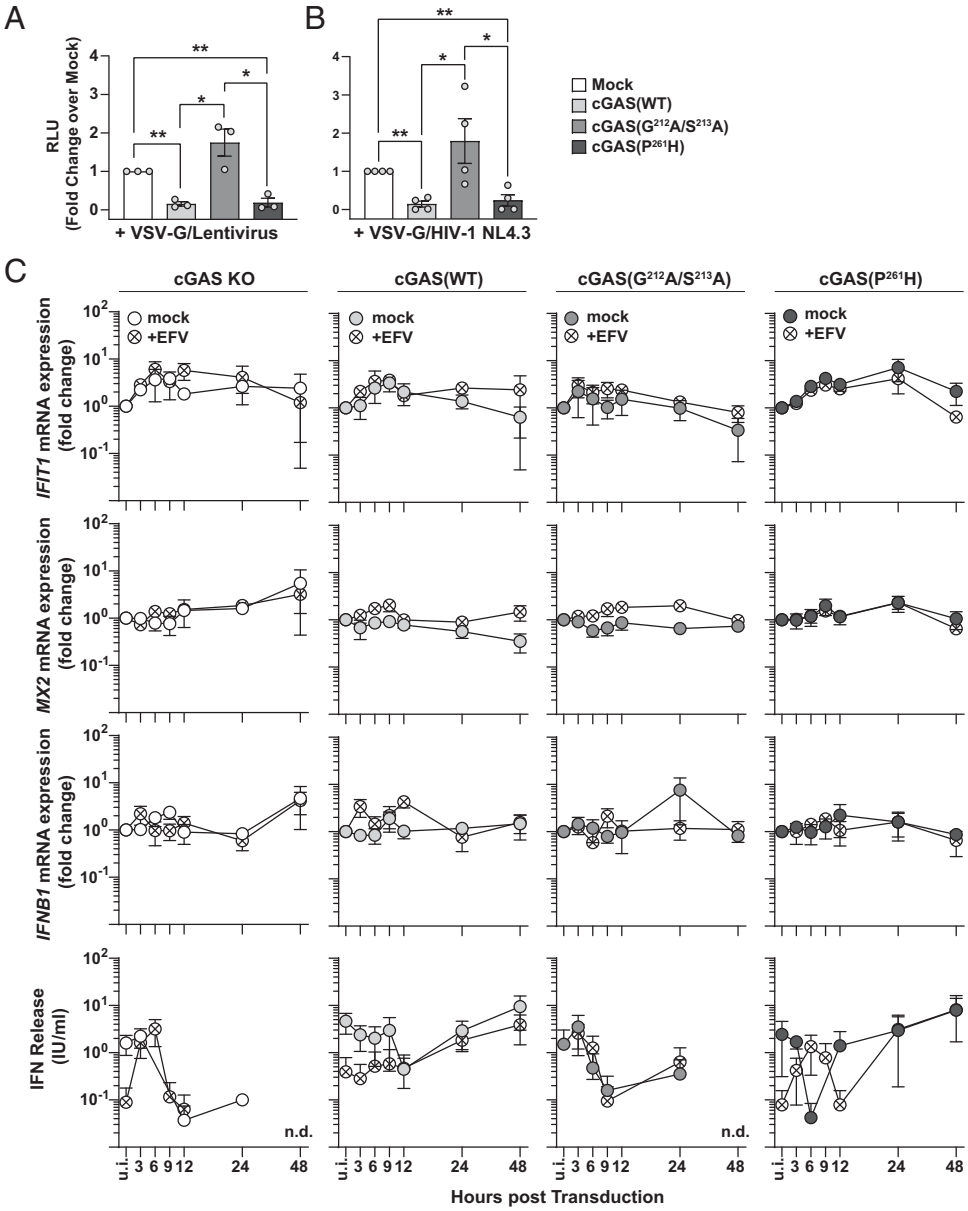

FIGURE 5. cGAS(WT) and cGAS(P261H) expression reduces susceptibility to lentiviral transduction in the absence of transduction-provoked innate immune responses. (**A**) THP-1 cells were transduced with VSV-G–pseudotyped lentiviral vectors and analyzed for luciferase reporter expression at 72 h posttransduction. Shown is the fold change over THP-1 cGAS KO cells ($n = 3$). (**B**) THP-1 cells were infected with VSV-G–pseudotyped HIV-1 NL4.3 luciferase, and luciferase reporter expression was analyzed at 72 h posttransduction. Shown is the fold change over THP-1 cGAS KO cells ($n = 4$). (**C**) Indicated THP-1 cells were transduced with VSV-G–pseudotyped lentiviral vectors in the presence or absence of the reverse transcriptase inhibitor efavirenz (EFV). Shown are *IFIT1*, *MX2*, and *IFNB* mRNA expression levels and the release of bioactive IFNs in cell culture supernatants at the indicated time points ($n = 3$). $^{*}p < 0.05$, $^{**}p < 0.01$, by Student *t* test.

IRF3, and TREX1 was not affected by complementation of cGAS expression in HEK293T cells (Supplemental Fig. 2C, 2D). Reconstitution with both cGAS and STING expression largely restored the cGAS-dependent base-level induction of *IFIT1*, *MX2*, and *IFNB1* expression in HEK293T cells (Supplemental Fig. 2E). Based on these observations, we considered cGAS/STING-expressing HEK293T cells as a suitable model to monitor cGAS-dependent restriction of viral infections. As a prototypic DNA virus, we used an HSV-1 strain that encodes a truncated version of pUL41, a well-characterized cGAS antagonist (6, 38). Cells expressing cGAS(WT) or cGAS (P261H) were less susceptible to infection with HSV-1 Δ*UL41*N. Their rate of HSV-1 Vp5-positive cells scored to 57.8% and 50.8%, respectively, as opposed to 69.5% in cGAS(G212A/S213A)-expressing cells and 65.9% in cGAS-negative cells, although only the differences between cGAS(WT)- or cGAS(P261H)- and cGAS (G212A/S213A)-expressing cells and cGAS(P261H) and cGAS KO cells reached statistical significance (Fig. 6A). Strikingly, the same pattern was observed in the context of CHIKV strain 181/25, an RNA virus (Fig. 6B). In this study, cGAS(WT)- or cGAS(P261H)-expressing cells displayed luciferase reporter expression of 5.180 and 5.177 relative light units, respectively, as compared with cGAS(G212A/S213A)-expressing cells that yielded a mean value of 16.760 relative light units. Taken together, these data support the idea that cGAS maintains a baseline antiviral milieu that acts in a broad manner against invading viral pathogens. Conclusively, beyond sensing viral DNA intermediates or stress-induced host DNA released from intracellular compartments during an ongoing infection, cGAS expression and steady-state activity may maintain a static antiviral state that represents a hurdle for viral infections that are sensitive to the cGAS--controlled antiviral ISG program.

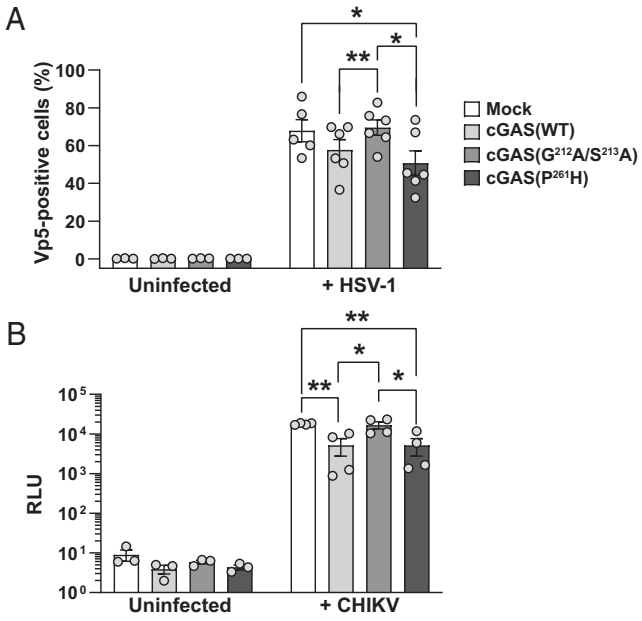

FIGURE 6. Baseline antiviral state mediated by cGAS(WT) and cGAS(P261H) expression renders cells less susceptible to HSV-1 and CHIKV infection. (**A**) 293T mCherry-STING cells stably expressing cGAS variants were challenged with HSV-1 Δ*UL41*N followed by quantification of intracellular HSV-1 Vp5 protein expression by flow cytometry. (**B**) 293T mCherry-STING cells stably expressing cGAS variants were infected with CHIKV 181/25 luciferase reporter strain followed by luciferase detection at 48 h postinfection. Error bars indicate SEM from three or more individual experiments. *$p < 0.05$, **$p < 0.01$, by Student *t* test; n.s., not significant.

cGAS(P261H) and cGAS(WT) share an overall similar ability to sense DNA in THP-1 cells

We next investigated the functionality of cGAS-mediated DNA sensing and induction of the type I IFN response of THP-1 cells expressing cGAS(P261H) as compared with cGAS(WT) by quantifying the type I IFN response provoked upon electroporation with endotoxin-free plasmid DNA. Of note, human cGAS is efficiently activated upon binding to long dsDNA, as opposed to binding to short DNA fragments (26, 27). Electroporation of plasmid DNA resulted in the release of bioactive IFN at concentrations of 11,158 and 33,652 IU/ml into supernatants of cells expressing cGAS(WT) or cGAS(P261H), respectively (Fig. 7A). In contrast, cGAS KO cells and cells expressing the inactive cGAS(G212A/S213A) mutant barely responded to plasmid DNA challenge and displayed responses that did not exceed the levels of mock-electroporated cells. Electroporation with the STING agonist cGAMP, but not the control cyclic dinucleotide c-di-UMP, induced release of similar levels of bioactive IFNs in all tested cell lines, indicating the intactness of the STING signaling axis (Fig. 7A). Similarly, phosphorylation of STING, TBK1, and IRF3 upon plasmid DNA challenge was detectable as early as 0.5 and 1 h after plasmid DNA challenge in cells expressing cGAS(WT) and cGAS(P261H), whereas lysates from both THP-1 cGAS KO cells and THP-1 cells expressing cGAS(G212A/S213A) scored negative in this assay, as expected (Fig. 7B). Although the quality and kinetics of the type I IFN response upon challenge with a fixed plasmid copy number did not reveal gross differences between cGAS(WT) and cGAS(P261H), titration of plasmid DNA uncovered a slightly inferior ability of cGAS(P261H) over cGAS(WT) to induce *IFIT1* mRNA expression (Fig. 7C), but not release of bioactive IFNs in the cell culture supernatant (Fig. 7D). Although stimulation with a short 18-bp dsDNA fragment did not result in any cGAS-dependent *IFIT1* mRNA induction, as expected (26), stimulation with 45- and 70-bp dsDNA fragments both resulted in a dose-dependent *IFIT1* mRNA induction that was largely dependent on catalytically active cGAS (Supplemental Fig. 3). However, no statistically significant differences between cells expressing cGAS(WT) or cGAS(P261H) were detectable. To unravel potentially different inherent catalytic activities of cGAS(WT) and cGAS(P261H), both proteins were expressed in *E. coli*, purified and incubated with dsDNA fragments of 1-, 4-, or 6-kb length in the presence of ATP and GTP. Both proteins presented similar in vitro enzymatic activities as judged by cGAMP quantification by liquid chromatography–tandem mass spectrometry, with a trend toward higher cGAMP production by cGAS(P261H) as compared with cGAS(WT) (Fig. 7E). For both cGAS variants, the enzymatic activity increased with augmenting dsDNA length, in accordance with other reports on cGAS(WT) (26, 51). In summary, while our in vitro data seem to suggest a slightly inferior in vitro catalytic activity of cGAS (WT) as compared with cGAS(P261H), our functional data in cells indicate a slightly superior sensitivity of the WT protein to DNA that manifests at suboptimal DNA quantities.

rs610913 homozygosity results in a trend toward a lower cell-intrinsic response to plasmid DNA, but not to LPS and poly(I:C) challenge

According to data from the 1000 Genomes Project (24), the SNP rs610913 displays an allele frequency of 35.6–63.1% in humans. PBMCs from a cohort of healthy individuals were isolated and stratified upon genotyping of corresponding whole blood. Steady-state *IFIT1* mRNA expression levels were similar in PBMCs from individuals homozygous for the WT variant and individuals homozygous for rs610913 (Fig. 8A). *IFIT1* mRNA expression was slightly, but not significantly, increased in the rs610913 SNP group

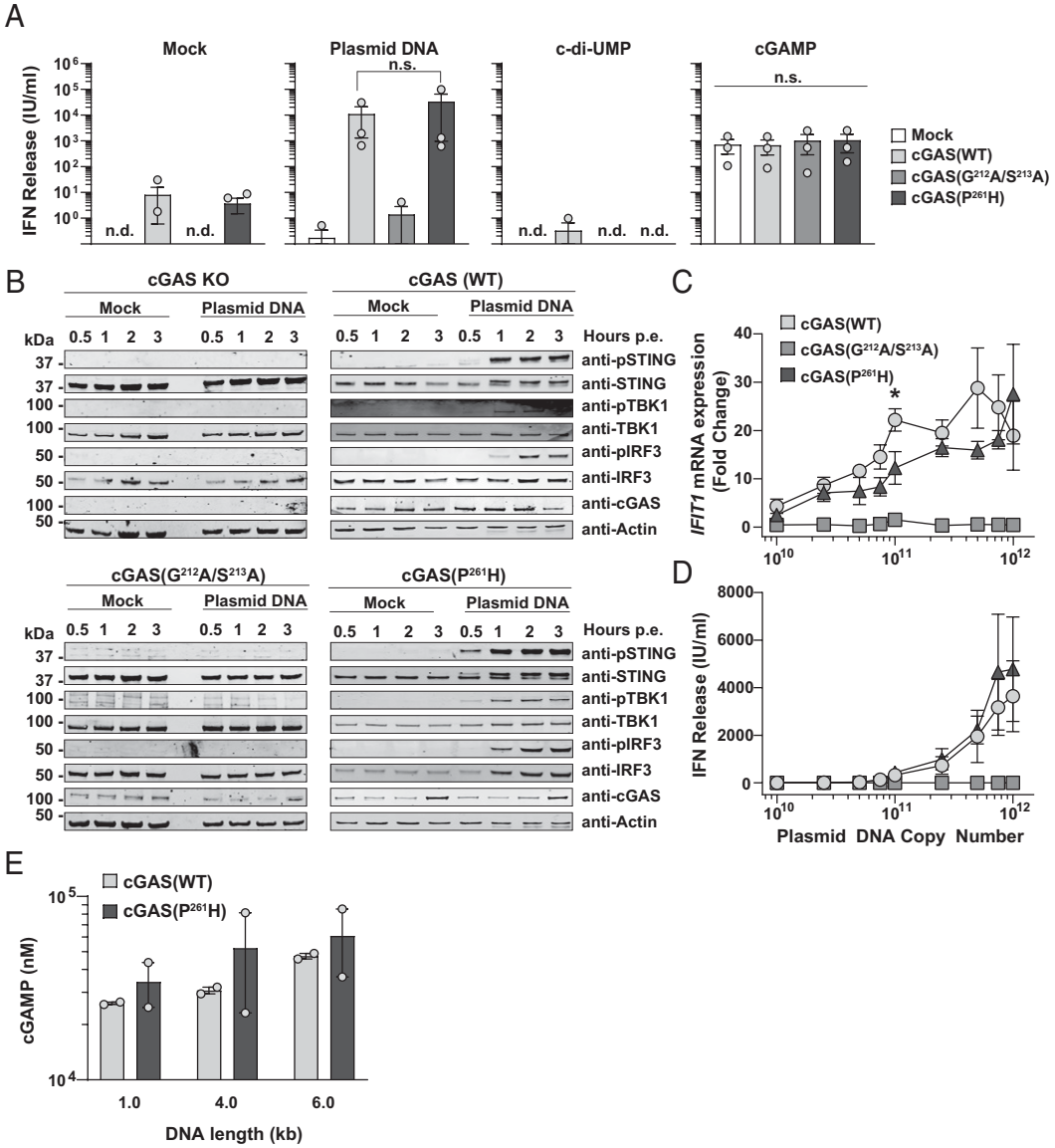

FIGURE 7. cGAS(P261H) and cGAS(WT) share an overall similar ability to sense DNA in THP-1 cells. (**A**) Indicated THP-1 cells were electroporated with plasmid DNA (12 μg), c-di-UMP (6 μg), cGAMP (6 μg), or mock electroporated. Shown is the release of bioactive IFNs in cell culture supernatants. (**B**) Immunoblotting of indicated total and phosphorylated proteins was performed using lysates from indicated THP-1 cells electroporated with plasmid DNA (12 μg) or mock electroporated and collected at the indicated time points postchallenge. One representative blot of two is shown. (**C**) *IFIT1* mRNA expression of indicated THP-1 cells electroporated with increasing amounts of plasmid DNA. (**D**) Release of bioactive IFNs in cell culture supernatant indicated THP-1 cells electroporated with increasing amounts of plasmid DNA. (**E**) The in vitro activity of purified cGAS(WT) and cGAS(P261H) proteins in the presence of dsDNA fragments of various lengths (1, 4, and 6 kb) is shown. The in vitro activity was measured in terms of cGAMP production by cGAS incubated with its substrates ATP and GTP. Error bars indicate SEM of two experiments performed with two individual protein purifications. Unless otherwise stated, error bars indicate SEM from three individual experiments. n.d., not detectable; p.e., postelectroporation.

compared with the cGAS(WT) group after both LPS and poly(I:C) challenge (Fig. 8B). In contrast, plasmid DNA challenge revealed a trend toward slightly decreased *IFIT1* mRNA expression in the rs610913 SNP group compared with the cGAS(WT) group, although not reaching statistical significance.

Discussion

This study aimed at characterizing the impact of a single amino acid exchange, that is, proline-to-histidine at position 261 of the cGAS protein. The SNP rs610913 encoding for cGAS(P261H) attracted our attention because of its high allele frequency. With the exception of the protective deleting polymorphism in the *CCR5* gene (*CCR5Δ32*), little genetic contribution on HIV acquisition was identified in previous genome-wide association studies (25, 52). The mild apparent overrepresentation of the rs610913 allele in HIV-1–positive individuals prompted us to hypothesize that it associates with a higher risk of HIV-1 acquisition. Of note, rs610913 appeared to be enriched in bacillus Calmette–Guérin-vaccinated healthy controls compared with tuberculosis-positive vaccinated individuals, suggesting an association of rs610913 with bacillus Calmette–Guérin vaccine-mediated protection to tuberculosis infection (53). Given the lack of additional data on rs610913, we aimed at evaluating its role in vitro, in cellulo, and ex vivo.

Interestingly, we first detected a strong association of cGAS expression and maintenance of base-level innate immunity, in the

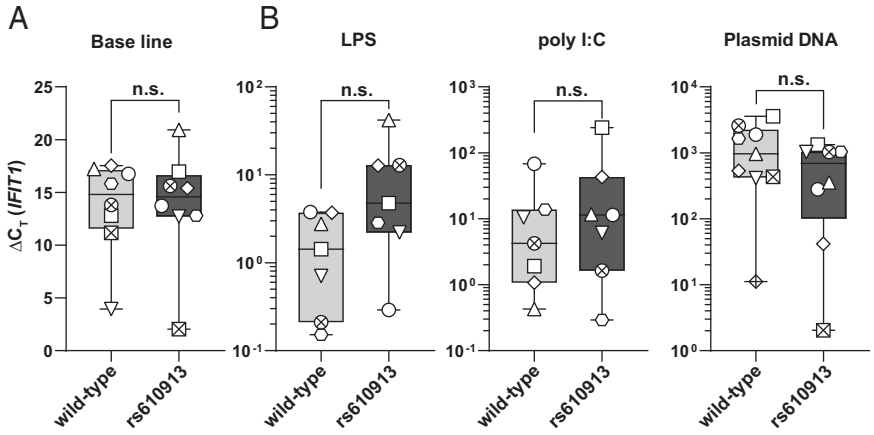

FIGURE 8. rs610913 homozygosity results in a trend toward a lower cell-intrinsic response to plasmid DNA, but not to LPS and poly(I:C) challenge. IL-2/PHA–stimulated PBMCs from healthy donors with indicated genotype were analyzed with respect to (**A**) basal level *IFIT1* mRNA expression of IL-2/PHA–stimulated PBMCs, and (**B**) *IFIT1* mRNA expression in IL-2/PHA–stimulated PBMCs upon poly(I:C), LPS, or plasmid DNA challenge. The symbols indicate individual donors. Error bars display SEM.

absence of infection or external stimuli. Both the expression of individual tested ISGs and the global transcriptomic profile shifted significantly toward an antiviral state in THP-1 cGAS KO cells upon restoration of cGAS expression. This observation was corroborated in HEK293T cells equipped with both cGAS and STING expression. Also, components of the IFN signaling cascade, such as *STAT1* and *IRF7*, were expressed at higher levels in the presence of functional cGAS, potentially allowing bystander cells to mount more rapid paracrine responses. This observation is reminiscent of our previous findings in mouse $CD4^+$ T cells, which equally displayed a cGAS-dependent ISG expression profile in the absence of exogenous stimuli (10). Work by other groups linked the cGAS-mediated priming of innate immunity to the release and sensing of mitochondrial DNA as a response to cellular stress (54, 55), a pathway that can be triggered by both DNA or RNA virus infection (16, 54, 56) and to the baseline sensing of endogenous retroviruses. It is therefore conceivable that cGAS-mediated activity may not only target viruses with dsDNA genomes or DNA intermediates, but also RNA viruses. Along this line, several RNA viruses indeed evolved strategies to actively counteract the cGAS/STING signaling axis (17, 57).

However, comparison of cells expressing cGAS(P261H) and cGAS(WT) protein failed to reveal consistent or pronounced differences in their ability to maintain a baseline innate immunity in any experimental system we studied, suggesting a similar efficiency of cGAS(P261H) enzymatic function, at least at steady-state conditions. At baseline levels, we identified a differential regulation of *TCP-1*, which encodes for a molecular chaperone that is part of the TRiC complex (58). Upon challenge with high amounts of plasmid DNA, cells expressing either cGAS(WT) or cGAS(P261H) supported a robust release of similar concentrations of bioactive IFNs, as opposed to cells expressing the nonfunctional cGAS mutant and cGAS KO cells. Also, kinetics of phosphorylation of STING, TBK1, and IRF3 were similar in cGAS(P261H)- and cGAS(WT)-expressing cells. In the context of challenge with suboptimal DNA quantities, induction of *IFIT1* mRNA expression was significantly reduced in cGAS(P261H)-expressing cells compared with cGAS(WT) cells. Likewise, PBMCs from homozygous rs610913 carriers displayed a statistically nonsignificant trend toward reacting at lower magnitudes to DNA challenge than cells from homozygous WT allele carriers. These data point toward a possibly reduced DNA binding affinity of cGAS(P261H) or differential requirement of cGAS cofactor interaction. The latter idea is supported by the results of our molecular modeling attempts, which hinted toward the possibility of a potential additional cofactor binding site in the cGAS(P261H) protein. The topology and the surface charge distribution of the head-to-head hcGAS(P261H) cleft containing the two H261 residues create a favorable binding site for a potential cellular cofactor that might increase the stability of the hcGAS P261H·dsDNA ladder-like assembly in vivo. This stability increase would contribute to the nucleation-cooperativity-based mechanism of cGAS (26) and enhanced enzymatic activity. The latter is supported by the observation that a slightly higher in vitro catalytic activity of cGAS(P261H) can be attributed to the additional stabilization of the head-to-head area by the two hydrogen bonds between H261 and the side chains of S201 and E259 of the same monomer, which are absent in the WT enzyme. Additionally, the presence of two histidine residues in the cleft makes this site more suitable for specific recognition and high-affinity binding compared with proline. Intriguingly, a previous report suggested a loss of helix and glycosylation of the mutated cGAS(P261H) protein, and a better capacity for binding interactions (53).

Individual expression of cGAS(WT) or cGAS(P261H) conferred a decreased susceptibility to VSV-G–pseudotyped lentiviral vector-mediated and HIV-1 transduction. This inhibition occurred in the absence of detectable induction of an innate immune response upon transduction. These data support the idea that the cGAS-induced baseline antiviral state of the cells, rather than the cGAS-mediated detection of viral DNA intermediates or infection-triggered release of mitochondrial DNA, is responsible for lower transduction efficiencies. Of note, the absence of innate immune activation upon HIV-1 infection has been linked to the intactness of viral capsids that permit capsid uncoating closely tied to nuclear pores or in proximity to integration sites within the nucleus, thereby preventing exposure of HIV-1 reverse transcriptase products to cytosolic DNA sensors (11, 12, 59, 60). In line with our working model, cGAS expression reduced susceptibility also to infection with HSV-1 and CHIKV, an RNA virus. Schoggins et al. (15) proposed cGAS-mediated inhibition of RNA virus infection through exerting an IRF3-dependent but STAT-independent mechanism. Alphaviruses including CHIKV are sensitive to STING/IRF3-mediated restriction of infection (61, 62). In contrast, herpesvirus infection can be accompanied by accidental leakage of viral DNA into the cytosol, allowing cGAS-mediated recognition of the viral nucleic acids and subsequent type I IFN responses (63, 64). Although we detected a

protective role of functional cGAS in our experiments, we failed to establish a specific phenotype of cGAS(WT) compared with the cGAS(P261H) variant, indicating that both proteins' expression establishes a cellular antiviral state that sufficiently restricts infection by diverse viruses.

In conclusion, we demonstrate the overall intact functionality of rs610913 SNP-encoded cGAS(P261H). This protein, similarly to cGAS(WT), mounts an efficient IFN response upon sensing of dsDNA and decreases susceptibility to infection by different viruses by maintenance of a cGAS-dependent baseline expression of multiple antiviral factors.

Acknowledgments

We thank Sandra Pelligrini, Veit Hornung, and Jens Bohne for the gift of the HL116 cell line, THP-1 cGAS KO cells, and HEK293T-mCherry-STING and HEK293T cells. We thank Oya Cingöz for providing the plasmid HIV-1 NL4.3 ΔEnv ΔVpr luciferase. We thank Victor Tarabykin for granting access to the StepOnePlus real-time PCR system at Charité Universitätsmedizin. We thank the Genomics Platform of the Berlin Institute of Health for next-generation sequencing. We thank Rune Hartmann and Andreas Holleufer for help with the in vitro activity experiments. We are very grateful to Dietmar Manstein, Rune Hartmann, and Karl-Peter Hopfner for many fruitful discussions. We thank Thomas Pietschmann and Christian Drosten for constant support. We thank the HIV Reagent Program for providing essential reagents. We thank Sabine Dickhöfer for genotyping support and technical assistance. We thank all study subjects and their families, as well as voluntary healthy blood donors, for participating in the study.

Disclosures

The authors have no financial conflicts of interest.

References

1. Ablasser, A., M. Goldeck, T. Cavlar, T. Deimling, G. Witte, I. Röhl, K.-P. Hopfner, J. Ludwig, and V. Hornung. 2013. cGAS produces a 2′-5′-linked cyclic dinucleotide second messenger that activates STING. *Nature* 498: 380–384.
2. Gao, P., M. Ascano, Y. Wu, W. Barchet, B. L. Gaffney, T. Zillinger, A. A. Serganov, Y. Liu, R. A. Jones, G. Hartmann, et al. 2013. Cyclic [G(2′,5′)pA(3′,5′)p] is the metazoan second messenger produced by DNA-activated cyclic GMP-AMP synthase. *Cell* 153: 1094–1107.
3. Stempel, M., B. Chan, and M. M. Brinkmann. 2019. Coevolution pays off: herpesviruses have the license to escape the DNA sensing pathway. *Med. Microbiol. Immunol. (Berl.)* 208: 495–512.
4. Ma, Z., S. R. Jacobs, J. A. West, C. Stopford, Z. Zhang, Z. Davis, G. N. Barber, B. A. Glaunsinger, D. P. Dittmer, and B. Damania. 2015. Modulation of the cGAS-STING DNA sensing pathway by gammaherpesviruses. *Proc. Natl. Acad. Sci.* 112: E4306–E4315
5. Zhu, H., and C. Zheng. 2020. The race between host antiviral innate immunity and the immune evasion strategies of herpes simplex virus 1. *Microbiol. Mol. Biol. Rev.* 84: e00099-20.
6. Su, C., and C. Zheng. 2017. Herpes simplex virus 1 abrogates the cGAS/STING-mediated cytosolic DNA-sensing pathway via its virion host shutoff protein, UL41. *J. Virol.* 91: e02414-16.
7. Christensen, M. H., S. B. Jensen, J. J. Miettinen, S. Luecke, T. Prabakaran, L. S. Reinert, T. Mettenleiter, Z. J. Chen, D. M. Knipe, R. M. Sandri-Goldin, et al. 2016. HSV-1 ICP27 targets the TBK1-activated STING signalsome to inhibit virus-induced type I IFN expression. *EMBO J.* 35: 1385–1399.
8. Bodda, C., L. S. Reinert, S. Fruhwürth, T. Richardo, C. Sun, B.-C. Zhang, M. Kalamvoki, A. Pohlmann, T. H. Mogensen, P. Bergström, et al. 2020. HSV1 VP1-2 deubiquitinates STING to block type I interferon expression and promote brain infection. *J. Exp. Med.* 217: e20191422.
9. Cingöz, O., and S. P. Goff. 2019. HIV-1 is a poor inducer of innate immune responses. *MBio* 10: e02834-18.
10. Elsner, C., A. Ponnurangam, J. Kazmierski, T. Zillinger, J. Jansen, D. Todt, K. Döhner, S. Xu, A. Ducroux, N. Kriedemann, et al. 2020. Absence of cGAS-mediated type I IFN responses in HIV-1-infected T cells. *Proc. Natl. Acad. Sci. USA* 117: 19475–19486.
11. Siddiqui, M. A., A. Saito, U. D. Halambage, D. Ferhadian, D. K. Fischer, A. C. Francis, G. B. Melikyan, Z. Ambrose, C. Aiken, and M. Yamashita. 2019. A novel phenotype links HIV-1 capsid stability to cGAS-mediated DNA sensing. *J. Virol.* 93: e00706-19.
12. Sumner, R. P., L. Harrison, E. Touizer, T. P. Peacock, M. Spencer, L. Zuliani-Alvarez, and G. J. Towers. 2020. Disrupting HIV-1 capsid formation causes cGAS sensing of viral DNA. *EMBO J.* 39: e103958.
13. Yan, N., A. D. Regalado-Magdos, B. Stiggelbout, M. A. Lee-Kirsch, and J. Lieberman. 2010. The cytosolic exonuclease TREX1 inhibits the innate immune response to human immunodeficiency virus type 1. *Nat. Immunol.* 11: 1005–1013.
14. Kumar, S., J. H. Morrison, D. Dingli, and E. Poeschla. 2018. HIV-1 activation of innate immunity depends strongly on the intracellular level of TREX1 and sensing of incomplete reverse transcription products. *J. Virol.* 92: e00001-18.
15. Schoggins, J. W., D. A. MacDuff, N. Imanaka, M. D. Gainey, B. Shrestha, J. L. Eitson, K. B. Mar, R. B. Richardson, A. V. Ratushny, V. Litvak, et al. 2014. Pan-viral specificity of IFN-induced genes reveals new roles for cGAS in innate immunity. [Published erratum appears in 2015 *Nature* 525: 144.] *Nature* 505: 691–695.
16. Moriyama, M., T. Koshiba, and T. Ichinohe. 2019. Influenza A virus M2 protein triggers mitochondrial DNA-mediated antiviral immune responses. *Nat. Commun.* 10: 4624.
17. Webb, L. G., J. Veloz, J. Pintado-Silva, T. Zhu, M. V. Rangel, T. Mutetwa, L. Zhang, D. Bernal-Rubio, D. Figueroa, L. Carrau, et al. 2020. Chikungunya virus antagonizes cGAS-STING mediated type-I interferon responses by degrading cGAS. *PLoS Pathog.* 16: e1008999.
18. Patel, S., S. M. Blaauboer, H. R. Tucker, S. Mansouri, J. S. Ruiz-Moreno, L. Hamann, R. R. Schumann, B. Opitz, and L. Jin. 2017. The common R71H-G230A-R293Q human TMEM173 is a null allele. *J. Immunol.* 198: 776–787.
19. Yi, G., V. P. Brendel, C. Shu, P. Li, S. Palanathan, and C. Cheng Kao. 2013. Single nucleotide polymorphisms of human STING can affect innate immune response to cyclic dinucleotides. *PLoS One* 8: e77846.
20. Jin, L., L.-G. Xu, I. V. Yang, E. J. Davidson, D. A. Schwartz, M. M. Wurfel, and J. C. Cambier. 2011. Identification and characterization of a loss-of-function human MPYS variant. *Genes Immun.* 12: 263–269.
21. Nissen, S. K., J. G. Pedersen, M. Helleberg, K. Kjær, K. Thavachelvam, N. Obel, M. Tolstrup, M. R. Jakobsen, and T. H. Mogensen. 2018. Multiple homozygous variants in the STING-encoding TMEM173 gene in HIV long-term nonprogressors. *J. Immunol.* 200: 3372–3382.
22. Everitt, A. R., S. Clare, T. Pertel, S. P. John, R. S. Wash, S. E. Smith, C. R. Chin, E. M. Feeley, J. S. Sims, D. J. Adams, et al.; MOSAIC Investigators. 2012. IFITM3 restricts the morbidity and mortality associated with influenza. *Nature* 484: 519–523.
23. Ge, D., J. Fellay, A. J. Thompson, J. S. Simon, K. V. Shianna, T. J. Urban, E. L. Heinzen, P. Qiu, A. H. Bertelsen, A. J. Muir, et al. 2009. Genetic variation in *IL28B* predicts hepatitis C treatment-induced viral clearance. *Nature* 461: 399–401.
24. Auton, A., L. D. Brooks, R. M. Durbin, E. P. Garrison, H. M. Kang, J. O. Korbel, J. L. Marchini, S. McCarthy, G. A. McVean, G. R. Abecasis, et al.; 1000 Genomes Project Consortium. 2015. A global reference for human genetic variation. *Nature* 526: 68–74.
25. McLaren, P. J., C. Coulonges, S. Ripke, L. van den Berg, S. Buchbinder, M. Carrington, A. Cossarizza, J. Dalmau, S. G. Deeks, O. Delaneau, et al. 2013. Association study of common genetic variants and HIV-1 acquisition in 6,300 infected cases and 7,200 controls. *PLoS Pathog.* 9: e1003515.
26. Andreeva, L., B. Hiller, D. Kostrewa, C. Lässig, C. C. de Oliveira Mann, D. Jan Drexler, A. Maiser, M. Gaidt, H. Leonhardt, V. Hornung, and K.-P. Hopfner. 2017. cGAS senses long and HMGB/TFAM-bound U-turn DNA by forming protein-DNA ladders. *Nature* 549: 394–398.
27. Zhou, W., A. T. Whiteley, C. C. de Oliveira Mann, B. R. Morehouse, R. P. Nowak, E. S. Fischer, N. S. Gray, J. J. Mekalanos, and P. J. Kranzusch. 2018. Structure of the human cGAS-DNA complex reveals enhanced control of immune surveillance. *Cell* 174: 300–311.e11.
28. Emsley, P., and K. Cowtan. 2004. Coot: model-building tools for molecular graphics. *Acta Crystallogr. D Biol. Crystallogr.* 60: 2126–2132.
29. Krissinel, E., and K. Henrick. 2004. Secondary-structure matching (SSM), a new tool for fast protein structure alignment in three dimensions. *Acta Crystallogr. D Biol. Crystallogr.* 60: 2256–2268.
30. Cornell, W. D., P. Cieplak, C. I. Bayly, I. R. Gould, K. M. Merz, D. M. Ferguson, D. C. Spellmeyer, T. Fox, J. W. Caldwell, and P. A. Kollman. 1995. A second generation force field for the simulation of proteins, nucleic acids, and organic molecules. *J. Am. Chem. Soc.* 117: 5179–5197.
31. Uzé, G., S. Di Marco, E. Mouchel-Vielh, D. Monneron, M. T. Bandu, M. A. Horisberger, A. Dorques, G. Lutfalla, and K. E. Mogensen. 1994. Domains of interaction between alpha interferon and its receptor components. *J. Mol. Biol.* 243: 245–257.
32. Zufferey, R., D. Nagy, R. J. Mandel, L. Naldini, and D. Trono. 1997. Multiply attenuated lentiviral vector achieves efficient gene delivery in vivo. *Nat. Biotechnol.* 15: 871–875.
33. Miyoshi, H., M. Takahashi, F. H. Gage, and I. M. Verma. 1997. Stable and efficient gene transfer into the retina using an HIV-based lentiviral vector. *Proc. Natl. Acad. Sci. USA* 94: 10319–10323.
34. Agarwal, S., B. Nikolai, T. Yamaguchi, P. Lech, and N. V. Somia. 2006. Construction and use of retroviral vectors encoding the toxic gene barnase. *Mol. Ther.* 14: 555–563.
35. Stewart, S. A., D. M. Dykxhoorn, D. Palliser, H. Mizuno, E. Y. Yu, D. S. An, D. M. Sabatini, I. S. Y. Chen, W. C. Hahn, P. A. Sharp, et al. 2003. Lentivirus-delivered stable gene silencing by RNAi in primary cells. *RNA* 9: 493–501.
36. Xu, S., A. Ducroux, A. Ponnurangam, G. Vieyres, S. Franz, M. Müsken, T. Zillinger, A. Malassa, E. Ewald, V. Hornung, et al. 2016. cGAS-mediated innate immunity spreads intercellularly through HIV-1 Env-induced membrane fusion sites. *Cell Host Microbe* 20: 443–457.
37. Connor, R. I., B. K. Chen, S. Choe, and N. R. Landau. 1995. Vpr is required for efficient replication of human immunodeficiency virus type-1 in mononuclear phagocytes. *Virology* 206: 935–944.

38. Strelow, L. I., and D. A. Leib. 1995. Role of the virion host shutoff (vhs) of herpes simplex virus type 1 in latency and pathogenesis. *J. Virol.* 69: 6779–6786.
39. Döhner, K., K. Radtke, S. Schmidt, and B. Sodeik. 2006. Eclipse phase of herpes simplex virus type 1 infection: efficient dynein-mediated capsid transport without the small capsid protein VP26. *J. Virol.* 80: 8211–8224.
40. Sodeik, B., M. W. Ebersold, and A. Helenius. 1997. Microtubule-mediated transport of incoming herpes simplex virus 1 capsids to the nucleus. *J. Cell Biol.* 136: 1007–1021.
41. Grosche, L., K. Döhner, A. Düthorn, A. Hickford-Martinez, A. Steinkasserer, and B. Sodeik. 2019. Herpes simplex virus type 1 propagation, titration and single-step growth curves. *Bio Protoc.* 9: e3441.
42. Döhner, K., A. Wolfstein, U. Prank, C. Echeverri, D. Dujardin, R. Vallee, and B. Sodeik. 2002. Function of dynein and dynactin in herpes simplex virus capsid transport. *Mol. Biol. Cell* 13: 2795–2809.
43. Engelmann, I., D. R. Petzold, A. Kosinska, B. G. Hepkema, T. F. Schulz, and A. Heim. 2008. Rapid quantitative PCR assays for the simultaneous detection of herpes simplex virus, varicella zoster virus, cytomegalovirus, Epstein-Barr virus, and human herpesvirus 6 DNA in blood and other clinical specimens. *J. Med. Virol.* 80: 467–477.
44. Levitt, N. H., H. H. Ramsburg, S. E. Hasty, P. M. Repik, F. E. J. Cole, Jr., and H. W. Lupton. 1986. Development of an attenuated strain of chikungunya virus for use in vaccine production. *Vaccine* 4: 157–162.
45. Döhner, K., A. Ramos-Nascimento, D. Bialy, F. Anderson, A. Hickford-Martinez, F. Rother, T. Koithan, K. Rudolph, A. Buch, U. Prank, et al. 2018. Importin α1 is required for nuclear import of herpes simplex virus proteins and capsid assembly in fibroblasts and neurons. *PLoS Pathog.* 14: e1006823.
46. Ashburner, M., C. A. Ball, J. A. Blake, D. Botstein, H. Butler, J. M. Cherry, A. P. Davis, K. Dolinski, S. S. Dwight, J. T. Eppig, et al.; The Gene Ontology Consortium. 2000. Gene Ontology: tool for the unification of biology. *Nat. Genet.* 25: 25–29.
47. The Gene Ontology Consortium. 2019. The Gene Ontology resource: 20 years and still GOing strong. *Nucleic Acids Res.* 47(D1): D330–D338.
48. Pablos, J. L., B. Santiago, P. E. Carreira, M. Galindo, and J. J. Gomez-Reino. 1999. Cyclooxygenase-1 and -2 are expressed by human T cells. *Clin. Exp. Immunol.* 115: 86–90.
49. Huang, C. C., K. E. Duffy, L. R. San Mateo, B. Y. Amegadzie, R. T. Sarisky, and M. L. Mbow. 2006. A pathway analysis of poly(I:C)-induced global gene expression change in human peripheral blood mononuclear cells. *Physiol. Genomics* 26: 125–133.
50. Civril, F., T. Deimling, C. C. de Oliveira Mann, A. Ablasser, M. Moldt, G. Witte, V. Hornung, and K.-P. Hopfner. 2013. Structural mechanism of cytosolic DNA sensing by cGAS. *Nature* 498: 332–337.
51. Luecke, S., A. Holleufer, M. H. Christensen, K. L. Jønsson, G. A. Boni, L. K. Sørensen, M. Johannsen, M. R. Jakobsen, R. Hartmann, and S. R. Paludan. 2017. cGAS is activated by DNA in a length-dependent manner. *EMBO Rep.* 18: 1707–1715.
52. Dean, M., M. Carrington, C. Winkler, G. A. Huttley, M. W. Smith, R. Allikmets, J. J. Goedert, S. P. Buchbinder, E. Vittinghoff, E. Gomperts, et al. 1996. Genetic restriction of HIV-1 infection and progression to AIDS by a deletion allele of the CKR5 structural gene. *Science* 273: 1856–1862.
53. Thada, S., S. Burkert, R. Sivangala, A. Hussain, S. Sur, N. Dittrich, M. L. Conrad, H. Slevogt, S. Latha Gaddam, and R. R. Schumann. 2020. A SNP upstream of the cyclic GMP-AMP synthase (cGAS) gene protects from relapse and extra-pulmonary TB and relates to BCG vaccination status in an Indian cohort. *Genes Immun.* 21: 13–26.
54. West, A. P., W. Khoury-Hanold, M. Staron, M. C. Tal, C. M. Pineda, S. M. Lang, M. Bestwick, B. A. Duguay, N. Raimundo, D. A. MacDuff, et al. 2015. Mitochondrial DNA stress primes the antiviral innate immune response. *Nature* 520: 553–557.
55. Maekawa, H., T. Inoue, H. Ouchi, T.-M. Jao, R. Inoue, H. Nishi, R. Fujii, F. Ishidate, T. Tanaka, Y. Tanaka, et al. 2019. Mitochondrial damage causes inflammation via cGAS-STING signaling in acute kidney injury. *Cell Rep.* 29: 1261–1273.e6.
56. Sun, B., K. B. Sundström, J. J. Chew, P. Bist, E. S. Gan, H. C. Tan, K. C. Goh, T. Chawla, C. K. Tang, and E. E. Ooi. 2017. Dengue virus activates cGAS through the release of mitochondrial DNA. *Sci. Rep.* 7: 3594.
57. Aguirre, S., P. Luthra, M. T. Sanchez-Aparicio, A. M. Maestre, J. Patel, F. Lamothe, A. C. Fredericks, S. Tripathi, T. Zhu, J. Pintado-Silva, et al. 2017. Dengue virus NS2B protein targets cGAS for degradation and prevents mitochondrial DNA sensing during infection. *Nat. Microbiol.* 2: 17037.
58. Melki, R., G. Batelier, S. Soulié, and R. C. J. Williams, Jr. 1997. Cytoplasmic chaperonin containing TCP-1: structural and functional characterization. *Biochemistry* 36: 5817–5826.
59. Burdick, R. C., C. Li, M. Munshi, J. M. O. Rawson, K. Nagashima, W.-S. Hu, and V. K. Pathak. 2020. HIV-1 uncoats in the nucleus near sites of integration. *Proc. Natl. Acad. Sci.* 117: 5486–5493.
60. Francis, A. C., and G. B. Melikyan. 2018. Single HIV-1 imaging reveals progression of infection through CA-dependent steps of docking at the nuclear pore, uncoating, and nuclear transport. *Cell Host Microbe* 23: 536–548.e6.
61. Sali, T. M., K. M. Pryke, J. Abraham, A. Liu, I. Archer, R. Broeckel, J. A. Staverosky, J. L. Smith, A. Al-Shammari, L. Amsler, et al. 2015. Characterization of a novel human-specific STING agonist that elicits antiviral activity against emerging alphaviruses. *PLoS Pathog.* 11: e1005324.
62. Gall, B., K. Pryke, J. Abraham, N. Mizuno, S. Botto, T. M. Sali, R. Broeckel, N. Haese, A. Nilsen, A. Placzek, et al. 2018. Emerging alphaviruses are sensitive to cellular states induced by a novel small-molecule agonist of the STING pathway. *J. Virol.* 92: e01913-17.
63. Sun, C., S. Luecke, C. Bodda, K. L. Jønsson, Y. Cai, B.-C. Zhang, S. B. Jensen, I. Nordentoft, J. M. Jensen, M. R. Jakobsen, and S. R. Paludan. 2019. Cellular requirements for sensing and elimination of incoming HSV-1 DNA and capsids. *J. Interferon Cytokine Res.* 39: 191–204.
64. Horan, K. A., K. Hansen, M. R. Jakobsen, C. K. Holm, S. Søby, L. Unterholzner, M. Thompson, J. A. West, M. B. Iversen, S. B. Rasmussen, et al. 2013. 2013. Proteasomal degradation of herpes simplex virus capsids in macrophages releases DNA to the cytosol for recognition by DNA sensors. *J. Immunol.* 190: 2311–2319.

Article

TRANSPARENT PROCESS OPEN ACCESS

molecular systems biology

Nonproductive exposure of PBMCs to SARS-CoV-2 induces cell-intrinsic innate immune responses

Julia Kazmierski[1,2,†], Kirstin Friedmann[1,†], Dylan Postmus[1,2], Jackson Emanuel[1], Cornelius Fischer[3], Jenny Jansen[1,2], Anja Richter[1], Laure Bosquillon de Jarcy[1,4], Christiane Schüler[1,2], Madlen Sohn[3], Sascha Sauer[3], Christian Drosten[1,5], Antoine-Emmanuel Saliba[6], Leif Erik Sander[4], Marcel A Müller[1,5], Daniela Niemeyer[1,5,*] & Christine Goffinet[1,2,**]

Abstract

Cell-intrinsic responses mounted in PBMCs during mild and severe COVID-19 differ quantitatively and qualitatively. Whether they are triggered by signals emitted by productively infected cells of the respiratory tract or result from physical interaction with virus particles remains unclear. Here, we analyzed susceptibility and expression profiles of PBMCs from healthy donors upon *ex vivo* exposure to SARS-CoV and SARS-CoV-2. In line with the absence of detectable ACE2 receptor expression, human PBMCs were refractory to productive infection. RT–PCR experiments and single-cell RNA sequencing revealed JAK/STAT-dependent induction of interferon-stimulated genes (ISGs) but not proinflammatory cytokines. This SARS-CoV-2-specific response was most pronounced in monocytes. SARS-CoV-2-RNA-positive monocytes displayed a lower ISG signature as compared to bystander cells of the identical culture. This suggests a preferential invasion of cells with a low ISG baseline profile or delivery of a SARS-CoV-2-specific sensing antagonist upon efficient particle internalization. Together, nonproductive physical interaction of PBMCs with SARS-CoV-2- and, to a much lesser extent, SARS-CoV particles stimulate JAK/STAT-dependent, monocyte-accentuated innate immune responses that resemble those detected *in vivo* in patients with mild COVID-19.

Keywords interferon; interferon-stimulated genes; PBMCs; SARS-CoV-2

Subject Categories Immunology; Microbiology, Virology & Host Pathogen Interaction

DOI 10.15252/msb.202210961 | Received 7 February 2022 | Revised 28 July 2022 | Accepted 28 July 2022

Mol Syst Biol. (2022) 18: e10961

Introduction

The current SARS-CoV-2 pandemic represents a global medical, societal, and economical emergency of increasing importance. Arising at the end of 2019 in the Hubei province in China, the causative agent of the coronavirus disease 2019 (COVID-19), SARS-CoV-2, has to date infected more than 555 million individuals worldwide (World Health Organization). Owing to SARS-CoV-2 infection, more than 6.3 million deaths were reported to date (as of 2022, July 5th). The predominant symptoms of symptomatic COVID-19 are fever, cough, and shortness of breath; however, in severe cases, the disease can progress to pneumonia, acute respiratory distress syndrome, and multiple organ failure (Chen *et al*, 2020; Wölfel *et al*, 2020). The management of the pandemic is complicated by a large interindividual spectrum of clinical courses ranging from asymptomatic to fatal outcomes, pre- and asymptomatic infectious phases (Rothe *et al*, 2020; Jones *et al*, 2021), and the ongoing emergence of variants with increased transmissibility and/or immune escape. The reasons for the high interindividual outcome of infection are insufficiently understood and may include different degrees of cross-reactive background immunity at the level of humoral (Anderson *et al*, 2021; Ng *et al*, 2020) and T-cell-mediated immunity (Bacher *et al*, 2020; Braun *et al*, 2020; Nelde *et al*, 2021; Schulien *et al*, 2021), polymorphisms in genes related to innate immunity (Zhang *et al*, 2020) and autoimmunity (Bastard *et al*, 2020). Currently, specific treatment regimens must be administered early postinfection. They include the RNA polymerase inhibitor Remdesivir that may reduce hospitalization time but not mortality (Wang *et al*, 2020b), the protease inhibitor Paxlovid (Hammond *et al*, 2022), the nucleoside analog Molnupiravir and monoclonal anti-spike antibodies with variant-specific neutralization potencies (Weinreich *et al*, 2021; RECOVERY Collaborative

1 Institute of Virology, Campus Charité Mitte, Charité – Universitätsmedizin Berlin, Berlin, Germany
2 Berlin Institute of Health, Berlin, Germany
3 Scientific Genomics Platforms, Laboratory of Functional Genomics, Nutrigenomics and Systems Biology, Max Delbrück Center for Molecular Medicine, Berlin, Germany
4 Department of Infectious Diseases and Respiratory Medicine, Charité - Universitätsmedizin Berlin, Corporate Member of Freie Universität Berlin, Humboldt-Universität zu Berlin, and Berlin Institute of Health (BIH), Berlin, Germany
5 German Center for Infection Research, Associated Partner Charité, Berlin, Germany
6 Helmholtz Institute for RNA-based Infection Research (HIRI), Helmholtz-Center for Infection Research (HZI), Würzburg, Germany
*Corresponding author. Tel: +0049 30 450 525 488; E-mail: daniela.niemeyer@charite.de
**Corresponding author. Tel: +0049 30 450 525 489; E-mail: christine.goffinet@charite.de
†These authors contributed equally to this work as first authors

Group, 2022). In the late phase of infection, the administration of the immune modulator dexamethasone (RECOVERY Collaborative Group, 2021) dampens the hyperactivation of cytokine-driven immune responses. While several effective vaccines are available, the necessity for specific treatment options will likely persist given the expected proportion of the population that will not have access to vaccines or will refuse vaccination.

To accelerate the establishment of immunomodulatory strategies, it is crucial to characterize *ex vivo* systems that correlate with cellular immunophenotypes of SARS-CoV-2 infection *in vivo* and that may contribute to preclinical testing. Furthermore, the usage of *ex vivo* platforms allows the systematic and comparative investigation of human cellular responses to exposure with different representatives of the species SARS-related coronaviruses (CoVs), including SARS-CoV. Peripheral immune cells are major contributors to human cellular responses upon infection. Given the recruitment of blood mononuclear cells to the lung compartment (Bost *et al*, 2020; Delorey *et al*, 2021; Wendisch *et al*, 2021), and the reported presence of viral RNA detectable in the peripheral blood of up to 10% of severely ill patients (Andersson *et al*, 2020; Prebensen *et al*, 2021), direct contact of PBMCs with infectious SARS-CoV-2 virions or defective viral particles is a likely scenario.

Here, we analyzed susceptibility to infection and cell-intrinsic innate responses of peripheral blood cells from healthy donors upon *ex vivo* exposure to SARS-CoV and SARS-CoV-2. Although both SARS-related CoVs failed to detectably replicate and spread in PBMCs, SARS-CoV-2 specifically triggered a JAK/STAT-dependent innate immune response that was most pronounced in monocytes. Single-cell, virus-inclusive RNA sequencing revealed relatively inefficient and ACE2-independent uptake of virus particles and a SARS-CoV-2 exposure-specific gene expression profile. Cellular responses, consisting of upregulation of the expression of interferon-stimulated genes (ISGs) but not proinflammatory cytokines, partially recapitulate expression profiles obtained by single-cell RNA sequencing of PBMCs from patients experiencing mild COVID-19 (Arunachalam *et al*, 2020; Schulte-Schrepping *et al*, 2020; Silvin *et al*, 2020). Our data demonstrate that cells from the peripheral blood, when undergoing contact with SARS-CoV-2 particles, mount cellular responses that potentially contribute to the control and/or pathogenesis of the infection.

Results

Absence of productive infection of human PBMCs by SARS-CoV and SARS-CoV-2

To address the ability of SARS-related CoVs to infect and propagate in cells of the peripheral blood, we exposed unstimulated PBMCs from healthy individuals to purified stocks of SARS-CoV and SARS-CoV-2, respectively, using equal infectious titers as determined on Vero E6 cells. As a reference, PBMCs were exposed to supernatants from uninfected Vero E6 cells (mock-exposed). For both SARS-related CoV, infectivity in cell-culture supernatants drastically decreased over time compared with the inoculum, reaching undetectable levels at 3 days postinoculation (Fig 1A), and pointing towards the absence of *de novo* production of infectious particles. Treatment of cells with the polymerase inhibitor Remdesivir did not further reduce infectivity in the supernatant, suggesting that the infectivity detectable in the mock-treated, virus-exposed cultures reflects virus input (Fig 1B). By contrast, infection of Vero E6 cells with the identical SARS-CoV-2 stock gave rise to a productive and Remdesivir-sensitive infection (Appendix Fig S1). In our experiments, virus-containing supernatant was replaced with a fresh medium 4 h postinoculation. Nevertheless, low levels of viral RNA genome equivalents remained detectable in the culture supernatant until the end of the experiment for both SARS-CoV and SARS-CoV-2 (up to 192 h postexposure; Fig 1C). Viral RNA was abundant also in supernatants from Remdesivir-treated cultures and cultures exposed to heat-inactivated SARS-CoV-2 until 192 h postexposure, arguing for high stability of the residual viral RNA of the inoculum, and against a constant replenishment of extracellular viral RNA pools as a reason for the stable RNA quantities (Fig 1D), in line with reported longevity of the incoming genomic viral RNA (Lee *et al*, 2022). Notably, blunting signaling by type I interferons (IFNs) through the constant presence of the JAK/STAT inhibitor Ruxolitinib failed to enable secretion of infectious particles and viral RNA in the supernatant, suggesting that JAK/STAT-dependent cell-intrinsic innate immunity is not the underlying reason for the absence of detectable virus production (Fig 1A and C).

To elucidate if PBMCs, despite being nonpermissive, are nevertheless susceptible to SARS-related CoV entry and initial RNA replication, we monitored cell-associated viral RNA species in the cultures over time. Because adherence of cells was incomplete before 48 h, we were able to separate adherent and the suspension cell fractions only starting at 72 h postculture start. Cell-associated viral genome equivalents (Fig 1E) and subgenomic viral E and N RNA (Fig EV1), the latter produced during discontinuous viral transcription, remained stable over time, and did not differ quantitatively for both SARS-related CoVs. Ruxolitinib treatment did not detectably enable RNA replication (Figs 1E and EV1), suggesting the absence of essential cofactors at the level of entry and/or RNA replication rather than the antiviral activity of IFN-regulated restriction factors. In line with this idea, we failed to detect the expression of the SARS-CoV receptor, angiotensin-converting enzyme 2 (ACE2) in PBMCs, as judged by immunoblotting, flow cytometry, and Q-RT–PCR using ACE2-specific antibodies and primer/probes, respectively (Fig EV2A–C). Also, we failed to detect relevant quantities of NRP-1 expression by flow cytometry (Fig EV2D), which has been suggested as an alternative entry receptor in conditions of low-to-absent ACE2 abundance (Cantuti-Castelvetri *et al*, 2020; Daly *et al*, 2020). In conclusion, freshly isolated, unstimulated PBMCs are devoid of expression of ACE2 and putative alternative receptor NRP-1. Furthermore, they appear to be nonsusceptible and nonpermissive to infection with either SARS-related CoV, at least *ex vivo*. However, the continuous presence of viral RNA associated with cells and in the culture supernatant suggests that virus particles attach to and/or internalize into PBMCs in an ACE2-independent manner and remain cell-associated for up to several days.

Exposure of PBMCs to SARS-CoV-2 and, to a much lower extent SARS-CoV, triggers a JAK/STAT-dependent cell-intrinsic innate immune response

To identify potential cell-intrinsic innate immune responses to SARS-CoV and SARS-CoV-2 exposure, we analyzed *IFIT1* and *IL6*

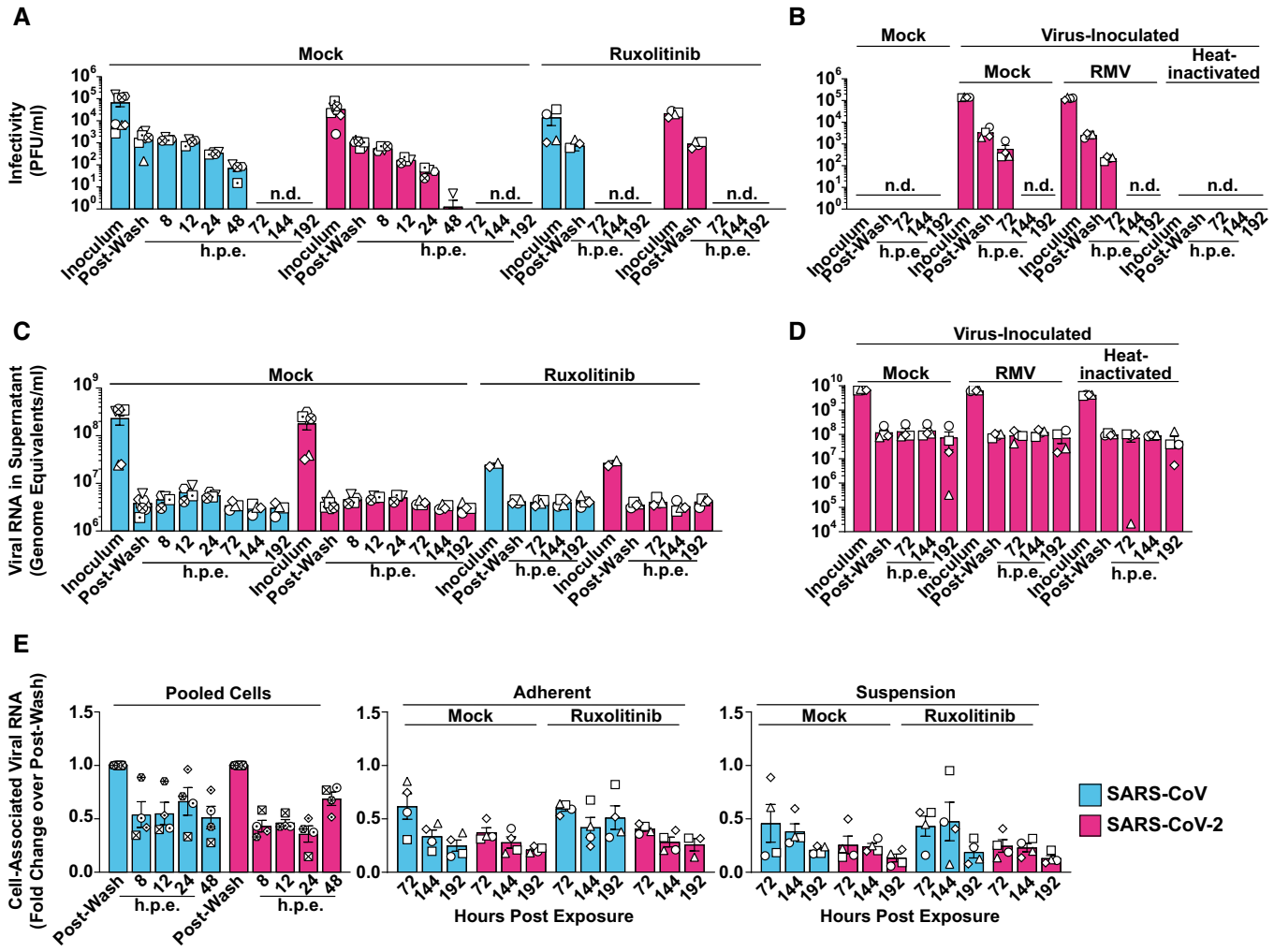

Figure 1. Absence of productive infection of PBMCs by SARS-CoV and SARS-CoV-2.

Untreated or Ruxolitinib (10 μM)-treated PBMCs from four individual donors were exposed to SARS-CoV or SARS-CoV-2 (MOI 0.5). PBMCs inoculated with supernatant from Vero E6 cell cultures mixed with PBS and OptiPro serum-free medium supplemented with 0.5% gelatine were used as a control condition (Mock). Supernatants and individual cell fractions were collected at indicated time points postinoculation and analyzed for:

A, B Infectivity in cell-culture supernatants by plaque titration assay.

C, D Viral RNA (genome equivalents/ml) concentrations in cell-culture supernatants by Q-RT–PCR.

E Relative changes of cell-associated viral genomic RNA quantities by Q-RT–PCR and normalized to *RNASEP* levels.

Data information: Data were generated in four individual experiments using cells from at least four individual donors represented by different symbols, bars represent the mean, and error bars indicate the SEM. Statistical significance was tested using the paired Student's *t*-test comparing mock- and Ruxolitinib-treated samples. *P*-values > 0.05 were considered not significant and are not shown in the figure. n.d., not detectable; h.p.e., hours postexposure; RMV, Remdesivir; Ruxo., Ruxolitinib.

mRNA expression over time (Figs 2A and EV3). We selected *IFIT1* and *IL6* as prototypic target genes that are transcribed by IRF3- and NF-κB-dependent promoter activation, respectively (Honda & Taniguchi, 2006). In contrast to SARS-CoV-inoculated cells, SARS-CoV-2-exposed cells displayed Ruxolitinib-sensitive, significantly upregulated *IFIT1* mRNA expression at 16, 24, and 48 h postinoculation (Fig 2A). Inhibition of potential low-level SARS-CoV-2 RNA replication through treatment of cells with Remdesivir, and heat inactivation of the SARS-CoV-2 stock inoculum did not prevent induction of *IFIT1* mRNA expression (Appendix Fig S2), corroborating the idea that the latter is triggered by exposure to virions but not by productive infection. By contrast, *IL6* expression was barely induced after exposure to SARS-CoV and SARS-CoV-2 (Fig EV3). Together, SARS-CoV-2 exposure specifically triggered IRF3-induced *IFIT1* but not NF-κB-induced *IL6* gene expression. We next analyzed if type I IFN expression preceded *IFIT1* mRNA expression in SARS-CoV-2-exposed PBMCs. Despite a slight trend for elevated *IFNA1* and *IFNB1* mRNA expression at 16 h, levels failed to reach significant upregulation at 4, 16, and 24 h, when compared to mock-exposed cultures (Fig 2B). However, IFN-α2 and IFN-stimulated IP-10, MCP-1, and MCP-3 proteins, as opposed to IL-6 and several other cytokines (Appendix Fig S3) were secreted in the supernatant of exposed PBMCs in a Ruxolitinib-sensitive manner, with overall higher levels in SARS-CoV-2- than in SARS-CoV-exposed cultures

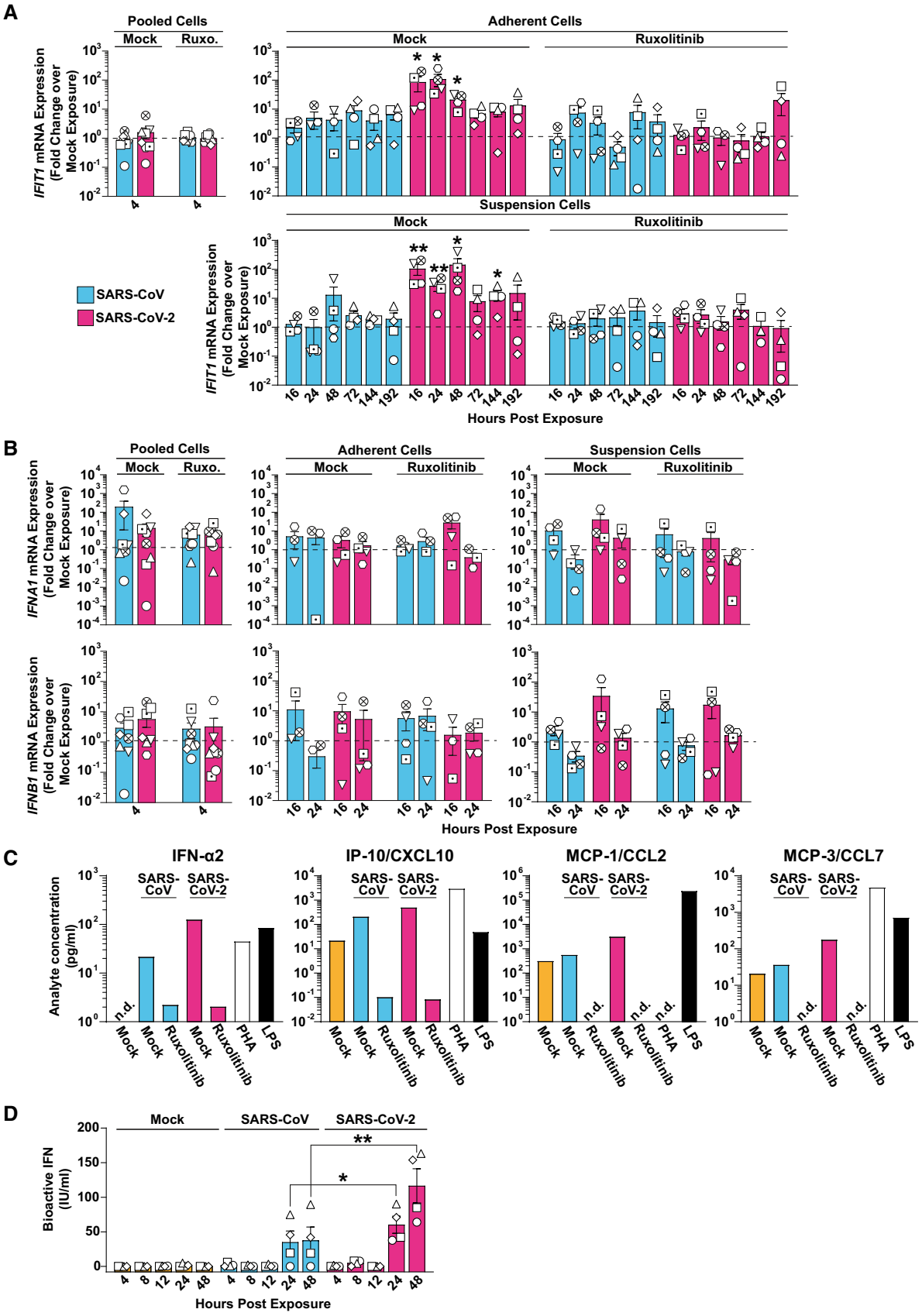

Figure 2.

Figure 2. Exposure of PBMCs to SARS-CoV-2 and, to a much lower extent SARS-CoV, triggers a JAK/STAT-dependent cell-intrinsic innate immune response.

A–C RNA extracted from Ruxolitinib-treated or mock-treated, and SARS-CoV-, SARS-CoV-2-, or mock-exposed PBMCs was analyzed for (A) *IFIT1*, (B) *IFNA1* and *IFNB1*, (C) mRNA expression by Q-RT–PCR at indicated time points. Suspension and adherent cell fractions were analyzed separately, except at the 4 h time point. Values were normalized to cellular *RNASEP* expression and are shown as fold change over mock-inoculated conditions. The dotted line indicates the expression level of mock-inoculated cell cultures and is set to 1. (C) Supernatants from Ruxolitinib- or mock-treated and SARS-CoV-, SARS-CoV-2-, or mock-inoculated PBMCs were collected 48 h postexposure, and cytokine expression of IFN-α2, IP-10/CXCL10, MCP-1/CCL2, and MCP-3/CCL7 were quantified using a Luminex-based immunoassay. PHA- or LPS-treated PBMCs were used as a positive control. Bars represent the results of a pool of four individual samples per condition.

D Supernatants collected from SARS-CoV-, SARS-CoV-2-, or mock-exposed PBMCs at indicated time points were analyzed for the release of bioactive IFN using the HL116 reporter cell assay.

Data information: Data were generated in four individual experiments using PBMCs from four or more individual donors represented by different symbols, bars represent the mean, and error bars indicate the SEM (A, B, and D). Statistical significance between mock- and Ruxolitinib-treated samples was tested using the paired Student's *t*-test and comparing SARS-CoV with SARS-CoV-2-treated samples from the same donor and time points. *P*-values < 0.05 were considered significant (*), < 0.01 very significant (**), or ≥ 0.05 not significant (not shown). n.d., not detectable.

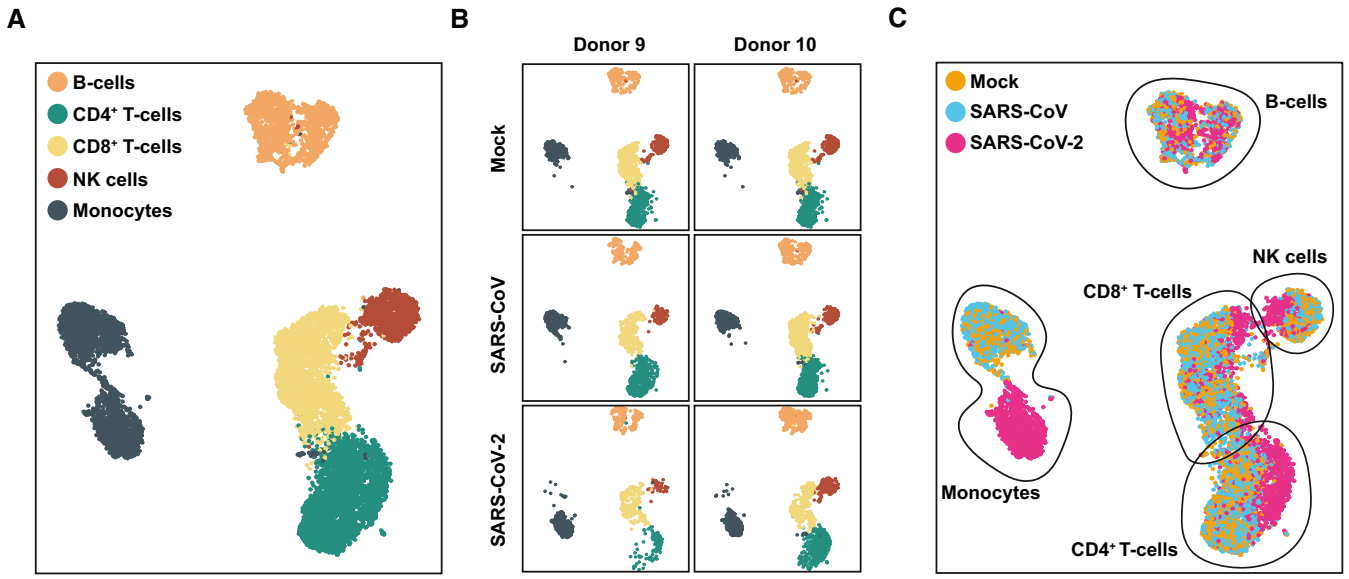

Figure 3. SARS-CoV-2 exposure causes transcriptional changes in most cell types.

PBMCs isolated from two donors were exposed to SARS-CoV, SARS-CoV-2, or mock-exposed, and analyzed by scRNA-sequencing 24 h postexposure.

A UMAP displaying all identified cell types,

B UMAP indicating the data obtained from the PBMCs of the two donors,

C Identified cell types according to condition.

(Fig 2C). Furthermore, bioactive IFN was detected in the supernatant of corresponding cultures, with highest levels upon SARS-CoV-2 exposure, while SARS-CoV inoculation induced the release of bioactive IFN at inferior levels that were statistically indistinguishable from those in mock-exposed cultures (Fig 2D). These results suggest that, although both SARS-related CoV failed to establish a productive infection in PBMCs, SARS-CoV-2 appears to induce cell-intrinsic, IFN-mediated, and JAK/STAT-dependent responses in several cell types comprised in PBMCs. By contrast, SARS-CoV induced very mild, if any, innate immune responses.

SARS-CoV-2 exposure causes transcriptional changes in most cell types

To explore cell-intrinsic responses in individual cell types, we performed single-cell RNA sequencing of PBMCs exposed to SARS-CoV and SARS-CoV-2, respectively. We identified the five major cell types, namely B cells, $CD4^+$ and $CD8^+$ T cells, NK cells, and monocytes (Fig 3A) based on the expression of discriminatory marker mRNAs (see Materials and Methods). Separated based on experimental conditions, PBMCs of both donors shared a similar relative cell type distribution (Fig 3B) and similar cell type-specific transcriptional profile (Appendix Fig S4), and data of both donors were merged for the following analyses. In line with our bulk analyses (Fig EV2A–C), *ACE2* mRNA was undetectable, as was *TMPRSS2* mRNA (Fig EV2E). By contrast, the protease-encoding *FURIN*, *BSG*, and *NRP1* mRNAs were expressed in all cell types and most abundantly in monocytes (Fig EV2E). Graphical mapping indicated transcriptomic changes within individual cell types for SARS-CoV-2-exposed, but not for SARS-CoV-exposed cultures, compared with mock-inoculated cells (Fig 3C). Notably, SARS-CoV-2 monocytes clustered separately from the other conditions in the UMAP despite library batch correction, implying a pronouncedly altered transcriptome. The T- and NK-cell clusters slightly and partially shifted, indicating a change in their

transcriptional profile (Fig 3C). The relative abundance of T cells and monocytes in SARS-CoV-2-exposed cells as compared to mock-exposed PBMCs remained constant, as judged by flow cytometric analysis (Appendix Fig S5). Together, this analysis revealed that transcriptomic changes occurred in most cell types upon SARS-CoV-2 exposure, particularly in the monocytic fraction.

Exposure to SARS-CoV-2 induces a global innate immunity-related gene profile in PBMCs with cell type-specific signatures

We next investigated in more detail the cell type-specific response to SARS-CoV-2. For each cell type, cells from all three treatments were subclustered and genes differentially expressed between clusters were used as input for cell trajectory analysis using the Pseudotime algorithm from the monocle R package (Trapnell *et al*, 2014). We aimed to identify whether cells from different treatments, especially those exposed to different viruses, developed along the same trajectory as a result of the exposure or if a different cell fate was induced (Fig 4A). For all five major cell types, cells inoculated with SARS-CoV-2 developed towards a separate cell fate and largely branched off from mock-exposed and SARS-CoV-exposed cells, which, conversely, shared a common trajectory. Interestingly, B-cell analysis resulted in four branching points, from which only two (#1 and #3) were specific for SARS-CoV-2-exposed cells, suggesting a high transcriptional heterogeneity of B cells independently of virus exposure. Though progression through pseudotime resulted in a distinct and highly pronounced trajectory of all SARS-CoV-2-exposed cell types, this effect was most clear in monocytes (Fig 4A). Analysis of expression of specific genes, including *ISG15* and *IFIT1*, confirmed that in general, all cell types contributed to gene expression changes upon SARS-CoV-2 challenge, and monocytes displayed the most pronounced elevation of expression of both genes (Fig 4B). Identification of differentially expressed genes (DEGs) in mock-exposed compared with SARS-CoV-2-inoculated PBMCs revealed a significant upregulation of gene expression in all cell types, especially in monocytes (Fig 4C). Interestingly, the majority of DEGs were identified as known ISGs (defined by the interferome database; colored in green (interferome.org; v2.01)). Scoring the individual cell types and conditions by their expression of an IFN-signaling module revealed a SARS-CoV-2-specific induction of ISGs in all cell types, though this was most prominent in monocytes (Fig 4D). Moreover, IFN module scores were colinear with Pseudotime scores along the SARS-CoV-2 trajectory, supporting the notion that SARS-CoV-2 exposure induces a development of PBMCs towards an antiviral phenotype. Increased expression of several ISGs, including *ISG15*, *IFIT1*, *IFITM3*, *DDX58*, *IFIH1*, *LY6E*, *MX2*, *IFI6*, *BST2*, was detectable predominantly, but not exclusively, in monocytes (Fig 4E), supporting the hypothesis that monocytes play a key role in the induction of cell-intrinsic innate immune response to SARS-CoV-2 stimulation. In line with our previous findings (Fig 2), SARS-CoV-2- and SARS-CoV-exposed cells scored virtually negative for the expression of various cytokines, including *IL6* (Fig 4E) and *IFN* mRNAs (Appendix Fig S6), although they express IFN receptors (Appendix Fig S6). In conclusion, these data reveal a strong induction of cell-intrinsic innate immunity in SARS-CoV-2-exposed PBMCs that manifests predominantly in monocytes.

Transcriptome differences in viral RNA-positive and bystander monocytes

Next, we aimed at identifying viral RNA-positive cells and their specific transcriptional profile that we hypothesized to differ from cells without detectable viral RNA of the identical culture. SARS-CoV-2 RNA was detectable in all cell types but predominantly in monocytes (Fig 5A). Identified viral reads were distributed over the viral genome sequence, with a high over-representation of the 3' RNA sequences that all subgenomic and genomic viral RNA have in common, corresponding to the 3' part of the N-coding sequence and polyA tail (Fig 5B). Specifically, in SARS-CoV- and SARS-CoV-2-exposed PBMC cultures, we identified 99 (2.13%) and 212 (2.88%) viral RNA-positive cells, respectively (Fig 5C). Among those, we identified 56 (7.8%) and 173 (15.3%) viral RNA-positive monocytes among all monocytes, respectively. First of all, no statistically significant differences in expression of individual genes of RNA-positive and RNA-negative monocytes were identified. However, the IFN module score (Fig 4) was slightly, but statistically highly significantly, elevated in SARS-CoV-2-exposed monocytes with undetectable viral RNA (Fig 5D and E). Specifically, within the 94 genes that were expressed marginally more abundantly in cells lacking detectable SARS-CoV-2 RNA, 18 represented ISGs, including *ISG15*, *IFITM2*, *IFITM3*, *IFI27*, and *HLA* genes that tended to be upregulated in viral RNA-negative bystander cells. Importantly, the presence of viral RNA did not specifically associate with the expression of *BSG/CD147* and *NRP1*, and *ACE2* and *TMPRSS2* expression was undetectable, suggesting that particles internalize in a manner that is independent of these proposed and confirmed receptors, respectively. In SARS-CoV-2 RNA-positive cells as compared to SARS-CoV-2 RNA-negative cells of the identical cultures, among others, *CD163* reads tended to be slightly more abundant. Expression of the hemoglobin-haptoglobin scavenger receptor CD163 has been associated with the regulation of inflammation (Kowal *et al*, 2011) and

Figure 4. Exposure to SARS-CoV-2 induces a global innate immunity-related gene profile in PBMCs with cell type-specific signatures.

A Pseudotime cell trajectory analysis and GSEA analysis using genes differentially regulated between mock-, SARS-CoV-, and SARS-CoV-2-challenged conditions for indicated cell types.

B Representative UMAPs showing *IFIT1* and *ISG15* mRNA expression in the indicated conditions.

C Volcano plot of all DEGs in SARS-CoV-2-exposed cells compared with mock-exposed cells in the indicated cell types. Known ISGs were colored in green based on their presence in the interferome database (http://www.interferome.org/; v2.01).

D Cell trajectory maps of indicated cell types with cells colored by expression of the genes in an IFN module gene set.

E Dot plot depicting expression of selected ISGs and cytokines. Expression levels are color-coded, and the percentage of cells expressing the respective gene is coded by symbol size.

Data information: Data shown in this figure are based on the analysis of two donors.

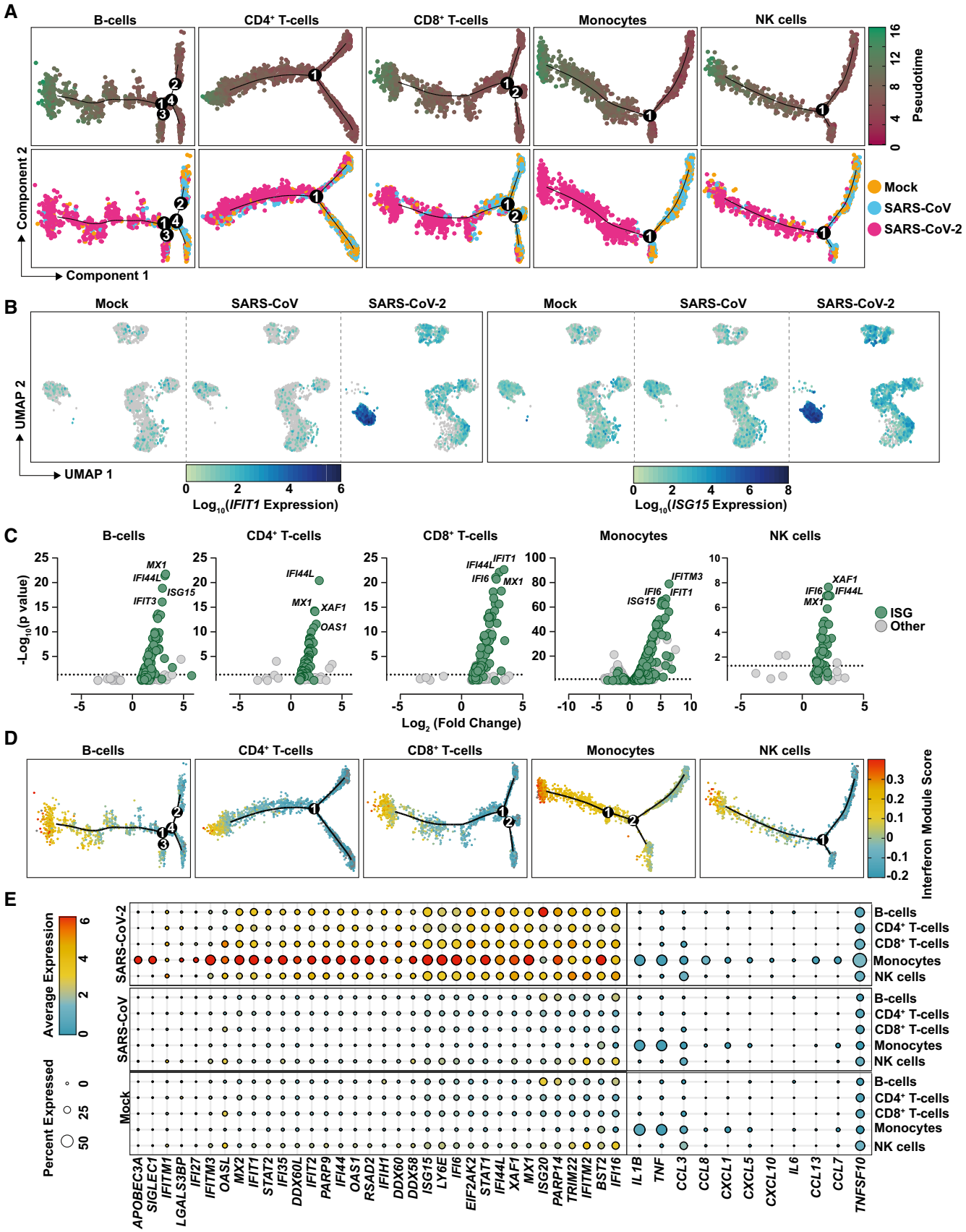
A
B-cells
CD4⁺ T-cells
CD8⁺ T-cells
Monocytes
NK cells
Pseudotime
Component 2
Component 1
Mock
SARS-CoV
SARS-CoV-2
B
UMAP 2
UMAP 1
Log10(IFIT1 Expression)
Log10(ISG15 Expression)
C
-Log10(p value)
Log2 (Fold Change)
MX1
IFI44L
ISG15
IFIT3
IFI44L
MX1
XAF1
OAS1
IFIT1
IFI6
IFITM3
XAF1
ISG
Other
D
Interferon Module Score
E
Average Expression
Percent Expressed
SARS-CoV-2
SARS-CoV
Mock
APOBEC3A
SIGLEC1
IFITM1
LGALS3BP
IFI27
IFITM3
OASL
MX2
IFIT1
STAT2
IFI35
DDX60L
IFIT2
PARP9
IFI44
OAS1
RSAD2
IFIH1
DDX60
DDX58
ISG15
LY6E
IFI6
EIF2AK2
STAT1
IFI44L
XAF1
MX1
ISG20
PARP14
TRIM22
IFITM2
BST2
IFI16
IL1B
TNF
CCL3
CCL8
CXCL1
CXCL5
CXCL10
IL6
CCL13
CCL7
TNFSF10

Figure 4.

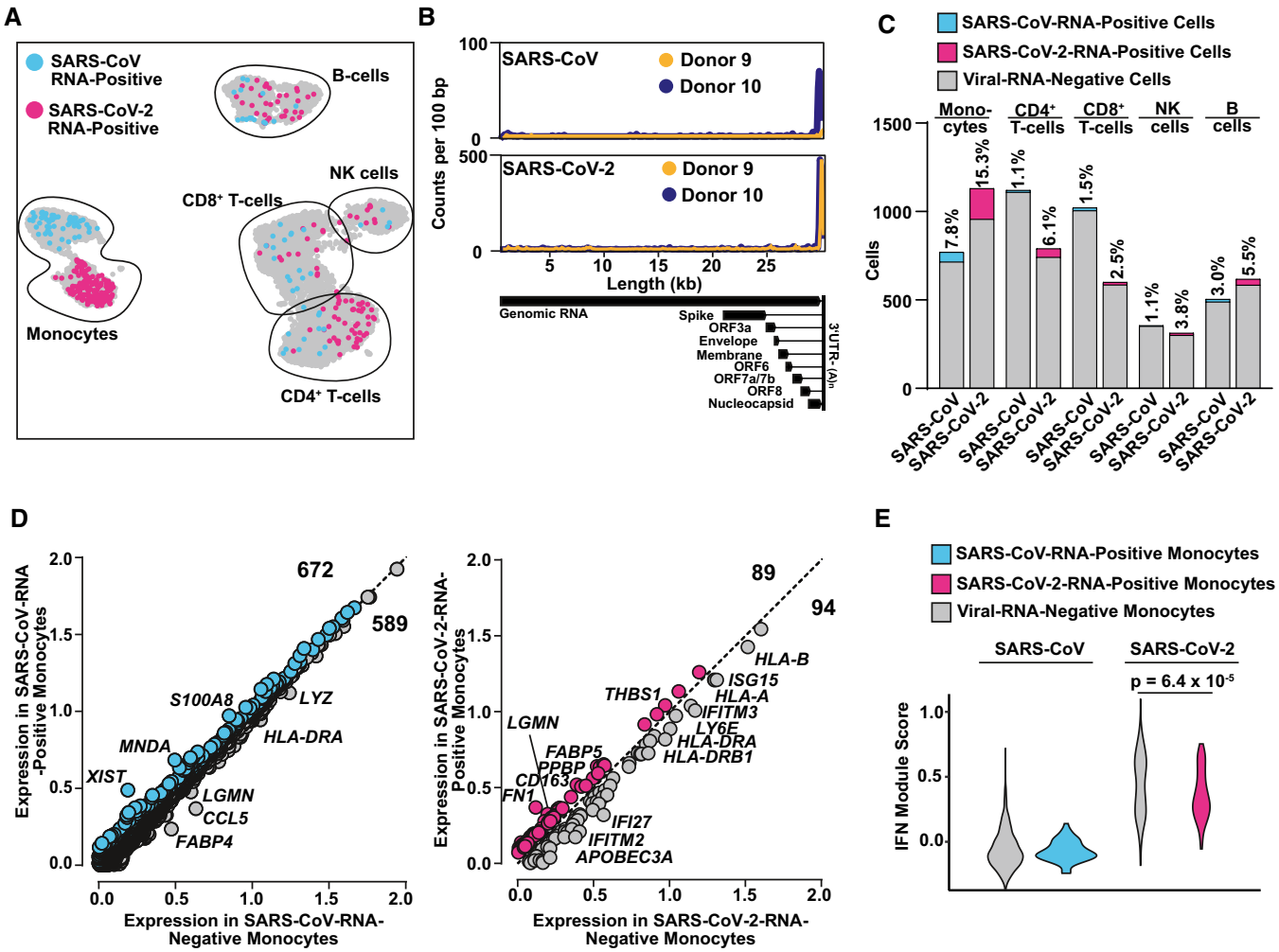

Figure 5. Viral RNA-positive monocytes trend towards downregulation of ISGs and upregulation of fibrosis-associated genes.

A UMAP highlighting cells in which transcripts of either SARS-CoV RNA (blue) or SARS-CoV-2 RNA (magenta) were identified.

B Virus-specific reads were aligned to the SARS-CoV or SARS-CoV-2 genome. Coverage of the genome is shown in counts per 100 bp.

C Bar graph showing the absolute number (bars) and relative percentage of cells that were identified as virus RNA-positive in SARS-CoV- and SARS-CoV-2-inoculated cultures, respectively.

D Plot of Log_{10} average expression of genes showing a Log_2(fold change) > 0.2 in viral RNA-positive versus viral RNA-negative monocytes from the SARS-CoV- (left panel) and SARS-CoV-2- (right panel) inoculated PBMCs with genes showing the highest expression fold change between both conditions.

E IFN Module Score of viral RNA-negative (gray; 715 and 958 cells in SARS-CoV and SARS-CoV-2 exposed cultures, respectively), SARS-CoV-RNA-positive (blue; 56 cells), and SARS-CoV-2-RNA-positive (magenta; 173 cells) monocytes. Statistical significance was tested using a Wilcoxon rank-sum test with continuity correction. *P*-values < 0.05 were considered significant (*), < 0.01 very significant (**), or ≥ 0.05 not significant.

Data information: Data shown in this figure are based on the analysis of two donors.

has interestingly been linked to immunological changes in monocytes and monocyte-derived macrophages from SARS-CoV-2-infected individuals (Gómez-Rial *et al*, 2020; Trombetta *et al*, 2021; Wendisch *et al*, 2021). Looking specifically at the *CD163*^{HIGH} monocyte population, we found that it displayed high expression levels of genes with profibrotic functions, including *VCAN*, *LGMN*, *MERTK*, *TFGB1*, *MRC1*, *TGFBI*, and *MMP9*, and enhanced the expression of cytokines including *CCL2*, *CXCL8*, or *IL1B* and the cytokine receptor *CCR5* (Fig EV4). Furthermore, SARS-CoV-2 RNA-positive cells displayed a preferential upregulation of genes implicated in migration and integrin binding (*FN1*, *PPBP*, *THBS1*), and differentiation, including *FABP5* and *LGMN*. Together, cells that internalized SARS-CoV-2 particles exhibit a slightly distinct gene expression profile characterized by a consistent reduction in antiviral ISGs and an upregulation of profibrotic genes as opposed to bystander cells with undetectable viral RNA.

Finally, we were intrigued whether preactivation would result in an altered ability of PBMCs to interact with, internalize, and sense SARS-CoV-2, as opposed to freshly isolated PBMCs from healthy donors. To mimic the environment of circulating PBMCs of a SARS-CoV-2-infected individual, we individually pretreated PBMCs with type I IFN, with supernatant from SARS-CoV-2-infected lung epithelial cell cultures, and with serum obtained at an early stage postinfection from mildly COVID-19 diseased individuals (Fig EV5). IFN-

α2a pretreatment did not influence the amount of detectable viral RNA, neither in the cell-associated fraction (Fig EV5A, left panel) nor in the supernatant (Fig EV5B, left panel), despite expected IFN-mediated enhancement of *IFIT1* (Fig EV5C) but not *IL6* mRNA (Fig EV5D) expression.

Pretreatment of PBMCs with virus-free, cytokine-containing supernatant derived from SARS-CoV-2-infected Calu-3 cell cultures resulted in a mild (1.6-fold), but statistically significant increase in cell-associated viral RNA copies (Fig EV5B, middle panel) when compared to cells stimulated with supernatant from uninfected Calu-3 cells, in the absence of changes concerning viral RNA quantities (Fig EV5A, middle panel) in the culture supernatant, and *IFIT1* and *IL6* mRNA expression (Fig EV5C and D, middle panels).

Similarly, cultivation of PBMCs in the presence of serum from COVID-19 patients, as opposed to mock or control serum treatment prior to SARS-CoV-2 exposure, was followed by a 1.8-fold higher abundance of viral genomic RNA in the cellular fraction (Fig EV5B, right panel). In summary, these results suggest that PBMCs that are "primed" by stimulation with a cytokine milieu that is characteristic of an ongoing systemic SARS-CoV-2 infection display a slightly increased ability to physically interact with viral particles, in the absence of detectable changes of *IFIT1* and *IL6* mRNA expression.

Discussion

In this study we characterized the response of peripheral immune cells, at the cell type level and at individual cells´ level, to *ex vivo* SARS-CoV-2 exposure as compared to SARS-CoV. While *ex vivo* experiments inherently do not recapitulate systemic immune cell interactions and lack the context of complex tissues´ and organs´ interplay and communication, they uniquely allow the side-by-side comparison of two genetically closely related but functionally different viruses under standardized conditions. Furthermore, they allow assessing the direct consequence of virus exposure on individual cell types.

Our results indicate that SARS-CoV-2 and SARS-CoV share the inability to detectably infect PBMCs. Previous studies with SARS-CoV and MERS-CoV yielded partially conflicting results regarding the susceptibility of human PBMCs to infection. *Ex vivo*, one publication reported the absence of SARS-CoV replication in PBMCs (Castilletti *et al*, 2005), while another work suggested susceptibility and permissiveness of PBMCs to SARS-CoV infection with a high interdonor variability (Ng *et al*, 2004). Another report suggested inefficient *de novo* SARS-CoV production in CD14-purified monocytes, despite detectable virus particle uptake, presumably through phagocytosis (Yilla *et al*, 2005). *In vivo*, *in situ* hybridization and electron microscopy analyses reported the presence of SARS-CoV material in lymphocytes and monocytes derived from infected patients (Gu *et al*, 2005). MERS-CoV was suggested to efficiently replicate in *ex vivo*-infected monocytes (Chu *et al*, 2014) but to only abortively infect human T cells (Chu *et al*, 2016). Of note, the confirmed receptor for SARS-CoV-2 cell entry (Hoffmann *et al*, 2020) has been reported to be virtually absent in PBMCs (Song *et al*, 2020; Xiong *et al*, 2020; Zou *et al*, 2020; Xu *et al*, 2020b), a finding that is in line with our own inability to detect *ACE2* mRNA and ACE2 protein expression in PBMCs by various methods. Therefore, we hypothesize that virus particles attach and/or internalize in an ACE2-independent manner, resulting in viral RNA associated with and/or internalized into cells. Interestingly, prestimulation of PBMCs in a cytokine-containing milieu using virus-free supernatants from infected lung epithelial cell cultures and sera from COVID-19 patients sensitized cells for a slightly more efficient uptake of particles. Given that receptor-independent phagocytosis is a hallmark of monocytes, our observation that the majority of the viral reads were retrieved in monocytic cells underlines this idea. Furthermore, as SARS-CoV ORF7a is a virion-associated protein (Huang *et al*, 2006) and SARS-CoV-2 ORF7a was reported to efficiently interact with PBMC-derived monocytes (Zhou *et al*, 2021), ORF7a may contribute to the attachment to monocytes. Interestingly, the binding capability of SARS-CoV ORF7a protein was reported to be significantly weaker as compared to SARS-CoV-2 ORF7a (Zhou *et al*, 2021), which is consistent with the observed two-fold reduced proportion of virus RNA-positive monocytes in SARS-CoV-exposed PBMCs as compared to SARS-CoV-2.

In vivo, a multitude of cytokines, including IL-1β, IL-1RA, IL-7, IL-8, IL-9, IL-10, CXCL10, IFN-γ, and TNF-α are upregulated in the plasma of COVID-19 patients, especially in cases with the severe outcome (Huang *et al*, 2020). By contrast, mild COVID-19 associates with effective type I IFN responses, including expression of type I IFNs themselves and IFN-stimulated genes, which are probably essential to clear the virus infection and orchestrate adaptive immunity accordingly (Arunachalam *et al*, 2020; Schulte-Schrepping *et al*, 2020; Stephenson *et al*, 2021). To date, it remains largely unclear which cell populations are the drivers of these individual responses. Productively infected epithelial cells in the respiratory tract may initiate some of these responses directly; alternatively, or in addition, immune cells may be stimulated by signals released by productively infected cells or by virions and/or viral proteins directly. Studies on the consequence of the physical interaction of SARS-CoV-2 with infection-refractory primary immune cells, as opposed to susceptible cell types in the respiratory tract, are largely missing. Of note, cytokines levels and composition differ in serum and bronchoalveolar lavage fluid of patients with COVID-19 (Xiong *et al*, 2020), suggesting that productively infected epithelial tissue in the respiratory tract and nonsusceptible peripheral immune cells initiate different cytokine responses. Proinflammatory monocytes that infiltrate the lung have been proposed to represent major cytokine producers in the lung microenvironment (Liao *et al*, 2020). In line with this idea, SARS-CoV-2-susceptible infected cell lines and primary cells (Blanco-Melo *et al*, 2020) display imbalanced host responses, with strong cytokine and ablated ISG responses, when compared to other respiratory virus infections. Also, studies performed in the SARS-CoV-2 Syrian hamster model uncovered an early and strong cytokine response in the myeloid compartment of the lung (Nouailles *et al*, 2021). Here, our data provide the first insights into the response of refractory PBMCs upon exposure to virus particles in the absence of co-stimulating infected cell types. The lack of expression of proinflammatory cytokines, including IL-6, TNFa, and IL-1 in SARS-CoV-2-exposed PBMCs, is in line with the idea that these cytokines are mainly derived from the respiratory tract representing the site of productive infection, and it may partially explain the absence of lymphocyte depletion in our experimental setting that is observed *in vivo* (Huang *et al*, 2020; Qin *et al*, 2020; Wang *et al*, 2020a). In our *ex vivo* PBMC setting, which

is devoid of productive infection, SARS-CoV-2 and, to a much lower extent, if at all, SARS-CoV particles induced innate immune responses in the absence of coculture with infected epithelial cells, indicating that direct exposure to virions can trigger responses in PBMCs.

Immune responses were initiated in different cell types with a focus on monocytes and were characterized by ample induction of expression of *IFIT1* and several other ISGs, as opposed to proinflammatory cytokines, including *IL6* mRNA expression. Our data suggest that this response may be triggered, at least to a certain extent, in a virus replication-independent manner. Despite our failure to detect *IFNA1* mRNA expression at the time points investigated, which might be related to its transient presence, the Ruxolitinib-sensitive induction of *IFIT1* mRNA expression, the secretion of IFN-α and IFN-induced cytokines, and bioactive IFN strongly suggest an underlying IFN-signaling-dependent mechanism. This observation is well in line with *ex vivo* data from PBMCs derived from COVID-19 patients showing highest, monocyte-specific induction of IFN-mediated responses that are inversely proportional to the degree of disease (Arunachalam *et al*, 2020; Schulte-Schrepping *et al*, 2020; Stephenson *et al*, 2021), and the absence of proinflammatory cytokine expression (Arunachalam *et al*, 2020; Xu *et al*, 2020a; Stephenson *et al*, 2021). Because our cellular model lacks the complexity of interactions occurring *in vivo* between circulating immune cells and tissue-resident cells, including those of the productively infected respiratory tract, we hypothesize that it approaches the situation in mildly infected individuals with a transient, rapidly controlled phase of virus replication involving a limited amount of virus-induced cell damage and immune dysregulation.

Comparison of cells with and without detectable SARS-CoV-2 RNA revealed quantitative differences regarding gene expression. Genes associated with fibrosis, migration, and integrin binding were mildly upregulated in cells with detectable viral RNA when compared to bystander cells, defined as cells of the SARS-CoV-2-exposed cell culture, which lacked detectable viral reads. Interestingly, monocytes developing profibrotic functions have recently been established in the context of COVID-19 *in vivo* and to be marked by high expression of CD163 (Wendisch *et al*, 2021). The literature suggests that CD163 expression in monocytes and macrophages is tightly regulated by pro- and anti-inflammatory cytokines (reviewed in Etzerodt & Moestrup, 2013) but is also inducible following Toll-like receptor (TLR) signaling, indicating multiple mechanisms of CD163 regulation (Weaver *et al*, 2007). Our *ex vivo* exposure approach does not mirror the cytokine-containing environment monocytes and macrophages of SARS-CoV-2-infected individuals are exposed to, which might, among other reasons, explain the overall mild induction of CD163 in this cellular compartment observed in our data as opposed to data from COVID-19 patients (Gómez-Rial *et al*, 2020; Wendisch *et al*, 2021). Our single-cell RNA-sequencing dataset, however, allows us to speculate about another potential layer of SARS-CoV-2-induced CD163 upregulation in monocytes in the absence of proinflammatory cytokines as a consequence of virus uptake and innate sensing of viral compartments through pattern recognition receptors, such as TLRs.

Bystander cells displayed enhanced ISG expression, suggesting that sensing of viral PAMPs in cells, which internalized virion particles (identified by detectable viral reads) is largely dampened by the delivery of virion-packaged antagonists, whereas cells internalizing virions at a level below our detection limit remain sensing-competent and alert bystander cells, resulting in an elevated IFN module score in the latter. A potentially additional phenomenon is that virion-packaged antagonists lower the overall base-line IFN/ISG level in invaded cells, conversely resulting in a comparably elevated IFN module score in bystander cells. We favor this model because in our experimental set-up, we identified changes of the IFN module score at the single-cell level as a consequence of virus exposure. Interestingly, and in analogy to our findings, uptake of SARS-CoV by CD14-purified monocytes was found to correlate with a low-to-absent baseline level of IFN expression (Yilla *et al*, 2005). However, virus preparations were not cleared from contaminating cytokines originating from the producer cell during virus stock production, and whether the low IFN state was a cause or consequence of SARS-CoV-2 exposure was not investigated in that particular study (Yilla *et al*, 2005), making it difficult to draw analogies to our findings. Indeed, our data cannot exclude the potentially additionally contributing reciprocal scenario of a more efficient and more probable internalization specifically into cells with a low ISG profile, which, however, would imply the existence of an essential, IFN-sensitive step in the uptake of virions that we deem unlikely given the receptor-independent uptake and the nonreproductive nature of the particle uptake. Indeed, IFN treatment prior to SARS-CoV-2 exposure failed to change quantities of viral RNA uptake upon IFN stimulation as judged in a bulk approach. Multiple SARS-related CoV-encoded IFN antagonists, including structural components of the incoming virion that do not require productive infection for expression and function, dampen innate immune responses when ectopically expressed, including membrane and nucleocapsid proteins (Lei *et al*, 2020). In addition, virion components including ORF3- and ORF6-encoded proteins (Bai *et al*, 2021; Cheng Huang *et al*, 2007; Ito *et al*, 2005) have type I IFN evasion properties (Lei *et al*, 2020; Li *et al*, 2020; Schroeder *et al*, 2021). Interestingly, among those, ORF6 from SARS-CoV-2 was described to be inferior in counteracting phospho-IRF3 nuclear translocation in infected cells, compared with SARS-CoV ORF6, resulting in higher ISG induction (Schroeder *et al*, 2021). Therefore, incoming viral RNA sensing may be less efficiently prevented by SARS-CoV-2 ORF6 as compared to SARS-CoV ORF6. Finally, the large absence of a detectable ISG expression profile in SARS-CoV-exposed PBMCs is consistent with a previous report analyzing abortively infected monocyte-derived macrophages (Cheung *et al*, 2005).

By contrast, endemic human CoVs, including 229E, have been shown to actively enter and replicate in blood-derived monocytic cells and macrophages (Desforges *et al*, 2007; Funk *et al*, 2012), in line with the detectable expression of the cellular 229E-specific receptor CD13/APN (Yeager *et al*, 1992; Funk *et al*, 2012) and triggering a strong infection-induced type I interferon responses in the monocytic cell compartments (Cheung *et al*, 2005; Desforges *et al*, 2007). In contrast to 229E, *ex vivo* exposure of monocytes or macrophages to SARS-CoV-2 triggers a type I IFN-dependent response in the absence of productive infection (this manuscript; Zheng *et al*, 2020; Zankharia *et al*, 2022); however, *in vivo* studies clearly demonstrate the contribution of monocytes and macrophages to the SARS-CoV-2-induced disease progression as a consequence of the constant exposure to cytokines and viral PAMPs, eventually resulting in a gradually increasing dysregulated myeloid

cell compartment (Schulte-Schrepping *et al*, 2020; Kosyreva *et al*, 2021; Leon *et al*, 2022). By contrast, the high IFN induction of the low pathogenic HCoV 229E early upon infection, is thought to be beneficial for a rapid, immune-mediated viral clearance, whereas the highly pathogenic HCoVs SARS-CoV and SARS-CoV-2 encode numerous viral antagonists to evade innate signaling, eventually resulting in blunted activation of the host cellular immunity and delayed viral clearance *in vivo* (Fung & Liu, 2019; Kim & Shin, 2021).

Together, our study provides an analysis of gene expression in PBMCs exposed *ex vivo* to SARS-CoV and SARS-CoV-2 at the cell type and individual cell level. Our data suggest that direct stimulation of monocytes through physical contact with SARS-CoV-2 particles is followed by strong ISG induction, despite the absence of detectable productive infection.

Materials and Methods

Cell lines and primary cells

Vero E6 (ATCC CRL-1586) cells, Calu-3 (ATCC HTB-55) cells, and HEK293T (ATCC CRL-3216) cells were cultivated in Dulbecco's modified Eagle's medium (DMEM) supplemented with 10% heat-inactivated fetal calf serum, 1% nonessential amino acids (Thermo Fisher Scientific), and 1% sodium pyruvate (Thermo Fisher Scientific) in a 5% CO_2 atmosphere at 37°C. Cell lines were routinely monitored for the absence of mycoplasma and paramyxovirus simian virus 5.

Withdrawal of blood samples from healthy humans and cell isolation was conducted with approval of the local ethics committee (Ethical review committee of Charité Berlin, votes EA4/166/19 and EA4/167/19). Human PBMCs were isolated from buffy coats by Ficoll–Hypaque centrifugation. PBMCs were cultured at 2×10^6/ml in RPMI 1640 containing 10% heat-inactivated fetal calf serum (Sigma Aldrich), 1% penicillin–streptomycin (Thermo Fisher Scientific), and 2 mM L-glutamine (Thermo Fisher Scientific). The experiments conformed to the principles set out in the WMA Declaration of Helsinki and the Department of Health and Human Services Belmont Report.

Viruses

SARS-CoV isolate HKU-39849 (accession no. JQ316196.1, Zeng *et al*, 2003; van den Worm *et al*, 2012) and the SARS-CoV-2 BetaCoV/Munich/ChVir984/2020 isolate (B.1 lineage, EPI_ISL_406862, Wölfel *et al*, 2020) were used.

Virus was grown on Vero E6 cells and concentrated using Vivaspin® 20 concentrators with a size exclusion of 100 kDa (Sartorius Stedim Biotech) in order to remove cytokines of lower molecular weight, including IFNs. Virus stocks were stored at −80°C, diluted in OptiPro serum-free medium supplemented with 0.5% gelatine and PBS. Titer was defined by plaque titration assay. Cells inoculated with culture supernatants from uninfected Vero cells mixed with OptiPro serum-free medium supplemented with 0.5% gelatine and PBS, served as mock-infected controls. All infection experiments were carried out under biosafety level three conditions with enhanced respiratory personal protection equipment.

Plaque titration assay

The amount of infectious virus particles was determined via plaque titration assay. Vero E6 cells were plated at 3.5×10^5 cell/ml in 24-well and infected with 200 µl of a serial dilution of virus-containing cell-culture supernatant diluted in OptiPro serum-free medium. One hour after adsorption, supernatants were removed and cells overlaid with 2.4% Avicel (FMC BioPolymers) mixed 1:1 in 2x DMEM. Three days postinfection, the overlay was removed, cells were fixed in 6% formaldehyde and stained with 0.2% crystal violet, 2% ethanol, and 10% formaldehyde. Plaque forming units were determined from at least two dilutions for which distinct plaques were detectable.

Virus exposure of PBMCs

Thirty minutes prior to virus exposure, PBMCs were left mock-treated or treated with Ruxolitinib (10 µM) or Remdesivir (20 µM). Treatment was maintained for the duration of the entire experiment. Virus challenge occurred by inoculation of 0.4×10^6 cells/ml in RPMI cell-culture medium supplemented with 2% FCS. Four hours postchallenge, cells were centrifuged and supernatants were collected (referred to as inoculum). Cells were resuspended in RPMI cell-culture medium supplemented with 10% FCS and plated at 0.4×10^6 cell/1.5 ml in 12-wells. In addition, post-wash samples were collected. For further sampling, cell-culture supernatant was centrifuged, the supernatant was collected and mixed with OptiPro serum-free medium supplemented with 0.5% gelatine for titration on Vero E6 cell or mixed with RAV1 buffer for viral RNA extraction and stored at −80°C until sample processing. Suspension cells and adherent cells were lysed in Trizol reagents and subjected to total RNA extraction. In PBMC prestimulation experiments, cells were prestimulated for 18 h, stimuli were removed by washing with PBS, and cells were inoculated with SARS-CoV-2 for 24 h as described above. For stimulation, cells were mock-treated or treated with 100 IU/ml IFN-α2a (Roferon), cultured in the presence of supernatants from mock- or SARS-CoV-2-infected Calu-3 cells, either crude or processed by Vivaspin® 20 filtration to obtain the cytokine-containing, but a virus-free fraction of the supernatant, or cultured in the presence of 10% serum collected from three mildly diseased COVID-19 patients (WHO 3; see Appendix Table S1) or healthy control sera. Three hospitalized COVID-19 patients' sera and clinical data were collected at Charité—Universitätsmedizin Berlin in the context of the *PaCOVID-19 Study* (Kurth *et al*, 2020). Patients were recruited between March and November 2020. All patients provided a positive SARS-CoV-2 by RT–PCR from respiratory specimens. The study was approved by the ethics committee of Charité (EA2/066/20). Written informed consent was obtained from all patients or legal representatives.

Reagents and inhibitors

Ruxolitinib was purchased from InvivoGen and used at 10 µM concentration. Remdesivir (Gilead Sciences) was kindly provided by the Department of Infectious Diseases and Respiratory Medicine, Charité – Universitätsmedizin Berlin. IFN-α2a (Roferon) was obtained from Roche.

Quantitative Q-RT–PCR

Viral RNA was extracted from cell-culture supernatants using the NucleoSpin RNA virus isolation kit (Macherey-Nagel) according to the manufacturer's instructions. Total RNA extraction from cells and DNase treatment were performed with Direct-zol RNA extraction kit (Zymo Research). Viral genome equivalents were determined using a previously published assay specific for both SARS-CoV and SARS-CoV-2 E gene (Corman *et al*, 2020). Subgenomic E gene expression was analyzed using the same probe and reverse primer combined with a forward primer, which is located in the SARS-CoV-2 leader region (sgLead-CoV-F: CGA TCT CTT GTA GAT CTG TTC TC; Wölfel *et al*, 2020). Subgenomic N gene expression was quantified with the following primers and probe: nCoV sgN Fwd: 5'-CGA TCT CTT GTA GAT CTG TTC TC-3', nCoV sgN Rev: 5'-CAG TAT TAT TGG GTA AAC CTT GG-3' and nCoV sgN prb: 5'-56-FAM/ CAG TAA CCA GAA TGG AGA ACG CAG /3BHQ-1-3. To analyze human gene expression, extracted RNA was subjected to cDNA synthesis (NEB, Invitrogen). Quantification of relative mRNA levels was performed with the LightCycler 480 Instrument II (Roche) using Taq-Man PCR technology. For human *IFIT1* and *IFNB1*, a pre-made primer-probe kit was used (Applied Biosystems, assay IDs: Hs01911452_s1; Hs01077958_s1, respectively). For human *ACE2* (ACE2-F: TGCCTATCC TTCCTATATCAGTCCAA, ACE2-R:GAGTA CAGATTTGTCCAAAATCTAC, ACE2-P: 6-FAM/ATGCCTCCCTGCT CATTTGCTTGGT/IBFQ), *IL-6* (IL-6-F: GGATTCAATGAGGAGACT TGC, IL-6-R: CACAGCTCTGGCTTGTTCC, IL-6-P: 6-FAM/AATCAT CAC/ZEN/TGGTCTTTTGGAGTTTGAGG/IBFQ), and *IFNA1* (IFNA1-F:GGGATGAGGACCTCCTAGACAA, IFNA1-R:CATCACACAGGCTT CCAAGTCA, IFNA1-P:6-FAM/TTCTGCACCGAACTCTACCAGCAGC TG/BHQ), customer-designed oligonucleotides were synthesized by Integrated DNA Technologies (IDT). Relative mRNA levels were determined using the ΔΔCt method using human *RNASEP* (Applied Biosystems) as the internal reference. Data analysis was performed using LightCycler Software 4.1 (Roche).

Immunoblotting

Cells were washed once with ice-cold PBS and lysed in 60 µl RIPA Lysis Buffer (Thermo Fisher Scientific) supplied with 1% protease inhibitor cocktail set III (Merck Chemicals) for 30 min at 4°C. Cell debris was pelleted for 10 min at 13,000 *g* and 4°C, and the supernatant was transferred to a fresh tube. Protein concentration was determined with Thermo Scientific's Pierce™ BCA protein assay kit according to the manufacturer's instructions. Protein lysates were mixed with 4 X NuPAGE LDS Sample Buffer (Invitrogen), supplied with 10% 2-mercaptoethanol (Roth), and inactivated for 10 min at 99°C. Proteins were separated by size on a 12% sodium dodecyl sulfate polyacrylamide gel and blotted onto a 0.2 µm PVDF membrane (Thermo Scientific) by semi-dry blotting (BioRad). Human ACE2 was detected using a polyclonal goat anti-human ACE2 antibody (1:500, R&D Systems), a horseradish peroxidase (HRP)-labeled donkey anti-goat antibody (1:5,000, Dinova), and Super Signal West Femto Chemiluminescence Substrate (Thermo Fisher Scientific). As a loading control, samples were analyzed for β-Actin expression using a mouse anti-β-actin antibody (1:5,000, Sigma Aldrich) and an HRP-labeled goat anti-mouse antibody (1:10,000, Dianova).

HL116 cell-based detection of bioactive IFNs

Cell-culture supernatants of individual cell lines were titrated on HL116 cells that express the luciferase gene under the control of the IFN-inducible 6–16 promoter (Uzé *et al*, 1994). Cells were PBS-washed, and luciferase expression was quantified using Cell-Culture Lysis Buffer and the Luciferase Assay System (both Promega). The concentration of IFN was quantified using an IFN-α2a (Roferon) standard curve.

Cytokine profiling

Supernatants from untreated or Ruxolitinib-pretreated and mock-, SARS-CoV-, or SARS-CoV-2-inoculated PBMCs from four donors were collected 48 h postexposure. As a positive control, PBMCs were treated with 1 µg/ml Lipopolysaccharide (LPS, Sigma Aldrich) or 1 µg/ml Phytohaemagglutinin (PHA, Sigma Aldrich) for 48 h. For each condition, samples from four donors were pooled. Cytokines were quantified using a Human/Cytokine/Chemokine/Growth Factor Panel A 48-Plex Premixed Magnetic Bead Multiplex Assay (Merck Millipore), using the Luminex MAGPIX System according to the manufacturer's instructions. Calibration and verification checks were met for all of the analytes. All analytes had standard curves with R^2 values > 0.9, except for FGF-2, GM-CSF, IL-9, IL-27, MCP-3, MIP-1β, and PDGF-AA/BB, which had standard curves with R^2 values > 0.75.

Single-Cell RNA-seq

Single-Cell RNA-seq libraries were prepared with the 10× Genomics platform using the Chromium Next GEM Single Cell 3' Reagent Kits v.3.1 following the manufacturer's instructions. Samples were multiplexed using TotalSeq-A Antibodies purchased from BioLegend (A0256, A0258, and A0259). Antibody staining and the subsequent library preparation were performed following the manufacturer's instructions. Quality control of the libraries was performed with the KAPA Library Quantification Kit and Agilent TapeStation. Libraries were sequenced on a HiSeq4000 using the following sequencing mode: read 1: 28 bp, read 2: 91–100 bp, Index i7: 8 bp. The libraries were sequenced to reach ~20,000 reads per cell.

Single-Cell RNA-seq data analysis

BCL files from the sequencing protocol were processed using the Cell Ranger pipeline v 3.1.0 (10× Genomics) and further analyzed using the Seurat v3.1.4 package (Butler *et al*, 2018) in R v3.6 (https://www.r-project.org/). Preprocessing of the data was performed using the recommended SCTransform procedure and the IntegrateData with PrepSCTIntegration workflows to eliminate batch effects. A comprehensive description of the code used in the analysis of data is available at https://github.com/GoffinetLab/SARS-CoV-2_PBMC-study. Cell types were identified based on marker gene expression (Schulte-Schrepping *et al*, 2020): B cells (*CD3D*$^-$, *MS4A1*$^+$), CD4$^+$ T cells (*CD3D*$^+$, *CD8A*$^-$), CD8$^+$ T cells (*CD3D*$^+$, *CD8A*$^+$), NK cells (*CD3D*$^-$, *CD8A*$^-$, *NKG7*$^+$, *GNLY*$^+$), Monocytes (*CD3D*$^-$, *CD14*$^+$, *FCGR3A*$^+$). Reads aligning to the SARS-CoV or SARS-CoV-2 genome were identified by alignment to

a combined SARS-Cov (AY310120.1, GenBank) and SARS-CoV-2 (NC_045512.2, GenBank) reference using the same Cell Ranger pipeline and visualized in a coverage plot using pyGenomeTracks (Lopez-Delisle *et al*, 2021).

Cell trajectory analysis

Cell trajectory analysis was performed using the Monocle v2.14.0 package (Trapnell *et al*, 2014) according to the guidelines set out by the developers. Different cell types were subclustered and processed as mentioned above. A resolution parameter of 0.3 was used for clustering. DEGs between clusters were determined using Seurat's FindAllMarkers function (Wilcoxon rank-sum test); of these, genes with a Bonferroni-corrected *P*-value of < 0.05 were imputed as ordering genes to generate the minimum spanning tree using the DDRTree algorithm. Code available at https://github.com/GoffinetLab/SARS-CoV-2_PBMC-study.

IFN module score

The IFN-signaling pathway gene set [R-HSA-913531] from the Reactome database (Gillespie *et al*, 2022) was retrieved from the Molecular Signatures Database (MSigDB; Liberzon *et al*, 2015). Cells were scored on their expression of these genes using the AddModuleScore function in Seurat, which is referred to as the IFN module score as the pathway includes genes canonically differentially regulated in response to interferon signaling.

Flow cytometry analysis

PBS-washed cells were PFA-fixed and immunostained for individual surface protein expression using the following antibodies: Anti-CD3-FITC (#561807; BD Biosciences), anti-CD4-APC (#555349; BD Biosciences), anti-CD14-PE (#561707; BD Biosciences), anti-CD19-FITC (#21270193; ImmunoTools), anti-NRP1/CD304-APC-R700 (#566038, BD Biosciences), anti-PD-1/CD279-PE (#21272794; ImmunoTools), and anti-TIM-3/CD366-FITC (#345022; Biolegend). To determine ACE2 cell surface expression, cells were immunostained with a goat anti-human ACE2 antibody (#AF933, R&D Systems) followed by immunostaining with a secondary antibody donkey anti-goat Alexa Fluor 488 (#A-11055, Thermo Fisher). ACE2-positive HEK293T cells were generated by transduction of cells with retroviral vectors generated by transfection of HEK293T cells with MLV gag-pol (Bartosch *et al*, 2003), pCX4bsrACE2 (Kamitani *et al*, 2006), and pVSV-G (Stewart *et al*, 2003). A FACS Lyric device (Becton Dickinson, Franklin Lakes, NJ, USA) with BD Suite Software was used for analysis.

Data presentation and statistical analysis

If not stated otherwise, bars show the arithmetic mean of the indicated amount of repetitions. Error bars indicate SEM from the indicated amount of individual experiments. The thumbnail image was generated with Biorender. If not stated otherwise, statistical significance was calculated by performing the Student's *t*-test using GraphPad Prism. *P*-values < 0.05 were considered significant and marked accordingly: $P < 0.05$ (*), $P < 0.01$ (**), or $P < 0.001$ (***); n.s. = not significant (≥ 0.05).

Data availability

The raw sequencing datasets generated during this study are available at the NCBI Gene Expression Omnibus GSE197665 (https://www.ncbi.nlm.nih.gov/geo/query/acc.cgi?acc=GSE197665).

Expanded View for this article is available online.

Acknowledgements

We thank Julian Heinze for excellent technical support. We thank J. S. M. Peiris, University of Hong Kong, China for providing the SARS-CoV isolate HKU-39849. We thank Sandra Pelligrini for the kind gift of the HL116 cell line. We are grateful for access to the BIH Core Facility Sequencing. This work was supported by funding from the Berlin Institute of Health (BIH) to CG. JK is supported by the Center of Infection Biology and Immunity (ZIBI) and Charité PhD Program. Part of this work was supported by Deutsche Forschungsgemeinschaft (DFG) (SFB-TR 84 to CD) and Bundesministerium für Bildung und Forschung (BMBF) through the projects RAPID-II (01KI2006A) to CD. JE and MAM are supported by VW Foundation Grant no. 9A890. A-ES thanks FOR-COVID (Bayerisches Staatsministerium für Wissenschaft und Kunst) and the Helmholtz Association for financial support. Open Access funding enabled and organized by Projekt DEAL.

Author contributions

Julia Kazmierski: Conceptualization; data curation; formal analysis; validation; investigation; visualization; methodology; writing – review and editing. **Kirstin Friedmann:** Conceptualization; formal analysis; validation; investigation; visualization; methodology; writing – review and editing. **Dylan Postmus:** Formal analysis; visualization; writing – review and editing. **Jackson Emanuel:** Formal analysis; investigation; visualization. **Cornelius Fischer:** Data curation; formal analysis. **Jenny Jansen:** Investigation. **Anja Richter:** Investigation. **Laure Bosquillon de Jarcy:** Investigation. **Christiane Schüler:** Investigation. **Madlen Sohn:** Investigation. **Sascha Sauer:** Supervision. **Christian Drosten:** Resources. **Antoine-Emmanuel Saliba:** Resources. **Leif Erik Sander:** Resources. **Marcel A Müller:** Resources; supervision; writing – review and editing. **Daniela Niemeyer:** Conceptualization; data curation; supervision; writing – original draft; writing – review and editing. **Christine Goffinet:** Conceptualization; resources; data curation; formal analysis; supervision; funding acquisition; investigation; visualization; writing – original draft; project administration; writing – review and editing.

In addition to the CRediT author contributions listed above, the contributions in detail are:

JK, KF, DN, and CG conceived and designed the experiments; JK, KF, JE, JJ, AR, LBJ, CS, MS, and DN performed the experiments, JK, KF, DP, JE, CF, LBJ, DN, and CG analyzed the data; CD, A-ES, LES, and MAM provided resources; DN and CG drafted the manuscript; JK, KF, DP, MAM, DN, and CG reviewed and edited the manuscript; SS, DN, and CG supervised the research.

Disclosure and competing interests statement

Technische Universität Berlin, Freie Universität Berlin and Charité – Universitätsmedizin have filed a patent application for siRNAs inhibiting SARS-CoV-2 replication with DN as co-author. The other authors declare that they have no conflict of interest.

References

Anderson EM, Goodwin EC, Verma A, Arevalo CP, Bolton MJ, Weirick ME, Gouma S, McAllister CM, Christensen SR, Weaver J *et al* (2021) Seasonal

human coronavirus antibodies are boosted upon SARS-CoV-2 infection but not associated with protection. *Cell* 184: 1858 – 1864

Andersson MI, Arancibia-Carcamo CV, Auckland K, Baillie JK, Barnes E, Beneke T, Bibi S, Brooks T, Carroll M, Crook D *et al* (2020) SARS-CoV-2 RNA detected in blood products from patients with COVID-19 is not associated with infectious virus. *Wellcome Open Res* 5: 181

Arunachalam PS, Wimmers F, Mok CKP, Perera RAPM, Scott M, Hagan T, Sigal N, Feng Y, Bristow L, Tak-Yin Tsang O *et al* (2020) Systems biological assessment of immunity to mild versus severe COVID-19 infection in humans. *Science* 369: 1210 – 1220

Bacher P, Rosati E, Esser D, Martini GR, Saggau C, Schiminsky E, Dargvainiene J, Schröder I, Wieters I, Khodamoradi Y *et al* (2020) Low-avidity $CD4^+$ T cell responses to SARS-CoV-2 in unexposed individuals and humans with severe COVID-19. *Immunity* 53: 1258 – 1271

Bai Z, Cao Y, Liu W, Li J (2021) The SARS-CoV-2 nucleocapsid protein and its role in viral structure, biological functions, and a potential target for drug or vaccine mitigation. *Viruses* 13: 1115

Bartosch B, Dubuisson J, Cosset F-L (2003) Infectious hepatitis C virus pseudo-particles containing functional E1-E2 envelope protein complexes. *J Exp Med* 197: 633 – 642

Bastard P, Rosen LB, Zhang Q, Michailidis E, Hoffmann HH, Zhang Y, Dorgham K, Philippot Q, Rosain J, Béziat V *et al* (2020) Auto-antibodies against type I IFNs in patients with life-threatening COVID-19. *Science* 370: eabd4585

Blanco-Melo D, Nilsson-Payant BE, Liu W-C, Uhl S, Hoagland D, Møller R, Jordan TX, Oishi K, Panis M, Sachs D *et al* (2020) Imbalanced host response to SARS-CoV-2 drives development of COVID-19. *Cell* 181: 1036 – 1045

Bost P, Giladi A, Liu Y, Bendjelal Y, Gang X, David E, Blecher-Gonen R, Cohen M, Medaglia C, Li H *et al* (2020) Host-viral infection maps reveal signatures of severe COVID-19 patients. *Cell* 181: 1475 – 1488

Braun J, Loyal L, Frentsch M, Wendisch D, Georg P, Kurth F, Hippenstiel S, Dingeldey M, Kruse B, Fauchere F *et al* (2020) SARS-CoV-2-reactive T cells in healthy donors and patients with COVID-19. *Nature* 587: 270 – 274

Butler A, Hoffman P, Smibert P, Papalexi E, Satija R (2018) Integrating single-cell transcriptomic data across different conditions, technologies, and species. *Nat Biotechnol* 36: 411 – 420

Cantuti-Castelvetri L, Ojha R, Pedro LD, Djannatian M, Franz J, Kuivanen S, van der Meer F, Kallio K, Kaya T, Anastasina M *et al* (2020) Neuropilin-1 facilitates SARS-CoV-2 cell entry and infectivity. *Science* 370: 856 – 860

Castilletti C, Bordi L, Lalle E, Rozera G, Poccia F, Agrati C, Abbate I, Capobianchi MR (2005) Coordinate induction of IFN-alpha and -gamma by SARS-CoV also in the absence of virus replication. *Virology* 341: 163 – 169

Chen N, Zhou M, Dong X, Jieming Q, Gong F, Han Y, Qiu Y, Wang J, Liu Y, Wei Y *et al* (2020) Epidemiological and clinical characteristics of 99 cases of 2019 novel coronavirus pneumonia in Wuhan, China: a descriptive study. *Lancet* 395: 507 – 513

Cheung CY, Poon LLM, Ng IHY, Luk W, Sia S-F, Wu MHS, Chan K-H, Yuen K-Y, Gordon S, Guan Y *et al* (2005) Cytokine responses in severe acute respiratory syndrome coronavirus-infected macrophages in vitro: possible relevance to pathogenesis. *J Virol* 79: 7819 – 7826

Chu H, Zhou J, Wong BH-Y, Li C, Chan JF-W, Cheng Z-S, Yang D, Wang D, Lee AC-Y, Li C *et al* (2016) Middle East respiratory syndrome coronavirus efficiently infects human primary T lymphocytes and activates the extrinsic and intrinsic apoptosis pathways. *J Infect Dis* 213: 904 – 914

Chu H, Zhou J, Wong BH-Y, Li C, Cheng Z-S, Lin X, Poon VK-M, Sun T, Lau CC-Y, Chan JF-W *et al* (2014) Productive replication of Middle East respiratory syndrome coronavirus in monocyte-derived dendritic cells modulates innate immune response. *Virology* 454–455: 197 – 205

Corman VM, Landt O, Kaiser M, Molenkamp R, Meijer A, Chu DK, Bleicker T, Brünink S, Schneider J, Schmidt ML *et al* (2020) Detection of 2019 novel coronavirus (2019-nCoV) by real-time RT-PCR. *Euro Surveill* 25: 2000045

Daly JL, Simonetti B, Klein K, Chen K-E, Williamson MK, Antón-Plágaro C, Shoemark DK, Simón-Gracia L, Bauer M, Hollandi R *et al* (2020) Neuropilin-1 is a host factor for SARS-CoV-2 infection. *Science* 370: 861 – 865

Delorey TM, Ziegler CGK, Heimberg G, Normand R, Yang Y, Segerstolpe Å, Abbondanza D, Fleming SJ, Subramanian A, Montoro DT *et al* (2021) COVID-19 tissue atlases reveal SARS-CoV-2 pathology and cellular targets. *Nature* 595: 107 – 113

Desforges M, Miletti TC, Gagnon M, Talbot PJ (2007) Activation of human monocytes after infection by human coronavirus 229E. *Virus Res* 130: 228 – 240

Etzerodt A, Moestrup SK (2013) CD163 and inflammation: biological, diagnostic, and therapeutic aspects. *Antioxid Redox Signal* 18: 2352 – 2363

Fung TS, Liu DX (2019) Human coronavirus: host-pathogen interaction. *Annu Rev Microbiol* 73: 529 – 557

Funk CJ, Wang J, Ito Y, Travanty EA, Voelker DR, Holmes KV, Mason RJ (2012) Infection of human alveolar macrophages by human coronavirus strain 229E. *J Gen Virol* 93: 494 – 503

Gillespie M, Jassal B, Stephan R, Milacic M, Rothfels K, Senff-Ribeiro A, Griss J, Sevilla C, Matthews L, Gong C *et al* (2022) The reactome pathway knowledgebase 2022. *Nucleic Acids Res* 50: D687 – D692

Gómez-Rial J, Currás-Tuala MJ, Rivero-Calle I, Gómez-Carballa A, Cebey-López M, Rodríguez-Tenreiro C, Dacosta-Urbieta A, Rivero-Velasco C, Rodríguez-Núñez N, Trastoy-Pena R *et al* (2020) Increased serum levels of sCD14 and sCD163 indicate a preponderant role for monocytes in COVID-19 immunopathology. *Front Immunol* 11: 560381

Gu J, Gong E, Zhang B, Zheng J, Gao Z, Zhong Y, Zou W, Zhan J, Wang S, Xie Z *et al* (2005) Multiple organ infection and the pathogenesis of SARS. *J Exp Med* 202: 415 – 424

Hammond J, Leister-Tebbe H, Gardner A, Abreu P, Bao W, Wisemandle W, Baniecki M, Hendrick VM, Damle B, Simón-Campos A *et al* (2022) Oral Nirmatrelvir for high-risk, nonhospitalized adults with Covid-19. *N Engl J Med* 386: 1397 – 1408

Hoffmann M, Kleine-Weber H, Schroeder S, Krüger N, Herrler T, Erichsen S, Schiergens TS, Herrler G, Wu N-H, Nitsche A *et al* (2020) SARS-CoV-2 cell entry depends on ACE2 and TMPRSS2 and is blocked by a clinically proven protease inhibitor. *Cell* 181: 271 – 280

Honda K, Taniguchi T (2006) IRFs: master regulators of signalling by Toll-like receptors and cytosolic pattern-recognition receptors. *Nat Rev Immunol* 6: 644 – 658

Huang C, Wang Y, Li X, Ren L, Zhao J, Yi H, Zhang L, Fan G, Xu J, Gu X *et al* (2020) Clinical features of patients infected with 2019 novel coronavirus in Wuhan, China. *Lancet* 395: 497 – 506

Huang C, Ito N, Tseng C-TK, Makino S (2006) Severe acute respiratory syndrome coronavirus 7a accessory protein is a viral structural protein. *J Virol* 80: 7287 – 7294

Huang C, Peters CJ, Makino S (2007) Severe acute respiratory syndrome coronavirus accessory protein 6 is a virion-associated protein and is released from 6 protein-expressing cells. *J Virol* 81: 5423 – 5426

Ito N, Mossel EC, Narayanan K, Popov VL, Huang C, Inoue T, Peters CJ, Makino S (2005) Severe acute respiratory syndrome coronavirus 3a protein is a viral structural protein. *J Virol* 79: 3182 – 3186

Jones TC, Biele G, Mühlemann B, Veith T, Schneider J, Beheim-Schwarzbach J, Bleicker T, Tesch J, Schmidt ML, Sander LE *et al* (2021) Estimating infectiousness throughout SARS-CoV-2 infection course. *Science* 373: eabi5273

Kamitani W, Narayanan K, Huang C, Lokugamage K, Ikegami T, Ito N, Kubo H, Makino S (2006) Severe acute respiratory syndrome coronavirus nsp1 protein suppresses host gene expression by promoting host mRNA degradation. *Proc Natl Acad Sci USA* 103: 12885 – 12890

Kim Y-M, Shin E-C (2021) Type I and III interferon responses in SARS-CoV-2 infection. *Exp Mol Med* 53: 750 – 760

Kosyreva A, Dzhalilova D, Lokhonina A, Vishnyakova P, Fatkhudinov T (2021) The role of macrophages in the pathogenesis of SARS-CoV-2-associated acute respiratory distress syndrome. *Front Immunol* 12: 682871

Kowal K, Silver R, Sławińska E, Bielecki M, Chyczewski L, Kowal-Bielecka O (2011) CD163 and its role in inflammation. *Folia Histochem Cytobiol* 49: 365 – 374

Kurth F, Roennefarth M, Thibeault C, Corman VM, Muller-Redetzky H, Mittermaier M, Ruwwe-Glosenkamp C, Heim KM, Krannich A, Zvorc S *et al* (2020) Studying the pathophysiology of coronavirus disease 2019: a protocol for the Berlin prospective COVID-19 patient cohort (pa-COVID-19). *Infection* 48: 619 – 626

Lee JY, Wing PA, Gala DS, Noerenberg M, Järvelin AI, Titlow J, Zhuang X, Palmalux N, Iselin L, Thompson MK *et al* (2022) Absolute quantitation of individual SARS-CoV-2 RNA molecules provides a new paradigm for infection dynamics and variant differences. *Elife* 11: e74153

Lei X, Dong X, Ma R, Wang W, Xiao X, Tian Z, Wang C, Wang Y, Li L, Ren L *et al* (2020) Activation and evasion of type I interferon responses by SARS-CoV-2. *Nat Commun* 11: 3810

Leon J, Michelson DA, Olejnik J, Chowdhary K, Hyung Suk O, Hume AJ, Galván-Peña S, Zhu Y, Chen F, Vijaykumar B *et al* (2022) A virus-specific monocyte inflammatory phenotype is induced by SARS-CoV-2 at the immune–epithelial Interface. *Proc Natl Acad Sci USA* 119: e2116853118

Liao M, Liu Y, Yuan J, Wen Y, Gang X, Zhao J, Cheng L, Li J, Wang X, Wang F *et al* (2020) Single-cell landscape of bronchoalveolar immune cells in patients with COVID-19. *Nat Med* 26: 842 – 844

Liberzon A, Birger C, Thorvaldsdóttir H, Ghandi M, Mesirov JP, Tamayo P (2015) The Molecular Signatures Database (MSigDB) hallmark gene set collection. *Cell Syst* 1: 417 – 425

Li J-Y, Liao C-H, Wang Q, Tan Y-J, Luo R, Qiu Y, Ge X-Y (2020) The ORF6, ORF8 and nucleocapsid proteins of SARS-CoV-2 inhibit type I interferon signaling pathway. *Virus Res* 286: 198074

Lopez-Delisle L, Rabbani L, Wolff J, Bhardwaj V, Backofen R, Grüning B, Ramírez F, Manke T (2021) pyGenomeTracks: reproducible plots for multivariate genomic datasets. *Bioinformatics* 37: 422 – 423

Nelde A, Bilich T, Heitmann JS, Maringer Y, Salih HR, Roerden M, Lübke M, Bauer J, Rieth J, Wacker M *et al* (2021) SARS-CoV-2-derived peptides define heterologous and COVID-19-induced T cell recognition. *Nat Immunol* 22: 74 – 85

Ng KW, Faulkner N, Cornish GH, Rosa A, Harvey R, Hussain S, Ulferts R, Earl C, Wrobel AG, Benton DJ *et al* (2020) Preexisting and de novo humoral immunity to SARS-CoV-2 in humans. *Science* 370: 1339 – 1343

Ng LFP, Hibberd ML, Ooi E-E, Tang K-F, Neo S-Y, Tan J, Krishna Murthy KR, Vega VB, Chia J-M, Liu ET *et al* (2004) A human in vitro model system for investigating genome-wide host responses to SARS coronavirus infection. *BMC Infect Dis* 4: 34

Nouailles G, Wyler E, Pennitz P, Postmus D, Vladimirova D, Kazmierski J, Pott F, Dietert K, Muelleder M, Farztdinov V *et al* (2021) Temporal omics analysis in Syrian hamsters unravel cellular effector responses to moderate COVID-19. *Nat Commun* 12: 4869

Prebensen C, Myhre PL, Jonassen C, Rangberg A, Blomfeldt A, Svensson M, Omland T, Berdal J-E (2021) Severe acute respiratory syndrome coronavirus 2 RNA in plasma is associated with intensive care unit admission and mortality in patients hospitalized with coronavirus disease 2019. *Clin Infect Dis* 73: e799 – e802

Qin C, Zhou L, Hu Z, Zhang S, Yang S, Tao Y, Xie C, Ma K, Shang K, Wang W *et al* (2020) Dysregulation of immune response in patients with coronavirus 2019 (COVID-19) in Wuhan, China. *Clin Infect Dis* 71: 762 – 768

RECOVERY Collaborative Group, Horby P, Lim WS, Emberson JR, Mafham M, Bell JL, Linsell L, Staplin N, Brightling C, Ustianowski A *et al* (2021) Dexamethasone in hospitalized patients with Covid-19. *N Engl J Med* 384: 693 – 704

RECOVERY Collaborative Group (2022) Casirivimab and Imdevimab in patients admitted to hospital with COVID-19 (RECOVERY): A randomised, controlled, open-label, platform trial. *Lancet* 399: 665 – 676

Rothe C, Schunk M, Sothmann P, Bretzel G, Froeschl G, Wallrauch C, Zimmer T, Thiel V, Janke C, Guggemos W *et al* (2020) Transmission of 2019-nCoV infection from an asymptomatic contact in Germany. *N Engl J Med* 382: 970 – 971

Schroeder S, Pott F, Niemeyer D, Veith T, Richter A, Muth D, Goffinet C, Müller MA, Drosten C (2021) Interferon antagonism by SARS-CoV-2: a functional study using reverse genetics. *Lancet Microbe* 2: e210 – e218

Schulien I, Kemming J, Oberhardt V, Wild K, Seidel LM, Killmer S, Sagar, Daul F, Salvat Lago M, Decker A *et al* (2021) Characterization of pre-existing and induced SARS-CoV-2-specific $CD8^+$ T cells. *Nat Med* 27: 78 – 85

Schulte-Schrepping J, Reusch N, Paclik D, Baßler K, Schlickeiser S, Zhang B, Krämer B, Krammer T, Brumhard S, Bonaguro L *et al* (2020) Severe COVID-19 is marked by a dysregulated myeloid cell compartment. *Cell* 182: 1419 – 1440

Silvin A, Chapuis N, Dunsmore G, Goubet A-G, Dubuisson A, Derosa L, Almire C, Hénon C, Kosmider O, Droin N *et al* (2020) Elevated calprotectin and abnormal myeloid cell subsets discriminate severe from mild COVID-19. *Cell* 182: 1401 – 1418

Song X, Hu W, Yu H, Zhao L, Zhao Y, Zhao X, Xue H-H, Zhao Y (2020) Little to no expression of angiotensin-converting Enzyme-2 on Most human peripheral blood immune cells but highly expressed on tissue macrophages. *Cytometry A* 2020: 1 – 10

Stephenson E, Reynolds G, Botting RA, Calero-Nieto FJ, Morgan MD, Tuong ZK, Bach K, Sungnak W, Worlock KB, Yoshida M *et al* (2021) Single-cell multi-omics analysis of the immune response in COVID-19. *Nat Med* 27: 904 – 916

Stewart SA, Dykxhoorn DM, Palliser D, Mizuno H, Yu EY, An DS, Sabatini DM, Chen IS, Hahn WC, Sharp PA *et al* (2003) Lentivirus-delivered stable gene silencing by RNAi in primary cells. *RNA* 9: 493 – 501

Trapnell C, Cacchiarelli D, Grimsby J, Pokharel P, Li S, Morse M, Lennon NJ, Livak KJ, Mikkelsen TS, Rinn JL (2014) The dynamics and regulators of cell fate decisions are revealed by Pseudotemporal ordering of single cells. *Nat Biotechnol* 32: 381 – 386

Trombetta AC, Farias GB, Gomes AMC, Godinho-Santos A, Rosmaninho P, Conceição CM, Laia J, Santos DF, Almeida ARM, Mota C *et al* (2021) Severe COVID-19 recovery is associated with timely acquisition of a myeloid cell immune-regulatory phenotype. *Front Immunol* 12: 691725

Uzé G, Di Marco S, Mouchel-Vielh E, Monneron D, Bandu MT, Horisberger MA, Dorques A, Lutfalla G, Mogensen KE (1994) Domains of interaction between alpha interferon and its receptor components. *J Mol Biol* 243: 245 – 257

Wang D, Hu B, Hu C, Zhu F, Liu X, Zhang J, Wang B, Xiang H, Cheng Z, Xiong Y *et al* (2020a) Clinical characteristics of 138 hospitalized patients with

2019 novel coronavirus-infected pneumonia in Wuhan, China. *JAMA* 323: 1061 – 1069

Wang Y, Zhang D, Guanhua D, Ronghui D, Zhao J, Jin Y, Shouzhi F, Gao L, Cheng Z, Lu Q *et al* (2020b) Remdesivir in adults with severe COVID-19: a randomised, double-blind, placebo-controlled, multicentre trial. *Lancet* 395: 1569 – 1578

Weaver LK, Pioli PA, Wardwell K, Vogel SN, Guyre PM (2007) Up-regulation of human monocyte CD163 upon activation of cell-surface toll-like receptors. *J Leukoc Biol* 81: 663 – 671

Weinreich DM, Sivapalasingam S, Norton T, Ali S, Gao H, Bhore R, Xiao J, Hooper AT, Hamilton JD, Musser BJ *et al* (2021) REGEN-COV antibody cocktail clinical outcomes study in Covid-19 outpatients. *N Engl J Med* 385: e81

Wendisch D, Dietrich O, Mari T, von Stillfried S, Ibarra IL, Mittermaier M, Mache C, Chua RL, Knoll R, Timm S *et al* (2021) SARS-CoV-2 infection triggers profibrotic macrophage responses and lung fibrosis. *Cell* 184: 6243 – 6261

Wölfel R, Corman VM, Guggemos W, Seilmaier M, Zange S, Müller MA, Niemeyer D, Jones TC, Vollmar P, Rothe C *et al* (2020) Virological assessment of hospitalized patients with COVID-2019. *Nature* 581: 465 – 469

van den Worm SHE, Eriksson KK, Zevenhoven JC, Weber F, Züst R, Kuri T, Dijkman R, Chang G, Siddell SG, Snijder EJ *et al* (2012) Reverse genetics of SARS-related coronavirus using vaccinia virus-based recombination. *PLoS ONE* 7: e32857

Xiong Y, Liu Y, Cao L, Wang D, Guo M, Jiang A, Guo D, Hu W, Yang J, Tang Z *et al* (2020) Transcriptomic characteristics of bronchoalveolar lavage fluid and peripheral blood mononuclear cells in COVID-19 patients. *Emerg Microbes Infect* 9: 761 – 770

Xu G, Qi F, Li H, Yang Q, Wang H, Wang X, Liu X, Zhao J, Liao X, Liu Y *et al* (2020a) The differential immune responses to COVID-19 in peripheral and lung revealed by single-cell RNA sequencing. *Cell Discov* 2020: 73

Xu H, Zhong L, Deng J, Peng J, Dan H, Zeng X, Li T, Chen Q (2020b) High expression of ACE2 receptor of 2019-nCoV on the epithelial cells of Oral mucosa. *Int J Oral Sci* 12: 8

Yeager CL, Ashmun RA, Williams RK, Cardellichio CB, Shapiro LH, Look AT, Holmes KV (1992) Human aminopeptidase N is a receptor for human coronavirus 229E. *Nature* 357: 420 – 422

Yilla M, Harcourt BH, Hickman CJ, McGrew M, Tamin A, Goldsmith CS, Bellini WJ, Anderson LJ (2005) SARS-coronavirus replication in human peripheral monocytes/macrophages. *Virus Res* 107: 93 – 101

Zankharia U, Yadav A, Yi Y, Hahn BH, Collman RG (2022) Highly restricted SARS-CoV-2 receptor expression and resistance to infection by primary human monocytes and monocyte-derived macrophages. *J Leukoc Biol* 2022: 1 – 8

Zeng FY, Chan CWM, Chan MN, Chen JD, Chow KYC, Hon CC, Hui KH, Li J, Li VYY, Wang CY *et al* (2003) The complete genome sequence of severe acute respiratory syndrome coronavirus strain HKU-39849 (HK-39). *Exp Biol Med* 228: 866 – 873

Zhang Q, Bastard P, Liu Z, Le Pen J, Moncada-Velez M, Chen J, Ogishi M, Sabli IKD, Hodeib S, Korol C *et al* (2020) Inborn errors of type I IFN immunity in patients with life-threatening COVID-19. *Science* 370: eabd4570

Zheng J, Wang Y, Li K, Meyerholz DK, Allamargot C, Perlman S (2020) Severe acute respiratory syndrome coronavirus 2–induced immune activation and death of monocyte-derived human macrophages and dendritic cells. *J Infect Dis* 223: 785 – 795

Zhou Z, Huang C, Zhou Z, Huang Z, Su L, Kang S, Chen X, Chen Q, He S, Rong X *et al* (2021) Structural insight reveals SARS-CoV-2 ORF7a as an immunomodulating factor for human $CD14^+$ monocytes. *iScience* 24: 102187

Zou X, Chen K, Zou J, Han P, Hao J, Han Z (2020) Single-cell RNA-seq data analysis on the receptor ACE2 expression reveals the potential risk of different human organs vulnerable to 2019-nCoV infection. *Front Med* 14: 185 – 192

Absence of cGAS-mediated type I IFN responses in HIV-1–infected T cells

Carina Elsner[a,b,1], Aparna Ponnurangam[a,1], Julia Kazmierski[a,c,d], Thomas Zillinger[e], Jenny Jansen[c,d], Daniel Todt[f,g], Katinka Döhner[h], Shuting Xu[a], Aurélie Ducroux[a], Nils Kriedemann[a], Angelina Malassa[a], Pia-Katharina Larsen[i], Gunther Hartmann[e], Winfried Barchet[e,j], Eike Steinmann[f], Ulrich Kalinke[i], Beate Sodeik[h,k], and Christine Goffinet[a,c,d,2]

[a]Institute for Experimental Virology, TWINCORE, Centre for Experimental and Clinical Infection Research, 30625 Hanover, Germany; [b]Institute for Virology, University of Duisburg-Essen, University Hospital Essen, 45147 Essen, Germany; [c]Institute of Virology, Charité–Universitätsmedizin Berlin, 10117 Berlin, Germany; [d]Berlin Institute of Health, 10178 Berlin, Germany; [e]Institute of Clinical Chemistry and Clinical Pharmacology, University Hospital, University of Bonn, 53127 Bonn, Germany; [f]Department of Molecular and Medical Virology, Ruhr University Bochum, 44801 Bochum, Germany; [g]European Virus Bioinformatics Center, 07743 Jena, Germany; [h]Institute of Virology, Hanover Medical School, 30625 Hanover, Germany; [i]Institute for Experimental Infection Research, TWINCORE, Centre for Experimental and Clinical Infection Research, 30625 Hanover, Germany; [j]German Center for Infection Research, 50935 Cologne-Bonn, Germany; and [k]Cluster of Excellence Resolving Infection Susceptibility (Excellence Cluster 2155), Hanover Medical School, 30625 Hanover, Germany

Edited by Stephen P. Goff, Columbia University Medical Center, New York, NY, and approved June 28, 2020 (received for review February 12, 2020)

The DNA sensor cGAS catalyzes the production of the cyclic dinucleotide cGAMP, resulting in type I interferon responses. We addressed the functionality of cGAS-mediated DNA sensing in human and murine T cells. Activated primary CD4$^+$ T cells expressed cGAS and responded to plasmid DNA by upregulation of ISGs and release of bioactive interferon. In mouse T cells, cGAS KO ablated sensing of plasmid DNA, and TREX1 KO enabled cells to sense short immunostimulatory DNA. Expression of *IFIT1* and *MX2* was downregulated and upregulated in cGAS KO and TREX1 KO T cell lines, respectively, compared to parental cells. Despite their intact cGAS sensing pathway, human CD4$^+$ T cells failed to mount a reverse transcriptase (RT) inhibitor-sensitive immune response following HIV-1 infection. In contrast, infection of human T cells with HSV-1 that is functionally deficient for the cGAS antagonist pUL41 (HSV-1Δ*UL41*N) resulted in a cGAS-dependent type I interferon response. In accordance with our results in primary CD4$^+$ T cells, plasmid challenge or HSV-1Δ*UL41*N inoculation of T cell lines provoked an entirely cGAS-dependent type I interferon response, including IRF3 phosphorylation and expression of ISGs. In contrast, no RT-dependent interferon response was detected following transduction of T cell lines with VSV-G-pseudotyped lentiviral or gammaretroviral particles. Together, T cells are capable to raise a cGAS-dependent cell-intrinsic response to both plasmid DNA challenge or inoculation with HSV-1Δ*UL41*N. However, HIV-1 infection does not appear to trigger cGAS-mediated sensing of viral DNA in T cells, possibly by revealing viral DNA of insufficient quantity, length, and/or accessibility to cGAS.

HIV-1 | HSV-1 | cGAS | innate sensing | T cells

The ability of mammalian cells to sense invading pathogens by cellular pattern recognition receptors is crucial for mounting of an effective cellular defense response and for initiating adequate adaptive immunity. cGMP-AMP synthetase (cGAS) senses DNA of aberrant subcellular localization in a sequence-independent, but length-dependent manner. Binding of DNA by cGAS is implicated in antiviral and antimicrobial defense, and autoimmunity. Activated cGAS catalyzes the cyclization of ATP and GTP, resulting in the small molecule and cyclic dinucleotide cGAMP (1, 2). cGAMP induces a STING/TBK1/IRF3-dependent signaling cascade that culminates in the expression of IRF-3–induced genes and type I interferons (IFNs), which, in turn, elicit an antiviral state by transactivating multiple IFN-stimulated genes (ISGs). The exonuclease TREX1 constitutes an important counterplayer of cGAS and prevents immune hyperactivation by cleaving cytoplasmic DNA that would otherwise be sensed (3, 4).

It is widely accepted that herpesviral infections trigger cGAS/STING-dependent cellular responses that are essential for the host to overcome the infection in vivo. Herpesviruses have evolved numerous strategies to dampen this cellular surveillance machinery (reviewed in refs. 5 and 6). It is debated to which extent retroviruses, including HIV-1, are prone to cGAS-mediated sensing, especially in primary HIV-1 target cells. Many studies on HIV-1 and cGAS have been conducted in immortalized adherent cell lines of limited physiological relevance, including A549 lung epithelial cells, monocytic THP-1 cells, mouse L929 fibroblast cells (7–10), and primary human dendritic cells. The latter produce reverse transcripts efficiently only if transduced with HIV-1 particles that copackage SIV or HIV-2 Vpx (11, 12), a scenario that does not occur during natural HIV-1 infection. HIV-1 infection fails to trigger a detectable type I IFN expression in primary monocyte-derived macrophages unless capsids are destabilized genetically or pharmacologically (13), interferences which may induce leakage of reverse transcripts into the cytoplasm. The limited data available on the role of cGAS in HIV-1–infected T cells is controversial. One study in HIV-1–infected T cells proposed cGAS-dependent responses, which appeared to be triggered

Significance

Whether HIV-1 infection triggers cGAS-mediated immune responses in CD4$^+$ T cells remains debated. It is important to investigate to which extent HIV-1–infected T cells contribute to IFN production and expression of antiviral interferon-stimulated genes. By analyzing cellular responses upon productive HIV-1 infection or transduction, we demonstrate that lentiviruses and gammaretroviruses can infect and spread in primary CD4$^+$ T cells and T cell lines without alarming the cGAS-mediated DNA sensing machinery, probably due to their replication strategy that minimizes the abundance of cGAS-sensitive DNA PAMPs.

Author contributions: C.E., A.P., J.K., B.S., and C.G. designed research; C.E., A.P., J.K., T.Z., J.J., D.T., K.D., S.X., A.D., N.K., A.M., and P.-K.L. performed research; C.E., A.P., J.K., T.Z., J.J., D.T., S.X., A.D., and C.G. analyzed data; C.E., A.P., J.K., T.Z., D.T., K.D., P.-K.L., U.K., and C.G. wrote the paper; and G.H., W.B., E.S., U.K., B.S., and C.G. supervised research.

Competing interest statement: W.B. is an employee of IFM Therapeutics.

This article is a PNAS Direct Submission.

Data deposition: The RNA-sequencing (seq) data discussed in this publication has been deposited in National Center for Biotechnology Information's Gene Expression Omnibus (GEO), https://www.ncbi.nlm.nih.gov/geo (accession no. GSE150753).

[1]C.E. and A.P. contributed equally to this work.

[2]To whom correspondence may be addressed. Email: christine.goffinet@charite.de.

This article contains supporting information online at https://www.pnas.org/lookup/suppl/doi:10.1073/pnas.2002481117/-/DCSupplemental.

First published July 24, 2020.

postintegration, potentially through release of mitochondrial DNA in the course of productive infection (14). In that study, the accessory protein Vpr was reported to potentiate, while Vpu dampened these responses (14). In contrast, another study suggested that DNA sensing is generally blunted in T cells (15). Our work revealed that productive HIV-1 infection does not induce type I IFN expression in IL-2/PHA-activated PBMCs (16). Here, we readdressed the integrity of cGAS-mediated DNA sensing in primary and immortalized human and mouse CD4$^+$ T cells. We find that the integral components of the cGAS-mediated DNA sensing pathway are expressed and functional in CD4$^+$ T cells from both species. Challenge of T cells with a HSV-1 mutant with reduced ability to counteract cGAS elicited dramatic cGAS-dependent responses. HIV-1 infection, on the contrary, failed to induce detectable cGAS-dependent or reverse transcriptase (RT) inhibitor-sensitive type I IFN responses.

Results

Plasmid DNA Challenge Elicits a Type I IFN Response in Activated Human and Murine Primary CD4$^+$ T Cells. We first assessed cGAS expression in purified, resting, and activated primary human and mouse CD4$^+$ T cells. Immunoblotting revealed detectable levels of cGAS expression in IL-2/PHA–stimulated human CD4$^+$ T cells (Fig. 1*A* and *SI Appendix*, Fig. S1*A*) and anti-CD3/28–stimulated

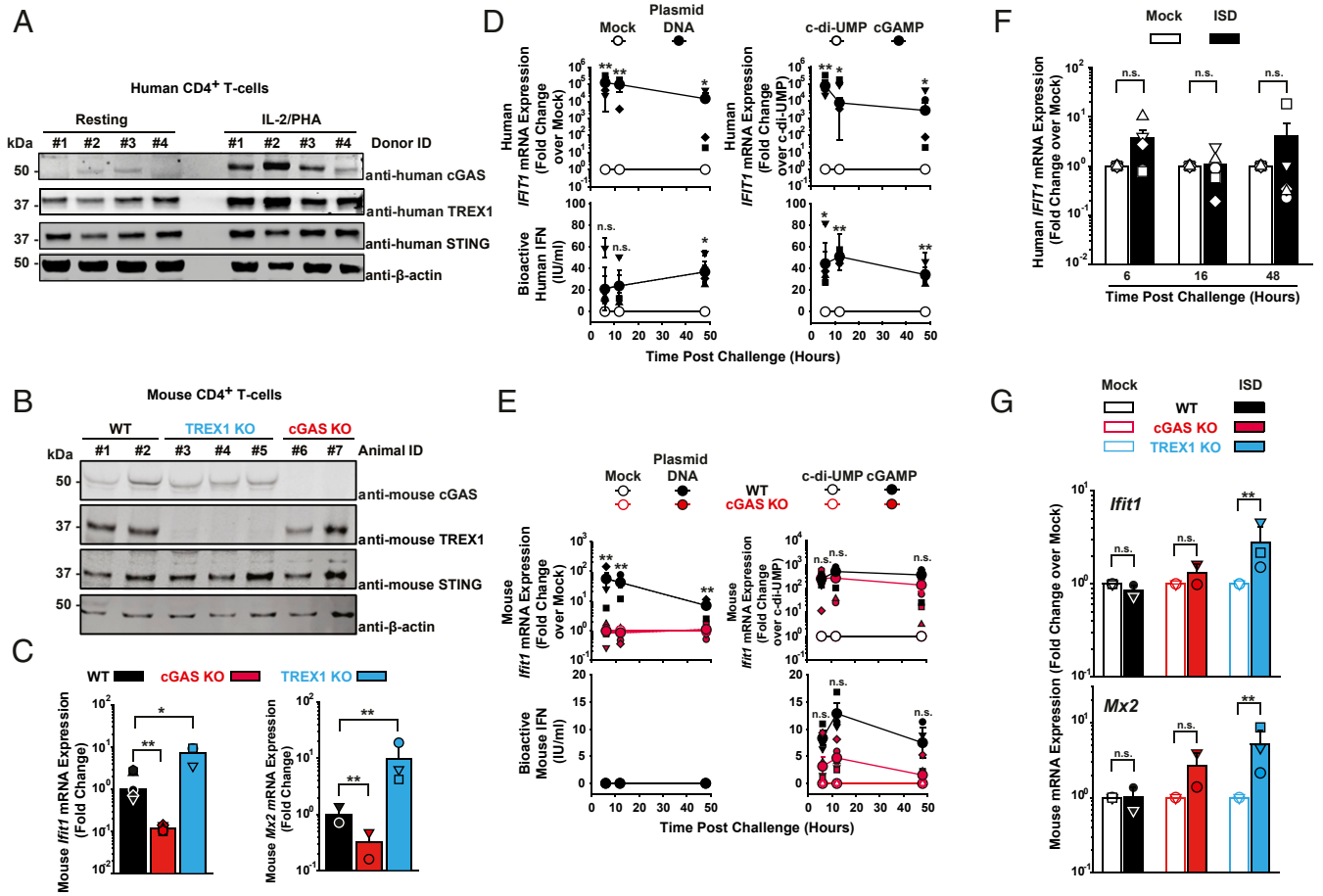

Fig. 1. Plasmid DNA challenge elicits a type I IFN response in activated human and murine primary CD4$^+$ T cells. (*A*) Immunoblotting of lysates of primary human CD4$^+$ T cells using indicated antibodies. (*B*) Immunoblotting of lysates of primary anti-CD3/28–activated and IL-2–activated CD4$^+$ T cells from WT, TREX1 KO, and cGAS KO mice using indicated antibodies. (*C*) Relative steady-state *Ifit1* and *Mx2* mRNA levels were determined by qRT-PCR in activated CD4$^+$ T cells of mice of indicated genotype (n = 2–3). Error bars indicate SEM from values obtained from cell cultures of two to three individual animals of each genotype. Small symbols represent levels obtained in individual animals; bars represent the arithmetic mean of values of all cell cultures of a given condition. (*D*) Activated human CD4$^+$ T cells were either mock-electroporated or electroporated with plasmid DNA (*Left*), and electroporated either with c-di-UMP or cGAMP (*Right*). Cultures were monitored at indicated time points postchallenge for relative *IFIT1* mRNA expression by qRT-PCR (*Upper*) and release of bioactive type I IFN using a luminometric HL116-based assay (*Lower*). Error bars indicate SEM from values obtained from cells from four individual donors whose values are depicted as small symbols. Large symbols represent the arithmetic mean of values of all cell cultures of a given condition. (*E*) Activated mouse CD4$^+$ T cells of WT and cGAS KO animals were either mock-electroporated or electroporated with plasmid DNA (*Left*), and electroporated either with c-di-UMP or cGAMP (*Right*). Cultures were monitored at indicated time points postchallenge for *Ifit1* mRNA expression by qRT-PCR (*Upper*) and release of bioactive type I IFN using a luminometric MEF-based assay (*Lower*). Error bars indicate SEM from values obtained from cells from three individual animals of each genotype whose values are depicted as small symbols. Large symbols represent the arithmetic mean of values of all cell cultures of a given condition. Statistical significance was calculated for T cells from cGAS KO versus WT animals. (*F*) Activated human CD4$^+$ T cells were mock-electroporated or electroporated with short ISD and monitored at indicated hours postchallenge for *IFIT1* mRNA expression by qRT-PCR. Error bars indicates SEM from values obtained from cells from four to five individual donors whose values are depicted as small symbols; bars represent the arithmetic mean of values of all cell cultures of a given condition. (*G*) Activated mouse CD4$^+$ T cells of indicated animals were mock-electroporated or electroporated with short ISD and monitored at 6 h postchallenge for *Ifit1* mRNA expression by qRT-PCR. Error bars indicates SEM from cells of three individual animals of each genotype whose values are depicted as small symbols; bars represent the arithmetic mean of values of all cell cultures of a given condition. P values <0.05 were considered significant (*) and <0.01 very significant (**); n.s. = not significant (≥0.05).

mouse CD4+ T cells (Fig. 1*B* and *SI Appendix*, Fig. S1*B*). In human CD4+ T cells, cGAS messenger RNA (mRNA) and protein levels were drastically lower in resting than in activated cultures, consistent with published data (17) (Fig. 1*A* and *SI Appendix*, Fig. S1 *A* and *C–D*), while cGAS expression was clearly detectable in both unstimulated and anti-CD3/28–activated mouse CD4+ T cells (*SI Appendix*, Fig. S1*B*). STING and the exonuclease TREX1 were expressed in activated CD4+ T cells of humans (Fig. 1*A*) and WT mice (Fig. 1*B*). In murine-activated CD4+ T cells, basal expression levels of *Ifit1* and *Mx2* mRNAs were reduced and elevated in the context of cGAS KO and TREX1 KO, respectively (Fig. 1*C*), suggesting that basal activities of cGAS and TREX1 modulate steady-state expression levels of cellular ISGs in T cells.

Next, we tested the DNA sensing abilities of activated CD4+ T cells of both species. Electroporation of IL-2/PHA–activated human CD4+ lymphocytes with endotoxin-free plasmid DNA gave rise to a more than 100,000-fold induction of *IFIT1* mRNA expression compared to mock electroporation (Fig. 1 *D*, *Upper Left*). Importantly, mock electroporation of primary CD4+ T cells did not induce detectable cellular responses (*SI Appendix*, Fig. S2*A*). Of note, *IFIT1* is transactivated directly by IRF3 and independently of type I IFNs (18). Up to 60 IU bioactive type I IFN/mL were secreted in the culture supernatant following plasmid DNA challenge (Fig. 1 *D*, *Lower Left*), while mock electroporation failed to induce significant changes of both readouts. Direct challenge with cGAMP, the catalytic product of cGAS, but not c-di-UMP, which does not activate STING, up-regulated *IFIT1* mRNA expression up to 100,000-fold (Fig. 1 *D*, *Upper Right*) and triggered the release of up to 80 IU bioactive IFN/mL (Fig. 1 *D*, *Lower Right*).

Analogous experiments in mouse CD4+ T cells (Fig. 1*E*) revealed that *Ifit1* mRNA induction upon plasmid DNA electroporation is strictly cGAS-dependent, suggesting that cGAS is the unique functional cytosolic DNA sensor expressed in this cell type, at least in the mouse species (Fig. 1 *E*, *Upper Left*). In contrast to human CD4+ T cells, intriguingly, no secretion of bioactive type I IFN into the culture supernatant was detectable upon DNA challenge (Fig. 1 *E*, *Lower Left*). Irrespective of their cGAS expression status, mouse CD4+ T cells scored positive for *Ifit1* mRNA induction (Fig. 1 *E*, *Upper Right*) and type I IFN release (Fig. 1 *E*, *Lower Right*) upon delivery of cGAMP, indicating that IFN release is not inherently blunted in this cell line. Sensing of short immunostimulatory DNA (ISD) was effective and cGAS-dependent in THP-1 cells (*SI Appendix*, Fig. S3, but occurred neither in human CD4+ T cells (Fig. 1*F*) nor in CD4+ T cells from WT and cGAS KO mice (Fig. 1*G*), but was detectable in cells from TREX1 KO mice (Fig. 1*G*), suggesting that TREX1 reduces the abundance of ISD molecules that are otherwise susceptible to cGAS sensing.

De Novo HIV-1 Infection, as Opposed to HSV-1 Infection, Fails to Trigger a Type I IFN Response in Human CD4+ T Cells. We next interrogated to which extent HIV-1 infection triggers cell-intrinsic innate immunity in human CD4+ T cells. Primary IL-2/PHA-activated CD4+ T cells were inoculated with HIV-$1_{Ba\text{-}L}$ and monitored for different parameters over a period of up to 13 d postinfection. We used R5-tropic HIV-$1_{Ba\text{-}L}$ because the extent of HIV-$1_{Ba\text{-}L}$–induced CD4+ T cell death was moderate and allowed us to conduct the experiment over a prolonged time period. In contrast, extensive cell death in cultures infected with the prototypic X4-tropic HIV-1 NL4.3 strain precluded any long-term kinetic experiments. Furthermore, HIV-$1_{Ba\text{-}L}$ stock was produced by serial passaging on susceptible T cell lines and did not rely on transfection of producer cells, a procedure that is inherently linked to contamination of viral stocks with proviral plasmid DNA. This potential contamination is problematic especially in the context of studies addressing DNA sensing and can only be removed by excessive DNase treatment of particles (19, 20).

RT inhibitor efavirenz (EFV)-sensitive and, thus, de novo production of HIV-1 p24 capsid, was detectable from 2 d postinfection on and typically peaked at day 6 postinfection, followed by a steady decrease until the end of the experiment at day 13 postinfection (Fig. 2*A*). Detectable de novo synthesis of HIV-1 late RT products started at 8 h postinfection (Fig. 2*B*). HIV-1 DNA synthesis peaked at day 6 postinfection, reaching 1,000 copies per cell and subsequently plateaued at around 200–300 copies per cell (Fig. 2*B*), suggesting multiple infection events per cell under these experimental conditions that favor viral spread from cell-to-cell. Strikingly, in these very same cultures, *IFIT1* mRNA expression was only 10-fold increased at 2 to 4 h. At 10 and 13 d postinfection, a 40- and 80-fold induction of *IFIT1* mRNA expression was detected. However, these increases were neither sensitive to EFV treatment nor grossly exceeded the level of *IFIT1* mRNA expressed in uninfected cells at the end of the experiment (day 13 postinfection) (Fig. 2 *C*, *Top*). This result suggests that the increases in *IFIT1* mRNA expression very early (3 and 4 h) and late (10 and 13 d) after viral inoculation indicate sensing of virus-associated PAMPs or DAMPs that are independent of reverse transcription. Alternatively, they may simply reflect fluctuations of the steady-state *IFIT1* mRNA levels in these activated primary CD4+ T cell cultures. Similarly, levels of *MX2* (Fig. 2 *C*, *Middle*) and *IFN*-β mRNA (Fig. 2 *C*, *Bottom*) expression fluctuated between unchanged and 4-fold increased and almost superimposed the levels detected in cells that had been treated with EFV prior to HIV-1 inoculation.

The small molecule inhibitor PF74, which binds a groove in the N-terminal domain of HIV-1 capsid, has been suggested to provoke premature disassembly of the viral core post entry (21–23). Interestingly, PF74-induced premature HIV-1 uncoating has been recently linked to increased cGAS-dependent immune responses (10, 24). We thus explored if PF74 treatment of CD4+ T cells during HIV-1 infection may force viral DNA leakage and accumulation in the cytoplasm, potentially followed by sensing. As expected, PF74 treatment potently inhibited productive infection of CD4+ T cells in the absence of detectable cell death (*SI Appendix*, Fig. S4*A*). However, no statistically significant induction of mRNA expression of *IFIT1*, *MX2*, and *IFN*-β was detectable (*SI Appendix*, Fig. S4*B*). Although values in PF74-treated, HIV-1–infected T cell cultures tended to be elevated compared to mock-treated, HIV-1–infected counterparts, no statistical significant difference between those two conditions could be established. In addition, treatment of cells with PF74 per se slightly induced *IFN*-β mRNA expression, although again, no statistically significant difference to levels of HIV-1–infected samples was obtained.

In order to explore whether primary human CD4+ T cells are competent for sensing of a DNA-viral infection at all, we assessed their response to HSV-1 inoculation. In vivo, HSV-2–infected T cells have been detected in lesions (25). Ex vivo, T cell lines and activated primary T cells appear to be susceptible to HSV-1 infection, as judged by detection of intracellular HSV-1 antigens upon exposure to virus (25–27). Owing to its genomic DNA of 152-kbp length, which is directly introduced into the infected cell upon entry of the capsid associated to tegument proteins and which has been reported to be released from a subset of capsids into the cytosol (28–30), we reasoned that HSV-1 might represent a useful control with a potentially high susceptibility to cGAS-mediated DNA sensing in T cells. We made use of an HSV-1 mutant (HSV-1 Δ*UL41*N), which lacks a large part of the 5′ part of the immunoevasion gene *UL41*, whose gene product pUL41 targets cGAS mRNA to degradation (31). Inoculation with HSV-1 Δ*UL41*N yielded 6% VP5 capsid protein-positive CD4+ T cells at day 2 postinfection, and sensitivity of the VP5 positivity to acyclovir (ACV) provides first evidence for a productive HSV-1 infection in this cell type, at least ex vivo (Fig. 2*D*). We detected an average of 32 viral DNA copies per cell directly upon

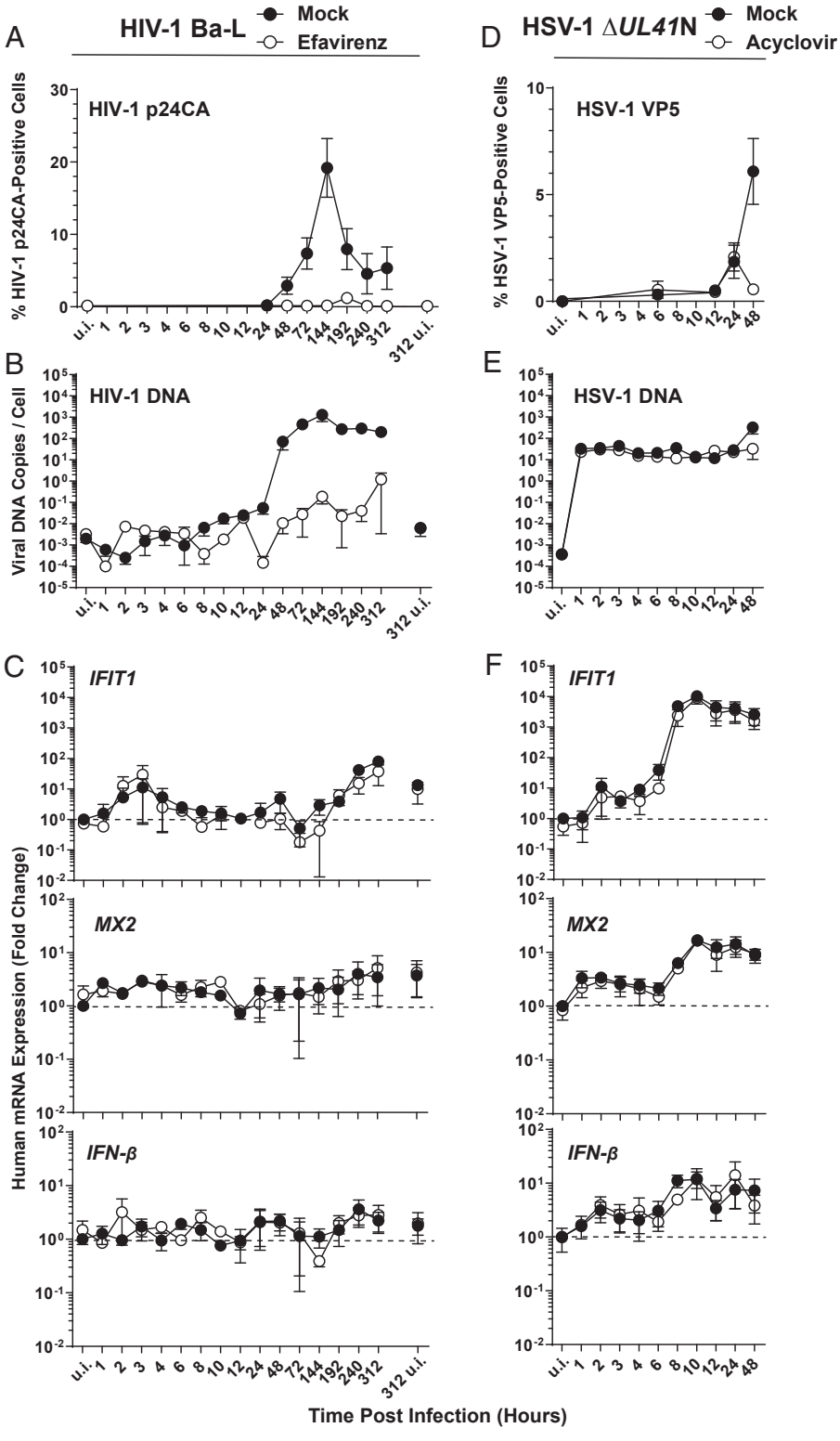

Fig. 2. De novo HIV-1 infection, as opposed to HSV-1 infection, fails to trigger a type I IFN response in human CD4$^+$ T cells. (*A*–*C*) Primary human CD4$^+$ T cells were infected with HIV-$1_{Ba\text{-}L}$ in the absence and presence of EFV and monitored, at indicated time points, for: (*A*) HIV-1 p24 capsid expression by intracellular immunostaining followed by FACS analysis. (*B*) De novo synthesis of HIV-1 late RT products by absolute qPCR. (*C*) Relative expression of *IFIT1*, *MX2*, and *IFN*-β by qRT-PCR. (*D*–*F*) Primary human CD4$^+$ T cells were inoculated with HSV-1 Δ*UL41*N in the absence and presence of ACV and monitored, at indicated time points, for: (*D*) HSV-1 VP5 capsid protein expression by intracellular immunostaining followed by FACS analysis. (*E*) Genomic HSV-1 DNA copy numbers by absolute qPCR. (*F*) Relative expression of *IFIT1*, *MX2*, and *IFN*-β by qRT-PCR. Error bars show SEM from values obtained from CD4$^+$ T cells from three to five individual donors.

HSV-1 inoculation, a quantity that was maintained over 24 h irrespective of absence or presence of ACV. This DNA most likely represents incoming genomic DNA prior to HSV-1 DNA replication. At 48 h, the level of HSV-1 Δ*UL41*N DNA copies per cell increased 10-fold in untreated cells in an ACV-sensitive fashion, suggesting active viral DNA replication in $CD4^+$ T cells (Fig. 2*E*). In these very same infected T cell cultures, *IFIT1* mRNA expression clearly increased over time in an ACV-insensitive manner and reached up to 14,000-fold higher levels than uninfected cells at 8 h postinfection, suggesting that the incoming viral DNA or a PAMP/DAMP independent of viral DNA replication triggered IRF3-mediated *IFIT1* mRNA expression (Fig. 2 *F*, *Top*). mRNA expression of *MX2* (Fig. 2 *F*, *Middle*) and *IFN*-β (Fig. 2 *F*, *Bottom*) was increased 29-fold and 25-fold, respectively.

Together, these results point toward the absence of a robust cell-intrinsic immunity response to HIV-1 infection in primary human $CD4^+$ T cells despite productive infection and abundant synthesis of de novo HIV-1 RT products. In contrast, a control HSV-1 Δ*UL41*N infection, although accompanied by the intracellular delivery of viral DNA copies 10-fold less in numbers or at best approaching those measured at the peak of spreading HIV-1 infection, clearly elicited cell-intrinsic innate immunity.

Global Analysis of the Cellular Transcriptome of HIV-$1_{Ba\text{-}L}$–Infected Primary $CD4^+$ T Cells. To assess the cellular response of primary $CD4^+$ T cells to HIV-1 infection on a global scale, we sequenced RNA isolated from infected cultures. Transcript abundance for 28 individual genes implicated in or induced by the IFN signaling pathway were calculated and mean RPKM values were compared (Fig. 3*A*). None of them were notably deregulated with respect to EFV treatment, indicating that productive infection did not provoke a detectable type I IFN response, in line with our qRT-PCR–based measurements of *IFIT1*, *MX2*, and *IFN*-β mRNA expression (Fig. 2*C*). Plotting of raw RPKM values greater than 0.5 of all RNAs revealed only very minor differences in the overall transcriptome of cells productively infected compared to cells treated with EFV prior to infection (Fig. 3*B*). Those genes that were statistically significantly deregulated (34 at 3 h, 10 at 8 h, and 78 at 144 h) were only modulated at very mild levels (Fig. 3*C*) and are predominantly associated with cell cycle-associated pathways. Complete linkage clustering did not reveal patterns of ISGs differentially regulated in cells with productive HIV-1 replication over time (Fig. 3*D*). Finally, HIV-1 RNA reads retrieved from the identical samples confirmed de novo production of HIV-1 mRNAs at 144 h postinfection (Fig. 3*E*).

The Human T Cell Line PM1 Expresses Functional cGAS. We next studied the role of cGAS during HIV-1 and HSV-1 Δ*UL41*N infection of T cells. To this end, we first screened a panel of immortalized human T cell lines frequently used in HIV-1 research for endogenous cGAS expression. Interestingly, the collection displayed drastic cell line-specific differences in cGAS mRNA and protein expression. PM1 and CEM T cell lines displayed high and moderate cGAS levels, respectively, whereas SUPT1, A3.01, and Jurkat T cell lines expressed low levels of cGAS mRNA and scored negative for cGAS protein (Fig. 4*A*). Because PM1 T cells shared high levels of endogenous cGAS expression with primary human activated $CD4^+$ T cells, they were chosen for mechanistic studies and subjected to CRISPR/Cas9-mediated *knock-out* of cGAS (Fig. 4*B*). Delivery of plasmid DNA into the cytoplasm of parental PM1 T cells by electroporation increased the abundance of *IFIT1* mRNAs up to 133,000-fold (Fig. 4 *C*, *Upper Left*) and induced release of up to 17 IU/mL bioactive IFN (Fig. 4 *C*, *Lower Left*). Mock electroporation per se did not induce cellular responses (*SI Appendix*, Fig. S2*B*). These responses were almost entirely abrogated in cGAS KO PM1 T cells. The efficiency of plasmid DNA sensing in the other T cell lines largely correlated with their individual cGAS expression status, with the exception of A3.01 T cells, which reacted to plasmid DNA in the absence of detectable endogenous cGAS protein expression (*SI Appendix*, Fig. S5*A*), pointing toward the potential contribution of other DNA sensors than cGAS in this cell line to DNA sensing. Reconstitution of normally cGAS-negative Jurkat T cells with WT, but not with catalytically inactive, cGAS (G212A/S213A) mutant enabled *IFIT1* up-regulation as an early response to plasmid DNA challenge (*SI Appendix*, Fig. S5*A*). cGAMP-triggered enhancement of *IFIT1* mRNA expression and IFN release was generally detectable irrespective of the cGAS expression status (*SI Appendix*, Fig. S5*B*), although appearing more pronounced in cGAS KO PM1 T cells as compared to parental PM1 T cells (Fig. 4 *C*, *Right*). Conclusively, PM1 T cells recapitulate the expression status of endogenous cGAS and the plasmid DNA sensing ability of primary activated human $CD4^+$ T cells, suggesting that they may serve as a valuable model for investigating cGAS-mediated sensing of DNA in T cells upon viral infections. Most importantly, cGAS appears to be the only and essential sensor of plasmid DNA in this model T cell line.

Absence of cGAS-Mediated Innate Immune Responses in PM1 T Cells upon Lentiviral Vector Transduction, as Opposed to HSV-1 Infection. To unravel the contribution of cGAS in PM1 T cells during sensing of HIV-1 infection, we transduced parental and cGAS KO cells with VSV-G–pseudotyped lentiviral vectors containing a CMV-driven GFP-encoding transfer vector and monitored the cellular response over time. VSV-G–pseudotyped vectors do not express HIV-1 accessory genes, some of which have been suggested to counteract cell-intrinsic immune sensing (14, 32) and enable a robust transduction efficiency during a single round of replication. We thus hypothesized that any potential cellular sensing of HIV-1 should have the highest chance of being detected in this experimental system. Inoculation of PM1 T cell lines resulted in 30–35% GFP-positive cells at 3 d postinfection, irrespective of the cGAS expression status, and EFV-mediated inhibition of RT almost entirely abolished transduction (Fig. 5*A*). During the entire experiment, transduced parental PM1 T cells displayed virtually unchanged *IFIT1* and slightly (10-fold) elevated *MX2* mRNA expression, which however was neither cGAS-dependent nor EFV-sensitive (Fig. 5*B*). Genetic modification of the HIV-1 capsid at specific positions (N74D and P90A) has been reported to prevent the interaction with capsid-stabilizing cellular cofactors and, thereby, reduce the stability of the viral core (33–35), inducing a premature capsid disassembly resulting in a type I IFN response in THP-1 cell lines and primary macrophages (13, 36). As expected (36), individual inoculation of parental PM1 T cells with equal p24 capsid equivalents of HIV-1 (CA N74D) and HIV-1 (CA P90A) (*SI Appendix*, Fig. S6*A*) resulted in a 10-fold reduced transduction efficiency, as compared to cells infected with WT counterpart (*SI Appendix*, Fig. S6*B*). Our data do not exclude the possibility that the capsid mutations resulted in less-efficient reverse transcription and nuclear import. However, both mutations are well-described to destabilize the capsid (33–35) and, even if reduced in quantity, leaky and/or abortive RT products were shown to become accessible to cellular sensors at least in other cell types (13, 36). Strikingly, HIV-1 (CA N74D) and HIV-1 (CA P90A) failed to trigger a detectable elevation of *IFIT1* and *MX2* mRNA expression in PM1 T cells (*SI Appendix*, Fig. S6*C*).

In stark contrast, inoculation of parental PM1 T cell lines with HSV-1 Δ*UL41*N (Fig. 5*C*) was followed by an up to 1,500-fold up-regulated *IFIT1* mRNA expression, which was strictly cGAS-dependent until 12 h post infection (Fig. 5 *D*, *Upper*), and a constantly cGAS-dependent, up to 300-fold up-regulated *MX2* mRNA expression (Fig. 5 *D*, *Lower*). ACV treatment did not prevent *IFIT1* and *MX2* mRNA expression, consistent with the idea that the incoming viral genome is sensed by cGAS. In line with our observations in primary human $CD4^+$ T cells infected with HIV-$1_{Ba\text{-}L}$, parental PM1 T cells fail to induce robust immune

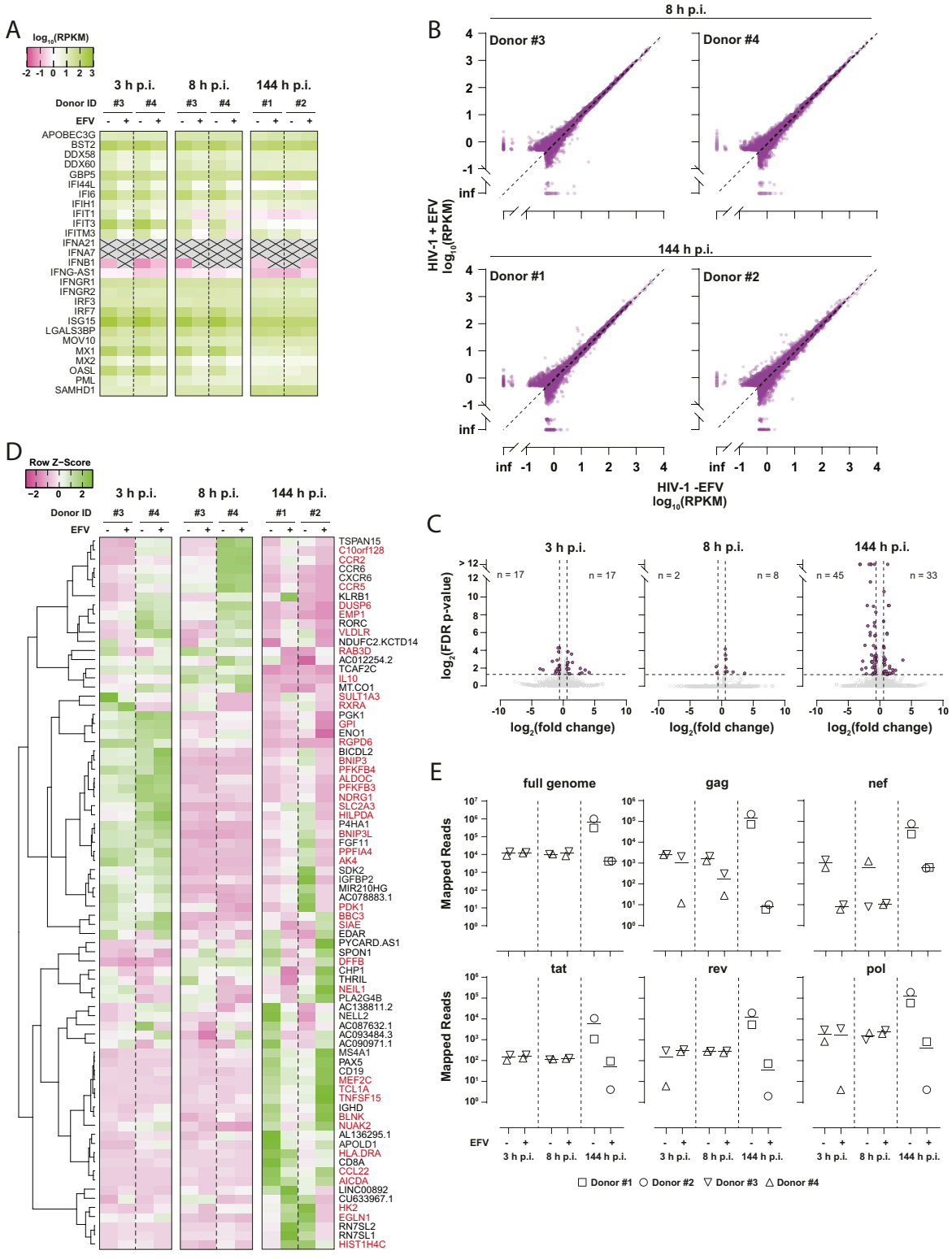

Fig. 3. Global analysis of the cellular transcriptome of HIV-$1_{Ba\text{-}L}$–infected primary $CD4^+$ T cells. (*A*) RPKM values of 28 individual genes implicated in or induced by the IFN signaling pathway are depicted as heatmap. Shown is the temporal expression in ex vivo HIV-$1_{Ba\text{-}L}$–infected $CD4^+$ T cells at 3, 8, and 144 h postinfection (p.i.), in the presence or absence of EFV treatment. Transcripts with RPKM < 0.01 are crossed out. (*B*) Plot of raw RPKM values greater than 0.5 of RNAs of all donors obtained from productively infected cells (HIV-1 -EFV) versus cells treated with EFV (HIV-1 +EFV) prior to and during infection. (*C*) Plot of fold change (untreated versus EFV-treated cells) versus FDR *P* value of all mapped human genes at indicated time points p.i. with HIV-$1_{Ba\text{-}L}$ (gray circles). The numbers of transcripts deregulated more than twofold with FDR *P* values <0.05 (purple circles) are shown in the plots. (*D*) Heatmap displaying row z-scores of the 78 genes that were statistically significantly deregulated in untreated versus EFV-treated infected cells at 144 h p.i. Complete linkage clustering of genes using the Pearson distance measurement method was performed with heatmapper 2 (www2.heatmapper.ca). Genes labeled in red are known ISGs according to interferome v2.01 (www.interferome.org; search parameters were set to "any", except, Species: "Homo sapiens" and System: "Haemopoietic/Immune"). (*E*) Number of RNA-seq reads mapping to HIV-$1_{Ba\text{-}L}$ reference sequence at indicated time points postinfection.

responses upon lentiviral transduction, despite a high transduction efficiency and absence of HIV-1 accessory gene expression. In strong contrast, PM1 T cells mount drastic cell-intrinsic responses to HSV-1 Δ*UL41*N inoculation in a strictly cGAS-dependent fashion early after infection.

Our data did not exclude the possibility of an active suppression of innate sensing by an incoming component of the lentiviral particle, e.g., capsid-mediated inhibition of IRF3 phosphorylation. However, pulsing cells with the GFP-expressing lentivirus (Fig. 5*E*) did not interfere with cGAS-mediated innate sensing of a subsequent HSV-1 Δ*UL41*N infection (Fig. 5*F*), arguing against the idea of a lentivirus-induced suppression of the innate sensing machinery.

cGAS and TREX1 Modulate Sensing of Plasmid DNA and of ISD, Respectively. Mouse T cell lines are refractory to productive HIV-1 infection, even upon circumvention of the mouse-specific entry block by usage of VSV-G–pseudotyped virus (37–40). We initially hypothesized that this postentry block may be related to a mouse T cell-specific sensing property. Since mouse $CD4^+$ T cells expressed functional cGAS (Fig. 1 *B* and *E* and *SI Appendix*, Fig. S1*B*), we tested its role during lentiviral and gammaretroviral transduction. In analogy to the human T cell line screen, we identified a remarkable diversity in cGAS expression levels among a panel of mouse T cell lines. While YAC-1 and S1A.TB T cells expressed cGAS, L1210, R1.1, and TIMI.4 cell lines scored negative (Fig. 6*A*). We thus introduced cGAS and TREX1 *knock-outs* in YAC-1 T cell lines via CRISPR/Cas9 gene editing (Fig. 6*B*).

In mouse YAC-1 T cells, the induction of *Ifit1* and *Mx2* mRNA expression upon plasmid DNA challenge was almost entirely dependent on endogenous cGAS expression (Fig. 6 *C*, *Top* and *Middle*). The remaining four cell lines failed to induce significant *Ifit1* mRNA expression upon plasmid DNA electroporation (*SI Appendix*, Fig. S7*A*). Among the parental T cell line panel, only YAC-1 T cells secreted detectable amounts of bioactive type I IFN in the culture supernatant upon plasmid DNA electroporation, and this process occurred in an entirely cGAS-dependent manner (Fig. 6 *C*, *Bottom* and *SI Appendix*, Fig. S7*B*). TREX1 KO and parental YAC-1 T cells shared a common *Ifit1* and *Mx2* mRNA induction pattern upon DNA challenge, and differed only by a slightly elevated, but very transient (only at 6 h) secretion of bioactive type I IFN in the culture supernatant of TREX1 KO cells. These results probably reflect the overall resistance of the electroporated circular plasmid DNA to the exonuclease activity of TREX1 (41). All tested mouse T cell lines reacted to cGAMP by up-regulation of *Ifit1* mRNA expression (*SI Appendix*, Fig. S7*C*) and most of them by release of bioactive type I IFN. Paralleling our results obtained in cGAMP-transfected human PM1 T cells (Fig. 4 *C*, *Right*), cGAMP challenge of cGAS KO YAC-1 T cells was followed by an enhanced *Ifit1* mRNA expression as compared to parental YAC-1 T cells (Fig. 6 *C*, *Top Right*). In contrast, expression of *Mx2* mRNA and release of bioactive IFN were of similar quantities in cGAS KO and parental YAC-1 T cells (Fig. 6 *C*, *Middle* and *Bottom Right*), suggesting that cGAS expression does not grossly modulate the magnitude of cGAMP-induced IFN production, but may potentially enforce IRF3-mediated responses. TREX1 KO did not display overt changes in any readout monitored after cGAMP challenge compared to parental cells.

While eletroporation of parental and cGAS KO YAC-1 T cells with short ISD did not induce detectable changes of *Ifit1* and *Mx2* mRNA expression as compared to mock treatment, TREX1 KO clearly augmented cell-intrinsic immune responses (Fig. 6*D*) in accordance with our findings in primary mouse T cells (Fig. 1*G*) and in line with the predominant exonuclease activity of TREX1 (41).

Conclusively, in analogy to human PM1 T cells, YAC-1 T cells express endogenous cGAS and sense plasmid DNA in a cGAS-dependent manner. In addition, TREX1 prevents sensing of short ISD, while it does not prevent sensing of circular and/or long DNA species.

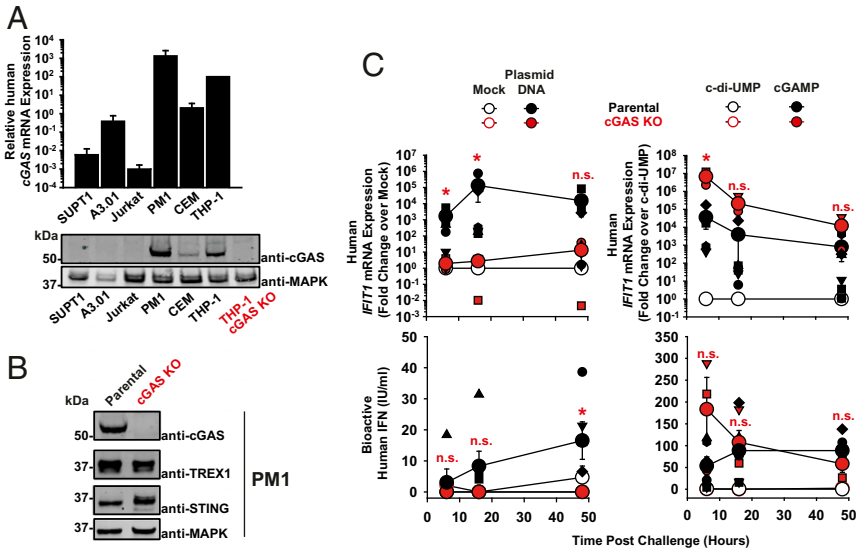

Fig. 4. The human T cell line PM1 expresses functional cGAS. (*A*) Relative levels of cGAS mRNA expression in indicated cell lines (bar diagram). The level detected in THP-1 cells is set to 100. Immunoblotting of indicated cell lysates using anti-cGAS and anti-MAPK antibodies. Lysates of parental and cGAS KO THP-1 cells serve as specificity control for the anti-human cGAS antibody. (*B*) Immunoblotting of lysates of parental and cGAS KO PM1 T cell lines using indicated antibodies. (*C*) Parental and cGAS KO PM1 T cells were either mock-electroporated or electroporated with plasmid DNA (*Left*), or electroporated either with c-di-UMP or cGAMP (*Right*). Cultures were monitored at indicated time points postchallenge for relative *IFIT1* mRNA expression by qRT-PCR (*Upper*) and release of bioactive type I IFN using a luminometric HL116-based assay (*Lower*). Error bars show SEM from three to four independent experiments whose values are shown as small symbols. The arithmetic means of values of all cell cultures of a given condition are shown as large symbols. Statistical significance was calculated for cGAS KO versus parental T cells. *P* values <0.05 were considered significant (*) and <0.01 very significant (**); n.s. = not significant (≥0.05).

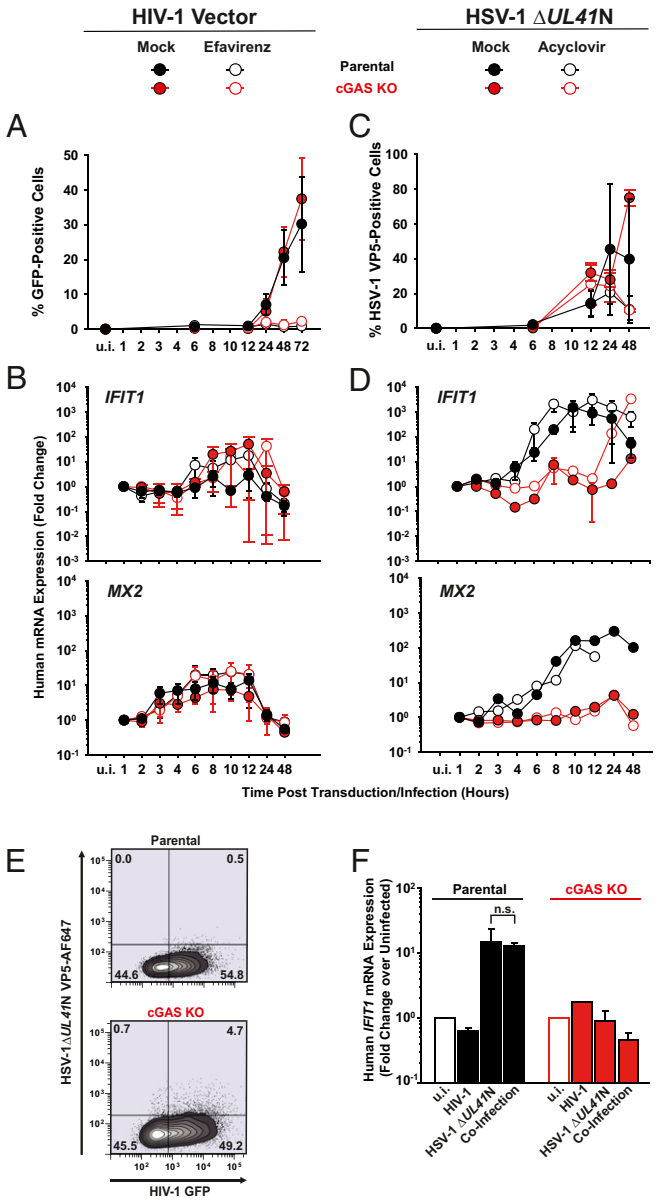

Fig. 5. Absence of cGAS-mediated innate immune responses in PM1 T cells upon lentiviral vector transduction as opposed to HSV-1 infection. (*A* and *B*) Parental and cGAS KO PM1 T cells were transduced with VSV-G–pseudotyped HIV-1 GFP vectors in the absence and presence of EFV and monitored, at indicated time points, for: (*A*) Reporter GFP expression by FACS analysis. (*B*) Relative expression of *IFIT1* and *MX2* by qRT-PCR. (*C* and *D*) Parental and cGAS KO PM1 T cells were inoculated with HSV-1 Δ*UL41*N in the absence and presence of ACV and monitored, at indicated time points, for: (*C*) HSV-1 VP5 capsid protein expression by intracellular immunostaining followed by FACS analysis. (*D*) Relative expression of *IFIT1* and *MX2* by qRT-PCR. (*E*) Parental and cGAS KO T cells were transduced with HIV-1 vectors, followed by inoculation with HSV-1 Δ*UL41*N 24 h later. Shown is a representative dot plot of dually infected cells at 48 h post-HSV-1 inoculation. (*F*) Relative *IFIT1* mRNA expression in indicated cells 48 h post-HSV-1 inoculation. *P* values <0.05 were considered significant (*) and <0.01 very significant (**); n.s. = not significant (≥0.05).

Lack of cGAS-Mediated Innate Immune Sensing of HIV-1 and MLV Transduction in Mouse YAC-1 T Cells. Lentiviral transduction of YAC-1 T cells yielded very low GFP positivity (Fig. 7*A*), in agreement with their documented block at the level of nuclear import/integration in mouse T cells (37–40). A parallel transduction of human SUP-T1 T cells confirmed the infectivity of the used lentiviral stock. Despite the occurrence of EFV-sensitive reverse transcription, reaching up to 20 HIV-1 DNA copies per cell (Fig. 7*B*), *Ifit1* and *Mx2* mRNA expression hardly increased upon transduction (Fig. 7*C*). In addition, phosphorylation of IRF3 was undetectable in transduced YAC-1 T cells (Fig. 7*D*). All values obtained from cGAS KO T cells equaled those obtained for parental T cells, supporting the idea that HIV-1 transduction does not induce cGAS-dependent type I IFN responses in T cells. TREX1 KO did not result in any phenotypic changes, except a mild, but EFV-insensitive, trend toward higher *Mx2*, but not *Ifit1*, mRNA induction.

HSV-1 Δ*UL41*N inoculation of parental YAC-1 T cells resulted in 10% VP5-positive cells (Fig. 7*E*) and the delivery of up to 100 copies of HSV-1 genomes per cell (Fig. 7*F*), which was accompanied by an up to 500-fold and 1,500-fold up-regulation of *Ifit1* and *Mx2* mRNA expression, respectively (Fig. 7*G*), and a clear induction of phosphorylation of IRF3 (Fig. 7*H*). Again, those responses were insensitive to ACV, but strictly cGAS-dependent (Fig. 7 *G* and *H*), suggesting that the incoming HSV-1 genome or a DNA replication-independent PAMP or DAMP is sensed by cGAS. HSV Δ*UL41N*-inoculated TREX1 KO T cells displayed a slightly enhanced induction of *Ifit1* and *Mx2* mRNA expression. Finally, transduction of YAC-1 T cells with a cognate retrovirus, murine leukemia virus (MLV) pseudotyped with VSV-G, failed to trigger detectable innate immune responses, despite robust transduction efficiency (*SI Appendix*, Fig. S8).

Discussion

The cGAS/STING-mediated DNA sensing pathway is implicated in surprisingly diverse biological processes in different cell types, ranging from antiviral and antimicrobial defense, autoimmunity, sensing of endogenous retroviruses, senescence, DNA repair, and even to inflammation after myocardial infarction (reviewed in ref. 42). Viruses which replicate via DNA or DNA intermediates are generally considered as likely candidates prone to cGAS sensing. In addition, viral infection-caused stress responses may trigger release of mitochondrial DNA, which may result in cGAS-dependent responses to both DNA- and RNA-viral infections (43). Consequently, many viruses have evolved to prevent recognition by cGAS (5, 6).

The initial goal of our study was to define whether T cells contribute to sensing of DNA PAMPs or DAMPs in the context of exogenous DNA challenge and of viral infections. Activated $CD4^+$ T cells are the predominant target cell type of productive HIV-1 infection and support the de novo synthesis of reverse transcription products more efficiently than resting $CD4^+$ T cells, macrophages, and dendritic cells, probably due to reasons including optimal intracellular dNTP levels. Furthermore, human cGAS is expressed in activated T cells (14, 17), as opposed to resting T cells (14, 17). Although not belonging to classical antigen-presenting cells, we wondered whether T cells contribute to the immune system's defense against viral infection via cGAS/STING.

A first interesting observation was the markedly reduced and enhanced level of *Ifit1* and *Mx2* mRNA expression in mouse $CD4^+$ T cells devoid of cGAS and TREX1 expression, respectively. These results indicate a basal catalytic activity of cGAS, even in uninfected T cells, which has been also proposed for other cell types, including bone marrow-derived mouse macrophages (44). Basal activity of cGAS has been suggested to be triggered when cGAS is expressed at high levels (1), by binding to DNA originating from endogenous retroviruses and by the release of mitochondrial DNA (45, 46). cGAS activity is counteracted by TREX1 that degrades cytosolic DNA and, thus, precludes interaction of DNA with cGAS (3). The steady-state cGAS activity might therefore represent an important innate barrier to any invading pathogen that is sensitive to proteins expressed in the context of basal cGAS stimulation, since it may ensure maintenance of a basal antiviral state (44).

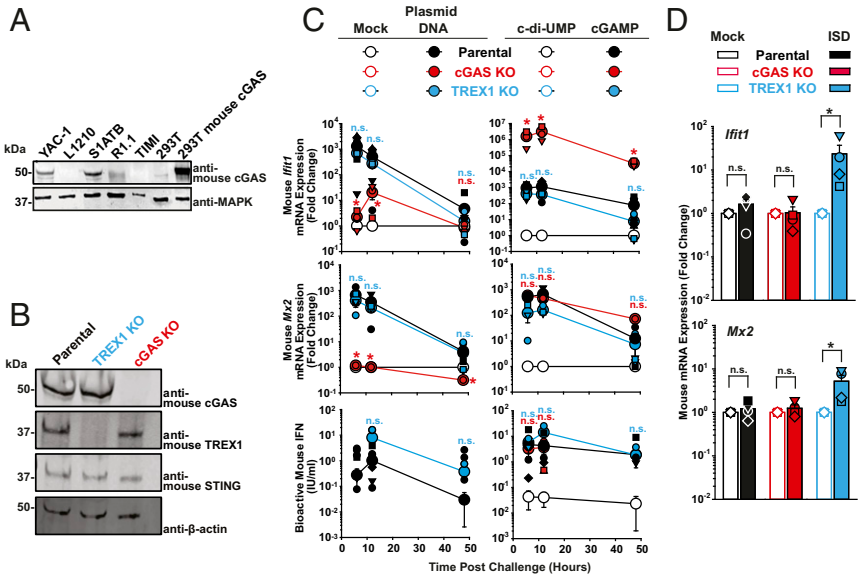

Fig. 6. cGAS and TREX1 modulate sensing of plasmid DNA and of ISD, respectively. (*A*) Immunoblotting of indicated cell lysates using anti-mouse cGAS and anti-MAPK antibodies. Lysates of parental HEK293T and mouse cGAS-expressing HEK293T serve as specificity controls for the anti-mouse cGAS antibody. (*B*) Immunoblotting of lysates of parental and cGAS KO YAC-1 T cell lines using indicated antibodies. (*C*) Parental, cGAS KO and TREX1 KO YAC-1 T cells were either mock-electroporated or electroporated with plasmid DNA (*Left*), or electroporated either with c-di-UMP or cGAMP (*Right*). Cultures were monitored at indicated time points postchallenge for relative *Ifit1* and *Mx2* mRNA expression by qRT-PCR (*Top* and *Middle*) and release of bioactive type I IFN using a luminometric MEF-based assay (*Bottom*). (*D*) Indicated YAC-1 T cell lines were mock-electroporated or electroporated with short ISD and monitored at 6 h postchallenge for *Ifit1* and *Mx2* mRNA expression by qRT-PCR. *P* values <0.05 were considered significant (*) and <0.01 very significant (**); n.s. = not significant (≥0.05).

The ability of activated CD4$^+$ T cells to respond to electroporated plasmid DNA and cGAMP indicated that this cell type has a functional DNA sensing machinery, which, as shown in mouse T cells, is cGAS-dependent. On the contrary, transfection of short ISD of 45 base pairs length failed to induce detectable responses. This is in line with cGAS′s reported ability to sense DNA in a length-dependent manner and to form intracellular cGAS protein-DNA ladder-like structures, thus requiring longer DNA molecules, and potentially cellular cofactors (47). On the contrary, in vitro stimulation of purified cGAS was reported to be effective with DNA fragments as small as 10–20 base pairs, at least when high concentration of both cGAS and DNA are present (47). Furthermore, our experiments in mouse CD4$^+$ T cells suggest that transfected ISDs might be prone to TREX1-mediated nucleic acid cleavage, since a detectable, but moderate, induction of *Ifit1* and *Mx2* mRNA expression was detected in TREX1 KO, but not in WT and cGAS KO cells. Together, this suggests that the discrepancy in the reported results regarding the response to ISD challenge in vitro and in living cells might be partially explained by the activity of TREX1.

In untreated CD4$^+$ T cells infected with HIV-1$_{Ba\text{-}L}$, intracellular p24 capsid positivity and quantities of reverse transcription products peaked 6 d postinfection, confirming productive infection at a level that is typically reached in primary CD4$^+$ T cells infected ex vivo with authentic HIV-1 (48). The biphasic *IFIT1* mRNA expression up-regulation observed in this context at early (2–3 h) and late (10–13 d) time points postinoculation could neither be attributed to sensing of de novo-synthesized viral DNA nor to productive infection, since EFV treatment did not alter the expression profile of *IFIT1*. These results were corroborated in a global transcriptomic approach, which indicated that IRF3-transactivated and IFN-related genes are generally not induced in productively infected cells at multiple time points, as compared to EFV-treated cultures. The lack of impact of both pharmacological and genetic destabilization of the viral capsid in T cells contrasts findings in macrophages and THP-1 cells (13, 24, 36), suggesting that viral DNA escaping the protective capsid is still unaccesssible to or quantitatively insufficient for cGAS-mediated sensing. An interesting hypothesis for this apparent cell type-specific phenomenon may be differential levels of TREX1 expression. Future studies are required to define the contribution of TREX1 to avoidance of HIV-1 sensing in T cells and macrophages. Short abortive RT products most likely resemble ISD, an experimental stimulus that triggered an immune response only in TREX1 KO T cells. Along this line, siRNA-mediated threefold reduction of *TREX1* mRNA expression resulted in a more potent induction of IFN genes in macrophages than in T cells (4). Nuclear export of unspliced viral RNA has been proposed to induce sensing of viral RNAs (49, 50). While our lentiviral virus particle approach is not an appropriate system to test this aspect in T cells based on a simple transfer vector, we believe that the absence of RT inhibitor-sensitive immune responses in HIV-1-$_{Ba\text{-}L}$–infected T cells argues against this possibility regarding induction of the tested ISGs. We conclude that HIV-1 can efficiently spread in activated CD4$^+$ T cells, the most susceptible target cell type, without provoking a notable type I IFN-mediated antiviral response. In stark contrast, efficient and ACV-insensitive induction of expression of *IFIT1*, *MX2*, and *IFN*-β mRNA in HSV-1 Δ*UL41N*-infected cells suggest that the incoming HSV-1 genomic DNA is prone to sensing in CD4$^+$ T cells. Interestingly, while the majority of HSV-1 DNA genomes are believed to be enclosed within a protective capsid, their leakage has already been suggested to occur in myeloid cells (28–30), and our data support the idea that this phenomenon occurs also in T cells.

The study by Vermeire et al. reporting cGAS-dependent sensing of HIV-1 infection postintegration in human CD4$^+$ T cells (14) is reminiscent of a reported sensing of HIV-1/Vpx in dendritic cells (11) and appears to contradict our findings. The reasons for these discrepancies may include the use of different virus production schemes and different virus strains. We chose HIV-1$_{Ba\text{-}L}$ because its production through serial passaging excludes the possibility of contaminating HIV-1 plasmid DNA in virion preparations and because it allowed us to monitor infection for up

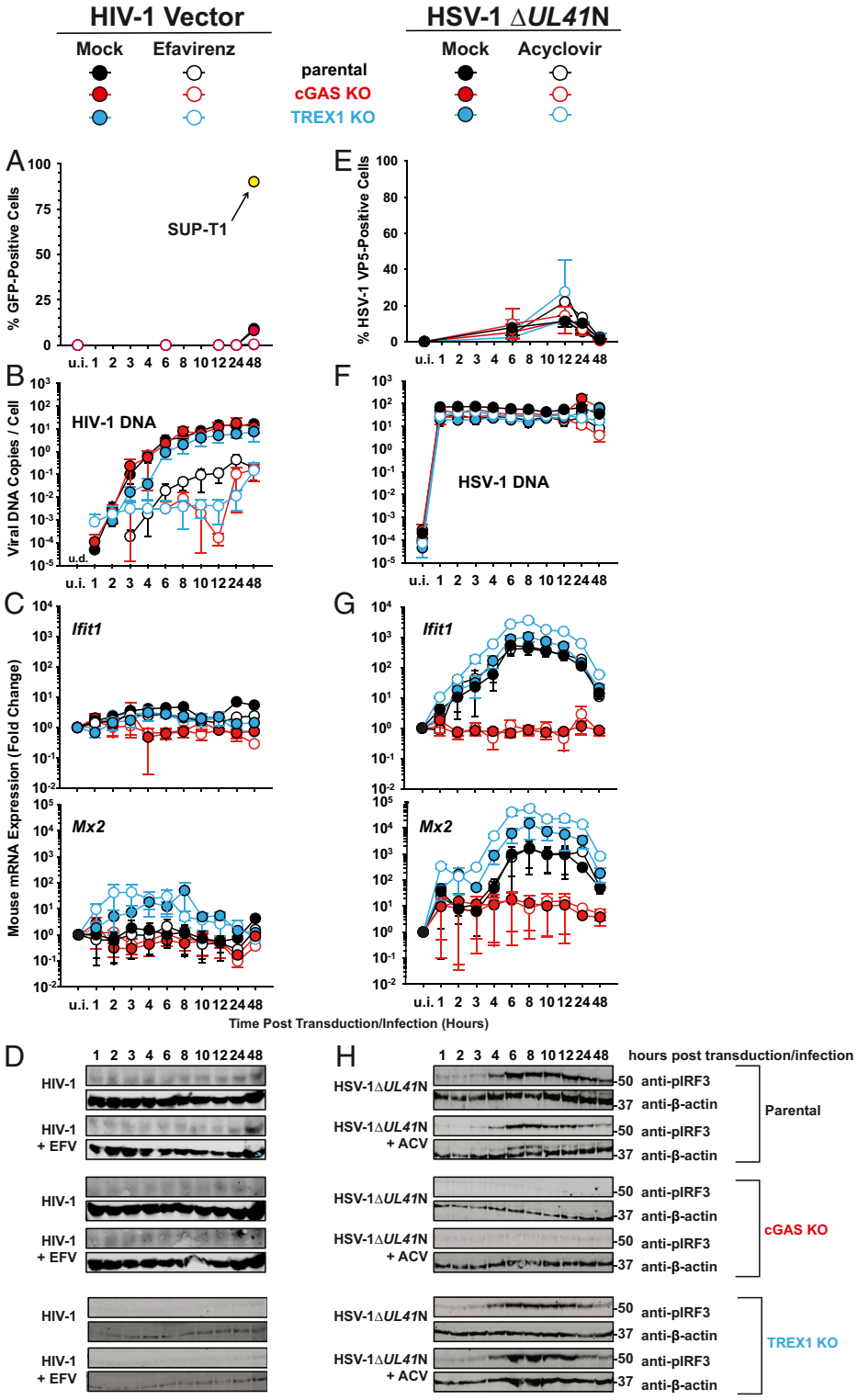

Fig. 7. Lack of cGAS-mediated innate immune sensing of HIV-1 and MLV transduction in mouse YAC-1 T cells. (*A–D*) Parental, cGAS KO, and TREX1 KO T cell lines were inoculated with VSV-G HIV-1 GFP vectors in the absence and presence of EFV and monitored, at indicated time points, for: Reporter GFP expression by FACS analysis (*A*), de novo synthesis of HIV-1 late RT products by absolute qPCR (*B*), relative expression of *Ifit1* and *Mx2* by qRT-PCR (*C*), and phosphorylated IRF3 by immunoblotting using a phospho-IRF3 antibody (*D*). (*E–H*) Parental, cGAS KO, and TREX1 KO T cell lines were inoculated with HSV-1 Δ*UL41*N in the absence and presence of ACV and monitored, at indicated time points, for: HSV-1 VP5 capsid protein expression by intracellular immunostaining followed by FACS analysis (*E*), genomic HSV-1 DNA copy numbers by absolute qPCR (*F*), relative expression of *Ifit1* and *Mx2* by qRT-PCR (*G*), phosphorylated IRF3 by immunoblotting using a phospho-IRF3 antibody (*H*).

to 13 d in the absence of extensive cell death. In contrast, Vermeire et al. generated virus stocks by calcium phosphate transfection and used, for the majority of experiments, the X4-tropic NL4.3 that, in our hands, induces massive death of $CD4^+$ T cells 2–3 d postinfection, a well-documented property of many X4-tropic HIV-1 strains. Whether the differential ability of NL4.3 and Ba-L to induce cell stress and death upon productive infection explain, at least partially, the different observations remains to be investigated.

Screening human and mouse cell lines revealed a surprising heterogeneity in cGAS expression among tested T cells. We therefore advise that DNA sensing studies in T cell lines should carefully validate the cGAS expression profile in the chosen T cell system. The absence of cGAS-dependent cellular responses upon productive HIV-1 and MLV vector transduction of PM1 and YAC-1 T cells, despite their full capability to sense DNA via cGAS, is consistent with the idea that HIV-1 infection either evades or antagonizes this DNA sensing machinery. Since no accessory HIV-1 proteins are expressed by the lentiviral vectors employed, absence of cGAS-dependent responses in transduced cells let us hypothesize that cGAS is not activated, neither in the context of spreading infection nor of lentiviral and retroviral transduction. Along this line, superinfection of lentivirally transduced cells with HSV-1 did not alleviate the induction of HSV-triggered *IFIT1* mRNA expression, arguing against a putative ability of lentiviruses to directly interfere with the cGAS-dependent signaling pathway. During lentiviral and gammaretroviral infection, a single full-length DNA genome is produced progressively during capsid migration to the nucleus and is then integrated into the cellular chromosome; no DNA replication during the rest of the replication cycle is required. In contrast, herpesviral genomes are 20-fold larger than HIV-1 genomes, and, in addition to being inevitably present as integral part of incoming virions, are also generated anew in large quantities in the context of progeny virus production. Thus, retroviruses including HIV-1 may have evolved a replication strategy that reduces the abundance of cytoplasmic DNA intermediates to a minimum, thus avoiding susceptibility to cGAS-mediated sensing in infected T cells.

Methods

Animals. cGAS KO mice on the C57BL/6 background (Mb21d1tm1d(EUCOMM)Hmgu/J) were kindly obtained from Charles Rice. TREX1 KO mice were kindly obtained from Tomas Lindahl (Francis Crick Institute, London). C57BL/6 (WT), cGAS KO and TREX1 KO mice were bred under specific pathogen-free conditions. Mouse experimental work was carried out using 8- to 14-wk-old mice in compliance with regulations of the German animal welfare law.

Cell Lines and Primary Cells. A3.01, SUPT1, Jurkat, CEM T cells were purchased from American Type Culture Collection. PM1 T cells were obtained from the NIH AIDS Reagent Program. S1A.TB, R1.1, TIMI.4 were kindly obtained from Oliver Keppler. Parental YAC-1 and L1210 cells were kindly obtained from Roland Jacobs, Hanover Medical School. CRISPR/Cas9-mediated knockouts were generated by transient electroporation of an EF1alpha-Cas9-2A-EGFP/U6-sgRNA expression plasmid, followed by FACS-sorting and single-cell cloning by limiting dilution. Parental HEK293T cells and HEK293T cells expressing cGAS (clone 17) are described in ref. 51. Parental THP-1, cGAS KO THP-1, and Jurkat T cells stably expressing WT cGAS and cGAS (G212A/S213A) are described in ref. 16. Withdrawal of blood samples from healthy humans and cell isolation were conducted with approval of the full study of the local ethics committees (ethical review committee of Hanover Medical School, vote ID 3025-2016; Ethical review committee of Charité–Universitätsmedizin Berlin, vote ID EA4/167/19). Purification of human $CD4^+$ T cells was performed by negative selection.

Single-cell suspensions of mouse splenocytes were prepared by pushing spleen tissue pieces through a 70-μm pore size nylon mesh screen (Fisher Scientific). Washed splenocytes were subjected to $CD4^+$ T cell isolation using the EasySep Mouse $CD4^+$ T-Cell Isolation kit (Stemcell Technologies).

Viruses. $HIV\text{-}1_{Ba\text{-}L}$ was obtained from the NIH AIDS Reagent Program and propagated on PM1 T cells. HSV-1 Δ*UL41*N (HSV-1(KOS) UL41NHB) was kindly provided by David A. Leib (52). It encodes a truncated version of pUL41, which fails to induce the degradation of cellular mRNAs and is unable to counteract cGAS. To prepare concentrated stocks, extracellular virions were pelleted from the medium of cells infected with a multiplicity of infection of 0.01 pfu per cell for 3 d (53, 54). Virus stocks were plaque-titrated on Vero cells (53, 55). To determine the genome/pfu ratio of HSV-1 stocks, we measured the number of HSV-1 genomes by qPCR as described previously (54, 56).

Lentiviral and Gammaretroviral Particles. VSV-G–pseudotyped HIV-1 GFP particles were generated by calcium phosphate-based transfection of HEK293T cells with the packaging plasmid pCMV ΔR8.91 (57) expressing WT capsid or CA(P90A) or pCMV ΔR8.2 (CA N74D), the GFP-encoding transfer plasmid pHR.GFP (58), and the pCMV-VSV-G plasmid (59). VSV-G–pseudotyped MLV GFP particles were generated by calcium phosphate-based transfection of HEK293T cells with the packaging plasmid pCMVi gag-pol (60), the GFP-encoding transfer plasmid pSER S11 SF GFP (61), and the pCMV-VSV-G plasmid (59).

Intracellular HIV-1 p24CA and HSV-1 VP5 Immunostaining. PBS-washed cells were paraformaldehyde (PFA)-fixed and immunostained for intracellular HIV-1 p24CA using fluorescein isothiocyanate (FITC)-conjugated mAb KC57 (Beckman Coulter) in 0.1% Triton in phosphate-buffered saline (PBS). VP5 immunostaining was performed with rabbit anti-HSV-1 VP5 (SY4563; ref. 62) and an appropriate fluorochrome-conjugated secondary antibody in 0.1% Triton in PBS.

qPCR of Viral DNA. DNA extraction from cells were performed with Maxwell 16 Blood DNA purification kit (Promega). Quantification of absolute copy numbers of HIV-1 late RT products was performed with the 7500 Fast Real-Time PCR System (Applied Biosystems) using a published Taq-Man–based PCR (63). The number of HSV-1 genomes was quantified as described previously (54, 56) using the LightCycler FastStart DNA Master HybProbe kit (Roche Diagnostics).

Human and Mouse Type I IFN Bioactivity Assays. Secretion of human type I IFN bioactivity was quantified using the human reporter cell line HL116 that carries the luciferase gene under the control of the IFN-inducible 6–16 promoter (ref. 64, a kind gift from Sandra Pellegrini, Institut Pasteur, France). Secretion of murine, bioactive type I IFN was quantified using the mouse reporter cell line MEF that expresses the luciferase gene under the control of the mouse *Mx2* promoter (ref. 65, a kind gift of Mario Köster, Helmholtz Center for Infection Research, Brunswick, Germany).

Data Availability. The RNA-sequencing data discussed in this publication have been deposited in National Center for Biotechnology Information's Gene Expression Omnibus (GEO) (66), https://www.ncbi.nlm.nih.gov/geo (accession no. GSE150753).

All relevant data and protocols are included in the paper. Requests for reagents should be directed to C.G.

Additional *Materials and Methods* are posted in *SI Appendix*.

ACKNOWLEDGMENTS. We thank Charles Rice (The Rockefeller University, New York) and Tomas Lindahl for providing the cGAS KO and *TREX1* KO mouse lines, respectively. We thank Sandra Pelligrini (Institut Pasteur, Paris), Frank Pessler (TWINCORE, Hanover, Germany), and Mario Köster for the kind gift of the HL116 cell line, THP-1 cells, and MEF-luciferase cells, respectively. We thank Oya Cingöz (Robert Koch Institute, Berlin) for kindly providing the ΔR8.92 CA (N74D) plasmid. We thank Oliver Dittrich-Breiholz (Hanover Medical School, Hanover, Germany) and Victor Tarabykin (Charité - Universitätsmedizin Berlin, Berlin) for granting access to the Step One Plus Real-Time PCR System and the ABI7500 Real-Time PCR System, respectively. We thank the NIH AIDS Research & Reference Reagent Program for providing essential reagents. We thank Thomas Pietschmann (TWINCORE, Hanover, Germany) and Christian Drosten (Charité - Universitätsmedizin Berlin, Berlin) for constant support. This work was supported by a postdoctoral fellowship from the Foundation Ernst & Margarete Wagemann (to A.D.); by a DAAD thesis completion fellowship (to A.P.); funding of Joint French-German Project cGAS-VAC Project 406922110 (to U.K.); funding from Deutsche Forschungsgemeinschaft (DFG) for Germany's Excellence Strategy, EXC 2155, Project 390874280 (to B.S.); DFG Collaborative Research Centre CRC900 "Microbial Persistence and its Control" Project 158989968, project C2 (to B.S.) and project C8 (to C.G.); and DFG SPP Priority Programm 1923 "Innate Sensing and Restriction of Retroviruses" GO2153/4 Grant (to C.G.); funding from Boehringer Ingelheim Foundation (Exploration Grant) (to C.G.); and funding of the Helmholtz Center for Infection Research and Berlin Institute of Health (to C.G.).

1. A. Ablasser *et al*., cGAS produces a 2′-5′-linked cyclic dinucleotide second messenger that activates STING. *Nature* **498**, 380–384 (2013).
2. P. Gao *et al*., Cyclic [G(2′,5′)pA(3′,5′)p] is the metazoan second messenger produced by DNA-activated cyclic GMP-AMP synthase. *Cell* **153**, 1094–1107 (2013).
3. A. Ablasser *et al*., TREX1 deficiency triggers cell-autonomous immunity in a cGAS-dependent manner. *J. Immunol.* **192**, 5993–5997 (2014).
4. N. Yan, A. D. Regalado-Magdos, B. Stiggelbout, M. A. Lee-Kirsch, J. Lieberman, The cytosolic exonuclease TREX1 inhibits the innate immune response to human immunodeficiency virus type 1. *Nat. Immunol.* **11**, 1005–1013 (2010).
5. Z. Ma *et al*., Modulation of the cGAS-STING DNA sensing pathway by gammaherpesviruses. *Proc. Natl. Acad. Sci. U.S.A.* **112**, E4306–E4315 (2015).
6. M. Stempel, B. Chan, M. M. Brinkmann, Coevolution pays off: Herpesviruses have the license to escape the DNA sensing pathway. *Med. Microbiol. Immunol. (Berl.)* **208**, 495–512 (2019).
7. O. Cingöz, S. P. Goff, HIV-1 is a poor inducer of innate immune responses. *MBio* **10**, e02834-18 (2019).
8. D. Gao *et al*., Cyclic GMP-AMP synthase is an innate immune sensor of HIV and other retroviruses. *Science* **341**, 903–906 (2013).
9. S. Kumar, J. H. Morrison, D. Dingli, E. Poeschla, HIV-1 activation of innate immunity depends strongly on the intracellular level of TREX1 and sensing of incomplete reverse transcription products. *J. Virol.* **92**, e00001-18 (2018).
10. M. A. Siddiqui *et al*., A novel phenotype links HIV-1 capsid stability to cGAS-mediated DNA sensing. *J. Virol.* **93**, e00706-19 (2019).
11. X. Lahaye *et al*., The capsids of HIV-1 and HIV-2 determine immune detection of the viral cDNA by the innate sensor cGAS in dendritic cells. *Immunity* **39**, 1132–1142 (2013).
12. S. M. Yoh *et al*., PQBP1 is a proximal sensor of the cGAS-dependent innate response to HIV-1. *Cell* **161**, 1293–1305 (2015).
13. J. Rasaiyaah *et al*., HIV-1 evades innate immune recognition through specific cofactor recruitment. *Nature* **503**, 402–405 (2013).
14. J. Vermeire *et al*., HIV triggers a cGAS-dependent, Vpu- and Vpr-regulated type I interferon response in $CD4^+$ T cells. *Cell Rep.* **17**, 413–424 (2016).
15. R. K. Berg *et al*., T cells detect intracellular DNA but fail to induce type I IFN responses: Implications for restriction of HIV replication. *PLoS One* **9**, e84513 (2014).
16. S. Xu *et al*., cGAS-mediated innate immunity spreads intercellularly through HIV-1 env-induced membrane fusion sites. *Cell Host Microbe* **20**, 443–457 (2016).
17. S. Cerboni *et al*., Intrinsic antiproliferative activity of the innate sensor STING in T lymphocytes. *J. Exp. Med.* **214**, 1769–1785 (2017).
18. N. Grandvaux *et al*., Transcriptional profiling of interferon regulatory factor 3 target genes: Direct involvement in the regulation of interferon-stimulated genes. *J. Virol.* **76**, 5532–5539 (2002).
19. C. Goffinet *et al*., Primary T-cells from human CD4/CCR5-transgenic rats support all early steps of HIV-1 replication including integration, but display impaired viral gene expression. *Retrovirology* **4**, 53 (2007).
20. K. B. Koh, M. Fujita, A. Adachi, Elimination of HIV-1 plasmid DNA from virus samples obtained from transfection by calcium-phosphate co-precipitation. *J. Virol. Methods* **90**, 99–102 (2000).
21. K. A. Matreyek, S. S. Yücel, X. Li, A. Engelman, Nucleoporin NUP153 phenylalanine-glycine motifs engage a common binding pocket within the HIV-1 capsid protein to mediate lentiviral infectivity. *PLoS Pathog.* **9**, e1003693 (2013).
22. J. Shi, J. Zhou, V. B. Shah, C. Aiken, K. Whitby, Small-molecule inhibition of human immunodeficiency virus type 1 infection by virus capsid destabilization. *J. Virol.* **85**, 542–549 (2011).
23. C. L. Márquez *et al*., Kinetics of HIV-1 capsid uncoating revealed by single-molecule analysis. *eLife* **7**, e34772 (2018).
24. R. P. Sumner *et al*., Disrupting HIV-1 capsid formation causes cGAS sensing of viral. bioRxiv:10.1101/838011 (11 November 2019).
25. M. Aubert, M. Yoon, D. D. Sloan, P. G. Spear, K. R. Jerome, The virological synapse facilitates herpes simplex virus entry into T cells. *J. Virol.* **83**, 6171–6183 (2009).
26. K. R. Jerome *et al*., Herpes simplex virus inhibits apoptosis through the action of two genes, Us5 and Us3. *J. Virol.* **73**, 8950–8957 (1999).
27. S. Lahmidi, U. Strunk, J. R. Smiley, A. Pearson, P. Duplay, Herpes simplex virus 1 infection of T cells causes VP11/12-dependent phosphorylation and degradation of the cellular protein Dok-2. *Virology* **511**, 66–73 (2017).
28. K. A. Horan *et al*., Proteasomal degradation of herpes simplex virus capsids in macrophages releases DNA to the cytosol for recognition by DNA sensors. *J. Immunol.* **190**, 2311–2319 (2013).
29. S. B. Rasmussen *et al*., Activation of autophagy by α-herpesviruses in myeloid cells is mediated by cytoplasmic viral DNA through a mechanism dependent on stimulator of IFN genes. *J. Immunol.* **187**, 5268–5276 (2011).
30. C. Sun *et al*., Cellular requirements for sensing and elimination of incoming HSV-1 DNA and capsids. *J. Interferon Cytokine Res.* **39**, 191–204 (2019).
31. C. Su, C. Zheng, Herpes simplex virus 1 abrogates the cGAS/STING-mediated cytosolic DNA-sensing pathway via its virion host shutoff protein, UL41. *J. Virol.* **91**, e02414-16 (2017).
32. M. Trotard *et al*., Sensing of HIV-1 infection in tzm-bl cells with reconstituted expression of STING. *J. Virol.* **90**, 2064–2076 (2015).
33. K. Lee *et al*., Flexible use of nuclear import pathways by HIV-1. *Cell Host Microbe* **7**, 221–233 (2010).
34. A. J. Price *et al*., CPSF6 defines a conserved capsid interface that modulates HIV-1 replication. *PLoS Pathog.* **8**, e1002896 (2012).
35. T. Schaller *et al*., HIV-1 capsid-cyclophilin interactions determine nuclear import pathway, integration targeting and replication efficiency. *PLoS Pathog.* **7**, e1002439 (2011).
36. L. Bulli *et al*., Complex interplay between HIV-1 capsid and MX2-independent alpha interferon-induced antiviral factors. *J. Virol.* **90**, 7469–7480 (2016).
37. J. G. Baumann *et al*., Murine T cells potently restrict human immunodeficiency virus infection. *J. Virol.* **78**, 12537–12547 (2004).
38. H. M. Tervo, C. Goffinet, O. T. Keppler, Mouse T-cells restrict replication of human immunodeficiency virus at the level of integration. *Retrovirology* **5**, 58 (2008).
39. N. Tsurutani *et al*., Nuclear import of the preintegration complex is blocked upon infection by human immunodeficiency virus type 1 in mouse cells. *J. Virol.* **81**, 677–688 (2007).
40. J. X. Zhang, G. E. Diehl, D. R. Littman, Relief of preintegration inhibition and characterization of additional blocks for HIV replication in primary mouse T cells. *PLoS One* **3**, e2035 (2008).
41. D. B. Stetson, J. S. Ko, T. Heidmann, R. Medzhitov, Trex1 prevents cell-intrinsic initiation of autoimmunity. *Cell* **134**, 587–598 (2008).
42. M. Motwani, S. Pesiridis, K. A. Fitzgerald, DNA sensing by the cGAS-STING pathway in health and disease. *Nat. Rev. Genet.* **20**, 657–674 (2019).
43. B. Sun *et al*., Dengue virus activates cGAS through the release of mitochondrial DNA. *Sci. Rep.* **7**, 3594 (2017).
44. J. W. Schoggins *et al*., Pan-viral specificity of IFN-induced genes reveals new roles for cGAS in innate immunity. *Nature* **505**, 691–695 (2014).
45. H. Maekawa *et al*., Mitochondrial damage causes inflammation via cGAS-STING signaling in acute kidney injury. *Cell Reports* **29**, 1261–1273.e6 (2019).
46. A. P. West *et al*., Mitochondrial DNA stress primes the antiviral innate immune response. *Nature* **520**, 553–557 (2015).
47. L. Andreeva *et al*., cGAS senses long and HMGB/TFAM-bound U-turn DNA by forming protein-DNA ladders. *Nature* **549**, 394–398 (2017).
48. A. Cooper *et al*., HIV-1 causes CD4 cell death through DNA-dependent protein kinase during viral integration. *Nature* **498**, 376–379 (2013).
49. H. Akiyama *et al*., HIV-1 intron-containing RNA expression induces innate immune activation and T cell dysfunction. *Nat. Commun.* **9**, 3450 (2018).
50. S. M. McCauley *et al*., Intron-containing RNA from the HIV-1 provirus activates type I interferon and inflammatory cytokines. *Nat. Commun.* **9**, 5305 (2018).
51. A. Ablasser *et al*., Cell intrinsic immunity spreads to bystander cells via the intercellular transfer of cGAMP. *Nature* **503**, 530–534 (2013).
52. L. I. Strelow, D. A. Leib, Role of the virion host shutoff (vhs) of herpes simplex virus type 1 in latency and pathogenesis. *J. Virol.* **69**, 6779–6786 (1995).
53. B. Sodeik, M. W. Ebersold, A. Helenius, Microtubule-mediated transport of incoming herpes simplex virus 1 capsids to the nucleus. *J. Cell Biol.* **136**, 1007–1021 (1997).
54. K. Döhner, K. Radtke, S. Schmidt, B. Sodeik, Eclipse phase of herpes simplex virus type 1 infection: Efficient dynein-mediated capsid transport without the small capsid protein VP26. *J. Virol.* **80**, 8211–8224 (2006).
55. K. Döhner *et al*., Function of dynein and dynactin in herpes simplex virus capsid transport. *Mol. Biol. Cell* **13**, 2795–2809 (2002).
56. I. Engelmann *et al*., Rapid quantitative PCR assays for the simultaneous detection of herpes simplex virus, varicella zoster virus, cytomegalovirus, Epstein-Barr virus, and human herpesvirus 6 DNA in blood and other clinical specimens. *J. Med. Virol.* **80**, 467–477 (2008).
57. R. Zufferey, D. Nagy, R. J. Mandel, L. Naldini, D. Trono, Multiply attenuated lentiviral vector achieves efficient gene delivery in vivo. *Nat. Biotechnol.* **15**, 871–875 (1997).
58. H. Miyoshi, M. Takahashi, F. H. Gage, I. M. Verma, Stable and efficient gene transfer into the retina using an HIV-based lentiviral vector. *Proc. Natl. Acad. Sci. U.S.A.* **94**, 10319–10323 (1997).
59. S. A. Stewart *et al*., Lentivirus-delivered stable gene silencing by RNAi in primary cells. *RNA* **9**, 493–501 (2003).
60. A. J. Fletcher *et al*., Trivalent RING assembly on retroviral capsids activates TRIM5 ubiquitination and innate immune signaling. *Cell Host Microbe* **24**, 761–775.e6 (2018).
61. A. Schambach *et al*., Overcoming promoter competition in packaging cells improves production of self-inactivating retroviral vectors. *Gene Ther.* **13**, 1524–1533 (2006).
62. K. Döhner *et al*., Importin α1 is required for nuclear import of herpes simplex virus proteins and capsid assembly in fibroblasts and neurons. *PLoS Pathog.* **14**, e1006823 (2018).
63. C. Goffinet, I. Allespach, O. T. Keppler, HIV-susceptible transgenic rats allow rapid preclinical testing of antiviral compounds targeting virus entry or reverse transcription. *Proc. Natl. Acad. Sci. U.S.A.* **104**, 1015–1020 (2007).
64. G. Uzé *et al*., Domains of interaction between alpha interferon and its receptor components. *J. Mol. Biol.* **243**, 245–257 (1994).
65. D. Kugel, J. E. Pulverer, M. Köster, H. Hauser, P. Staeheli, Novel nonviral bioassays for mouse type I and type III interferon. *J. Interferon Cytokine Res.* **31**, 345–349 (2011).
66. R. Edgar, M. Domrachev, A. E. Lash, Gene expression Omnibus: NCBI gene expression and hybridization array data repository. *Nucleic Acids Res.* **30**, 207–210 (2002).

XI. Curriculum vitae

Mein Lebenslauf wird aus datenschutzrechtlichen Gründen in der elektronischen Version meiner Arbeit nicht veröffentlicht.

XII. Publication list

First-author publications & comments

I. **Kazmierski J***, Friedmann K*, Postmus D, Emanuel J, Fischer C, Jansen J, Richter A, Bosquillon de Jarcy L, Schüler C, Sohn M, Sauer S, Drosten C, Saliba AE, Sander LE, Müller MA, Niemeyer D#, Goffinet C#. **Nonproductive exposure of PBMCs to SARS- CoV-2 induces cell-intrinsic innate immune responses**. Mol Syst Biol. 2022 Aug;18(8):e10961. doi: 10.15252/msb.202210961. **IF: 13.1**

II. **Kazmierski J**, Elsner C, Döhner K, Xu S, Ducroux A, Pott F, Jansen J, Thorball CW, Zeymer O, Zhou X, Fedorov R, Fellay J, Löffler MW, Weber ANR, Sodeik B, Goffinet C. **A Baseline Cellular Antiviral State Is Maintained by cGAS and Its Most Frequent Naturally Occurring Variant rs610913**. J Immunol. 2022 Jul 18:ji2100685. doi: 10.4049/jimmunol.2100685. **IF: 5.4**

III. **Kazmierski J**, Goffinet C. **Alert from a Distant Neighbor: Spread of Antiviral Immunity through Anion Channels**. Comment in Immunity. 2020 May 19;52(5):719-721. doi: 10.1016/j.immuni.2020.04.017. **IF: 31.7**

First-author publications (Preprints)

IV. **Kazmierski, J**., D. Postmus, E. Wyler, C. Fischer, J. Jansen, K. Meixenberger, S. N. Vitcetz, M. Sohn, S. Sauer, N. Bannert, M. Landthaler, and C. Goffinet. 2020**. Single Cell RNA-Sequencing-based Analysis of CD4$^+$ T-Cell Subset-Specific Susceptibility to Transcriptional Modulation by HIV-1 Latency-Reversing Agents**. *bioRxiv* 2020.05.04.075119.

Co-authored publications

V. Ebenig A, Muraleedharan S, **Kazmierski J**, Todt D, Auste A, Anzaghe M, Gömer A, Postmus D, Gogesch P, Niles M, Plesker R, Miskey C, Gellhorn Serra M, Breithaupt A, Hörner C, Kruip C, Ehmann R, Ivics Z, Waibler Z, Pfaender S, Wyler E, Landthaler M, Kupke A, Nouailles G, Goffinet C, Brown RJP, Mühlebach MD. **Vaccine-associated enhanced respiratory pathology in COVID-19 hamsters after TH2-biased immunization**. Cell Rep. 2022 Aug 16;40(7):111214. doi: 10.1016/j.celrep.2022.111214. **IF: 9.4**

VI. Wyler E*, Adler JM*, Eschke K, Teixeira Alves G, Peidli S, Pott F, **Kazmierski J**, Michalick L, Kershaw O, Bushe J, Andreotti S, Pennitz P, Abdelgawad A, Postmus D, Goffinet C, Kreye J, Reincke SM, Prüss H, Blüthgen N, Gruber AD, Kuebler

WM, Witzenrath M, Landthaler M, Nouailles G#, Trimpert J#. **Key benefits of dexamethasone and antibody treatment in COVID-19 hamster models revealed by single-cell transcriptomics**. Mol Ther. 2022 May 4;30(5):1952-1965. doi: 10.1016/j.ymthe.2022.03.014. **IF: 11.5**

VII. Nouailles G*, Wyler E*, Pennitz P, Postmus D, Vladimirova D, **Kazmierski J**, Pott F, Dietert K, Muelleder M, Farztdinov V, Obermayer B, Wienhold SM, Andreotti S, Hoefler T, Sawitzki B, Drosten C, Sander LE, Suttorp N, Ralser M, Beule D, Gruber AD, Goffinet C, Landthaler M, Trimpert J#, Witzenrath M#. **Temporal omics analysis in Syrian hamsters unravel cellular effector responses to moderate COVID-19**. Nat Commun. 2021 Aug 11;12(1):4869. doi: 10.1038/s41467-021-25030-7. **IF: 14.9**

VIII. Wendisch D*, Dietrich O*, Mari T*, von Stillfried S*, Ibarra IL, Mittermaier M, Mache C, Chua RL, Knoll R, Timm S, Brumhard S, Krammer T, Zauber H, Hiller AL, Pascual- Reguant A, Mothes R, Bülow RD, Schulze J, Leipold AM, Djudjaj S, Erhard F, Geffers R, Pott F, **Kazmierski J**, Radke J, Pergantis P, Baßler K, Conrad C, Aschenbrenner AC, Sawitzki B, Landthaler M, Wyler E, Horst D; Deutsche COVID-19 OMICS Initiative (DeCOI), Hippenstiel S, Hocke A, Heppner FL, Uhrig A, Garcia C, Machleidt F, Herold S, Elezkurtaj S, Thibeault C, Witzenrath M, Cochain C, Suttorp N, Drosten C, Goffinet C, Kurth F, Schultze JL, Radbruch H, Ochs M, Eils R, Müller-Redetzky H, Hauser AE, Luecken MD, Theis FJ, Conrad C, Wolff T, Boor P, Selbach M, Saliba AE#, Sander LE#. **SARS-CoV-2 infection triggers profibrotic macrophage responses and lung fibrosis**. Cell. 2021 Dec 22;184(26):6243-6261.e27. doi: 10.1016/j.cell.2021.11.033. **IF: 41.6**

IX. Trump S*, Lukassen S*, Anker MS*, Chua RL*, Liebig J*, Thürmann L*, Corman VM*, Binder M*, Loske J, Klasa C, Krieger T, Hennig BP, Messingschlager M, Pott F, **Kazmierski J**, Twardziok S, Albrecht JP, Eils J, Hadzibegovic S, Lena A, Heidecker B, Bürgel T, Steinfeldt J, Goffinet C, Kurth F, Witzenrath M, Völker MT, Müller SD, Liebert UG, Ishaque N, Kaderali L, Sander LE, Drosten C, Laudi S, Eils R, Conrad C, Landmesser U#, Lehmann I#. **Hypertension delays viral clearance and exacerbates airway hyperinflammation in patients with COVID-19**. Nat Biotechnol. 2021 Jun;39(6):705-716. doi: 10.1038/s41587-020-00796-1. **IF: 54.9**

X. Chua RL*, Lukassen S*, Trump S*, Hennig BP*, Wendisch D*, Pott F, Debnath O, Thürmann L, Kurth F, Völker MT, **Kazmierski J**, Timmermann B, Twardziok S, Schneider S, Machleidt F, Müller-Redetzky H, Maier M, Krannich A, Schmidt S, Balzer F, Liebig J, Loske J, Suttorp N, Eils J, Ishaque N, Liebert UG, von Kalle C, Hocke A, Witzenrath M, Goffinet C, Drosten C, Laudi S, Lehmann I, Conrad C, Sander LE, Eils R. **COVID-19 severity correlates with airway epithelium-**

immune cell interactions identified by single-cell analysis. Nat Biotechnol. 2020 Aug;38(8):970-979. doi: 10.1038/s41587- 020-0602-4. **IF: 54.9**

XI. Elsner C*, Ponnurangam A*, **Kazmierski J**, Zillinger T, Jansen J, Todt D, Döhner K, Xu S, Ducroux A, Kriedemann N, Malassa A, Larsen PK, Hartmann G, Barchet W, Steinmann E, Kalinke U, Sodeik B, Goffinet C. **Absence of cGAS-mediated type I IFN responses in HIV-1-infected T cells**. Proc Natl Acad Sci U S A. 2020 Aug 11;117(32):19475-19486. doi: 10.1073/pnas.2002481117. **IF: 12.8**

Co-authored preprints

XII. Nouailles, G.*, J. M. Adler*, P. Pennitz, S. Peidli, G. T. Alves, M. Baumgart, J. Bushe, A. Voss, A. Langenhagen, F. Pott, **J. Kazmierski**, C. Goekeri, S. Simmons, N. Xing, C. Langner, R. M. Vidal, A. Abdelgawad, S. Herwig, G. Cichon, D. Niemeyer, C. Drosten, C. Goffinet, M. Landthaler, N. Blüthgen, H. Wu, M. Witzenrath, A. D. Gruber, S. D. Praktiknjo, N. Osterrieder, E. Wyler#, D. Kunec#, and J. Trimpert#. 2022. **A live attenuated vaccine confers superior mucosal and systemic immunity to SARS-CoV-2 variants**. *bioRxiv* 2022.05.16.492138.

XIII. Niemeyer, D., S. Schroeder, K. Friedmann, F. Weege, J. Trimpert, A. Richter, S. Stenzel, J. Jansen, J. Emanuel, **J. Kazmierski**, F. Pott, L. M. Jeworowski, R. Olmer, M.-C. Jaboreck, B. Tenner, J. Papies, J. Heinze, F. Walper, M. L. Schmidt, N. Heinemann, E. Möncke-Buchner, T. Veith, M. Baumgardt, K. Hoffmann, M. Widera, T. T. N. Thao, A. Balázs, J. Schulze, C. Mache, M. Morkel, S. Ciesek, L. G. Hanitsch, M. A. Mall, A. C. Hocke, V. Thiel, K. Osterrieder, T. Wolff, U. Martin, V. M. Corman, M. A. Müller, C. Goffinet#, and C. Drosten#. 2021. **Post-entry, spike-dependent replication advantage of B.1.1.7 and B.1.617.2 over B.1 SARS-CoV-2 in an ACE2-deficient human lung cell line**. *bioRxiv* 2021.10.20.465121.

Legend

* Shared first-authorship

Shared last-authorship

XIII. Acknowledgments

First, I would like to thank Prof. Dr. Christian Drosten for giving me the providing the resources and giving me the opportunity to conduct my research in the Institute of Virology at the Charité University Hospital Berlin.

My deep gratitude goes to my supervisor Prof. Dr. Christine Goffinet for her exceptional way of mentoring, guiding and supporting me and my fellow colleagues on our individual scientific career paths. Your endless curiosity and enthusiasm to conduct research and teach young scientists based on their individual strengths is truly inspirational. I learned a lot from you!

I would like to thank Prof. Dr. Chiara Romagnani and Prof. Dr. Daniel Sauter for their co-supervision, fruitful discussions and support for my projects.

I would like to extend my gratitude to all the past and current members of the Goffinet lab in Hannover and Berlin. You created an amazing group atmosphere, where everyone was always committed to help and support each other, which made our everyday lab work - despite all the struggles that comes with experimental work from time to time - much more enjoyable. Thank you!

Many thanks to Dr. Oya Cingöz for her constant support on my research projects, this dissertation and beyond.

Thanks to the German AIDS foundation for covering the printing costs for this dissertation.

Finally, I would like to thank my family and especially my partner Dennis Prigann for encouraging me to pursue this career path and being my strongest supporters over the years.